Design and realization of a primary and secondary leak standards for the measurement of leak flow rates of refrigerants

Isabelle Morgado

ED n°432 : Sciences des Métiers de l'Ingénieur

N° attribué par la bibliothèque
|__|__|__|__|__|__|__|__|__|__|

T H E S E

pour obtenir le grade de

DOCTEUR DE L'ECOLE NATIONALE SUPERIEURE DES MINES DE PARIS

Spécialité "Energétique"

présentée et soutenue publiquement par
Isabelle MORGADO

le 14 novembre 2008

DESIGN AND REALIZATION OF A PRIMARY AND SECONDARY LEAK STANDARDS FOR THE MEASUREMENT OF LEAK FLOW RATES OF REFRIGERANTS

Directeur de thèse : Denis Clodic

Jury

M. Didier MAYER, EMP ..... Président
M. Daniel FAVRAT, EPFL ..... Rapporteur
M. François LEPOUTRE, CNAM ..... Rapporteur
M. Jean-Claude LEGRAS, LNE ..... Examinateur
M. Etienne MERLIN, ADEME..... Examinateur
M. Denis CLODIC, EMP ..... Examinateur

ACKNOWLEDGEMENTS

Rewinding 3 years of my life, I realize that this work could not have been done without many people who contributed in a way or another to the accomplishment and success of this thesis. I would like to express my gratitude to them.

Denis CLODIC, Deputy-Director of the "Centre for Energy and Processes" and thesis director, and **Jean-Claude LEGRAS**, Head of the Pressure and Vacuum laboratory of the "Laboratoire National de Métrologie et d'Essais", who integrated me in their teams and who advised me all over this work. I hope that I deserved their trust and that our collaboration will continue successfully.

Anne-Marie POUGIN, who is always available to take care of administrative questions and especially for the time she spent to read this dissertation and her advises for its improvement.

Franck FAYOLLE, of the CEP, who contributed actively in the success of this work, who helps me in the design of the test benches and in their realization.

The **members** of the examination board and especially the "rapporteurs". I appreciate their patience while evaluating my work.

Mr. MERLIN for his follow up and **ADEME** for fueling the study with financial support.

Aline GARNIER of the CEP, **Mrs COULLON** of the LNE, and **Mrs POIROT** of the LNE for the documentation research help.

Mr SUTOUR, of the LNE Chemistry laboratory, for his technical support in chemistry.

Mr JEANJACQUOT and **Mr MADEC,** of the LNE Mass and Volume laboratory, for their collaboration in the volume comparison.

Mr CAMUS, of the LNE Dimensional laboratory, for his contribution in the calibration of the standard volume.

Mr WETZEL and **Mr LOUCIF,** of LNE, for their contribution in the realization of some elements of the test bench.

Youssef RIACHI, of CEP, for his help to handle the FLUENT software.

Mr CAZAURAN and **Mr HUCHET,** of CETIM, for sharing their experience in the leak detection in an industrial environment.

My colleagues, who made my stay easy at the CEP and at the LNE. I hope we will continue in this good ambiance. Special thanks to **Yingzhong YU**, **David SOUSA**, **Assaad ZOUGHAIB** of CEP, **Roger MONTABORD**, **Frédéric BOINEAU**, **Djilali BENTOUATI**, **Pierre OTAL,** and **Thierry RABAULT** of LNE for their friendship and their technical support.

My Parents for their encouragement, support and help. They contributed enormously to my well being and happiness. I dedicate my work to them.

Table of contents

Nomenclature

Symbols

C	Concentration	/ µmol.mol^{-1}
C_0	Conductance	/ m^3.s^{-1}
C_p	Heat capacity at constant pressure	/ J.kg^{-1}.K^{-1}
C_v	Heat capacity at constant volume	/ J.kg^{-1}.K^{-1}
D	Diameter	/ m
D	Diffusion coefficient	/ m².s^{-1}
E	Energy	/ J
e	Wall thickness	/ m
f_{prob}	Density function of the probability	
g	Acceleration of gravity	/ m.s^{-2}
h	Enthalpy of 1 kg of gas	/ J.kg^{-1}
h	Convection coefficient	/W.m^{-2}.K^{-1}
I	Light intensity	/ Cd
i	Current intensity	/ A
K	Thermal conductivity	/ W.m^{-1}.K^{-1}
L	Luminance	/ Cd.m^{-2}
l	Length	/ m
l_m	Molecular mean free path	/ m
M	Molar Mass	/ g.mol^{-1}
m	mass	/ kg
M_{micro}	Sensitivity	/ V.Pa^{-1}
N	Molar Flow Rate	/ mol.s^{-1}
n	Molar quantity	/ mol
P	Pressure	/ Pa
p	Acoustical pressure	/ Pa
Q	Throughput	/ Pa.m^3.s^{-1}
$\bar{q}$	Arithmetic mean of a quantity q	
q	Observation value of a quantity q	
Q_m	Mass flow rate	/ kg.s^{-1}
Q_v	Volume flow rate	/ m^3.s^{-1}
RES	Resistance	/ ohm
S	Surface	/ m²
SENS	Sensibility	
T	Temperature	/ K
t	Time	/ s
T_f	Optical filter transmission	
F	Function of transmission of the optical filter (F depends on [ν-ν_0])	
U	Enlarged combined uncertainty (k=2)	
u	Standard combined uncertainty	
u²(a)	Variance of the quantity a	
U_T	Voltage	/ V
V	Volume	/ m^3
v	Speed	/ m.s^{-1}
V(a)	Variance of the quantity a	
W	Absorbed power per unit volume	/ W.m^{-3}
Z	Impedance	

Greek letter

α	Correction factor representing all the phenomenon that are not controlled	
α_T	Thermal dilatation coefficient of a gas	/ K^{-1}
β	Absorptivity coefficient (depends on ν)	
β_V	Volume dilatation coefficient	/ K^{-1}
χ_T	Isothermal compressibility coefficient of a gas	Pa^{-1}
$\Delta\nu$	Bandwidth of the light	/ Hz
$\Delta\Pi$	Pressure loss	/Pa
ε	Interaction energy	/ J
γ	Adiabatic coefficient of a gas	
λ	Wavelength of sound	/ m
μ	Dynamic viscosity	/ Pa.s
ν	Frequency band of the filter	/ Hz
Φ	Collision diameter	/ Angströms
θ	Half cone angle of the light cone	/ sr
ρ	Density	/ $kg.m^{-3}$
σ	Type A - Standard deviation	
τ	Expected value of a quantity	
Ω	Collision integral	
ω	Chopper pulsation	/ rad^{-1}
ξ	Kinematic viscosity	/ $m^2.s^{-1}$
ψ	Pressure loss coefficient	/ Pa

Adimensionnal number

Kn	Knudsen Number	$Kn = \frac{D}{l_m}$
N_u	Nusselt Number	$N_u = \frac{h \cdot D}{K}$
R_a	Rayleigh Number	$Ra = \frac{g \cdot \beta_V \cdot \rho^2 \cdot C_p \cdot \lvert T_{wall} - T_{gaz} \rvert \cdot D^3}{K \cdot \mu}$
R_a^*	Modified Rayleigh Number	$Ra^* = \frac{g \cdot \beta_V \cdot \rho^2 \cdot C_p \cdot (T_{wall} - T_\infty) \cdot r_h^4}{K \cdot \mu \cdot L}$
Re	Reynolds Number	$Re = \frac{\rho \cdot V \cdot D}{\mu}$

Constants

k_B	Boltzmann Constancy	$k_B = 1.3806 \times 10^{-23}$ $J.K^{-1}$
N_a	Avogadro Number	$N_a = 6.022 \times 10^{23}$ mol^{-1}
R_g	Perfect gas constant	$R_g = 8.314$ $J.K^{-1}.mol^{-1}$

Indices

0	Initial value inside the accumulation volume (Static expansion method)
1 ($R_{U/L}$)	Step 1 in the valving sequence to determine the ratio $R_{U/L}$
2 ($R_{U/L}$)	Step 2 in the valving sequence to determine the ratio $R_{U/L}$
100	Value of 100 Ω
110	Value of 110 Ω
∞	From the infinity, of the ambient environment
ν	At the frequency band of the filter ν
Acc	Accumulation volume
After expansion	After expansion (Static expansion system)
air	Air
Average	Average between the value of the quantity related to the standard volume and the one related to the accumulation volume
Before expansion	Before expansion (Static expansion system)
calibration	Calibration
corr	Corrected value
cyl	Cylinder or main cylinder
diluted	Diluted
downstream	downstream
e	Final value inside the equilibrate system {accumulation volume + Standard volume} (Static expansion method)
final	Final
fitting	Fitting (mathematical)
fittings	Fittings, connections
FM	Flowmeter
g	gas
h	Hydraulic
heat	Heat
initial	Initial
int	Internal
L	Leak
limit	Limit Detection
m	Mechanical
mano	Manometer
mixture	Mixture
mult	Multimeter
P	Pressure
p	Piston
PAS	Photo-acoustic spectrometer
PAC	Photo-acoustic cell
Pt100	Pt100
pump	pumping
pump1	Pumping in step 1
pump2	Pumping in step 2
pump3	Pumping in step 3
q	Quantity q
R-134a	R-134a
R-134a/air	Between R-134a and air molecules
r	Reference
read	Indication read from a measuring instrument
regular	Regular (pressure losses)
RES	Resistance
res	Initial value inside the standard volume (Static expansion method)

s	Standard
singular	Singular (pressure losses)
sound	sound
Spectrophotometer	Spectrophotometer
stability	Stability
U/L	Upper chamber / Lower chamber
u	Upper chamber
unitary	Unitary
upstream	Upstream
used	Used
X	Translation
Xp	Translation of the piston
walls	Walls
window	Germanium Window

Acronyms

ASHRAE	American Society of Heating, Refrigerating and Air-Conditioning Engineers
CEP	Centre for Energy and Processes.
INRIM	Istituto Nazionale di Ricerca Metrologica
LNE	Centre for Scientific and Industrial Metrology (Laboratoire National de Métrologie et d'Essais).
NIST	National Institute of Standards and Technology

Abbreviations & Definitions

Accumulation volume	Volume where the gas is accumulated during the suction of the gas by the monitor (for the photo-acoustic gas monitor, it means that the photo-acoustic cell is opened). It includes the accumulation cell.
Accumulation cell	2L- cylindrical volume where the refrigerant leaks is evacuated into. All valves are closed. It is a part of the accumulation volume.
CFC	Chlorofluorocarbons.
Corr	Correction
GWP	The GWP or Global Warming Potential classifies the gases based on their contribution to the greenhouse effect. CO_2 is the reference gas with a GWP equals to 1,0. The GWP value of each gas is expressed in kg of CO_2. It depends on a selected time frame.
HCFC	Hydrochlorofluorocarbons
HFC	Hydrofluorocarbons
MFR	Mass Flow Rate
NAC	Non applied correction
ODP	The ODP or Ozone Depletion Potential is a relative scale that ranks chemicals based on their potential do deplete the ozone layer. By definition, R-11 has a value of 1,0 and is the reference for all other chemicals.
OEM	Original Equipment Manufacturer
PAC	Photo-acoustic cell
PAS	Photo-acoustic spectrometer
R	Ratios
ran	Random
RMS	Root Mean Square
sys	Systematic
Throughput	The quantity of gas in pressure-volume units, at a specified temperature, flowing per unit time across a specified open cross section [28].
VFR	Volumetric Flow Rate

General introduction

Nowadays leak detection is widely used in various fields such as the automotive and the refrigeration industries. The leak tightness of installations charged with refrigerants must be controlled periodically by refrigerant detectors, qualified via refrigerant leaks. Consequently this dissertation aims at establishing the measurement chain from standard leaks to qualified detectors. The thesis is composed of 4 chapters. Chapters 1, 2, and 3 deal with the primary standard to measure refrigerant calibrated leak flow rates. The last one deals with the detectors qualification method and the precautions to be taken during a detection on site.

Chapter 1 describes the stakes that lead to a need for establishing a complete measurement chain to measure refrigerant leaks flow rate. An inventory of the main existing methods to measure gas leaks flow rates – usually they are vacuum techniques – is carried out to understand the need to establish a new measurement chain. Consequently, the existing techniques are enumerated and evaluated to define the capacity to adapt this method to measure refrigerant leaks in their operating conditions. From this analysis the main interests of the development for a new method is deduced: the infrared detection in an accumulation volume.

Chapter 2 presents the design of the primary standard using the infrared detection. Some test benches to measure refrigerant mass flow rate (MFR) through components have already been realized by the Center for Energy and Processes (CEP). Based on the CEP experience, the design of the bench aims at improving and optimizing the metrological performances of the measurement. The identified key point are: the concentration and the accumulation volume measurement. Therefore, in this chapter:

- two main infrared techniques are theoretically and experimentally compared in order to select the most efficient.
- three techniques to calibrate volumes are presented and metrologically compared in order to select the best suited.

The aim of this chapter is to design a primary standard to measure refrigerant leak flow rates with an uncertainty about 1%. The selection of the components of the primary standard is finally presented based on the CEP experience and on this study results.

Once the test bench to measure refrigerant leak flow rate is realized according to the specifications defined in Chapter 2, the measurement chain is qualified. The procedures to calibrate the leak flow rate and the uncertainty budget of the measurement of leak flow rate are then established in Chapter 3, using the theory of the uncertainty estimation, and the experimental and phenomenological results. The leak flow rate is calculated from the variations of the tracer gas concentration, the temperature, and the pressure in the accumulation volume, and from the capacity of the accumulation volume. Consequently, the methods to measure these quantities are developed and the uncertainty budget for each quantity is estimated in Chapter 3. As in Chapter 2, the key points of this qualification concern the concentration variation measurements – the infrared spectrometer is calibrated - and the capacity of the volumes - the method is qualified.

Those three chapters aims at realizing a primary standard to measure refrigerant calibrated leak flow rates with an uncertainty about 1%. The main goal of the study is to give the means to the industry to respect the regulations relative to the leak tightness of refrigerating equipment. The primary standard ensures the traceability of the calibrated leaks used to qualify leak detectors. However, to establish the complete measurement chain of the sensitivity threshold of refrigerant detectors, Chapter 4 deals with the qualification method to qualify the refrigerant detectors: it aims at defining the precautions that must be taken. Theory, experiments, and CFD simulation by Fluent are presented in this chapter, in order to identify the main parameters that can influence the measurement of the detector sensitivity threshold. Based on this knowledge, the precautions to be taken during the measurement according to the existing standards to qualify the leak detector performances can be identified. Finally, the chapter

finalize the study by the precautions to be taken when a qualified detector is used for real leak detection in an industrial environment.

Chapter 1 - Inventory of existing methods to calibrate gas leak flow rate

1.1 Regulations and needs

Due to the Montreal Protocol signed in 1987, the use of ozone-depleting refrigerants such as CFCs and HCFCs has been or is progressively stopped. Thereby, these gases were replaced by HFC gases, CO_2, and hydrocarbons. The Ozone Depletion Potential of R-134a is equal to zero. However, the most used refrigerants are greenhouse gases: their GWPs are really high (see Table 1.1). On that account, the Kyoto Protocol in 1997 tends to limit the emissions of these greenhouse refrigerants.

Table 1.1. Example of GWP (100 years) of HFC gases [CLO98-1].

Name of the gas	GWP (100 years) *kg of CO_2*
Pure Fluids	
R-134a	1 300
R-125	2 800
R-32	650
R-152a	140
R-143a	3 800
Mixtures	
R-404A	3 260
R-407C	1 530
R-410A	1 730
R-507	3 300
R-417A	1 955

However, actions aiming at the limitation of greenhouse refrigerant emissions were not determined. European countries tend to define these actions. Different national policies are being published. Some European countries (the Netherlands, France…) mention that leak-tightness inspections are a key point. On that account, the European regulation n°2037/2000 indicates the measures to be taken in order to limit refrigerant emissions. In particular, title 5 mentions mandatory annual leak-tightness inspections for installations charged with refrigerants except for domestic appliances [CLO00], [CLO02]. More recently, the new European regulation n°842/2006 published on 17th May 2006 [REGLEM06] relating to the refrigerant greenhouse gases defines the duties of the owners of this equipment. Thus, the owner of equipment confining more than 3 kg of refrigerant fluids must control periodically the tightness of their equipment. The tightness has to be controlled:

- every year for equipment containing more than 3 kg of refrigerant,
- every 6 months for equipment containing more than 30 kg of refrigerant,
- every 3 months for equipment containing more than 300 kg of refrigerant.

In France, the decree n°98-560 on 30th June 1998 [DECRET98], relating to refrigerants used in refrigerating and climatic equipment, and the first article of the French order established on 12th January 2000 define that the owner of equipment with more than 2 kg of refrigerant must control the tightness every year. More recently, French decree n°2007-737 was published the7th May 2007

[DECRET07], based on the specifications of the European regulation. However, some differences exist between the European regulation and the French decree: for instance, the owner of equipment confining more than 2 kg of refrigerant must also control the leak tightness every year. The French policy tends to be more precise than the European regulation. The French order established on 12th January 2000 [ARRETE00] specifies how the leak tightness must be controlled. Consequently, the leak tightness of the equipment containing refrigerant must be controlled by refrigerant leak detectors and room controllers whose respective sensitivity must be lower than 5 $g.yr^{-1}$ and 10 $\mu mol.mol^{-1}$ [ARRETE07].

Hence, the performances of these devices have to be confirmed. Thereby, the implementation of regulation on leak-tightness inspections requires the elaboration of standards for the performances of refrigerant leak detectors and room controllers. AFNOR (French Association for Standards) initiated the matter with the standard E 35422. This standard was proposed to the CEN to become a European standard, EN-14624. This European standard was published in 2005. In the order [ARRETE07], it is specified that the sensitivity of devices must be measured according to the standard EN-14624 [AFN05]. This tendency reached also North America. The SAE (Society of Automotive Engineers) and the ASHRAE (American Society of Heating, Refrigerating and Air-Conditioning Engineers) are taking the same path and similar standards are written or under elaboration. All these standards establish that refrigerant calibrated leaks from 1 g/yr to 50 g/yr are needed to qualify the performances of refrigerant leak detectors and room controllers. Performances of a detector are tested by comparing the calibrated leak MFR and the indication of the detectors.

The calibration of refrigerant leaks is now a key point in leak-tightness inspections. Therefore, calibrated leaks have to be traceable to the SI units. It means that there is no reference to define the unit of a refrigerant leak flow rate through its practical realization. Finally, the first key point of leak-tightness inspections is the calibration and the design of standard leaks. In the short term, a primary standard for the measurements of leak flow rates of refrigerant will be necessary for OEMs and suppliers of leak detectors, as standard leaks are definitely needed. At the present time, the NIST (National Institute of Standards and Technology) in the United States and the LNE ("Laboratoire National de Métrologie et d'Essais") in France for instance calibrate standard leaks of helium. The LNE has decided to provide a primary standard for the measurements of leak flow rates of refrigerant gases. The LNE and the CEP have agreed to share their abilities in order to develop this type of equipment.

1.2 Objectives

The objectives of this chapter are as follows:

- To analyze the suitability of the existing methods to measure a refrigerant leak MFR
- To present the chosen method to measure refrigerant leak MFR
- To deduce the interest of this method.

1.3 Existing calibration method of gas leak flow rate

To the best of our knowledge, neither a device, nor a protocol existed for the verification of leak MFR of HFC calibrated leaks. However, concerning helium, a primary standard is available at the NIST in the United States [NIST92]. In France, a primary standard based on another method has been developed [LEG97], [BOI06]. These standards aim at calibrating helium leaks in the range from 10^{-6} mol/s to 10^{-12} mol/s, which means helium leaks around (1.3×10^{-4}) $g.yr^{-1}$ and (1.3×10^{2}) $g.yr^{-1}$. This large range of leak MFRs is due to the fact that helium leaks are widely used for vacuum systems. That is why it exists flows about 10^{-4} g/yr, adapted to molecular flows.

Concerning the refrigerant leaks, the standards for qualifying refrigerant detectors only require leaks from 1 $g.yr^{-1}$ to 50 $g.yr^{-1}$ for typical HFC gases as R-134a corresponding to leaks to be detected in refrigerating systems. For R-134a 1 $g.yr^{-1}$ equals to 3.1×10^{-10} $mol.s^{-1}$ and 50 $g.yr^{-1}$ equals to 1.6×10^{-8} $mol.s^{-1}$. The range is smaller than for helium and the leaks are quite huge comparing to helium leaks, because the flow regimes are not similar. These leaks are operating at atmospheric pressure, the flow regime is in general viscous neither molecular nor intermediate.

Thus the range of the existing methods is wider than the one needed for helium and includes the range of refrigerant flows. It is then necessary to compare these methods and to analyze the possibilities of using one of them for developing a primary standard. In this part of the thesis, some methods to calibrate helium leaks used by the NIST and by the LNE are described. Then the relevance of similar methods to calibrate refrigerant leaks is analyzed and discussed. Next a method widely used by some refrigerant leak manufacturers to calibrate refrigerant leak flow rates directly at atmospheric pressure is analyzed: the weighing method. Finally, the principle of measurement of the primary standard of refrigerant leaks is presented and the interest of this method is analyzed.

1.3.1 NIST primary standard for the measurements of leak flow rates of helium

1.3.1.1 Operating principle

The primary standard developed by the NIST [NIST92], [EHR90] aims at calibrating leak flow rates of helium. The standard is divided into three major components [TOR02], [CLO00], [CLO02]:

- a main vacuum system composed by an upper chamber and a lower chamber,
- a constant-pressure flowmeter,
- a manifold on which the leak is mounted.

The primary standard can measure molar flow rates between 10^{-6} $mol.s^{-1}$ and 10^{-12} $mol.s^{-1}$, which correspond to helium leak MFRs between (1.26×10^{-4}) $g.yr^{-1}$ and 126 $g.yr^{-1}$. It also corresponds to R-134a leak MFR between (3.22×10^{-4}) $g.yr^{-1}$ and (3.22×10^{3}) $g.yr^{-1}$ [EHR96].
Two operating techniques are used to measure the leak flow rate. They are named:

- "Flow into the upper chamber", which is composed of 3 valving sequences (steps 1, 2, and 3) aiming at substituting a known flow to the one from the unknown leak: the evacuation of the unknown leak, the adjustment of the flowmeter and the evacuation of the standard leak from the flowmeter. This technique measures leak flow rates between 10^{-6} $mol.s^{-1}$ and 10^{-12} mol/s. However, the uncertainty of the leak flow rate measurement of 10^{-12} $mol.s^{-1}$ is about 12%.
- "Flow division technique", which is composed of a preliminary measurement of a relevant parameter to estimate the flow rate (2 valving sequences: steps 1 and 2) and of the measurement of the flow rate (3 valving sequences: steps 1, 2, and 3). This technique is developed to measure helium leak flow rates near 10^{-12} $mol.s^{-1}$ with a better uncertainty (7.2%) than that of the "flow into the upper chamber" technique.

Flow into the upper chamber

At the beginning, the pressure in the upper chamber is recorded with no gas flow for different valving conditions.

Step 1:
The unknown gas flow is directed into the upper chamber. It flows into the lower chamber before being evacuated by the vacuum pump. The gas flow is allowed stabilizing and then, the equilibrium pressure of the upper chamber is recorded: P_{u1} (see Figure 1.1). Due to the conservation of total number of molecules, the molar flow rate N_L of gas leaving the leak is the same as the molar flow rate

of gas passing through the orifice, and the same as the flow rate of gas through the pump [NIST92]. Therefore, N_L can be expressed by Equation [1.1].

$$N_L = \frac{P_{u1}}{R_g \cdot T_{01}} \cdot \left[\frac{v_{pump1} \cdot C_{01}}{C_{01} + v_{pump1}} \right] \qquad [1.1],$$

where

C_{01}	Conductance in step 1
N_L	Molar Flow Rate of the leak
P_{u1}	Pressure in the upper chamber in step 1
V_{pump1}	Pumping speed in step 1

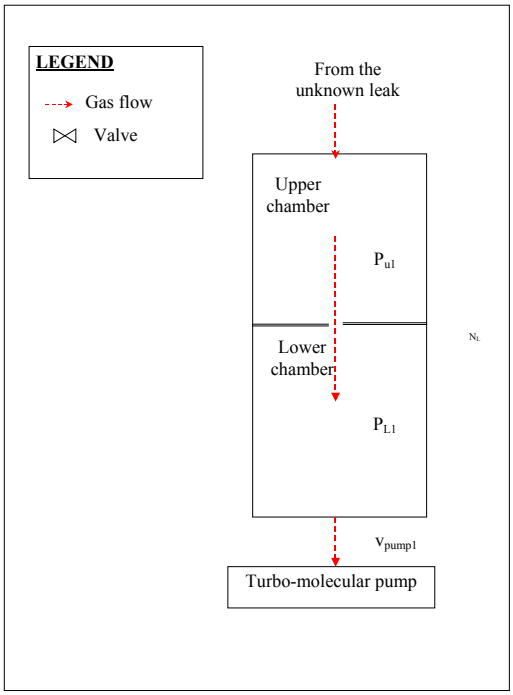

Figure 1.1. Step 1 of the sequence for calibrating leak flow rate through the upper chamber of the NIST primary standard.

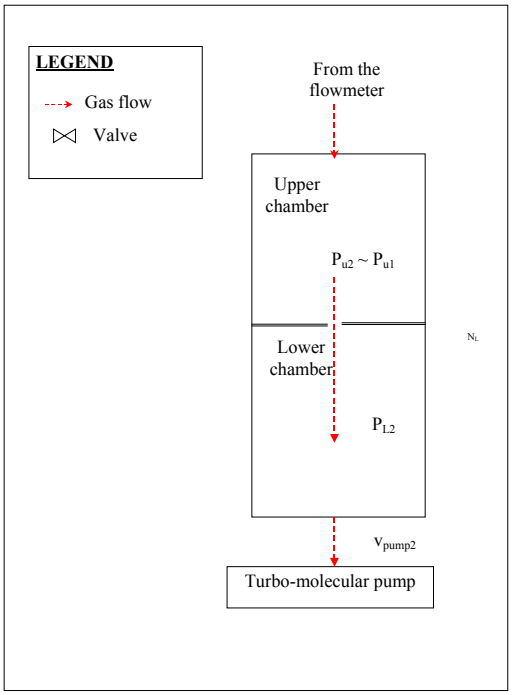

Figure 1.2. Step 2 of the sequence for calibrating leak flow rate through the upper chamber of the NIST primary standard.

Step 2:
Next, the unknown leak is valved out and gas is introduced into the flowmeter, which admits gas into the upper chamber. The flow rate is adjusted by a variable leak valve (see Figure 1.3), so that the pressure in the upper chamber is similar to the pressure P_{u1} generated in the upper chamber by the unknown leak in step 1. Then it is allowed stabilizing (see Figure 1.2: step 2).

Step 3:
This step aims at calibrating the generated leak flow rate from the flowmeter (see Figure 1.4). The apparatus is composed of a reference volume, a variable volume, two pistons, a piston advance control system, and pressure measurement devices. A flow of gas is generated by changing the volume of the variable volume at a measured rate such as the pressure in the variable volume remains constant. Therefore, in this step, gas introduction is stopped. The reference and the variable volumes, which were filled to the same pressure, are isolated from each other by closing the upstream valves. The pressure in the variable volume decreases due to the gas escaping through the leak valve, which produces a change in a differential capacitance diaphragm gauge installed between the two volumes. Then this gauge activates a control system, which controls the rate of advance of the piston to maintain a zero differential pressure between the two volumes. The pressure in the reference volume is experimentally measured: P_{r3}. The volume rate changes are experimentally determined as the change

in volume ΔV over a measured time interval Δt [NIST92], [CUL87], [JOU02]. The equilibrium pressure inside the upper chamber is then recorded: P_{u3}.

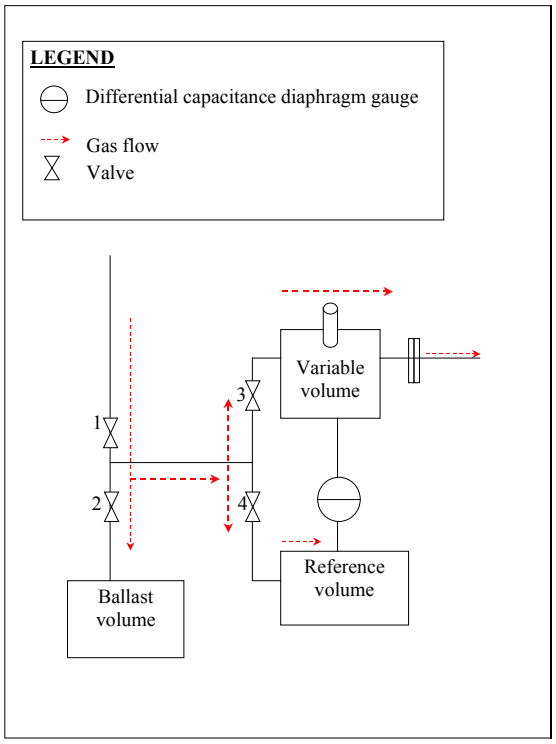

Figure 1.3. Generated leak flow by the flowmeter: step 2.

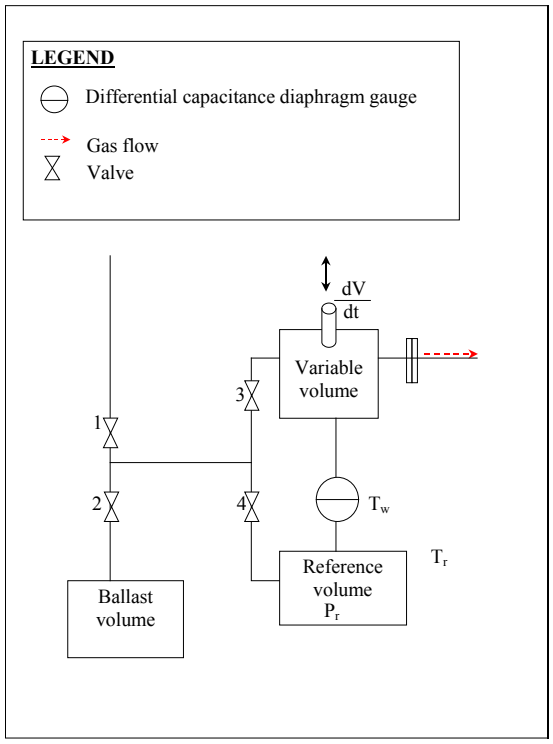

Figure 1.4. Measurement of the generated leak flow rate from the flowmeter: step 3.

Due to the conservation of total number of molecules, the molar flow rate of gas leaving the flowmeter N_L^{FM} is the same as the molar flow rate of gas passing through the orifice N_L^{03}, and the same as the flow rate of gas through the pump. It is worth noting that the NIST standard measures flow rate at each step: a flow rate passing through the orifice, a flow rate through a vacuum pump, a flow rate generated by a flowmeter, and measured via the variation of a volume. Therefore, this installation summarizes quite well the different means to measure a flow rate of an under vacuum system.

A loss of molar density in the upper volume means an increase in molar density in the lower volume. Considering the equation of state of perfect gases, the molar flow rate N_L^{03} through the orifice between the upper and the lower chambers can be expressed by Equation [1.2].

$$N_L^{FM} = N_L^{03} = -\frac{C_{03} \cdot (P_{u3} - P_{L3})}{R_g \cdot T_{03}} \qquad [1.2]$$

where

C_{03}	Conductance in step 3
N_L^{03}	Molar flow rate in step 3
N_L^{FM}	Flowmeter molar flow rate
P_{L3}	Pressure in the lower chamber in step 3
P_{u3}	Pressure in the upper chamber in step 3
R_g	Perfect gas constant
S_p	Piston surface
T_{03}	Temperature in the chambers in step 3

In order to maintain this flow rate constant, the differential pressure must remain constant. Therefore the capacity of the variable volume varies with the translation of a piston: the translation speed v_{XP} of the piston will be expressed by Equation [1.3].

$$v_{XP} = \frac{R_g \cdot T_{w3}}{P_{w3} \cdot S_p} \cdot N_L^{03} \Rightarrow N_L^{03} = \frac{P_{w3} \cdot \left(\Delta V / \Delta t\right)}{R_g \cdot T_{w3}} \approx \frac{P_{r3} \cdot \left(\Delta V / \Delta t\right)}{R_g \cdot T_{r3}} \qquad [1.3]$$

where

P_{r3}	Pressure in the reference volume in step 3
P_{w3}	Pressure in the variable volume in step 3
T_{r3}	Temperature in the reference volume of the flowmeter in step 3
T_{w3}	Temperature in the variable volume in step 3
V_{XP}	Translation speed of the piston
ΔV	Variation of the volume
Δt	Variation of the time

However, in this case, the system is evacuated: at the beginning the pressure is near zero. Therefore, the speed of the piston is almost infinite. The best solution is then to exhaust the gas in the lower chamber. Thus the pressure in the lower chamber will be expressed by [1.4].

$$P_{L3} = N_L^{03} \bullet \frac{R_g \cdot T_{03}}{v_{pump3}} \qquad [1.4]$$

where

P_{L3}	Pressure in the lower chamber chamber in step 3
T_{03}	Temperature in the upper chamber in step 3
v_{pump3}	Pumping speed in step 3

Therefore, P_{u3} can be expressed by Equation [1.5].

$$P_{u3} = P_{r3}\left(\frac{\Delta V}{\Delta t}\right)\left[\frac{T_{03}}{T_{r3}}\right]\left[\frac{C_{03} + v_{pump3}}{C_{03} \cdot v_{pump3}}\right] \qquad [1.5]$$

where

C_{03}	Conductance in step 3
P_{u3}	Pressure in the upper chamber in step 3

Finally, considering that the conductance is proportional to $\sqrt{T}$, the unknown flow rate is calculated by Equation [1.6].

$$N_L = N_L \cdot \frac{P_{u3}}{P_{u3}} = \frac{P_{r3}\left(\frac{\Delta V}{\Delta t}\right)}{R_g T_{r3}}\left[\frac{P_{u1}}{P_{u3}}\right]\left[\frac{T_{03}}{T_{01}}\right]^{1/2}\left[\frac{v_{pump1}}{v_{pump3}} \times \frac{C_{03} + v_{pump3}}{C_{01} + v_{pump1}}\right] \qquad [1.6]$$

Flow division technique

This technique aims at extending the dynamic range of the system. With the usual method, at flow rates of about 10^{-12} mol/s, the uncertainties associated with the flowmeter approach 10%. The principle behind the flow division technique is that, for constant orifice conductance and pumping speed, the ratio of the flow rate into the upper chamber at the pressure P_u to the flow rate into the lower chamber (result of the same pressure P_u in the upper chamber) is constant. This constancy is identical for any flow rates and it can be measured considering high flow rates. Thus, the range of measurements is not limited by the dynamic range of the flowmeter.

At first, the ratio must be determined. The following procedure aims at measuring this ratio. Figures 1.5 and 1.6 present the main valving sequences of this procedure. First, the variable and the

reference volumes of the flowmeter are filled with gas at the same pressure $P_{r1\ (RU/L)}$. The gas is admitted into the upper chamber. The gas supply is then switched off and the equilibrium is expected. The equilibrium pressure in the upper chamber is recorded: $P_{u1\ (RU/L)}$. The variation of the volume is measured (see Figure 1.5: step1).

Secondly, the variable and the reference volumes of the flowmeter are filled with gas at the same pressure $P_{r2\ (RU/L)}$. The gas from the flowmeter instead of being transferred into the upper chamber is directly admitted into the lower chamber. The flow rate is adjusted in order that the pressure in the upper chamber $P_{u2\ (RU/L)}$ is equal to $P_{u1\ (RU/L)}$ (see Figure 1.6: step 2). After the equilibrium, the flow rate is measured by the flowmeter: the volume variation is measured. Finally, the ratio is calculated by Equation [1.7].

$$R_{U/L} = \frac{P_{r2}(R_{U/L}) \cdot \left(\frac{\Delta V}{\Delta t}\right)_{2}(R_{U/L}) \cdot T_{r1}(R_{U/L})}{P_{r1}(R_{U/L}) \cdot \left(\frac{\Delta V}{\Delta t}\right)_{1}(R_{U/L}) \cdot T_{r2}(R_{U/L})} \cdot \left[\frac{P_{u1}(R_{U/L}) \cdot T_{02}(R_{U/L}) \cdot v_{pump1}(R_{U/L})}{P_{u2}(R_{U/L}) \cdot T_{01}(R_{U/L}) \cdot v_{pump2}(R_{U/L})}\right] \qquad [1.7]$$

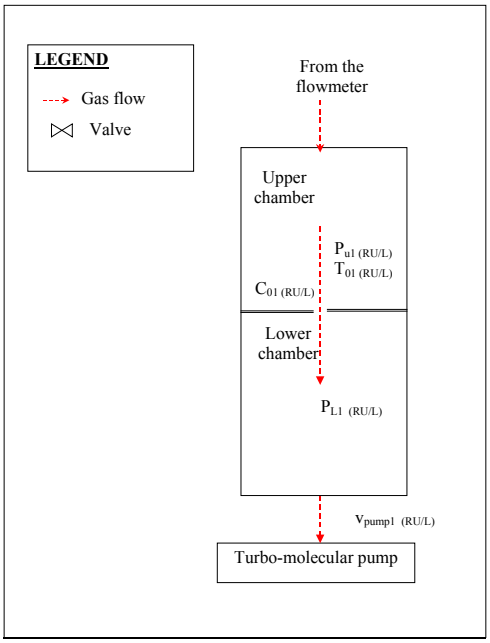

Figure 1.5. Valving sequence for measuring the leak flow rate ratio: step 1.

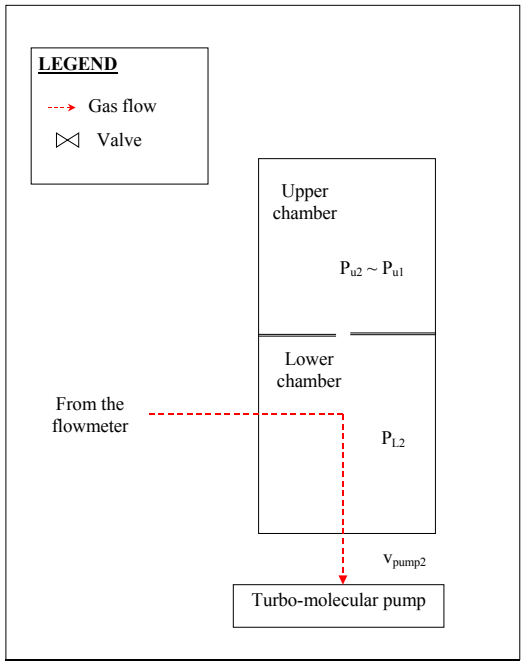

Figure 1.6. Valving sequence of the NIST primary standard for calibrating leak flow rate through the lower chamber: step 2.

Once the ratio is known, the unknown leak can be calibrated by the following procedure.
Step 1:
At first, the gas flow of the unknown leak is directed into the upper chamber, similarly to the previous method. It flows into the lower chamber before being evacuated by the vacuum pump. The equilibrium pressure of the upper chamber is recorded: P_{u1} (see Figure 1.1).

Step 2:
The unknown leak is then isolated and gas is introduced into the flowmeter, which delivers gas into the lower chamber. The flowmeter is adjusted (see Figure 1.3) such as the pressure in the upper chamber P_{u2} is about P_{u1}. Therefore, the leak flow rate from the flowmeter is related to the unknown

leak: $N_L = R_{U/L}.N_{FM}$. The variable and the reference volumes are at the same pressure P_{r2}. The flow rate is generated and allowed stabilizing (see Figure 1.7).

Step 3:
Then, as previously, the gas supply is switched off and the variable volume varies by the translation of the piston in order to compensate the leak of gas to maintain the pressure constant; the leak flow rate from the flowmeter is measured (see Figure 1.4) and calculated by Equation [1.8].

$$N_L = R_{U/L} \frac{P_{r3} \cdot \left(\frac{\Delta V}{\Delta t}\right)_3}{R_g \cdot T_{r3}} \cdot \left[\frac{P_{u1} \cdot T_{03} \cdot v_{pump1}}{P_{u3} \cdot T_{01} \cdot v_{pump3}}\right] \qquad [1.8]$$

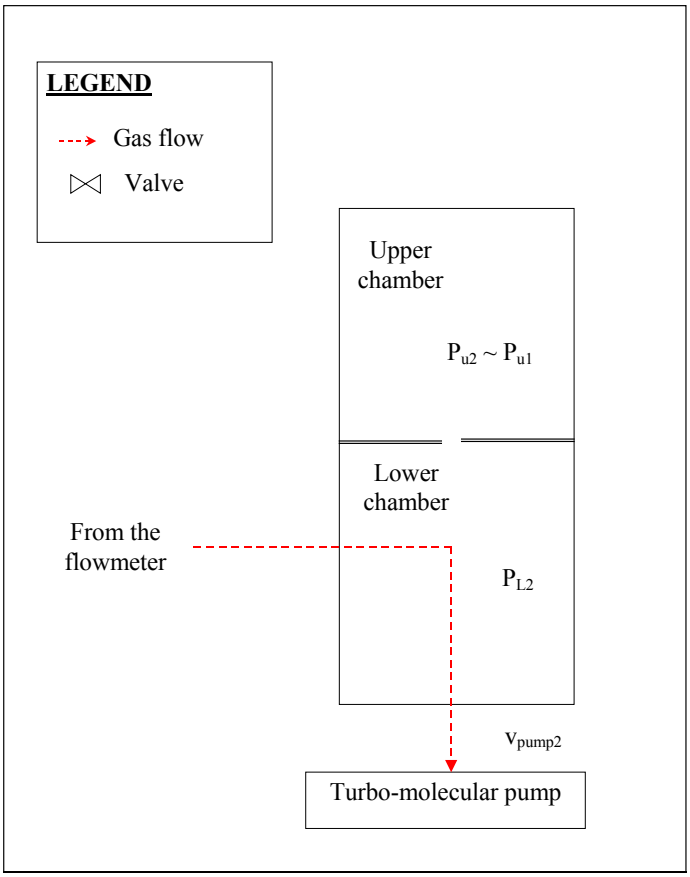

Figure 1.7. Valving sequence of the NIST primary standard for calibrating leak flow rate through the lower chamber: step 2.

1.3.1.2 Uncertainties

This operating principle used by the NIST presents a significant advantage: it is based on direct comparison of the unknown leak flow rate and of a flow rate generated by a flowmeter. It means that both quantities are flow rates, which implies a simplification of the measurement chain and an optimization of uncertainties.

The uncertainties of a leak flow rate measurement are reported in Table 1.2 (see [NIST92]) and are due to the uncertainties of:

- the measurement of the flow rate by the flowmeter [CUL87],
- the measurement of the pressure inside the upper chamber,
- the measurement of the chamber temperature,
- the measurement of the pump speed,
- the measurement of the conductance,
- the measurement of the "upper/lower ratio" when the flow division technique is considered.

Table 1.2 Summary of the uncertainties (in %) of the primary standard for the main technique (flow into the upper chamber) and for the flow division technique[1].

	Flow into the upper chamber			Flow division technique			
	Molar Flow Rate (mol/s)						
	10^{-6}-10^{-9}	10^{-10}-10^{-11}	10^{-12}	10^{-6}-10^{-9}	10^{-10}	10^{-11}	10^{-12}
Upper/lower ratio	-	-	-	-	4.0	4.0	4.0
Bellows flowmeter [2]	0.8	2.0	9.8	-	0.8	2.1	2.1
Bellows flowmeter [1]	0.02	0.1	1.5	-	0.5	0.5	1.0
Upper chamber pressure	0.3	0.3	0.3	-	0.3	0.3	0.3
Chamber temperature	0.1	0.1	0.1	-	0.1	0.1	0.1
Pump speed and conductance	0.06	0.06	0.06	-	0.1	0.1	0.1
Total	1.3	2.6	12	-	5.5	6.7	7.2

However it is difficult to adapt this method at an atmospheric system as the modeling is based on the molecular theory. Therefore, another method is discussed in next section. Contrary to the NIST method, the basic theory of this method is valid for atmospheric systems too. The LNE primary standard measuring helium leak flow rates in evacuated system is based on this method and is described as an example.

1.3.2 Pressure/Volume rise method

1.3.2.1 In an evacuated system

The correlation between the pressure and the temperature of an ideal gas in a chamber is calculated using Equation [1.10]. Then Equation [1.11] can be written deriving Equation [1.10] and considering that the temperature is constant [EHR92].

$$PV = nR_g T \quad , \qquad [1.10]$$

where n, P, V and R_g are respectively the molar quantity, the pressure, the volume and the perfect gas constant.

[1] [NIST92]

[2] The components of the uncertainty associated to the flowmeter are enumerated and explained in article [CUL87]. To sum up, the flowmeter measures the flow rate due to the variation of a volume. This variation is due to the displacement of a piston. The flow rate is calculated according to Equation [1.9]. The measurements of the parameters associated to the equation are causes of uncertainties.

$$\frac{dNL}{dt} = \frac{\Delta\left(\frac{PV}{R_g T}\right)}{\Delta t} - l - D \qquad [1.9]$$

$$Q = R_g T \frac{dn}{dt} = P \frac{dV}{dt} + V \frac{dP}{dt} \qquad [1.11]$$

where

Q	Throughput
t	Time

The variation of the volume or of the pressure allows determining the flow rate. Thereby, three possibilities are offered:

- only the value of the volume varies,
- only the value of the pressure varies,
- the values of both volume and pressure vary.

These possibilities are described in the literature [IVE82], [HYL96], [LEG97], [BOI06].

While the NIST uses the variation of a volume to measure the flow generated by the flowmeter, the LNE has adopted the "Pressure rise Method", whose schematic diagram is presented in Figure 1.8 and described in the literature [LEG97], [BOI06]. It means that sole the pressure value varies, while the volume and temperature are constants. As the pressure is measured by a capacitive manometer (the signal results from the deformation of a membrane), it is not correlated to the gas considered. The calculation of the flow rate is based on Equation [1.12].

$$Q = R_g T \frac{dn}{dt} = V \frac{dP}{dt} \qquad [1.12]$$

The measurement can be divided in 3 steps. The total volume of the test bench is composed of the standard volume, a chamber V_s, and the volume of the connections $V_{fittings}$.

First, valves 1, 2, 3, and 4 are opened. The temperature is recorded. When the pressure has reached a value around 1 Pa abs., valve 1 is closed. Pressure P_1 in the total volume is measured and recorded along the time. In this configuration, the pressure rise in the total volume can be measured and the flow rate of the leak directed into the total volume can be expressed by Equation [1.13].

$$Q_1 = \frac{dP_1}{dt_1} \cdot (V_s + V_{fittings}) \qquad [1.13]$$

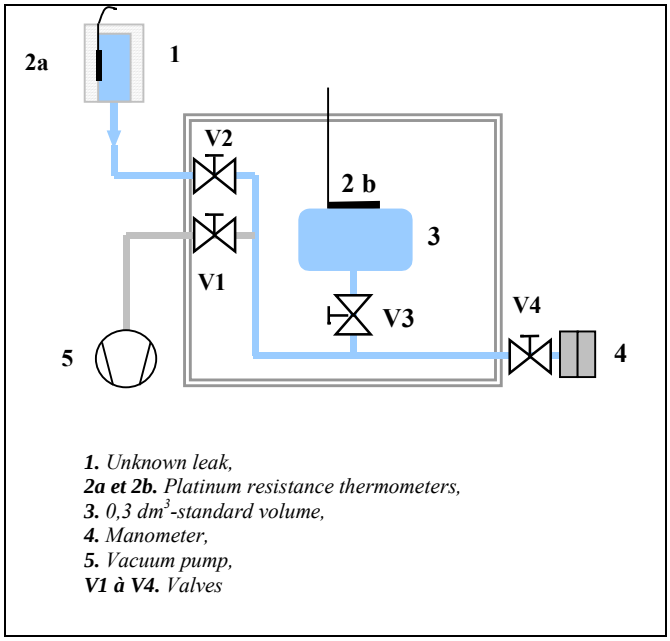

Figure 1.8. Schematic diagram of the operating principle of the pressure rise method [BOI06].

Secondly, valve 1 is opened again to evacuate the gas in the chamber. Then valves 1 and 3 are closed. The standard volume is isolated from the rest of the installation. It means that pressure P_2 in the connection volumes is recorded along time and the pressure rise is calculated by the least squares method. Therefore the flow rate of the leak directed into the total volume can be expressed by Equation [1.14].

$$Q_2 = \frac{dP_2}{dt_2} \cdot (V_{fittings}) \qquad [1.14]$$

Thirdly, as a residual flow may be detected, the pressure rise must be checked when the leak is not directed inside the volume of the installation. Valve 1 is opened until the pressure reaches a value around 1 Pa absolute. Next, valves 1 and 2 are closed and the variation of the residual pressure P_3 is determined by the least squares method. Then the residual flow rate can be expressed by Equation [1.15].

$$Q_3 = \frac{dP_3}{dt_3} \cdot (V_{\text{fittings}}) \qquad [1.15]$$

By combining Equations [1.13], [1.14] and [1.15], the leak flow rate can be expressed by Equation [1.16].

$$Q_L = V_s \cdot \frac{dP_1}{dt_1} \cdot \left(1 + \frac{\frac{dP_1}{dt_1} - \frac{dP_3}{dt_3}}{\frac{dP_2}{dt_2} - \frac{dP_1}{dt_1}} \right) \qquad [1.16]$$

This method allows measuring leak flow rates between (2 x 10^{-7}) Pa.m^3.s^{-1} (or 8 x 10^{-11} mol.s^{-1}) and (1 x 10^{-1}) Pa.m^3.s^{-1} (or (5 x 10^{-5}) mol.s^{-1}), whatever the gas [EHR96]. The uncertainties associated to this method are evaluated around 2% at (1 x 10^{-1}) Pa.m^3.s^{-1} and up to 8% at (2 x 10^{-7}) Pa.m^3.s^{-1}. Table 1.3 gives the uncertainty budget of the pressure rise method.

Table 1.3. Relative Standard Uncertainty of the pressure rise method.

Parameter	Relative uncertainty of the molar flow rate (%)
	Range of 10^{-6}-10^{-10} mol/s
Repeatability	0.50
ΔP/Δt	2.5
Volume	0.87
Temperature (1 °C)	0.20
Upstream pressure (200 Pa)	0.075
Residual leak flow	Negligible
Total	2.7

The comparison of Tables 1.2 and 1.3 underlines that both methods can measure the helium leak flow rate with an uncertainty between 1.3% and 2.7%. The NIST standards can extend the measurement to the range between 10^{-10} and 10^{-12} mol/s with relative uncertainties between 5.5% and 12%.

The span of refrigerant leaks to be detected can be considered as varying from 1 to 50 g/yr, which are included between (3.1 x 10^{-10}) mol/s and (1.6 x 10^{-8}) mol/s for leaks of R-134a: if a refrigerant leak works in an evacuated system, both methods could measure refrigerant leaks with an acceptable uncertainty. Therefore, the remaining issue is to determine if the method can be really adapted and gives a result with a reasonable uncertainty. As the NIST standard is based on the molecular theory, it seems to be easier to adapt the pressure rise method to calibrate leaks flow rates directed into a system at a pressure near the atmospheric pressure.

1.3.2.2 In a system at atmospheric pressure

While the principle of primary standard of NIST is based on the molecular statistics, the pressure rise method fits to leaks working at atmospheric pressure. The gas considered in this section is R-134a. The temperature of the installation is (20 ± 1) °C. If a leak of 10 g/yr is connected to the standard volume of the test bench (300 cm^3), the pressure raises by 1.5 Pa every minute.

An available absolute manometer has an expanded uncertainty about 10 Pa for a measurement of pressure about 101.3 kPa, while an absolute manometer measuring at pressures about 0.001 kPa to

10 kPa has a relative expanded uncertainty around U = 1.0 x 10^{-3}. The influence of the temperature in pressure measurement is higher when the pressure is about 10 kPa than when the pressure is about 20 Pa. The variation of 1 °C in the standard volume at 20 °C causes a variation of 0.35 kPa in a volume at a pressure near the atmospheric pressure. In an evacuated system like the one available at LNE, the standard volume pressure is close to 20 Pa. Therefore, a variation of 1 °C in the volume - whose temperature is 20 °C - causes a variation of 0.070 Pa in the volume.

Therefore, the uncertainty of the pressure rise-measurement at a pressure close to the atmospheric pressure is about a hundred times higher than in an evacuated system. Using an R-134a leak of 10 g/yr, it takes 80 minutes to obtain a pressure about the uncertainty inside the volume and 9 days to obtain a pressure one hundred times higher than the uncertainty of the pressure measurement. In that conditions, the calibration takes too much time. Because it takes too much time, some parameters that are not controlled may influence the result, such as the residual leakage of the installation and the temperature changes. To conclude, this method is not suitable to measure refrigerant leak flow rates at a pressure near the atmospheric pressure [CLO98-8].

1.3.3 Adaptability of measurements of refrigerant leaks in evacuated systems

A measurement chain already exists for the calibration of helium leaks in evacuated systems. But it cannot be adapted to refrigerant leaks in their working conditions (atmospheric pressure) and in the range from 1 g/yr to 50 g/yr. Then, the easiest solution would be to calibrate leaks filled with helium in evacuated systems and to convert the results for the same leak filled with R-134a and its downstream pressure about the atmospheric pressure. However, it needs reliable mathematical conversion fittings, which are not available yet. The reasons are discussed in this paragraph.

The leak flow rate mainly depends on the nature of the fluid and on the leak flow regime. Especially, three different models related to the Knudsen number can be defined [CLO98-6]. The Knudsen number Kn is described by a semi-empirical formula (Equation [1.20]):

$$Kn=\frac{D}{l_m}=0,7963\cdot\frac{\sqrt{\rho_{unitary}}}{\mu}\cdot D\cdot\frac{p_{upstream}+p_{downstream}}{2} \qquad [1.20]$$

where

D	Characteristic diameter of the capillary tube
e	Wall thickness
l_m	Molecular mean free path
$p_{upstream}$	Upstream pressure
$p_{downstream}$	Downstream pressure
μ	Dynamic viscosity
$\rho_{unitary}$	Unitary density

It allows classifying the flows between three classes [CLO98-6], [BLA91]:

- the molecular regime (Kn ≤ 2)
- the transient regime (2 ≤ Kn ≤ 200), and
- the viscous regime (Kn ≥ 200).

While helium leaks work at the molecular regime or transient regime, refrigerant leaks work at the viscous regime. Then, calibrating the refrigerant leaks in an evacuated system means studying these types of leaks in a molecular or transient regime, whereas they usually work in the viscous regime. It means that a conversion is necessary.

At first, it means that the regime of the leak is well known. It implies that the Knudsen number is calculated. However, the Knudsen number depends on the mean pressure across the leak and on the diameter of the leak, and most of the capillary leaks are crimped leaks. The issue is the definition of the diameter: is it the minimum diameter or a mean diameter of the tube? Without this data or a proper definition of this data, the regime cannot be predicted.

Secondly, the transient regime is not well-known [BER06]. For a capillary leak, some modeling expressions of the flow rate according to the flow regime are given[3]. The molar mass is the main parameter for a molecular regime, whereas the viscosity is the relevant parameter of a viscous regime [CLO02]. It seems logical that both parameters occur in the expression of the flow rate in the transition regime. The literature gives some fittings of the flow regimes [BLA91], [DELA61], [TIS93]. Some are reported in Equations [1.21], [1.22], and [1.23].

Molecular Regime

$$Q=\frac{1}{6}\sqrt{\frac{2\pi\cdot k_B\cdot T}{Na}}\cdot\frac{D^3}{l}\cdot\frac{1}{\sqrt{M}}\bullet\left(P_{upstream}-P_{downstream}\right) \qquad [1.21]$$

Transition regime (Knudsen formula)

$$Q=\frac{\pi}{128}\frac{D^4\left(\frac{P_{upstream}+P_{downstream}}{2}\right)}{\mu.l}+\frac{1}{6}\sqrt{\frac{2\pi\cdot k_B\cdot T}{Na}}\cdot\frac{D^3}{l}\cdot\frac{1}{\sqrt{M}}\cdot\left(\frac{1+\sqrt{\frac{Na.M}{k_B\cdot T}}\cdot\frac{D}{\mu}\cdot\left(\frac{P_{upstream}+P_{downstream}}{2}\right)}{1+1{,}24.\sqrt{\frac{Na.M}{k_B\cdot T}}\cdot\frac{D}{\mu}\cdot\left(\frac{P_{upstream}+P_{downstream}}{2}\right)}\right)\bullet\left(P_{upstream}-P_{downstream}\right) \qquad [1.22]$$

Viscous Regime

$$Q=\frac{\pi}{128}\frac{D^4\left(\frac{P_{upstream}+P_{downstream}}{2}\right)}{\mu.l}\bullet\left(P_{upstream}-P_{downstream}\right) \qquad [1.23]$$

However, the expression, which aims at quantifying gas flow rate in the transition region between molecular and viscous flows, based on first principles of the kinetic theory of gases, remains elusive [BER06], [NIST92]. Therefore, it is not possible already to deduce the behavior of a gas in the viscous region from its behavior in the under vacuum region. Refrigerant leaks must be calibrated at atmospheric pressure.

A study (EURAMET project n°911) including the LNE and the Istituto Nazionale di Ricerca Metrologica (INRIM) is being carried out. The aim of the project is to describe the gas-flow through a reference leak (generally geometrical leak of the capillary type) when the transition regime takes place in it with a simple equation that allows converting the throughput of one gas (He) specie to that of another gas. For instance, the same leak supplied with Helium or R-134a was measured by the LNE using the Pressure rise method. The results observed when the leak is supplied with Helium were compared with the INRIM's measurements via a flowmeter in the same conditions. The deviation between the two results is coherent with the uncertainty of the measurements in evacuated systems (< 2 %). At atmospheric pressure, the deviation is higher: about 10 %. The installation (pressure rise method) at LNE is qualified as an evacuated system. Therefore, the method used at atmospheric pressure implies an uncertainty superior to 10 %. The measurement range is a hundred times higher than the range of calibrated refrigerant leaks (1 g.yr^{-1} to 50 g.yr^{-1}). However, these results are sufficient to conclude that the flow rate clearly depends on the nature of the fluid, the flow rate regime, and the difference between the upstream and the downstream pressures (see Figure 1.9).

[3] [BER06], [DELA61], [TIS93]

The fact that the model to convert leak flow rate is not clearly defined implies that a long and complete study must be carried out between both laboratories to achieve some results. The flow rates of the capillary crimped leak, presented in Figure 1.9, are about 10^{-4} and 10^{-3} $Pa.m^3.s^{-1}$ corresponds to a range about 100-1000 g/yr of R-134a, which is more than 10 times higher than the range of the refrigerant leaks used to qualify leak detectors. Since the uncertainty is already superior or equal to 10 % for such a high leak, the method could be unreliable for smaller leaks at atmospheric pressure (about 1 g/yr to 50 g/yr). Therefore, as the available facilities are not reliable to measure efficiently low flow rates at atmospheric pressure, they do not allow determining a simple equation for converting the throughput of one gas (He) specie to that of another gas.

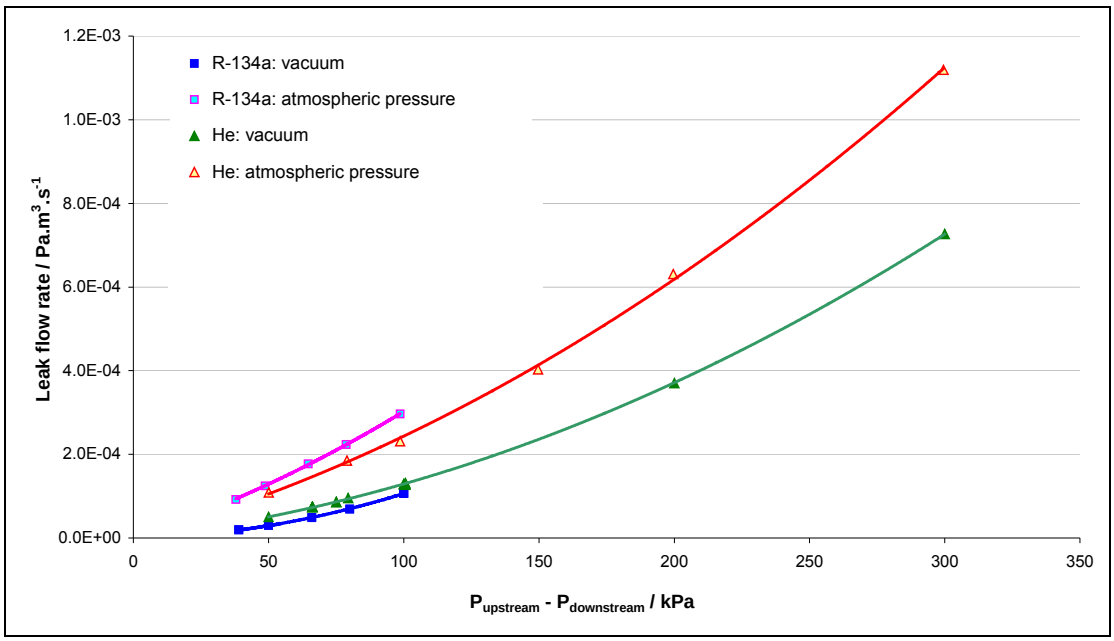

Figure 1.9. Crimped capillary leak filled with He or R-134a measured at 20 °C by the LNE. The lines represent the polynomial fittings for each gas and configuration.

1.3.4 Weighing method

As the impact of the leak flow regime is not negligible, the methods used to calibrate helium leaks cannot be used to calibrate refrigerant leaks. Some refrigerant leak manufacturer are aware of this matter. Because there was no primary standard available, they have developed a simple method to calibrate their leaks according to their working conditions (atmospheric pressure). However, they are not sure of their results. The following paragraph presents this method and aims at quantifying the expected minimum uncertainty of the results.

1.3.4.1 Operating principle

Because no primary standard for the calibration of the HFC leak flow rate exists, because they are aware that the leak MFR must be measured at atmospheric pressure, many leak suppliers, particularly in France, uses the weighing method. A leak implies a change of mass. Then the leak MFR can be expressed by Equation [1.23].

$$Qm = \frac{\Delta m}{\Delta t} \qquad [1.23]$$

where Δm (g) is the variation of mass during Δt (yr)

1.3.4.2 Limits

This method seems to be easy to carry out and cheap. However, some precautions have to be taken. The flow rate is so low that one measurement can take months or years in order to detect the mass variations. Let us consider the measurement uncertainty of the changes of mass only. If the balance has an uncertainty[4] of 0.10 g, a change of mass[5] around 1.0 g means that the MFR will be known with a relative uncertainty of 10%. To measure a leak flow rate around 10 g/yr, which is already a high leak, measurements must be done every two months. During this interval, the temperature and the pressure vary significantly. Since the flow rate depends on the temperature and pressure, the calibrated leak must be confined in a controlled-temperature chamber during all measurements. However, the temperature of the room in the LNE is in general controlled at (20 ± 1) °C. Considering that a R-134a leak is a capillary leak following the Poiseuille's law, that the upstream pressure is defined as the vapor-gas saturation pressure and the downstream pressure is about the atmospheric one. The MFR can be expressed by the following equation [1.24] [CLO98-6], [EHR92]:

$$Q_m = \frac{\pi . D^4}{128 \cdot e \cdot \mu} \cdot \frac{p_{upstream}^2 - p_{downstream}^2}{2}, \qquad [1.24]$$

where

D	Characteristic diameter of the capillary tube
e	Wall thickness
$p_{upstream}$	Upstream pressure
$p_{downstream}$	Downstream pressure
Q_m	Molar flow rate
μ	Dynamic viscosity

The value of the liquid-vapor saturation pressure versus the room temperature is determined using REFPROP, software developed by the NIST, and reported in Table 1.4.

Table 1.4. Liquid - vapor saturation pressure of the R-134a for temperatures between (20±1) °C.

T_{sat}	P_{sat}
°C	*kPa*
19	554,240
19.5	562,920
20	571,710
20.5	580,600
21	589,590

Therefore, $p_{upstream}$ can vary during the calibration between $P_{upstream}^{max}$ = 554.240 kPa and $P_{upstream}^{max}$ = 589.590 kPa. It means that the standard uncertainty of $p_{upstream}$ is higher than or equal to:

$$u_{p_{upstream}} = \frac{p_{upstream}^{max} - p_{upstream}^{min}}{\sqrt{12}} \approx 35.4 \ kPa .$$

[4] A permeation leak typically weighs around 600.00 g. It can be measured with a relative uncertainty of 1.10^{-5}.

[5] The calibrated leak flow rates are around 1g/yr and 50 g/yr. For a leak around 1 g/yr, the measurements must be done every year.

In a temperature6controlled room, the pressure in the room typically varies in the range (1013.3±20.0) hPa. Considering these values, a minimum value of the standard uncertainty on the difference ($P^2_{upstream}$-$P^2_{upstream}$) is estimated by Equation [1.25]:

$$u_{\left(p^2_{upstream} - p^2_{downstream}\right)} = \sqrt{\left(2 \cdot p_{upstream} \cdot \left[\frac{p^{max}_{upstream} - p^{min}_{upstream}}{\sqrt{12}}\right]\right)^2 + \left(2 \cdot p_{downstream} \cdot \frac{\Delta p_{Atmo}}{\sqrt{12}}\right)^2} \qquad [1.25].$$

It corresponds to a relative standard uncertainty of 13%. Therefore, the uncertainty due only to the stability of the upstream and downstream pressures in a controlled room implies a minimum expanded relative uncertainty (k = 2) of 26% on the value of the leak rate. It is higher than the uncertainty on a calibrated leak MFR tolerated by the standard EN 14624: it specifies a maximum relative uncertainty of 15%. The relative uncertainty of this leak calibration method is higher than 26%: there is not just the uncertainty on the pressure, but also the uncertainty on the viscosity (it also depends on the temperature and the pressure), the uncertainty on the temperature, and the uncertainty on the mass measurement. To conclude, this method is not adequate because the uncertainty is too high and makes the measurement irrelevant.

1.4 Infrared spectrometry method specific to refrigerant leaks

As there was a lack of reliable methods to measure refrigerant leak flow rates, the Center for Energy and Processes has developed a new method. It aims at measuring refrigerant leaks in their working conditions. The LNE, which is in charge of the metrology development, has decided to provide a primary standard for the measurements of leak flow rates of refrigerants. This primary standard is based on this method. In the following paragraph, the operating principle of this method is described and its interests are analyzed.

1.4.1 Operating principle

The method is based on the ability of an IR spectrometer to distinguish the concentration of the gas species absorbing IR light in mixture with gases non-absorbing IR light. It consists in measuring the accumulation of a tracer gas emitted by the refrigerant leak and diluted in an enclosed volume at atmospheric pressure (see Figure 1.10) [AFN02]. First, this volume (named accumulation volume) is evacuated and filled with reconstituted air (80% N_2 and 20% O_2) in order to avoid any pollution. Next the unknown leak is connected to the accumulation volume and the concentration raise of the refrigerant is measured continuously by an infrared spectrometer calibrated for the appropriate gas, as most of refrigerant gases absorb at waves length in the infrared range. Meanwhile, the temperature and the pressure in the accumulation volume are continuously measured [TOR02]. This method will be called the “infrared method”.

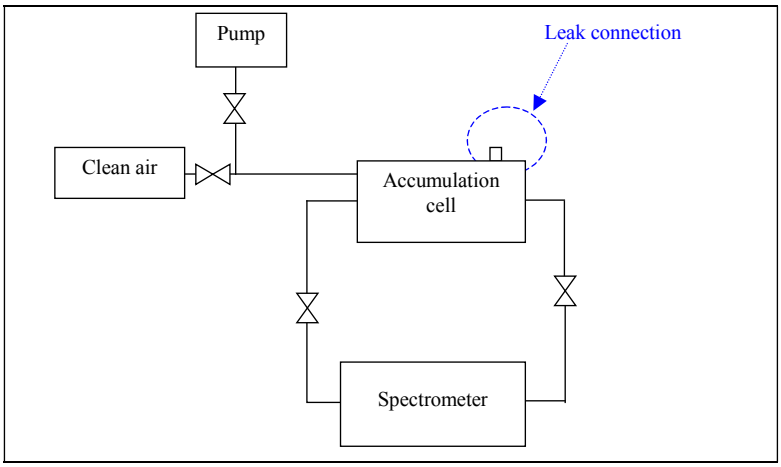

Figure 1.10. Diagram of an installation to calibrate refrigerant leaks using the infrared detection method.

The MFR is calculated by Equation [1.26]:

$$Q_m = \frac{M}{R_g}.V.\frac{\partial\left(\frac{P.C}{T}\right)}{\partial t} \qquad [1.26]$$

where Q_m, V, C, P, R_g and T are respectively the molar flow rate, the accumulation volume, the accumulated concentration, the pressure, the perfect gas constant and the temperature T inside the volume [TOR02], [CLO00], [CLO02].

1.4.2 Interests of the method

The main interests of this method are as follows:

- The measurements are made at atmospheric pressure and the tracer gas is the operating gas itself.
- It is an accumulation method.

This method uses the refrigerant gas itself as the tracer gas. On the working conditions of the refrigerant leaks, R-134a for instance, is indeed a better tracer gas than helium as demonstrated below. In the case of measurements in an evacuated system, molecular flows are considered: the molar mass is the main influence parameter on the flow rate. The helium gas is then a good tracer as its molar mass is small[6]: 4.0 g/mol. On the contrary, refrigerant leak flow rates are relative to viscous flow around 10^{-9}-10^{-8} mol/s (or 1-10 g/yr). In use, the value of the downstream pressure is around the atmospheric pressure. In this case, the main influence parameter becomes the viscosity. Therefore, because of its viscosity, R-134a is an excellent tracer gas[7] [CLO02]. The viscosity of R-134a is 30% lower than the viscosity of helium.

As the measurements are done at atmospheric pressure, infrared detection can be used. While a mass spectrometer only works in evacuated systems and measures flow rates, an IR spectrometer only works in "atmospheric systems" and measures concentrations. By using the IR detection techniques, it is possible to accumulate gas in a volume, which optimizes the sensitivity and the range of the method. As the concentration rises with time, it is not necessary to measure absolute concentrations. Only the changes of concentrations need to be detected. Detecting a low variation of concentration generated

[6] The detection sensitivities are all the better than the gas molar mass is low.

[7] The detection sensitivities are all the better than the gas viscosity is low.

by a low flow rate in a volume is then just a matter of time [TOR02]. Thus, not only the accumulation method deals with the limit detection issue, but also the uncertainty of the concentration measurements are reduced because only the changes in concentration are necessary to measure.

1.5 Conclusion

Since the European countries agreed the Kyoto protocol, they must reduce their greenhouse gases' emissions. As a consequence the leak tightness of refrigerating equipment must be controlled by leaks detectors and improved. Therefore, as calibrated refrigerant leaks must be used to qualify leak detectors, a measurement chain to measure refrigerant leak flow rate is necessary to ensure the traceability of the controls to the SI units.

A measurement chain to calibrate leak flow rate already exists for measuring gas flow rates. Two primary standards are presented: the NIST standard using a flowmeter and the LNE standard using the pressure rise method. However, it aims at measuring mainly helium leaks. Standards are adapted to evacuated systems. Therefore, as shown previously, the leak flow rates are characterized by a molecular or a transient regime. Since the refrigerant leaks are used at atmospheric pressure, their flows are characterized by a viscous regime. Those methods are then not directly adequate for measuring refrigerant leaks. It is not yet possible to convert a measured helium capillary leak flow rate in an evacuated system to a refrigerant flow rate at atmospheric pressure with an acceptable uncertainty (≤ 15% according to the European standard EN 14624 [AFN05]), as shown by a current European study to improve the knowledge of the behavior of capillary leaks, which is currently carried out by the LNE and the INRIM (EURAMET project n° 911).

As the implementation of regulation of leak tightness inspections requires refrigerant standard leaks, a new method was developed by the CEP. This method is the infrared method based on accumulation: it consists in measuring the gas accumulation due to the refrigerant leak inside a closed volume at atmospheric pressure. The advantages of this method have been presented:

- the calibration is done at atmospheric pressure, which respects the working flow regime of the leaks. Moreover, it uses R-134a as tracer gas: at atmospheric pressure these gases are excellent gas tracers
- the infrared detection is selective
- by using the infrared detection method, the accumulation principle can be used. Therefore, the longer the measure, the lower the uncertainty. Nevertheless an optimum measurement time can be determined (see Chapter 2).

Based on the method and on the experience of the CEP, a national primary standard to measure refrigerant calibrated leaks can be realized. The realization is composed of two main phases:

- the design of the test bench considering the metrology elements (see Chapter 2),
- the qualification of the test bench, i.e. the uncertainties estimation (see Chapter 3).

Chapter 2 - Design of the primary standard

2.1 Objectives

In the infrared method developed to measure refrigerant leak MFR – presented in the previous chapter -, the MFR is deduced from the concentration variation, the pressure and temperature in the accumulation volume, and the capacity of the accumulation volume. Pressure and temperature are easily measured with reasonable uncertainties. The key points of the design consist in selecting the best infrared spectrometer to measure the concentration variation in this volume and in determining the best method to measure the accumulation volume. Just a few infrared spectrometers measuring R-134a low concentrations (~ 1 $\mu mol.mol^{-1}$) are available. The monitors used by the CEP are based on different techniques of infrared detection. The first one is an IR photo-acoustic spectrometer and the second one is an IR spectrophotometer. Concerning the methods to measure the accumulation volume, three main methods are presented and compared to choose the most appropriate.

This chapter presents the steps for designing the primary standard that measure refrigerant leak MFR with an uncertainty about 1%. The objectives of this chapter are the following:

- To quantify and compare the performances of the two available infrared spectrometers in order to measure R-134a concentrations
- To study the methods to calibrate volumes, in order to choose the most appropriate
- To define the optimal capacity of volumes composing the primary standard
- To establish the design of the test bench.

2.2 Choice of the most appropriate infrared detection method

2.2.1 Theoretical basis of the infrared detection

In general, the infrared detection is based on the principle of absorption-desorption of photons by gas molecules. When a gas molecule is irradiated with light, it absorbs a photon. The molecule goes from its ground state E_0 to its excited state E_1. The energy difference between the states is $E_1-E_0 = h\nu$, where ν is the frequency of the absorbed photon.

The molecule can then lose this energy and return to the ground state in the following ways [ROS98]:

- It can radiate a photon again. The mechanism is a radiative de-excitation
- It can initiate a photochemical event such as bond re-arrangement. The mechanism is photochemistry
- It can collide with another molecule of the same species that is in the ground state E_0 and excite it to its excited state E_1. That is an inter-systems energy transfer
- It can collide with another molecule of the gas and transfer energy to translational or kinetic energy shared by both molecules.

The fourth way is usually the prevalent one for the molecule to lose the absorbed energy. Therefore, the infrared detection is usually based on this phenomenon.

Currently two apparatus of infrared detection are available to measure refrigerant gas concentrations: a photo-acoustic spectrometer and a spectrophotometer. Their operating principles are based on the fact

that a previously excited atom of gas will collide with another molecule of the gas and transfer its absorbed energy to translational or kinetic energy shared by both molecules. For the primary standard, it is essential to determine which infrared analyzer is best suited for measurements. Therefore, this section presents their operating principles and compares their efficiency. The two monitors are then experimentally compared in order to conclude on the most suited concentration measuring instrument.

2.2.2 Description of a photo-acoustic spectrometer

2.2.2.1 Operating principle

The concentration of R-134a is measured by a photo-acoustic spectrometer (PAS). The absorption of an infrared chopped and filtered light energy by an enclosed sample of gas is converted into sound pressure, which is measured by microphones [B&K90-1]. The PAS[8] (see Figure 2.1) is mainly composed of:

- a photo-acoustic cell (PAC), which encloses the sample gas,
- a light source,
- a parabolic mirror,
- a chopper,
- a filter wheel, and
- two microphones.

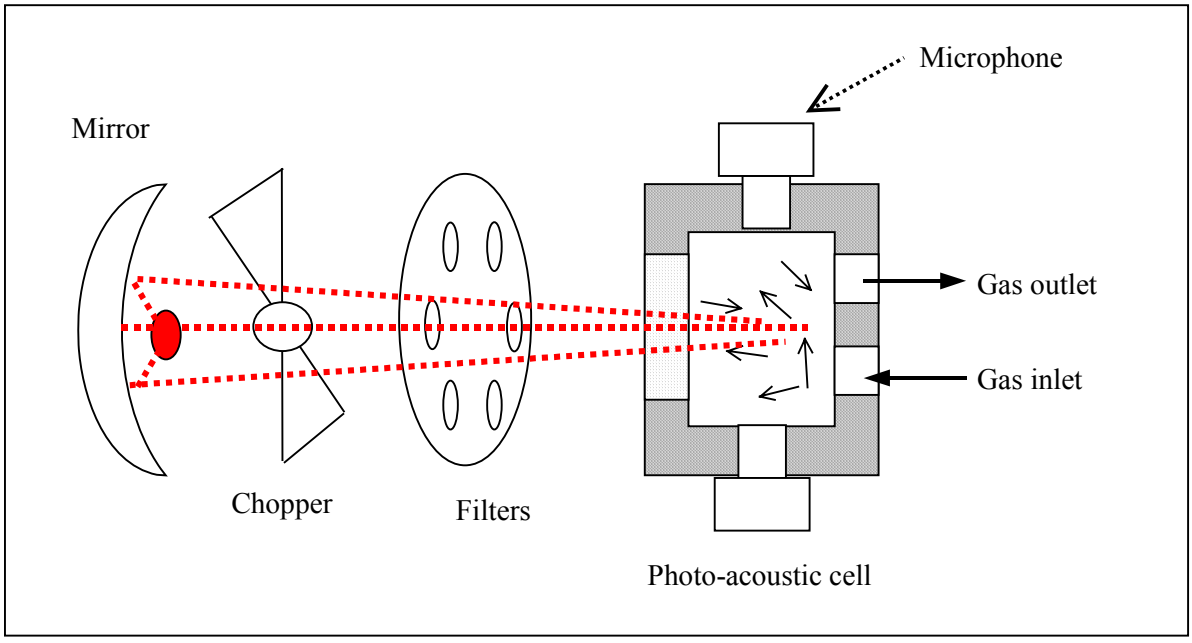

Figure 2.1. Example of a PAS [VECHT06].

A measurement cycle is done in two steps. First the spectrometer rinses its cell. Next it encloses a gas and measures the volume concentration of this sample. A measurement cycle lasts about 1 minute.

Before measuring the concentration of a sample of gas, the spectrometer sucks the gas from the accumulation volume inside the PAS cell and injects it back in the accumulation volume to rinse the cell continuously. After the rinsing that lasts about 45 s, a sample gas is hermetically sealed in the PAS cell.

[8] [MOR97], [VECHT06], [SHAF99], [ROS97], [AND93] and [B&K90-1]

Then the spectrometer measures the sample gas concentration enclosed in the PAC. Light from an infrared light source is reflected off a mirror with a half cone angle of the light cone θ. Light passes through a mechanical chopper, which pulses it at 20 Hz. Then, the light passes through one of the optical filters of the filter wheel, which selects the relevant frequencies, at which the gas sample mostly absorbs. This filter is an optical interference one. The pressure inside the PAC increases. As the light is pulsated, the pressure is modulated. An acoustic wave is then created and is measured by a condenser microphone (see [MOR97], [VECHT06], [SHAF99], [ROS97], [AND93] and [B&K90-1]). Finally the gas sample is injected back in the accumulation volume and the next cycle begins.

2.2.2.2 Relation between the acoustic pressure and the concentration

This chapter takes its source in the review [B&K90-1].

Expression of the acoustic signal

The acoustic signal generated by the absorbed light power is determined by the differential equation [2.1]:

$$K_g \cdot \nabla^2 T = \rho_g \cdot C_p \cdot \frac{\partial T}{\partial t} - \frac{\partial p}{\partial t} - W_{PAC}(t) \quad , \qquad [2.1]$$

where

C_p	Heat capacity at constant pressure
K_g	Gas thermal conductivity
p	Acoustic pressure
T	Temperature
t	Time
W_{PAC}	Absorbed power per unit volume relative to the photo-acoustic cell
ρ_g	Gas density

This equation is expressed assuming that the gas is a perfect gas and using the continuity equation [2.2]:

$$\frac{\delta}{\delta t}\left(p - \frac{\alpha_T}{\chi_T}.T \right) = \frac{\mathrm{div}(\vec{v})}{\chi_T}. \qquad [2.2]$$

and the energy equation [2.3]:

$$\frac{\delta T}{\delta t} + \frac{\gamma - 1}{\alpha_T}.\mathrm{div}(\vec{v}) - K_g.\nabla^2 T = \frac{W_{PAC}(t)}{\rho_g.C_{p_g}}, \qquad [2.3]$$

where

v	Speed
α_T	Thermal dilatation coefficient of a gas
χ_T	Isothermal compressibility coefficient of a gas
γ	Adiabatic coefficient of a gas

Expression of the absorbed power per unit volume in the PAC

To solve this equation, the absorbed power per unit volume in the PAC must be first expressed. When a perfectly reflecting mirror is used to focus light from a black-body source, the spectral density of the light at the focus point can be expressed by Equation [2.4]:

$$I_\nu = \pi \cdot L_\nu \cdot \sin^2\theta, \qquad [2.4]$$

where $I\nu$ is the light intensity at the frequency ϖ, $L\nu$ is luminance defined according to Planck's law of radiation and θ is the half cone angle of the light cone fixed at 30°.

Considering that the signal is sinusoidal at the chopper frequency, the intensity of the intermittent light entering the PAC can be expressed as:

$$I(t) = I_0 \cdot e^{j\varpi t} \text{ and } I_0 = 2 \cdot \alpha \cdot T_f \cdot L_\nu \cdot \sin^2\theta \cdot \Delta\nu . \quad [2.5]$$

where

I	Light intensity
j	Complex number
L_ν	Luminance at the frequency ν
T_f	Optical filter transmission
α	Correction factor representing all the phenomenon that are not controlled
Δν	Bandwidth of the light
θ	Half cone angle of the light cone
ω	Chopper pulsation

The transmission of light through an absorbing gas is described by Beer's law [2.6]:

$$I(l) = I(0) \cdot e^{-C\beta_g l}, \quad [2.6]$$

where l is the length of the light path.

C	Concentration
e	Exponential function
I	Light intensity
l	Length of the light path
β_g	Gas absorptivity coefficient (depends on ν)

Assuming that the gas absorbs slowly, the absorbed light is expressed by Equation [2.7]:

$$I(l) - I(0) = I(0) \cdot \left(1 - e^{-C\beta_g l}\right) \approx C \cdot \beta_g \cdot l \cdot I(0). \quad [2.7]$$

W(t) is then deduced from Equation [2.7]:

$$W_{PAC}(t) = 2 \cdot C \cdot \beta_g \cdot I(t) = W_0^{PAC} \cdot e^{j\varpi t},$$

$$\text{where } W_0^{PAC} = 4 \cdot \alpha \cdot T_f \cdot L_\nu \cdot \sin^2\theta \cdot C \cdot \beta_g \cdot \Delta\nu . \quad [2.8]$$

Solution of the equation

It is assumed that the signal is characterized by a sinusoidal at the chopper frequency. Therefore:

$$T(t) = T_0 \cdot e^{j\varpi t} \text{ and } p(t) = p_0 \cdot e^{j\varpi t}.$$

In order to solve the equation, the manufacturer of the PAS has assumed that the PAC is spherical. Therefore, T_0 only depends on the spherical coordinate r. On the contrary, the pressure can be considered uniform in the PAC, as the wavelength of sound λ_{sound} is much larger than the diameter of the cavity. λ_{sound} can be deduced from Equation [2.9]:

$$k_s = \frac{\varpi^2}{c_{sound}^2}\left(1 - j\frac{\varpi\xi}{c_{Sound}^2}\right) = \frac{4\pi}{\lambda_{sound}^2}, \quad [2.9]$$

where ω is the chopper pulsation speed, c_{sound} the sound speed, and ξ is defined as:

$\xi = \frac{\mu}{\rho}$ (laminar regime) or $\xi = \frac{4}{3}.\frac{\mu}{\rho}$ (turbulent regime).

Considering that the chopper frequency is low (20 Hz), the wavelength of sound is around 1000 m, while the diameter D of the PAC is around 2 cm.

Consequently, Equation [2.1] can be reduced to an equation depending only on the coordinate r:

$$\frac{\partial^2 T_0(r)}{\partial r^2} + \frac{2}{r}\cdot\frac{\partial T_0(r)}{\partial r} - j\cdot\frac{\varpi\cdot\rho_g\cdot C_{p_g}}{K_g}\cdot T_0(r) = -\frac{j\cdot\varpi\cdot p_0 + W_0^{PAC}}{K_g}. \qquad [2.10]$$

Assuming that the wall material has a much higher heat capacity than that of the gas, the boundary condition $T_0(D)$ is equal to zero. By solving Equation [2.10] and by using the perfect gases law, the amplitude of the acoustic signal for a spherical cavity is expressed as:

$$p_0 = \frac{W_0^{PAC}(\gamma-1)}{\omega}.e^{-j\frac{\pi}{2}}.\varphi\ , \qquad [2.11]$$

with the parameter φ used to simplify Equation [2.11]:

$$\varphi = \frac{1 - \frac{3}{\sqrt{j\cdot\frac{\varpi\cdot\rho_g\cdot C_{p_g}}{K_g}}\cdot\frac{D}{2}}\left[\coth\left(\sqrt{j\cdot\frac{\varpi\cdot\rho_g\cdot C_{p_g}}{K_g}}\cdot\frac{D}{2}\right) - \frac{1}{\sqrt{j\cdot\frac{\varpi\cdot\rho_g\cdot C_{p_g}}{K_g}}\cdot\frac{D}{2}}\right]}{1 + \frac{3(\gamma-1)}{\sqrt{j\cdot\frac{\varpi\cdot\rho_g\cdot C_{p_g}}{K_g}}\cdot\frac{D}{2}}\left[\coth\left(\sqrt{j\cdot\frac{\varpi\cdot\rho_g\cdot C_{p_g}}{K_g}}\cdot\frac{D}{2}\right) - \frac{1}{\sqrt{j\cdot\frac{\varpi\cdot\rho_g\cdot C_{p_g}}{K_g}}\cdot\frac{D}{2}}\right]}$$

As in reality the cavity is not a sphere but a cylinder with the presence in the volume of microphones and tubes, a factor of 0.85 is added to the equation to correct this hypothesis. The factor was calculated by Brüel & Kjaer [B&K90-1]. The root mean square of the acoustic pressure is then expressed as:

$$p_{PAS} = 2\sqrt{2}\times 0.85\times\frac{(\gamma-1)}{\varpi}\times|\varphi|\times\left(\alpha\cdot\sin^2\theta\cdot C\right)\times\int F(\upsilon-\upsilon_0)\cdot\beta_g(\upsilon)\cdot Tf\cdot L_\upsilon\cdot d\upsilon \qquad [2.12]$$

where

C	Concentration
F	Function of transmission of the optical filter (F depends on $[\nu-\nu_0]$)
L_ν	Luminance at the frequency ν
T_f	Optical filter transmission
α_T	Thermal dilatation coefficient of a gas
χ_T	Isothermal compressibility coefficient of a gas
γ	Adiabatic coefficient of a gas
ν	Frequency band of the filter
θ	Half cone angle of the light cone
ϖ	Chopper pulsation

The measurement is directly related to the unknown concentration [B&K90-1], [VECHT06]. For R-134a, |φ| is calculated equal to 0.97. For CO_2, |φ| is calculated equal to 0.98. The calculations are done according to the data in the review [B&K90-2].

During the measurement, variables are only the concentration and the acoustic pressure. Consequently Equation [2.12] becomes:

$$C_{PAS}=Z_{PAS}.p_{PAS} \qquad [2.13]$$

2.2.3 Description of the spectrophotometer

2.2.3.1 Operating principle

The second device available is the spectrophotometer [URAS] presented in Figure 2.2. It is mainly composed of an IR source, two similar cylinders, and a photometer. The first cylinder is closed and contains nitrogen. Nitrogen does not absorb at the IR range. This is called the "reference cylinder". The second one, called the "sample cylinder", is a cylinder through which a sample of gas of unknown concentration flows. The IR source – an incandescent filament – irradiates first the sample cylinder and next the reference cylinder. The light is directed via a chopper wheel.

When the light irradiates the sample cylinder, the sample gas absorbs the light at its resonant vibration frequency. This energy is transformed first into kinetic energy and then into heat. Thereby, the intensity of the incident light is attenuated and the value of this intensity at the cylinder outlet sample is noted I_l.

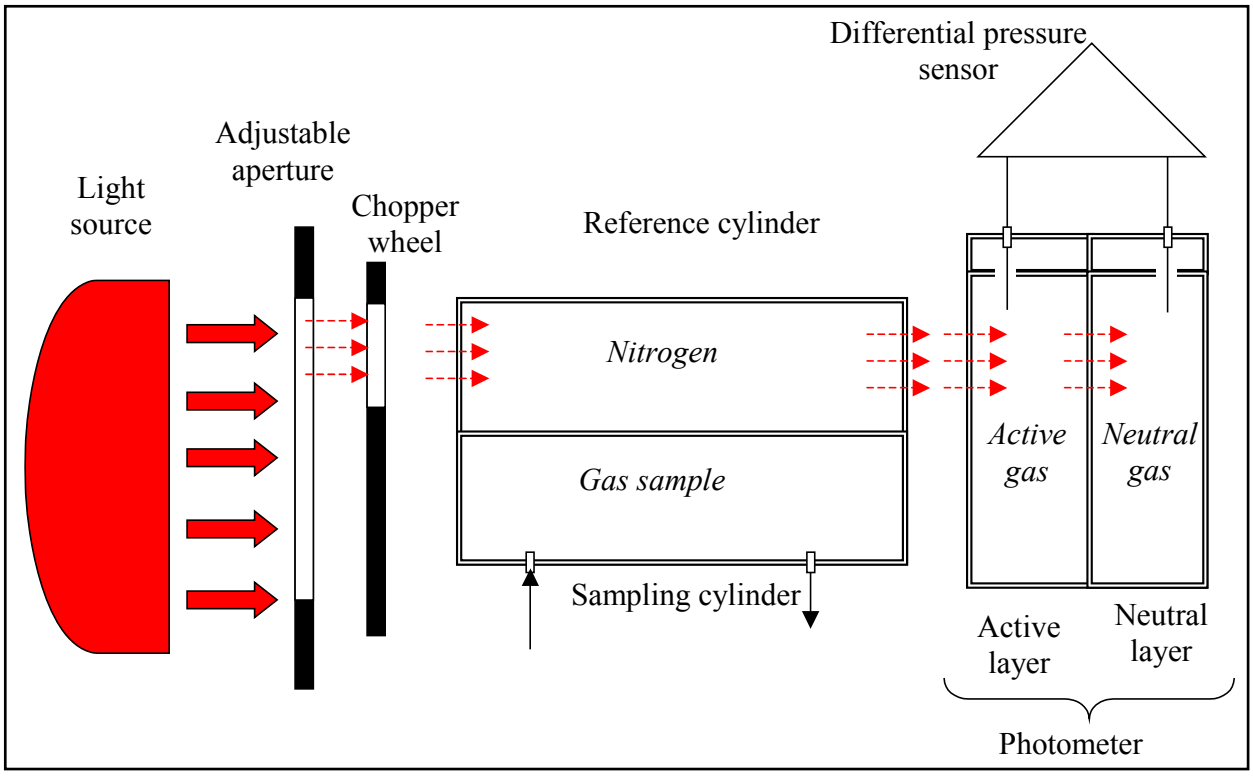

Figure 2.2. Example of a spectrophotometer (based on [URAS]).

Next the IR source irradiates the reference cylinder. As nitrogen does not absorb light, the intensity of the light is only attenuated because of the absorption of the walls. Cylinders are similar and the IR source is the same. The light absorbance is initially balanced by adjusting the aperture, the IR source radiates both cylinders with the same intensity of the incident light. Therefore, it can be considered that the intensity of the light at the outlet of the reference cylinder is similar to the intensity of the light at the inlet of the sample gas, considering the correction due to the absorption of the walls.

As soon as the light has gone through one of the cylinder, it reaches the photometer. The photometer is composed of two cavities. The first layer is filled with a gas whose absorption properties are similar to the studied one. This layer is called the "active layer". The gas concentration in this layer is well known. The second layer is not prone to absorb because filled with a neutral gas. This is called the

"neutral layer". The light with the intensity I_0 or I_l irradiates the first layer and next the second layer. As the active layer is filled with an absorbing gas while the neutral layer is filled with a neutral gas, the pressure in the active layer raises when the pressure in the neutral layer is stable. Although acoustic waves do not occur (the light is not modulated), there is a difference between the pressures in the first and in the second cavity that can be measured by a pressure sensor.

Relation between pressure and concentration

The pressure difference is proportional to the light intensity at the inlet of the photometer – ie. I_0 for the irradiation of the neutral cylinder or I_l for the irradiation of the sample cylinder. It is also proportional to the known concentration of the gas in the first layer (see Equation [2.14]):

$$\Delta P = \alpha_{Spectrophotometer} \cdot I \cdot (\gamma - 1) \cdot C_{detector} \qquad [2.14]$$

Due to the Beer-Lambert's law, the unknown concentration of the sample gas can be deduced from the ratio of I_0 and I_l: see Equation [2.15]:

$$I^{l}_{Spectrophotometer} = I^{0}_{Spectrophotometer} \cdot e^{-c.\beta g.l} \qquad [2.15]$$

where

$I^{0}_{Spectrophotometer}$ Intensity of the light that enters the photometer after attenuation through the reference cell

$I^{l}_{Spectrophotometer}$ Intensity of the light entering the photometer and attenuated by its passage through the cell filled with the gas the spectrometer must detect

l Length of the light trajectory inside the spectrometer during one cycle of measurement

As $\beta << 1$, Equation [2.15] can be expressed by Equation [2.16]:

$$I^{0}_{Spectrophotometer} - I^{l}_{Spectrophotometer} = c.Z_I.I^{0}_{Spectrophotometer} \qquad [2.16]$$

where

$$Z_I = \beta_g \cdot l$$

Then the relation between the difference of pressures in the cavities of the photometer and the concentration can be expressed by Equation [2.17].

$$C = \frac{1}{Z_I}\left[1 - \frac{\Delta P^{l}_{Spectrophotometer}}{\Delta P^{0}_{Spectrophotometer}}\right] \qquad [2.17]$$

where

$\Delta p^{0}_{Spectrophotometer}$ Acoustic pressure detected by the spectrophotometer, due to the absorption of the gas enclosed inside the photometer (for instance, CH_4 for R-134a) of the energy light $I^{0}_{Spectrophotometer}$

$\Delta p^{l}_{Spectrophotometer}$ Acoustic pressure detected by the spectrophotometer, due to the absorption of the gas enclosed inside the photometer (CH_4 for R-134a) of the energy light $I^{l}_{Spectrophotometer}$.

2.2.4 Theoretical comparison of the spectrophotometer and the PAS

According to the specifications of the suppliers, the PAS can provide measurement of concentrations of CO_2 or R-134a in the accumulation volume with a detection limit of 15 nmol.mol^{-1}, while the spectrophotometer can provide a measurement for both gases with a detection limit of 500 nmol.mol^{-1}. This difference is mainly due to their detection operating principles.

2.2.4.1 Comparison of the operating principle

The detection methods of the two spectrometers are based on the same phenomenon: the transformation of light energy in kinetic energy by the collision of molecules of the same species. One element of the uncertainty of the concentration measurement is due to the possible presence of gases that can pollute the signal. This uncertainty due to the IR detection methods must be considered for both apparatuses. However, the two IR detection methods are different. For the PAS, the light is modulated, which generates an acoustic pressure inside the PAC. For the spectrophotometer, the light is not modulated. The measurand is not an acoustic pressure but a pressure increase inside the photometer. The variation of pressure is alternatively proportional to the intensity:

- of the light at the outlet of the cell through which the gas to be detected passes: $I^{l}_{Spectrophotometer}$,
- of the light at the outlet of the reference cell: $I^{0}_{Spectrophotometer}$.

The difference between $I^{0}_{Spectrophotometer}$ and $I^{l}_{Spectrophotometer}$ is directly related to the concentration of the studied gas. Therefore, the photo-acoustic detection is more direct than the one used for the spectrophotometer: this explains the difference in their detection limits. In order to illustrate that, uncertainties in the chain of measurement of the two techniques are now compared.

To determine the most accurate method without considering the performance of the sensors inside the spectrometers, it will be assumed that the uncertainties relating to the measurement of Δp by both apparatuses are similar and equal to σ, i.e.:

$$\sigma_{PAS} = \sigma^{0}_{Spectrophotometer} = \sigma^{l}_{Spectrophotometer} = \sigma .$$

After calculations, the uncertainty relating to the PAS $u_{C_{PAS}}$ and the uncertainties relating to the spectrophotometer $u_{C_{Spectrophotometer}}$ are expressed by Equations [2.18] and [2.19]:

$$u_{C_{PAS}} = Z_{PAS}.\sigma \qquad [2.18]$$

$$u_{C_{Spectrophotometer}} = \sqrt{\frac{1}{\Delta P^{0}_{Spectrophotometer}{}^{2}} + \frac{1}{\Delta P^{l}_{Spectrophotometer}{}^{2}}} \cdot \left| \frac{\Delta P^{l}_{Spectrophotometer}}{Z_I.\Delta P^{0}_{Spectrophotometer}} \right| \sigma \qquad [2.19]$$

As the concentrations are very low (µmol.mol^{-1}), Equation [2.19] can be simplified assuming that $\left| \frac{\Delta P^{l}_{Spectrophotometer}}{\Delta P^{0}_{Spectrophotometer}} \right| \approx 1$:

$$u_{C_{Spectrophotometer}} \approx \frac{\sqrt{2}}{Z_I \cdot \Delta P_{Spectrophotometer}} \cdot \sigma \qquad [2.20]$$

Then, the ratio of the uncertainties relating to the PAS and to the spectrophotometer is approximated by Equation [2.21].

$$\frac{u_{C\,Spectrophotometer}}{u_{C\,PAS}} \approx \sqrt{2}\,\frac{1}{Z_I.Z_{PAS}}.\frac{1}{\Delta P_{Spectrophotometer}} \qquad [2.21].$$

Considering the values given by Brüel&Kjaer [B&K90-1] and [B&K90-2] and the properties of R-134a:
$Z_I = k.l = 0.385\ ppm^{-1}$, considering l = 50 cm and k = 0.77 (absorption coefficient of R-134a at 1190 cm^{-1}).

$Z_{PAS} \approx 0.06\ \ \mu mol \cdot mol^{-1} \cdot \mu Pa^{-1}$

Because of low concentrations, it can be assumed that $\Delta P^0_{Spectrophotometer} \approx 1\ \ \mu Pa$. Therefore, the ratio can be calculated: $\frac{u_{C\,Spectrophotometer}}{u_{C\,PAS}} \approx 50$. Thus, it seems that the PAS detection method is more sensitive than the operating principle of the spectrophotometer. However, it may be balanced by the properties of the pressure sensors.

2.2.4.2 Comparison of the pressure sensors

As the presence of the studied gas inside the PAS generates an acoustic pressure by absorption of modulated light, microphones can be used. This is not possible for the spectrophotometer. Microphones are extremely linear in a wide range of sound pressures. Their detection limits are defined as twice the detection limit of the pressure sensor [B&K90-1], which is about the μPa. A sound pressure around 1 μPa corresponds to a concentration detection limit around 15 $nmol.mol^{-1}$. For the spectrophotometer, the pressure sensor is not linear. The signal is converted numerically and linearized. The pressure sensor of the PAS seems to be more efficient. However, the specifications of the sensor are not known.

2.2.4.3 Influence of the environment

Finally, in the case of the spectrophotometer, the signal due to the absorption of light by the cell, through which the gas passes, is reduced: the apparatus measures the difference between the intensity of the light transmitted through a cell filled with the sample gas and the intensity of the light transmitted through a similar cell filled with the reference gas.

For the photo-acoustic spectrometer, the walls and the window of the PAC absorbs light, which influences the temperature inside. Therefore, the acoustic pressure is not only generated by the absorption of the light by the studied gas, but also by the walls and the window. The instability of the chopper can also be a source of uncertainty. According to the acoustic theory, at a low chopper frequency, the pressure inside the measuring cell only depends on the chopper frequency [B&K90-1], [HAR00]. If the chopper rate changes randomly, it generates a variation of the pressure. Although the use of two microphones, placed in opposition, tends to compensate the contribution of the noise vibrations during the measurement, the noise signal is clearly a component of the uncertainty.

Thus, the spectrophotometer seems to be more efficient to attenuate the noise signal. However as the characteristics of the sensors and the ratio of the noise signal over the measurement cannot be assessed, an experimental study has been carried out to complete the theoretical comparison.

2.2.5 Experimental comparison of the performance of the spectrometers at low concentrations

2.2.5.1 Relevant parameters

In order to compare the two apparatuses, it is first required to determine which data are really relevant for our application. The apparatuses are manufactured to measure concentrations and not flow rates. Therefore, all parameters used usually to define the performances of spectrometers may not be relevant [AFN75]. The usual criteria to describe the performances of a spectrometer are the bias error, the detection limit, the repeatability, the linearity, and the drift [VIM94].

The mass flow rate calculation of the refrigerant leak is based on the measurement of the variation of the concentration along the time. It means that only the concentration variation is relevant and not the absolute value of the concentration. The spectrometer accuracy is not a priority, whereas the detection limit, the repeatability, the linearity, and the stability of the spectrometers must be considered. To determine these parameters, a direct comparison with standard concentrations has been done.

2.2.5.2 Operating principle of the comparison

The chemistry department of the LNE has provided standard mixtures of CO_2 and R-134a in order to calibrate the gas monitor. They are manufactured using the gravimetric method [ISO06]. The concentrations $C_{mixture}$ of the standard mixtures are respectively (42.4 ± 0.1) µmol.mol^{-1} and (100.0 ± 0.1) µmol.mol^{-1}. These standards are diluted using mass flow controllers for gas in order to obtain several calibrated diluted concentrations C_s with an uncertainty about 3.0 %. An apparatus integrates both mass flow controllers in order to coordinate the dilution. A mass flow controller MFCgas with a measuring range of 0 - 100 mL.min^{-1} is connected to one of the standard gas mixtures and a mass flow controller MFCair with a measuring range of 0 - 10 L.min^{-1} is connected to clean air (see Figure 2.3). By controlling the mass flow rates, standard concentrations can be created in the respective ranges of 0.080 µmol.mol^{-1} to 1.3 µmol.mol^{-1} for R-134a and of 0.5 µmol.mol^{-1} to 5.5 µmol.mol^{-1} for CO_2.

Each mass flow controller was calibrated by comparison with a LNE standard with the same measuring range. For each mass flow controller, the MFR Qm_r versus the volume flow rate indicated by the apparatus Qv_{read} is then fitted as second order polynomials. The uncertainties of the mass flow controllers are mainly due to the least squares method fitting, the calibration of these controllers, the influence of the temperature, and the measurement of the pressure. The expanded combined uncertainties (k = 2) relative to both mass flow controllers have been calculated as:

MFCgas: U_{Qvr} [mL.min^{-1}]= 0.19 + 0.0047 x Qv_r[mL.min^{-1}], and

MFCair: U_{Qvr} [L.min^{-1}]= 0.12 + 0.0036 x Qv_r[L.min^{-1}].

The combined uncertainty of a diluted standard concentration C_s was then calculated. It was maximized by the expression $U_{Cs} = 0.027 \times C_s$.

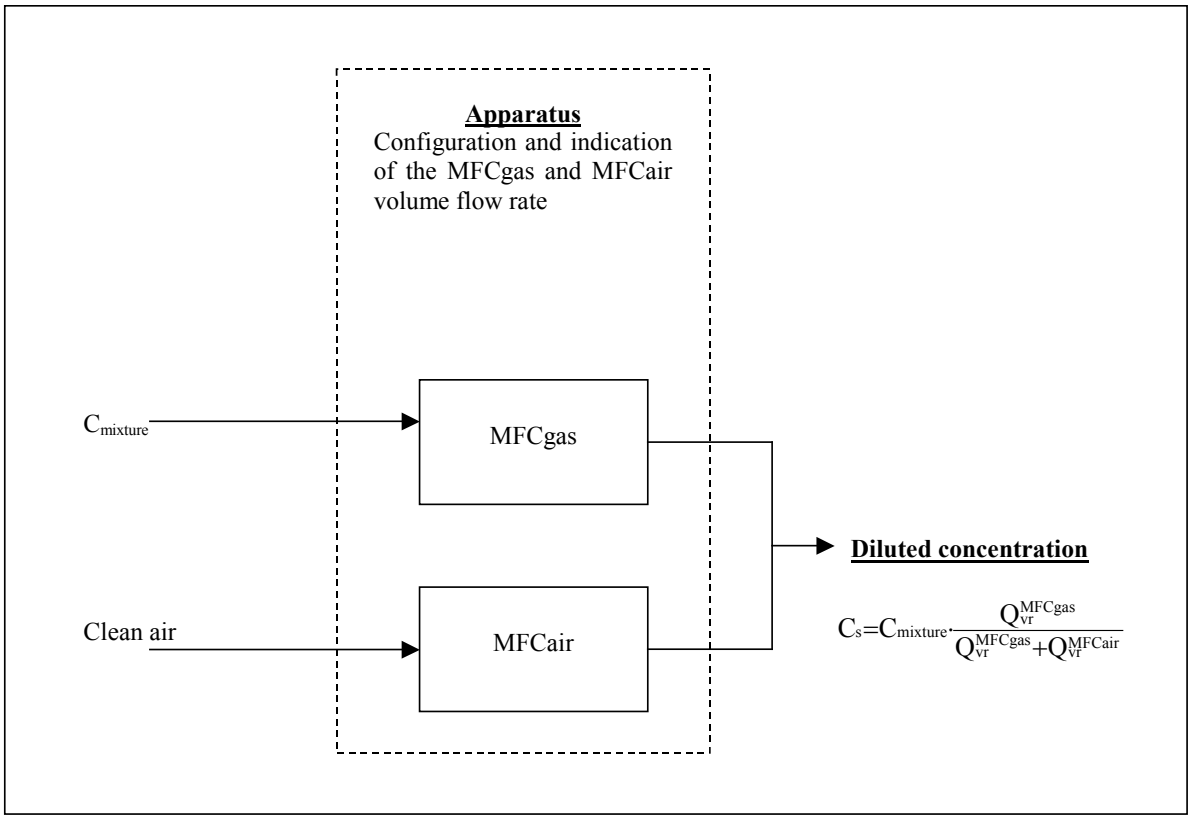

Figure 2.3. Dilution of the concentrations.

2.2.5.3 Results

The measurements of the standard concentrations of R-134a performed by the two spectrometers are presented Figure 2.4. This figure underlines that the photo-acoustic spectrometer repeatability is better than the one of the spectrophotometer. The repeatability and the linearity of both apparatuses are quantified and analyzed in next paragraphs.

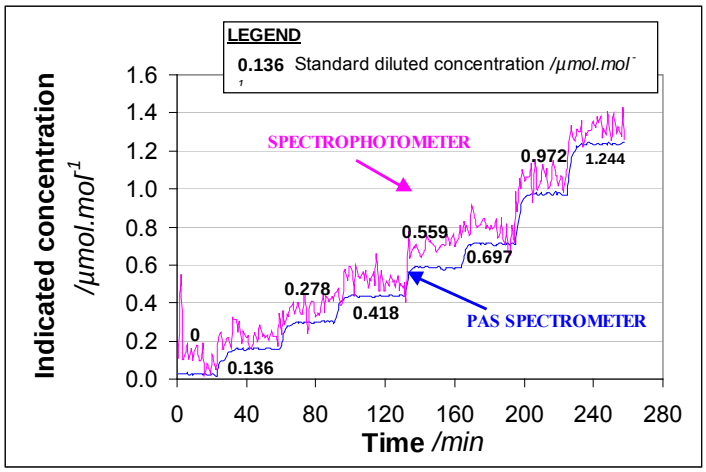

Figure 2.4. Measurements of a sample of standard concentrations of R-134a from 0 to 1.244 µmol.mol^{-1} at 23°C.

Repeatability

The repeatability of an instrument means its ability to provide closely similar indications for repeated applications of the same measurand under the same conditions of measurement. In this case, the repeatability is assimilated to the experimental standard deviation of a sample of 10 measurements, which characterizes the dispersion of the measurement. The repeatability of any apparatus is

consistent with its detection limit, whatever the gas. For R-134a, the repeatability is about 0.010 µmol.mol^{-1} for the PAS and about 0.070 µmol.mol^{-1} for the spectrophotometer (see Figure 2.5).

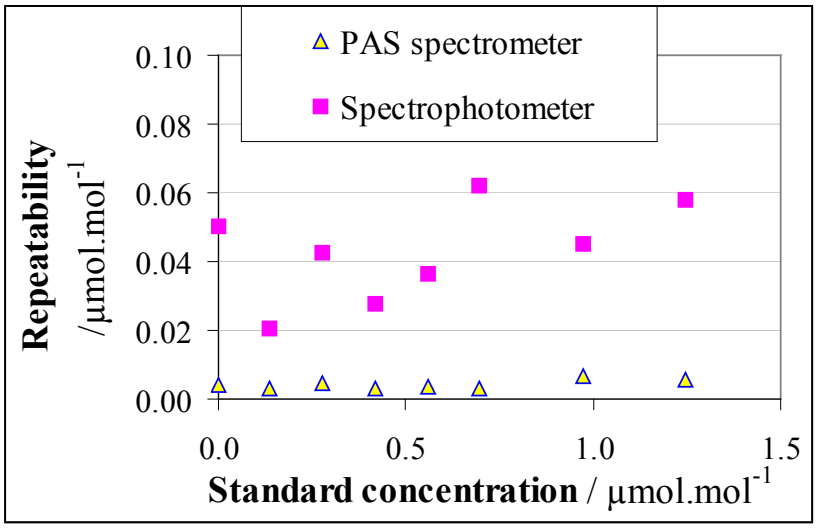

Figure 2.5. Repeatability of the PAS and the spectrophotometer indications of standard concentrations of R-134a from 0.00 to 1.3 µmol.mol^{-1} at 23°C.

Linearity

Verification of the linearity of an instrument means to verify if the relation between the readings and the standard concentrations is linear. The elements of comparison are the residuals from linear fittings, which are represented in Figure 2.6. For the detection of R-134a in a scale from 0.0 to 1.3 µmol.mol^{-1}, the maximum residual is about 0.015 µmol.mol^{-1} for the PAS and about 0.080 µmol.mol^{-1} for the spectrophotometer.

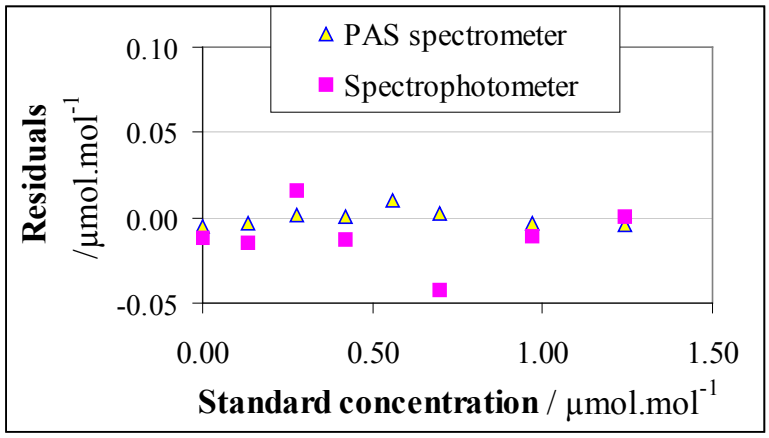

Figure 2.6. Residuals from a linear fitting relating the PAS and the spectrophotometer measurements of the standard concentrations (scale from 0.00 to 1.3 µmol.mol^{-1}) at 23°C.

Conclusion

Thus, the repeatability and the linearity of the PAS are about 10 times better than the spectrophotometer at low concentrations. The experimental analysis confirms both the theoretical study for R-134a and the resolutions claimed by the manufacturers. Performances of the photo-acoustic spectrometer are better than the spectrophotometer for detecting R-134a. To conclude, the photo-acoustic spectrometer is the most appropriate apparatus for the primary standard [MOR07].

2.3 Choice of the volume calibration method

For the design of the primary standard, the size of the accumulation volume has to be defined and its volume has to be precisely calibrated. In this section, three methods for volume calibration have been investigated. These investigations aim at determining the most appropriate method to calibrate the accumulation volume.

2.3.1 Dimensional method

2.3.1.1 Operating principle

The principle is to measure the dimensions of all elements composing the accumulation volume. Then the volume is calculated considering those measurements. It implies that the parallelism, the roughness of the walls composing the accumulation volume, and the tolerance of the dimensions are controlled.

2.3.1.2 Feasibility of the method

The control of the roughness and the parallelism of the walls imply that the volume is simple. However, the measurement of the leak flow rate implies the control of pressure, temperature, and concentration inside the accumulation volume.

Consequently the accumulation volume is composed of many dead volumes due to the valves, manometer, and fittings that connect the accumulation cell to the manometer, to the spectrometer, to the vacuum pump, and to the supplying system of clean air. The internal volume of the spectrometer cannot be measured. Thus this method is not appropriate to calibrate the accumulation volume.

2.3.2 Gravimetric method

2.3.2.1 Operating principle

In this method the mass of a pressurized cylinder is measured before and after charging a gas (argon for instance) into the formerly evacuated accumulation volume. The change in density of the gas collected in the accumulation volume is also calculated by measuring the variation of pressure and temperature in the accumulation volume: the gas is assimilated to a perfect gas. The accumulation volume is then calculated from the change in mass of the pressurized cylinder and the change in density inside the accumulation volume:

$$V=\frac{m_{cyl}^{initial}-m_{cyl}^{final}}{\rho_{Acc}^{final}-\rho_{Acc}^{initial}}-V_{fittings}\,, \qquad [2.22]$$

where $m_{cyl}^{\ i}$, $m_{cyl}^{\ f}$, $\rho_{Acc}^{\ i}$, $\rho_{Acc}^{\ f}$ and $V_{fittings}$ are respectively the initial and final masses of the pressurized cylinder, the initial and final densities of the gas in the accumulation volume, and the extra volume connected to the accumulation volume in order to introduce the gas from the cylinder [WRI03].

2.3.2.2 Analysis of the method

In this method, the accumulation volume must be evacuated. However, the spectrometer cannot bear pressure lower than 90 kPa or higher than 110 kPa. Therefore, the analyzer must be isolated during the calibration, which means that the volume of the circuit relative to the analyzer cannot be calibrated. The PAC is about 3 cm^3 according to the manufacturer. If the connecting tube diameter is

3 mm and length is more than 300 mm, its volume presents 1 % of the accumulation volume, which is not negligible. The calibration of this additional volume must be carried out at pressure between 90 kPa and 110 kPa. As the change in mass of the cylinder in these conditions is only around 0,6 g, a series of expansions of argon from the cylinder to the accumulation volume must be carried out. To protect the spectrometer, the calibration procedure has to be divided in two parts:

- the calibration of the accumulation cell,
- the calibration of the accumulation volume at pressure between 90 kPa and 110 kPa.

Considering the case of a 2-dm^3 volume initially at 3.5 kPa filled with argon up to the atmospheric pressure, a theoretical uncertainty can be estimated. The main components of the uncertainty are the uncertainties related to the temperature, pressure and mass measurements.

Typically, the temperature measurement follows a rectangular law with an uncertainty of U = 0.10 K. The pressure measurement follows a normal law with an uncertainty of U = 15 Pa. The mass measurement follows a normal law and its uncertainty is about U = 0.10 g for the measurement of the weight of a cylinder filled with argon. The nominal weight of the cylinder is about 10 kg. The measurement of the change of weight leads to the expression of a combined uncertainty, which is about U = 0.064 g (considering a correlation between the mass of 80%).

Considering this information, an uncertainty budget can be established (see Table 2.1). In this conditions, the expanded uncertainty is estimated to be U = (4.1 x 10^{-5}) m^3, which means a relative uncertainty of 2.1%. As the goal is to realize a primary standard for calibrating refrigerant leak flow rate with an uncertainty of about 1%, this method is not appropriate.

Table 2.1. Simulation of the uncertainty budget of a 2-dm^3 volume by the gravimetric method.

Quantity	Units of the quantity	Value of the quantity	Uncertainty	Standard uncertainty	Sensitivity	Standard uncertainty (m^3)
Mass difference	g	-3.131	0.064	0.032	$1/(\rho^f_{Acc} - \rho^i_{Acc})$	2.1 x 10^{-5}
Initial pressure P^i_{Acc}	Pa	3500	15	7.5	$R.T.(m^i_{cyl}-m^f_{cyl})/[M.(P^f_{Acc}-P^i_{Acc})^2]$	1.6 x 10^{-7}
Final pressure	Pa	101325	15	7.5	$-R.T.(m^i_{cyl}-m^f_{cyl})/[M.(P^f_{Acc}-P^i_{Acc})^2]$	1.6 x 10^{-7}
Temperature	°C	20	0.10	0.058	$R.(m^i_{cyl}-m^f_{cyl})/[M.(P^f_{Acc}-P^i_{Acc})]$	4.0 x 10^{-7}

2.3.3 Static volume expansion method

2.3.3.1 Operating principle

The accumulation volume is defined as the volume in which the gas emitted from the unknown leak is transferred during the measurement. It is composed of:

- a main cylindrical volume (named the accumulation cell) of approximately 2 dm^3 delimited by 5 valves,
- the PAC and all tubes connecting the spectrometer to the accumulation cell,
- the dead volume of the manometer measuring the pressure inside the accumulation volume.

The accumulation volume is measured by a static expansion method [WRI03], [VOLT00]. First, a standard volume V_s is evacuated at the pressure P_{res} and the accumulation volume V_{Acc} is pressurized at pressure P_0. A valve isolates the volumes. After measuring P_{res}, its associated temperature T_{res} and P_0 and its associated temperature T_0, the valve is opened. Due to the final pressure and temperature, respectively P_{eq} and T_{eq}, the gas density changes within the two volumes are used to calculate the unknown accumulation volume V_{Acc}. Applying the conservation of mass and the perfect gas law, the ratio of volumes can be calculated from the measurements of P_{res}, T_{res} and, P_0, T_0 via Equation [2.23].

$$R = \frac{V_{Acc}}{V_s} = \frac{\frac{P_e}{T_e} - \frac{P_{res}}{T_{res}}}{\frac{P_0}{T_0} - \frac{P_e}{T_e}} \quad . \qquad [2.23]$$

2.3.3.2 Advantages of the method

The pressure inside the accumulation volume can be adjusted in the range from 90 kPa to 110 kPa. The uncertainty of the result is reasonable even though the pressure conditions are imposed. Contrary to the gravimetric method, there is no need to carry out series of expansions to calibrate the fitting from the accumulation volume to the analyzer. Therefore, this method is easier to perform than the gravimetric method, in our case.

Considering the case of a 2-dm^3 measured volume initially filled at 110 kPa with clean air, isolated at the beginning from a standard volume about 0.5 dm^3 initially down at the pressure of 10 kPa: a theoretical uncertainty can be estimated as it was done for the gravimetric method. The main components of the uncertainty are related to:

- the calibration of the standard volume,
- the temperature measurement,
- the pressure measurement.

Typically, the calibration of the standard volume follows a normal law with a relative uncertainty of U = 0.10 %. The temperature measurement follows a rectangular law with an uncertainty of U = 0.10 K. The pressure measurement follows a normal law and its expanded uncertainty is about U = 15 Pa.

Considering this information, the uncertainty budget can be established (see Table 2.2). The expanded uncertainty is estimated as $U = (7.0 \times 10^{-6})$ m^3, which means a relative uncertainty of 0.35%. This method is the best suited for the accumulation volume determination.

Table 2.2. Simulation of the uncertainty budget of the measurement of a 2-dm^3 volume by the static expansion system method, using a standard volume of about 0.5 dm^3.

Quantity	Units of the quantity	Value of the quantity	Uncertainty	Standard uncertainty	Sensitivity	Standard uncertainty (m^3)
Pressure P_0	Pa	110000	15	7.5	$V_e.(P_{res}/T_{res}- P_e/T_e)$ / $[T_0.(P_e/T_e- P_0/T_0)^2]$	7.5×10^{-7}
Pressure P_{res}	Pa	10000	15	7.5	$V_e/[T_{res}.(P_e/T_e- P_0/T_0)]$	1.9×10^{-7}
Pressure P_e	Pa	90000	15	7.5	$V_e .(P_0/T_0 - P_{res}/T_{res})$ / $[T_e.(P_e/T_e- P_0/T_0)^2]$	9.4×10^{-7}
Temperature T_0	°C	20	0.1	0.058	$-P_0. V_e . (P_{res}/T_{res}- P_e/T_e)$ /$[T_0^2.(P_e/T_e- P_0/T_0)^2]$	2.2×10^{-6}
Temperature T_{res}	°C	20	0.1	0.058	$P_{res}.V_e/[T_{res}^2 .(P_e/T_e- P_0/T_0)]$	5.0×10^{-8}
Temperature T_e	°C	20	0.1	0.058	$P_e. V_e.(P_{res}/T_{res} -P_0/T_0)$ /$[T_e^2.(P_e/T_e- P_0/T_0)^2]$	2.3×10^{-6}
Standard Volume V_s	L	0.5000	0.0005	0.00025	$(P_{res}/T_{res}- P_e/T_e) / (P_e/T_e- P_0/T_0)$	1.0×10^{-6}

2.4 Optimization of the volumes composing the primary standard of leaks

2.4.1 Size of the accumulation volume

Time of measurement

As the method used to measure the leaks is based on an accumulation method, the duration of the calibration influences the quality of the measurement. The accumulation volume must be small in order to allow faster accumulation of gas. Indeed, high concentrations are more detectable than low ones. However, it must not be too small in order to allow several measurements of the high leaks in the range of 50 g/yr, as explained here after.

The optimal size of the accumulation volume can be determined by studying the relationship between the uncertainty of the calculated rate and the accumulation volume size in the measurement scale of leak flow rates ranging from 1 g/yr to 50 g/yr. A relationship between the concentration change, the duration of the calibration, and the volume can be expressed from Equation [2.24] of the flow rate:

$$\frac{\Delta C}{\Delta t} \cdot V_{Acc} \approx \frac{R_g \cdot T}{M \cdot P} \cdot Q_m \qquad [2.24].$$

For simulations, this equation has been applied to the accumulation volume, its volume size varying from 1 dm^3 to 10 dm^3. The uncertainty of the concentration measurement is expressed as the expression $u_C = (0.010 \times C + 0.015)$ µmol.mol^{-1}. Results of the simulation at 101.3 kPa and 20°C of the relative uncertainty of a leak of 1 g.yr^{-1} as a function of the duration of the calibration are presented Figure 2.7. If the accumulation volume is larger than another one, the calibration time has to be longer in order to keep the same relative uncertainty. Therefore the accumulation volume must be about 1 or 2 dm^3 in order to calibrate leak flow rate of about 1 g/yr in two to three hours with an uncertainty of about 1%. For larger volume, the calibration time would be too long [TOR02], [MOR07].

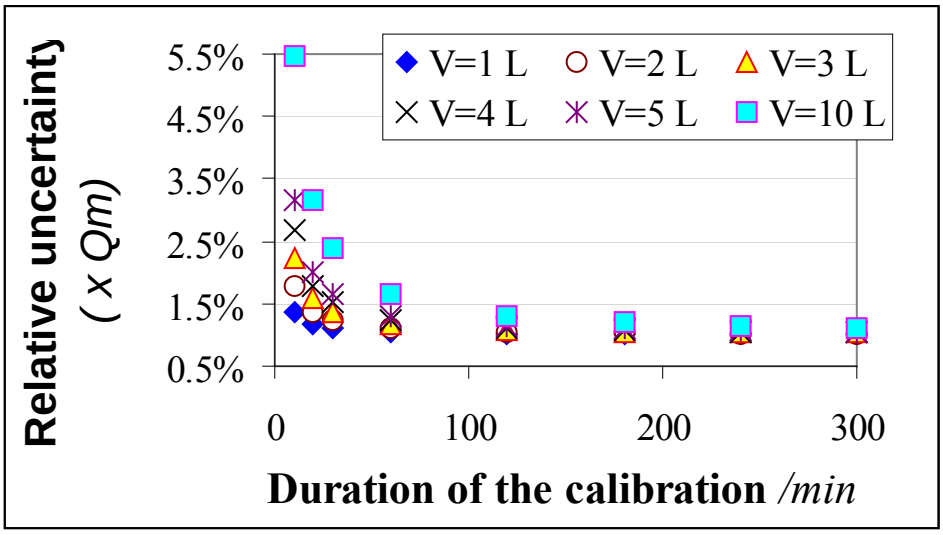

Figure 2.7. Theoretical relative uncertainty of the leak flow rate about 1 $g.yr^{-1}$ as a function of the duration of the calibration for different values of the capacity of the accumulation volume.

Number of data

A simulation of the variation of the concentration - inside the same volumes - during the calibration of a leak of 50 g/yr is compared to the recorded measurements of concentrations. As the measurement scale of the PAS varies from 0.015 $\mu mol.mol^{-1}$ to 150 $\mu mol.mol^{-1}$ and the PAS measures every minute, the size of the accumulation volume must be chosen in order to allow enough data for calibrating leak MFR of 50 g/yr [TOR02], [MOR07]. As the fitting of the relationship between concentration and time is a linear model, the minimum number of points is theoretically 3 measurements. However a sample of 10 points at least is more suited in order to determine significantly the uncertainty due to the model (see Figure 2.8).

To determine this number and validate the measurement, an experiment has been carried out. Figure 2.9 presents residuals of the linear fitting of the mass as a function of time for three cycles of 10 measurements for a leak flow rate of about 50 g/yr evacuated in a 2-dm^3 volume. The linear fitting is expressed thanks to the least-squares method. All measurements of the 3 cycles are considered. In the first cycle, the leak is not yet stabilized. If the second and third cycles are only considered, the repeatability of the leak flow rate measurement is calculated as 0.055 % of the value. Therefore, 10 measurements are sufficient to calibrate a leak of nominal value: 50 g/yr.

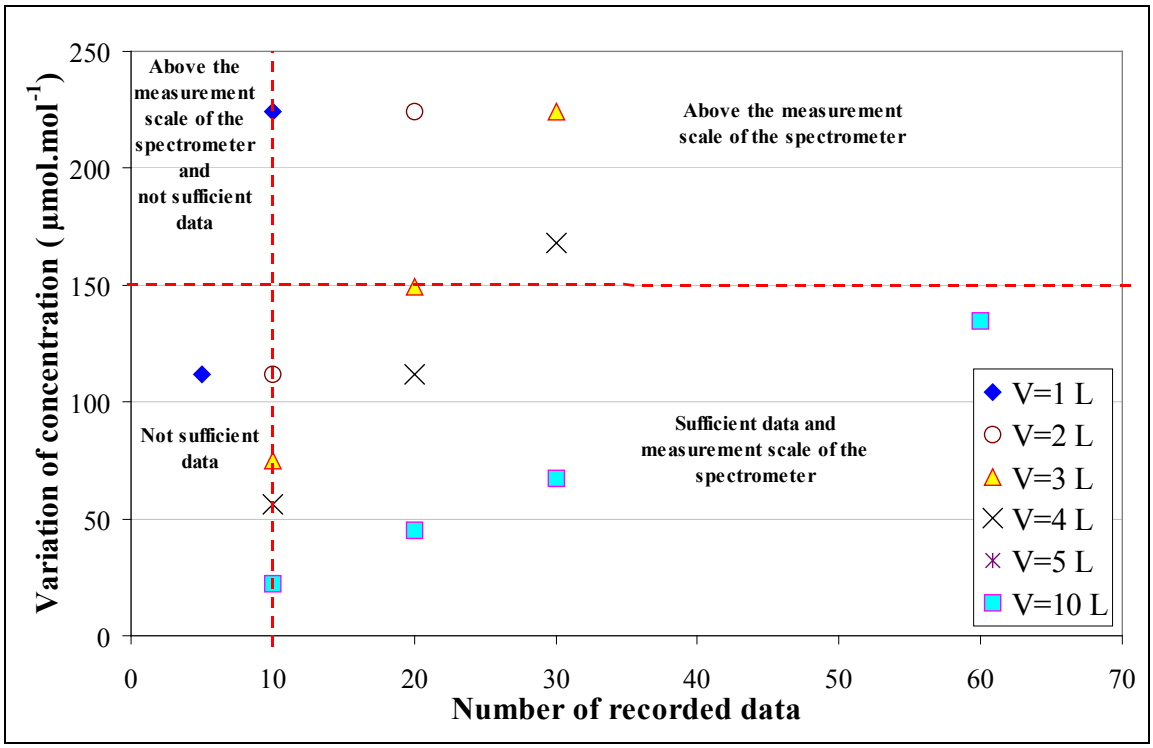

Figure 2.8. Variation of the concentration during the calibration of a leak flow rate about 50 g/yr as a function of the number of recorded data for different values of the size of the accumulation volume.

As a conclusion, taking into account the calibration time duration and the number of data for a 50 g/yr-leak calibration, the best compromise for the accumulation volume should be of 2 dm^3. For smaller leaks, the number of measurements can be adapted to reach this compromise.

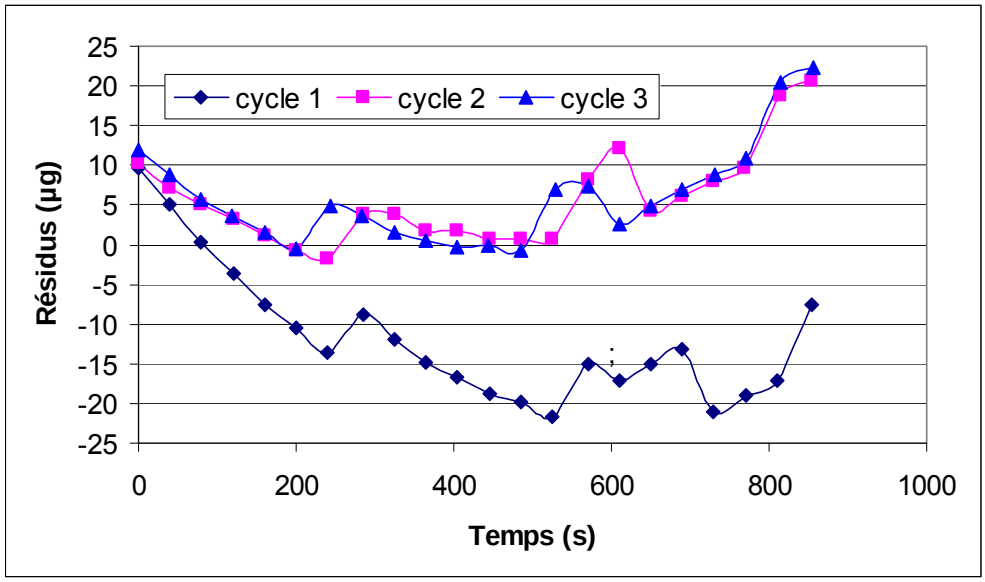

Figure 2.9. Residuals : fitting of the mass versus time considering all the cycles.

2.4.2 Optimization of the standard volume size

As the chosen method to calibrate the accumulation is the static expansion method, two volumes are necessary: an accumulation volume and a standard volume. The accumulation size previously estimated for the sake of limiting the number of measurements is now calculated from the value of the standard volume and from Equation [2.23]. The components of uncertainty are:

- the calibration of the thermometers whose uncertainty is estimated as U = 0.070 K
- the homogeneity in the volume whose uncertainty is estimated as a rectangular law U = 0.10 K
- the measurement of the pressure whose uncertainty is estimated as U = 15 Pa
- the calibration of the volume standard whose expected uncertainty is about 0.10 %.

Consequently, the standard volume size must be carefully defined, in order to minimize the uncertainties. Especially, as the combined uncertainty of the volume calibration by the static expansion method is strongly related to the size of the standard volume, the volume size must be defined in order to minimize this uncertainty. This section first describes the standard volume, in order to define its size. Then a simulation aiming at determining the optimal size of the standard volume compared to a first approximation size of the accumulation volume has been carried out.

The design of the standard volume aimed at making a volume as simple as possible, in order to calibrate it dimensionally [MOR07] with a relative uncertainty of 0.10% or better. Therefore, the volume is a cylinder made in stainless steel 316L - the "main cylinder" - sealed with O-rings and mainly composed of an opened cylinder and two flanges manufactured by the LNE. The combined uncertainty of the standard volume is mainly due to the tolerances related to the dimensions. Therefore, the roughness of the interior flanges and the parallelism of the opposite interior flanges were controlled in the manufacturing process. Additional volumes are also part of the standard volume:

- the tubes connecting the accumulation volume and the standard volume, including the appropriate dead volume of the valve VVE0,
- the tubes connecting the standard volume and the manometer,
- the dead volume of the manometer.

A simulation has been carried out for determining the optimal volume size of the standard volume in relation to the chosen size of 2 dm^3 defined for the accumulation volume. Only the uncertainties of measurements of pressures and temperatures have been considered. Thus, the expression of the combined variance underlines the influence of the initial pressures in both volumes. The size of the standard volume influences the combined uncertainty of the accumulation volume. The spectrometer works at a pressure between 90 kPa and 110 kPa only. Therefore, the initial pressure in the accumulation volume cannot exceed 110 kPa and the final pressure in both volumes must be fixed between 90 kPa and 110 kPa.

Considering these conditions, the optimal value of the ratio $\frac{V_{Acc}}{V_E}$ has been estimated about 4, which corresponds to a nominal value of the standard volume of 0.5 dm^3. The greater the difference of the initial pressures in both volumes, the more accurate the measurement. Therefore, the maximum size of the standard volume to obtain a final pressure higher than 90 kPa is about 0.5 dm^3 for an initial pressure of 10 kPa in the standard volume, and an initial pressure of 110 kPa in the accumulation volume. In these conditions of pressure, the theoretical relative uncertainty of the accumulation volume is minimized for a standard volume size of 0.5 dm^3, the uncertainty is about 0.35% (see Table 2.3).

Table 2.3. Relationship between the possible maximum capacity needed to maintain a pressure between 90 kPa and 110 kPa and the theoretical relative uncertainty of the accumulation volume.

Initial pressure in the accumulation volume = 110 kPa			Initial pressure in the accumulation volume = 105 kPa		
Initial Pressure in the standard *kPa*	Theoretical relative combined uncertainty (k=2)	Maximum capacity of the standard *L*	Initial Pressure in the standard *kPa*	Theoretical relative combined uncertainty (k=2)	Maximum capacity of the standard *L*
10000	0.35%	0,5	10000	0.98%	0,3
25000	0.36%	0,6	25000	0.99%	0,4
35000	0.47%	0,7	35000	1.1%	0,5
40000	0.37%	0,8	40000	1.0%	0,6
50000	0.39%	1,0	50000	0.5%	0,7

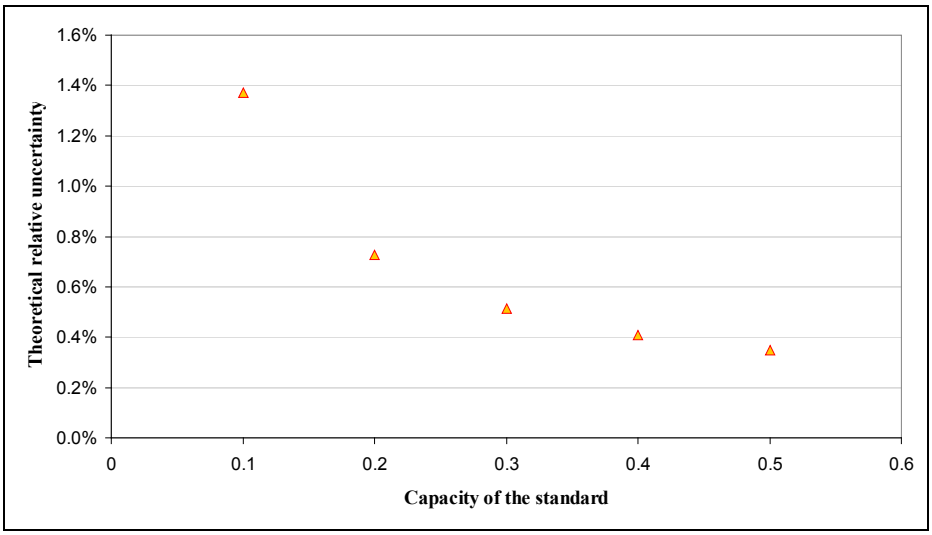

Figure 2.10. Theoretical relative uncertainty of the accumulation volume as a function the size of the standard, with the accumulation volume initially at 110 kPa and the standard volume initially at 10 kPa.

2.5 Design of the primary standard of leaks

Once the infrared spectrometer and the volume calibration method have been chosen, the selected design of the primary standard is realized. It implies to define the suitable complementary measurement devices and all the necessary circuits to make a qualified measurement.

2.5.1 Complementary measurement components

The method for measuring refrigerant leak flow rates needs two main components:

- the accumulation cell - where leaks will accumulate along the time,
- an infrared spectrometer measuring the raise of concentration inside the volume.

The calculation of leak flow rates needs to measure the concentration and the {pressure, temperature} associated to each measurement of concentration, the time, and the accumulation volume. The raise of concentration, the pressure and the temperature inside the accumulation volume and the standard volume must be measured respectively by a spectrometer, manometers, and thermometers. Thus, the primary standard needs the following instruments [TOR02]:

- an infrared detector,

- a manometer for each volume, and
- at least one thermometer for each volume.

In reality, to control the homogeneity of the temperature in the accumulation volume, four platinum resistance thermometers are installed: two inside the accumulation volume, and two in contact with the walls of the accumulation volume. Regarding the standard volume, as it is necessary to have the simplest volume to measure it dimensionally, a platinum resistance thermometer is installed in the middle of the lateral wall of the standard.

Concerning the operation of the photo-acoustic spectrometer, it does not measure continuously the concentration inside the accumulation volume. The photo-acoustic cell is rinsed by a gas sample circulating inside the accumulation volume. After rinsing, it takes the gas sample from the accumulation cell, encloses it in the photo-acoustic cell, and measures the concentration of this gas mixture sample. Each measurement takes about 1 minute. The shift from a dynamic mode to a static mode influences temporarily the pressure inside the accumulation volume. In order to minimize the uncertainty due to the measurement of the gas parameters, it is necessary to know the relative pressure and temperature at the moment of the sampling. With a differential pressure sensor, the dynamic mode and the static mode can be clearly identified (see Figure 2.11). When the differential pressure measurement is stable, the spectrometer measures the sample concentration. Finally a differential manometer is added between the spectrometer and the accumulation volume.

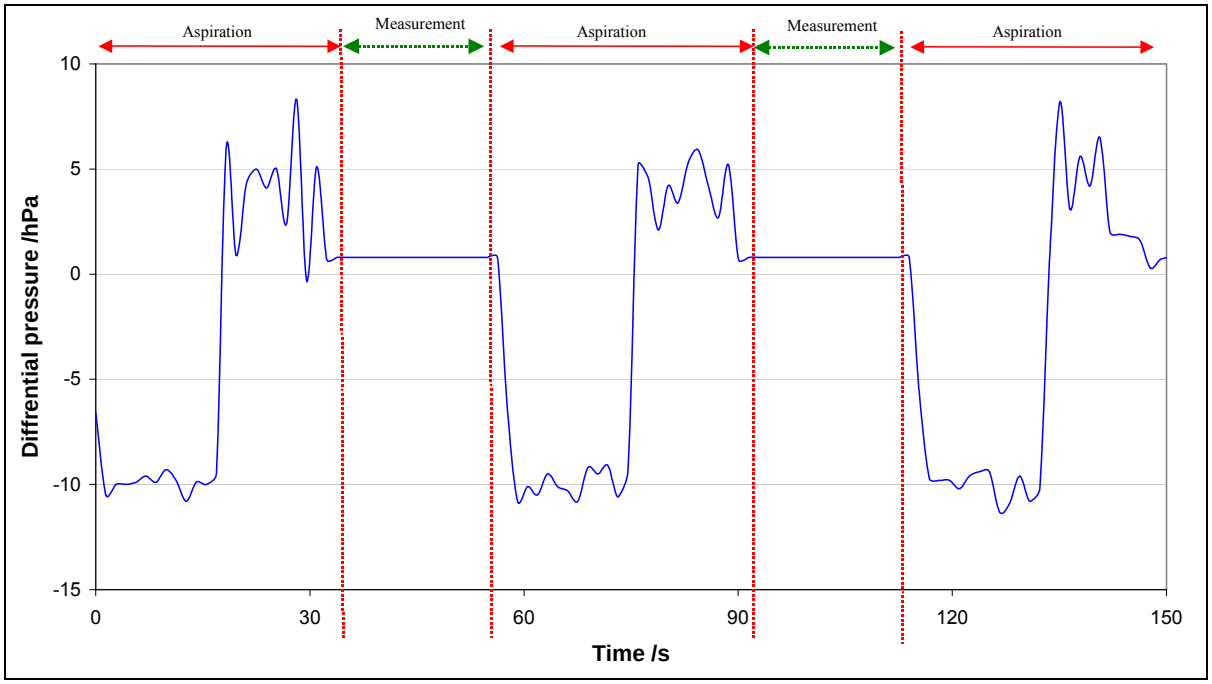

Figure 2.11. Identification of the dynamic and static modes via a differential pressure sensor.

To summarize, the primary standard is composed of two main volumes (the accumulation volume + the standard volume) and of the following complementary instruments:

- two Pt100 inside the accumulation volume,
- two Pt100 in contact with the walls of the accumulation volume,
- one Pt100 within the middle of the lateral wall of the standard volume,
- one barometer measuring the pressure inside the accumulation volume (full range scale from 3.5 kPa to 130 kPa),

- one barometer measuring the pressure inside the standard volume (full range scale from 3.5 kPa to 130 kPa),
- a differential pressure sensor to identify the moment where the spectrometer measures, and
- a photo-acoustic spectrometer to measure the concentration of the tracer gas accumulated inside the accumulation volume.

2.5.2 Circuits composing the primary standard

As it has been defined, the accumulation cell is a volume of about 2 dm^3 connected to a manometer to measure the inside pressure. Two platinum resistance thermometers are installed inside the accumulation volume. The accumulation cell is connected to the inlet and the outlet of the spectrometer. It can be isolated from the spectrometer by a valve.

The presence of water and CO_2 from the environment can influence the measurements of the infrared spectrometer, so the accumulation volume is filled with dry clean air (20% of oxygen and 80% of nitrogen, with a purity of 99.99%). In order to rinse the accumulation volume after a series of measurements, a circuit of evacuation connected to a vacuum pump has been integrated to the accumulation volume. Valves isolate the accumulation volume from this evacuation circuit. A supplying system is designed to fill the accumulation volume with dry clean air. It is isolated from the accumulation volume by a valve. The system includes a pressure controller. The pressure inside the accumulation volume is maintained at a pressure close to the atmospheric pressure [TOR02], [MOR07].

Finally, the standard volume is integrated in the test bench in order to calibrate regularly the accumulation volume by the static expansion method. The standard is isolated from the accumulation volume via valves. As the connecting volume between the accumulation volume and the standard volume has to be measured, it will be designed in order to be as small as possible. Figure 2.12 presents the circuits of the primary leak standard.

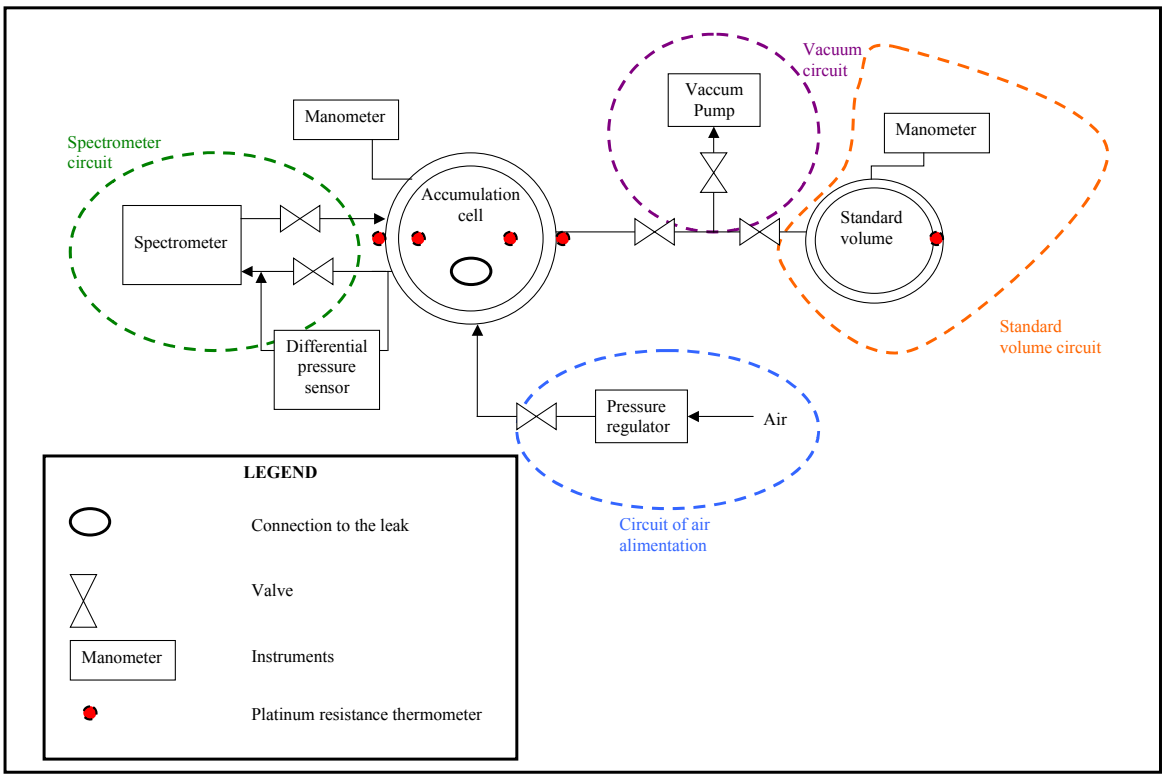

Figure 2.12. Diagram of the primary standard of leaks

2.5.3 Precaution for the static expansion method

The connecting tubes and the dead volumes are calibrated using the information supplied by the manufacturers or controlled by dimensional measurements. The main cylinder of the standard volume is calibrated using a tri-dimensional standard machine. Therefore, some design parameters must be controlled in order to fix the expanded relative uncertainty of the volume near 0.10%:

- the cylinder diameter at any height: the tolerance is fixed as U = 0.020 mm,
- the length of the cylinder: the tolerance is fixed as U = 0.030 mm,
- the roughness of internal walls fixed as U = 0.010 mm,
- the parallelism of the opposite interior flanges fixed as U = 0.010 mm.

2.5.4 Realization of the standard

A primary standard to calibrate leak flow rate of R-134a has been realized and installed at the LNE (see Figure 2.13 and Figure 2.14).

Figure 2.13. Photo of the primary standard *(Blue circle: volumes zoomed in Figure 2.14; red circle: photo-acoustic spectrometer)*

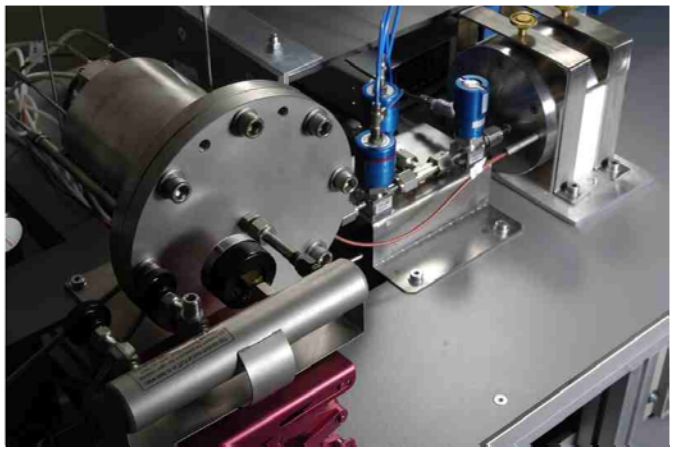

Figure 2.14. Zoom on the accumulation volume and the standard volume.

2.6 Conclusions

The measurement of the MFR is based on the data relative to the pressure, the temperature, the variation of the concentration, and on the knowledge of the accumulation volume. Pressure and temperature inside the accumulation volume are easily measured respectively by an absolute manometer and by a platinum thermometer. The key point of the design aims at determining how to measure the variation of the concentration and of the accumulation volume.

To measure R-134a (or CO_2) concentrations, two spectrometers - based on different techniques and used by the CEP - are available: an IR photo-acoustic spectrometer and an IR spectrophotometer. Both techniques have been analyzed. The relevant criterion of performance – defined as their repeatabilities and linearities - have been compared theoretically and experimentally in order to select

the more appropriate one for a primary standard that measures refrigerant leak MFR with an uncertainty of about 1%. Finally, the photo-acoustic spectrometer has been chosen.
To measure the accumulation volume, three methods has been considered:

- The dimensional method
- The gravimetric method, and
- The static volume expansion method.

The dimensional method and the gravimetric method are classic methods to calibrate the capacity of a volume. However, the volume must be simple to use the dimensional method. The theoretical and minimal uncertainty relative to the gravimetric method already reaches the relative value of 2.1%. It implies a value of 2.1% of the minimal relative uncertainty of the MFR. Using this method, it is not possible to realize a primary standard to measure refrigerant leak MFR with an uncertainty of 1%. Therefore, a static volume expansion method has been defined and analyzed. It is a vacuum technique used to measure pressure knowing two volumes. In this case, a volume is measured knowing the pressures and one of the two volumes. The theoretical and minimal uncertainty relative to this method reaches the value of 0.35%. This method has then been selected.

The test bench has then been designed based on the experience of the CEP, using the photo-acoustic spectrometer. Some metrological improvements have been done thanks to the studies:

- A standard volume has been added: in order to measure the accumulation volume using the static expansion system, a standard volume has been designed and integrated into the bench. This volume will be calibrated using the dimensional method: it must then be designed as simple as possible.
- A differential pressure gauge has been added thanks to the better understanding of the PAS operation. This gauge allows improving the measurement of the pressure inside the accumulation volume when the measurement is discontinue.

Besides, in order to optimize the uncertainty of the calibration and the calibration time, a study to determine the nominal capacity of the accumulation volume has been carried out to complete the design. The optimal capacity was defined as 2 dm^3 to measure MFR from 1 $g.yr^{-1}$ to 50 $g.yr^{-1}$.

The bench has then been realized considering the specifications described in this section. Once the installation is qualified, it will be the reference to measure the refrigerant leaks, which are needed to qualify the refrigerant leak detectors according to the European standard EN 14624 .

Chapter 3 - Qualification of the primary standard

3.1 Objectives

In Chapter 1, it was established that the realization of the primary standard implies a design phase and a qualification phase. Indeed, a standard is a "reference measuring system intended to define, realize, conserve or reproduce a unit or one or more values of a quantity to serve as a reference". In this case, the quantity to define is a leak flow rate and its unit is $g.yr^{-1}$. A primary standard is a specific standard: it is "designated or widely acknowledged as having the highest metrological qualities and whose value is accepted without reference to other standards of the same quantity" [VIM94].

The design of the test bench aimed at improving the previous test benches built by the CEP in order to optimize the uncertainty of components. It remains to qualify the measurement chain to obtain the value of a leak flow rate using values of other quantities: pressure, temperature, volume, and concentration.

The objectives of this chapter are as follows:

- To summarize the basics of the expression of the uncertainty of a measurement
- To identify and quantify the different error sources in the measurement of a refrigerant leak flow rate
- To establish the uncertainty budget of the calibration of a refrigerant leak flow rate whose nominal value is between 1 and 50 g/yr.

3.2 Basis of the expression of the uncertainty in measurement

The qualification of the leak primary standard consists of identifying the causes of errors and to quantify the uncertainty on the result of a leak calibration. In order to facilitate the understanding, let us remind the basis of the metrological definitions and the method to express the uncertainty of a measurement.

3.2.1 Causes of errors in the measurement

The objective of a measurement is to determine the value of a specific quantity. The result is only an estimation. It is meaningful only if it is accompanied by a statement of its uncertainty. A measurement has imperfections that give rise to an error in the measurement result. Traditionally the error is viewed as the combination of a random component and a systematic component [GUM99].

A random error presumably arises from unpredictable or stochastic temporal and spatial variations of influence quantities. Its effects give rise to variations in repeated observations of the value of the measured quantity. This error cannot be compensated, it can only be reduced by increasing the number of observations.

Like a random error, a systematic error cannot be eliminated. However, contrary to random errors, a systematic error is a predictable error. Therefore, it arises from a recognized effect of an influence quantity on a measurement result. If the effect can be quantified, a correction factor can be applied to compensate the effect. The value of the error due to this effect is then reduced to the value of the error in the correction value. However, it means that the systematic error must be clearly identified and quantified.

Qualifying a measurement installation implies that most of the sources of the random and systematic errors in the measurement results are clearly identified. The source of errors can be classified in five classes called:

- Measurand
- Means
- Environment
- Method
- Human competence

Measurand

The first class is called "Measurand". It includes the sources of errors related to the specific quantity subject to measurement: the incomplete definition of the specific quantity subject to measurement, the imperfect realization of this definition, the stability of the true value of this specific quantity, the non-representative sampling that may not represent this specific quantity, etc.

Means

The second class is called "Means". It gathers the sources of errors related to the means to measure as instruments, standards or other reference materials: their finite resolution or discrimination threshold, their inexact values, etc.

Environment

The third class is called "Environment". It gathers the sources of errors related to the environment influence: the inadequate knowledge of the effects of environmental conditions on the measurement, the lack of knowledge of the environmental conditions due for instance to imperfect measurement, etc. As an example, the measurement value can depend on the temperature of the system, which implies that a correction must be done based on the temperature value. Therefore, the temperature value must be known and then measured.

Method

The fourth class is called "Method". It gathers the sources of errors related to the method used to measure the quantity value. For instance, some approximations and assumptions are made to carry out the measurement procedure, which add some uncertainties in the final results. The inexact values of some constants can be used, like the perfect gas constant for instance.

Human competence

The last class is called "Human competence", because the sources of uncertainties are related to the operator: the personal bias in reading analogue instruments, the personal interpretation of the measurement procedure, the cleverness to carry out the measurement procedure, etc.

3.2.2 Main definitions

In the following dissertation, some terms are used considering metrological meaning. For better understanding, the definitions of these terms are provided in this paragraph. The definitions are quotation of an international standard [VIM94], written in order to give the same meaning to the main metrological terms for all its users.

Quantity: attribute of a phenomenon, body, substance that may be distinguished qualitatively and determined quantitatively.

Value (of a quantity): magnitude of a particular quantity generally expressed as a unit of a measurement multiplied by a number.

True value (of a quantity): value consistent with the definition of a given particular quantity.

Measurement: set of operations having the object of determining a value of a quantity. In this study, the term measurement can also be used as the abbreviation of "result of measurement".

Method of measurement: logical sequence of operations, described generically, used in the performance of measurements.

Result of a measurement: value attributed to a particular quantity, obtained by measurement.

Measurand: particular quantity subject to measurement.

Influence quantity: quantity that is not the measurand but that affects the result of the measurement.

Indication (of a measuring instrument): value of a quantity provided by a measuring instrument.

Accuracy of measurement: closeness of the agreement between the result of a measurement and a true value of the measurand.

Repeatability: closeness of the agreement between the results of successive measurements of the same measurand carried out under the same conditions of measurement.

Reproducibility: closeness of the agreement between the results of successive measurements of the same measurand carried out under changed conditions of measurement.

Uncertainty of measurement: parameter associated with the result of a measurement, that characterizes the dispersion of the values that could reasonably be attributed to the measurand.

Error of measurement: result of a measurement minus a true value of the measurand.

Detector: device or substance that indicates the presence of a phenomenon without necessarily providing a value of an associated quantity.

Linear scale: scale in which each scale spacing is related to the corresponding scale interval by a coefficient of proportionality that is constant throughout the scale.

Nominal value: rounded or approximate value of a characteristic of a measuring instrument that provides a guide to its use.

Stability: ability of a measuring instrument to maintain constant its metrological characteristics with time.

Standard: material measure, measuring instrument, reference material or measuring system intended to define, realize, conserve or reproduce a unit or one or more values of a quantity to serve as a reference.

Primary standard: standard that is designated or widely acknowledge as having the highest metrological qualities and whose value is accepted without reference to other standards of the same quantity.

Secondary standard: standard whose value is assigned by comparison with a primary standard of the same quantity.

Reference standard: standard, generally having the highest metrological quality available at a given location or in a given organization, from which measurements made there are derived.

3.2.3 Evaluation of standard uncertainty

In most cases, a measurand Y is not measured directly, but is determined from other quantities $(\tau_{qi})_i$ through a functional relationship f: $Y = f(\tau_{q1}, \tau_{q2}, \tau_{q3}, \ldots)$. The estimation of the measurand Y is notated y and the estimations of the other quantities τ_{qi} are notated q_i. Therefore: $y = f(q_1, q_2, q_3, \ldots)$.

Each input estimate qi and its associated standard uncertainty $u(q_i)$ is obtained from a distribution of possible values of the input quantity τ_{qi}. This probability distribution may be frequency based, that is, based on a series of observations of τ_{qi}, or it may be an a priori distribution. Type A evaluations of standard uncertainty components are founded on frequency distributions while Type B evaluations are founded on a priori distributions [GUM99].

3.2.3.1 Type A evaluation of standard uncertainty

In most cases, the best available estimate of the expected value τ_q of a quantity q, which varies randomly and for which n independent observations q_k have been obtained under the same conditions of measurement, is the arithmetic mean $\bar{q}$ of the n observations:

$$\bar{q} = \frac{1}{n} \cdot \sum_{k=1}^{n} q_k \,. \qquad [3.1]$$

The individual observations q_k differ in value because of random variations in the influence quantities or random effects. The experimental variance of the observations, which estimates the variance σ^2 of the probability distribution of q, is given by Expression [3.2]:

$$\sigma^2(q_k) = \frac{1}{n-1} \cdot \sum_{k=1}^{n} \left(q_k - \bar{q} \right)^2 . \qquad [3.2]$$

This estimate of the variance and its positive square root, which is termed the experimental standard deviation, characterize the dispersion of the observations from their arithmetic mean.

The experimental variance of the mean $\sigma^2(\bar{q})$ and the experimental standard deviation of the mean $\sigma(\bar{q})$ quantify how well $\bar{q}$ estimates the expectation τ_q of the quantity q. The experimental standard deviation of the mean may be used as a measure of the uncertainty of $\bar{q}$. This uncertainty is called Type A standard uncertainty.

3.2.3.2 Type B evaluation of standard uncertainty

For an estimate q of an input quantity τ_q that has not been obtained from repeated observations, the associated estimated variance or the standard uncertainty u(q) is evaluated by scientific judgment based on all available information on the possible variability of τ_q. It is based on an estimation of the probability density (distribution law).

The pool of information may include:

- previous measurement data,
- experience or general knowledge of the behavior and properties of relevant materials and instruments,
- manufacturer's specifications,
- data provided in calibration and other certificates,
- uncertainties assigned to reference data taken from handbooks.

The three main distribution laws that can be defined are:

- the normal distribution law,
- the rectangular law, or uniform distribution
- the triangular law.

Other distribution laws are described in the literature [GUM99].

Normal distribution law

The quantity value can follow a normal distribution law. The normal distribution is also called the Gaussian distribution (see Figure 3.1). It is defined by two parameters: the arithmetic mean (see Equation [3.1]) and the experimental standard deviation (see Equation [3.2]). Therefore, if these parameters are already known, the value can be characterized without making experimental observations. The continuous probability density function of the normal distribution is the Gaussian function [3.3]:

$$f_{prob} = \frac{1}{\sigma \cdot \sqrt{2 \cdot \pi}} \cdot e^{-\frac{(q_i - \bar{q})}{2 \cdot \sigma^2}} . \qquad [3.3]$$

For instance, calibration certificates, particularly the ones delivered under the logo COFRAC, are assuming that the quantity value follows a normal distribution law and the quoted uncertainty σ defines an interval having a 95% level of confidence. In that case, the standard uncertainty becomes the value $\frac{\sigma}{2}$.

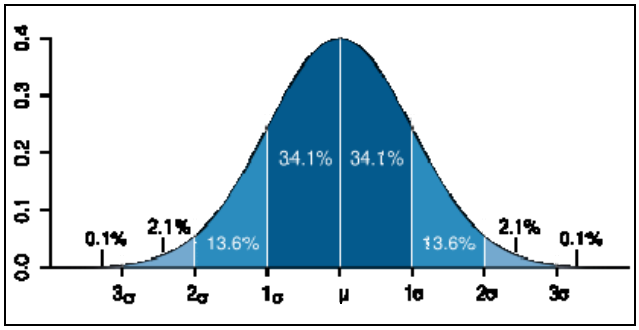

Figure 3.1. Example of a normal distribution with a mean value μ and a standard deviation σ: representation of the standard deviation and the confidence intervals.

Rectangular distribution law

In other cases, it may be possible to estimate only the upper and the lower limits for the quantity q, respectively q_{max} and q_{min}. If there is no more information, it is assumed that the probability of the quantity to take any value between the defined limits is equal. It is assumed that the probability to take a value outside these limits is equal to zero (see **Erreur ! Source du renvoi introuvable.**).

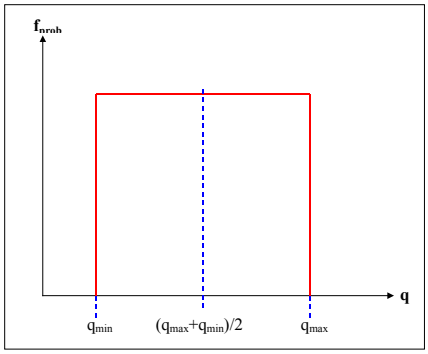

Figure 3.2. Example of a rectangular distribution law between the bounds [q_{min} ; q_{max}].

A study of the density of the probability determines that the expected value is still the arithmetic mean of values q_{min} and q_{max}, and the associated variance is expressed by Equation [3.4]:

$$u^2(q) = \frac{(q_{max} - q_{min})^2}{12}. \qquad [3.4]$$

Triangular distribution law

Because there is no specific knowledge about the possible values of τ_q within its estimated bounds q_{min} and q_{max}, it could be assumed that it is equally probable for τ_q to take any value within these bounds, with zero probability of being outside them (rectangular distribution law).

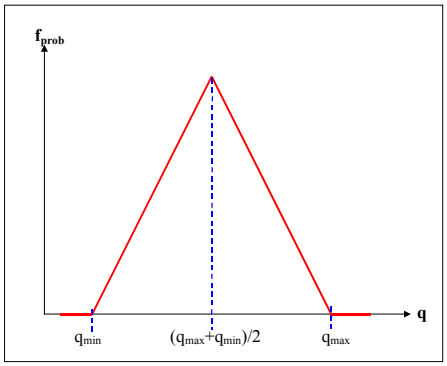

Figure 3.3. Example of a triangular distribution law between the bounds [q_{min} ; q_{max}].

However, it is more realistic to expect that values near the bounds are less likely than those near the midpoint, although it is not always the case. Therefore, if it is clearly justified, it can be more reasonable to consider a triangular distribution law (see Figure 3.3).

A study of the density of the probability determines that the expected value is still the arithmetic mean of values q_{min} and q_{max} and the associated variance is expressed by Equation [3.5]:

$$u^2(q) = \frac{(q_{max} - q_{min})^2}{6}. \qquad [3.5]$$

3.2.4 Expression of the combined uncertainty

Once Type A and Type B evaluations of the standard uncertainties associated to the estimate of the input quantities (q_1, q_2, q_3, …) are made, the uncertainty of the estimate of the measurand $Y=f(\tau_{q1}, \tau_{q2}, \tau_{q3}, \ldots)$ can be expressed. The standard uncertainty of the estimate y of the measurand Y is obtained by appropriately combining the standard uncertainties of the input estimates (q_1, q_2, q_3, …) of the quantities (τ_{q1}, τ_{q2}, τ_{q3}, …).

The combined standard uncertainty u(y) is the positive square root of the combined variance $u^2(y)$, given by Equation [3.6], which is called the propagation of variance uncertainties law**:**

$$u^2(y) = \sum_{j=1}^{\text{number of quantities}} \cdot \sum_{i=1}^{\text{number of quantities}} \frac{\partial f}{\partial q_i} \cdot \frac{\partial f}{\partial q_j} \cdot u(q_i,q_j), \qquad [3.6]$$

where q_i and q_j are the estimate of τ_{qi} and τ_{qj}, $u(q_i,q_j)$ with $i \neq j$ is the estimated covariance associated with q_i and q_j and where $u(q_i,q_i)=u^2(q_i)$ is the variance associated with q_i.

As previously seen, the standard that has been realized aims at measuring a leak flow rate (unit: $g.yr^{-1}$). It is a primary standard as the leak flow rate value is estimated with the reference of values of other quantities:

- the concentration measured by a PAS (see Section 3.3),
- the pressure measured by a manometer (see Section 3.4),
- the temperature measured by a platinum thermo-resistance (see Section 3.5), and
- the volume measured by using the expansion volumes method (see Section 3.6).

Like the design phase, measurements of the concentration and of the volume are the key points of the qualification. The pressure and the temperature are not the main components of the uncertainty as it is possible to measure the quantities with reasonable uncertainties. However, the qualification of the pressure and temperature measurements is presented for a better understanding of the qualification of the volume measurement.

3.3 Measurement of the concentration

One of the main components of the leak flow rate-measurement uncertainty is due to the concentration measurement. A relative uncertainty of 1% in the concentration measurement implies an uncertainty of 1% in the measurement of a leak flow rate. Therefore, the causes of errors in the measurement of the concentration by the PAS is analyzed and the uncertainty budget of the concentration measurement is experimentally established in the following paragraphs.

3.3.1 Analysis of the causes of errors in the concentration measurement by the PAS

The concentration of R-134a or CO_2 is measured by a PAS. A sample of gas enclosed in the cell of the spectrometer is excited by an infrared light energy, chopped and filtered appropriately. This photo-acoustic signal is converted into acoustic pressure, which is measured by microphones. As presented in Chapter 2, the PAS [VECHT06] is mainly composed of:

- a PAC, which enclosed the sample gas,
- a light source,
- a parabolic mirror
- a chopper,
- a filter wheel, and
- two microphones.

3.3.1.1 Photo-acoustic cell

A sample of an unknown concentration of gas is hermetically sealed in the PAC. The PAC is cylindrical and its volume around 3 cm^3. To avoid acoustical waves from the outside environment, the walls are thick. This cell is installed in a clean chamber in order to avoid the presence of dust. Small

particles of any kind in the PAC will absorb part of the light energy, which will generate a disturbing signal – named the dust signal.

Inside the cavity, the surface is polished and gold coated in order to obtain highly reflective walls. It aims at reducing the absorption of walls, which generates a wall signal. Due to the absorption of light, there is an increase in the temperature of the wall surface. This generated heat flows by conduction to the air layer in contact with the wall causing it to expand. As the light is modulated, the air in contact with the walls will expand and contract at the frequency of the chopper, which generates an acoustic signal. Considering that the cavity is spherical, the amplitude of this signal is expressed by the following expression [3.7] [B&K90-1]:

$$p_{walls} = \frac{3 \cdot \gamma \cdot P_0 \cdot W_{Walls}}{\varpi \cdot \frac{D}{2} \cdot T_0 \cdot \sqrt{\rho_{Walls} \cdot C_{Walls} \cdot K_{Walls} \cdot \frac{\rho_{0g} \cdot C_{p_g}}{K_g}}} \qquad [3.7]$$

where

$\mathbf{C_{pg}}$	Gas thermal capacity at constant pressure
$\mathbf{C_{walls}}$	Walls thermal capacity
D	Photo-acoustic cell diameter
$\mathbf{K_g}$	Gas thermal conductivity
$\mathbf{K_{walls}}$	Walls thermal conductivity
$\mathbf{P_0}$	Ambient pressure
$\mathbf{p_{walls}}$	Walls pressure
$\mathbf{T_0}$	Ambient temperature
W	Absorbed power per unit volume by the walls
γ	Adiabatic coefficient of the gas
ρ_g	Gas density
ρ_{walls}	Walls density
ϖ	Chopper pulsation

In order to minimize the wall signal, the absorptivity of the wall surface must be low, its reflectivity high, and the product of $\rho_w.C_{walls}.K_w$ high too. According to Brüel&Kjaer, the wall signal is typically 20 times the detection limit signal and this component of error is systematic.

The PAC is also composed with a germanium window through which the light passes. Contrary to the wall, it is not just the surface that absorbs the light but the whole bulk of the window material. Therefore the generated window acoustic signal is inversely proportional to $\omega^{3/2}$ instead of ω and is independent of the thermal conductivity of the window material:

$$p_{window} = \frac{2 \cdot \sqrt{2} \cdot \gamma \cdot P_0 \cdot \beta_{Window} \cdot I_0}{\varpi^{3/2} \cdot l_c \cdot \rho_{Window} \cdot C_{Window} \cdot \sqrt{\frac{\rho_{0g} \cdot C_{pg}}{K_g}}} . \qquad [3.8]$$

3.3.1.2 Light path

The infrared light source is assimilated to a black body. The light is maximum for all the infrared frequencies and a black body is easily modeled. However it is not selective and the model is for an ideal black body. Therefore there is a component of error due to the model.

The light is reflected off a mirror with a half-cone angle θ of the light cone. Light passes through a mechanical chopper, which pulses it at 20Hz. As the acoustic signal generated by the gas inside the PAC is dependent of the frequency of the chopper, it is necessary that the chopper pulses at a very stable frequency. The calculated concentration of the gas is inversely proportional to the pulsation of

the chopper. Therefore, an uncertainty on the pulsation of 1% implies an uncertainty of 1% on the result value of the concentration. Because the measurement of the leak flow rate implies the measurement of the increase of the concentration, the measured concentrations of the gas samples picked every minute can be associated for different rotation speeds of the chopper. Therefore, this error can impact the linearity of the spectrometer.

Once the light passes the chopper, it passes through one of the optical filters of the filter wheel, which selects the relevant frequencies at which the sample gas mostly absorbs. This filter is an optical interference one and its pass band transmission depends to some extent on the angle of the incident light. If the half-cone angle of the light cone after reflecting off the parabolic mirror, θ, is equal to $\pi/2$, the spectral intensity reaches its maximum value of πL_v. However, it is in practice not possible to reach the highest possible light intensity, because the frequency of an optical interference filter depends on the angle of light incidence. Therefore the value of θ is fixed as 30°. The uncertainty on the half-cone angle and on the function of transmission of the optical filter has the same impact on the concentration result than the uncertainty of the pulsation, as the concentration is proportional to these two quantities. Finally the filtered and chopped light passes the germanium window of the PAC. The pressure inside the PAC increases. As the light is pulsated, an acoustic wave is then created.

3.3.1.3 Measurement of the acoustic signal

This acoustic signal is measured by two condenser microphones, which are extremely linear in a wide range of sound pressures. This kind of microphone consists of thin metallic membrane in close proximity to a rigid back plate (see Figure 3.4). When the pressure increases and decreases in the measurement chamber, the flexible membrane moves in and out and the capacitance between the plates varies accordingly.

The sensitivity of the microphone M_p is defined as the ratio between the voltage U_T of the microphone when it is not electrically charged (i = 0) and the acoustic pressure submitted to the flexible membrane :

$$M_{micro}=\left(\frac{U_T}{p}\right)_{i=0}=-\frac{E_0.S}{j\omega' Z_m} \qquad [3.9]$$

Therefore, the acoustic pressure is expressed by the Equation [3.10]:

$$p=\frac{Z_m}{S}\times v=-\frac{E0}{j\cdot\omega' M_{micro}}.v \qquad [3.10].$$

The calibration of a microphone consists of determining its sensitivity. However, it is not the most sensitive.

The PAS system microphones are two ½ inch low noise microphones with built-in amplifiers. They are opposed in the PAC, which implies that the gas signal is doubled and that the addition in the random noise is only about 3 dB. Brüel&Kjaer have measured the RMS noise of microphones as a function of the frequency [B&K90-1]. At 20 Hz, in a room at 20°C and at 101.3 kPa, for a measurement in the chamber during 5 s, the RMS noise level corresponds to $2.5.10^{-6}$ Pa.

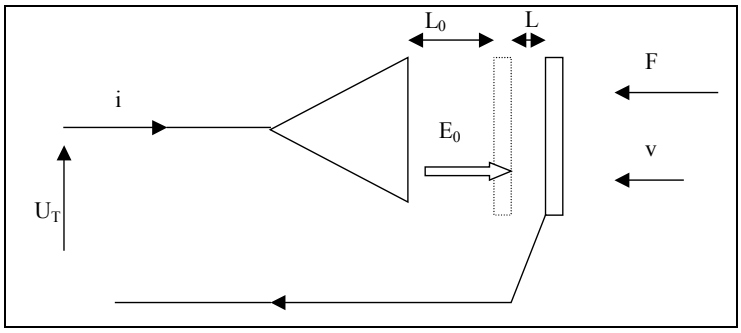

Figure 3.4. Diagram of a condenser microphone

3.3.1.4 Theoretical relationship between the sound pressure and the concentration

Equation [2.12] expressed that the concentration is proportional to the acoustic pressure. However, this fitting is based on several hypotheses (see Section 2.2.2.2). The modeling is linearized. Therefore, the relation may not be really linear and the modeling inserts some uncertainty components in the calculation of the concentration.

3.3.1.5 Limit detection

The limit detection of a gas C_{limit} is defined as the gas concentration causing a signal is equal to twice the RMS noise level of the transducer. As the RMS noise level is about $2.5.10^{-6}$ Pa, the detection limit signal corresponds to a sound pressure of $5.0.10^{-6}$ Pa [B&K90-1]. The detection limit is the concentration relative to a sound pressure of $2.p_{RMS} = 5.0.10^{-6}$ Pa, ie.:

$$C_{limit} = \frac{2 \cdot P_{RMS}}{2\sqrt{2} \times 0.85 \times \frac{(\gamma - 1)}{\omega} \times .|S|.(\alpha.sin^2\theta).\int F(\upsilon - \upsilon_0).k(\upsilon)Tf.L_\upsilon.d\upsilon} . \qquad [3.11]$$

Therefore, the detection limit specially depends on the nature of the gas and on the filter. For instance, this spectrometer can provide measurement of CO_2 or R-134a concentration in the accumulation volume with a detection limit respectively about 10 $nmol.mol^{-1}$ and 15 $nmol.mol^{-1}$.

Finally, the detection limit can be improved. As the P_{RMS} depends on the duration time t of the measurement on the cell, the longer the measurement, the lower the detection limit:

$$C_{limit1} = \frac{C_{limit0}}{\sqrt{\frac{t_1}{t_0}}} . \qquad [3.12]$$

3.3.1.6 Summary of the errors components

Table 3.1 summarizes the error components underlined in those paragraphs. The error components are classified according to the main source of errors that can be theoretically identified.

Table 3.1. Analysis of the potential causes of uncertainty in the measurement of the concentration by the PAS.

Index	Uncertainty causes
0	**Non identified : Type A standard uncertainties** Fidelity of the method.
1	**Measurand** Gas purity : dust, hygrometry, presence of other gas that absorbs at the same frequency.
2	**Instruments** Resolution of the PAS. Detection limit of the PAS. Calibration of the PAS. LIGHT Luminance Chopper frequency Half cone angle Function of transmission of the optical filter Model of a black body PAC Diameter of the cell Shape of the cell (non spherical, dead volumes …) MICROPHONE Calibration of the microphone (Sensitivity, linearity, fidelity).
3	**Operating Principle** Modeling Difference between the concentration of the gas sample and the concentration in the accumulation cell. Absorption of the light by the wall surfaces of the PAC. Absorption of the light by the germanium window of the PAC. Vibrations in the environment.
4	**Influence quantity** Pressure. Temperature.
5	**Humans means** Influence of the operator.

3.3.2 Calibration of the PAS

The estimation of the value of the combined uncertainty on the concentration measurement is complex by considering all the error components. Therefore, a calibration of the PAS by comparing the measurement with standard values suits better.

Operating principle

Standard mixtures of R-134a in clean air are provided by the chemistry department of the LNE using the gravimetric method: a well-known quantity of each gas is successively inserted into an evacuated gas cylinder. Their values $C_{mixture}$ are:

- Mixture M1 : (10.660 ± 0.055) µmol.mol^{-1} ;
- Mixture M2 : (42.40 ± 0.10) µmol.mol^{-1} and
- Mixture M3 : (1023.5 ± 5.2) µmol.mol^{-1}.

At first, these concentration mixtures were diluted using gas mass flow controllers in order to obtain several calibrated diluted concentrations $C_{diluted}$. The gas monitor was then calibrated by direct comparison with these diluted standard concentrations in the range of 0.020 to 100 µmol.mol^{-1}.

However, the experimental results showed a significant deviation between the low concentrations made by the dilution of M1 and M2 and the concentrations made by the dilution of M3 (see Figure 3.5). The mixtures were checked and coherent. A study of the coherence between the ratio of dilution has been carried out. It is based on the fact that a same concentration value can be created with different values of air flow rate and gas flow rate, while the standard mixture is the same: (1023.5 ± 5.2) µmol.mol^{-1}. The study has been carried out with R-134a. Results are reported in Figure 3.5. It can be concluded that the deviation is mainly due to the air flow rate: while a same concentration was expected for different values of volume flow rate, the spectrometer measures different values. The deviation can reach about 1.5 µmol.mol^{-1} for a concentration value about 10 µmol.mol^{-1}. The best examples are given for a concentration about 10 µmol.mol^{-1} and about 15 µmol.mol^{-1} (see Figure 3.6).

The combined uncertainty of a diluted standard concentration $C_{diluted}$ is maximized by the expression $U_{Cdiluted} = 0.027 \times C_{diluted}$ (see Section 2.2.5.2). It implies that the uncertainty due to the calibration of the spectrometer on the leak flow rate is higher than 2.7%.

As the objective is to measure a refrigerant leak flow rate with an uncertainty near 1%, this method is not adapted. Therefore, it was decided that the measurements of the PAS would be directly compared to the standard mixture provided by the chemistry department of the LNE. An addition of two mixtures was made: (77.83 ± 0.14) µmol.mol^{-1} ; (148.42 ± 0.30) µmol.mol^{-1}. A linear fitting can be calculated: $C_s = 1.0591 \times C_{read} - 0.46$ µmol.mol^{-1}. However, the maximal residual is equal to 0.95 µmol.mol^{-1}. Moreover, the residual repartition is not random. Rather than a linear fitting, a second order polynomial fitting is used to correct the concentration indications: $C_s = 0.00001792 \times C^2_{read} + 1.037 \times C_{read} - 0.203$ µmol.mol^{-1}. The maximal residual is then 0.074 µmol.mol^{-1} (see Figure 3.7).

However, even if the second order polynomial fitting will be considered, it needs to be confirmed by using more concentrations. The measurements of the spectrometer are correlated and the standard concentrations are also correlated. Therefore, the generalized least squares method will be developed in the future to improve the calibration quality of the spectrometer.

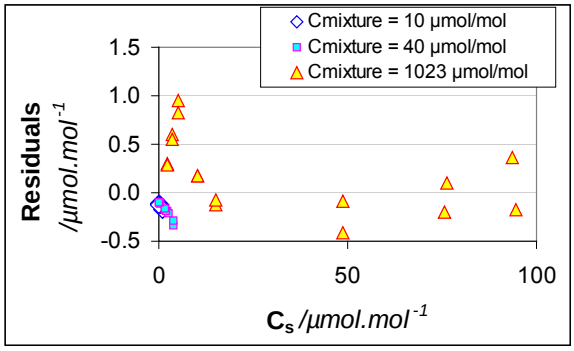

Figure 3.5. Residuals of a second order polynomial fitting of C_s=f(C_{read}) as a function of the diluted concentrations C_s made from the 3 standard mixtures (10.660 ± 0.055) µmol.mol^{-1}, (42.40 ± 0.10) µmol.mol^{-1} and (1023.5 ± 5.2) µmol.mol^{-1}.

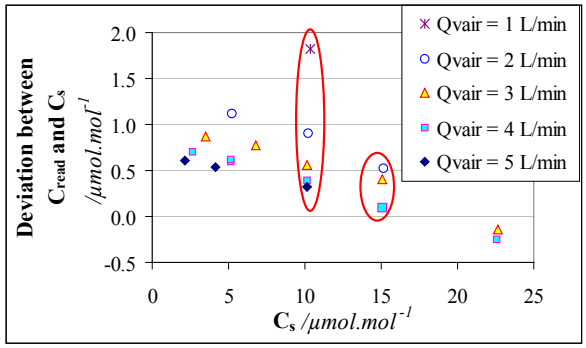

Figure 3.6. Deviation between the measurement of the spectrometer C_{read} and the diluted concentration C_s made from the standard mixture (1023.5 ± 5.2) µmol.mol^{-1}.with different ratios of gas/air volume flow rates, versus C_s.

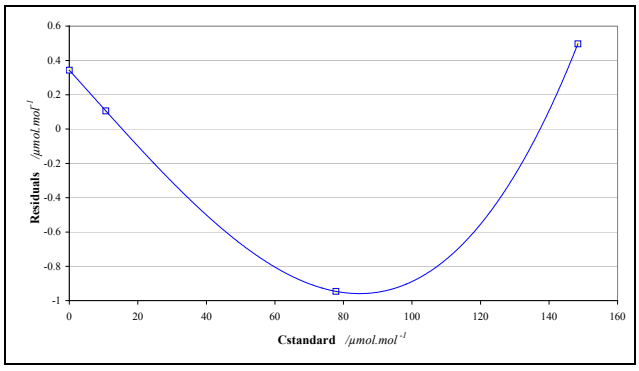

First order polynomial fitting

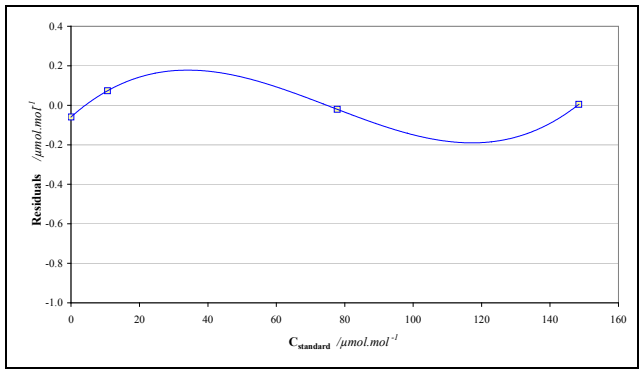

Second order polynomial fitting

Figure 3.7. Residual from the fitting of $C_{mixture}$=f(C_{read}).

Resolution of the PAS

The reading resolution of the gas monitor is limited to 3 digits. Therefore, the resolution is estimated to 1% of the measured value and the detection limit of the gas monitor is 0.015 µmol.mol^{-1}. As the resolution follows a rectangular distribution law, the uncertainty due to the resolution is (0.0087 + 0.0058 x C) µmol.mol^{-1}.

However, the resolution of the apparatus impacts the linearity of the apparatus. Therefore, it is considered that the component of uncertainty due to the resolution of the apparatus is included in the uncertainty of the variation of *PC/T* as a function of time. It will not appear in the uncertainty budget related to the calibration of the photo-acoustic spectrometer.

Environment

The PAS is sensitive to the pressure and the temperature of the environment. According to the manufacturer data, the spectrometer varies of 0.0015 µmol.mol^{-1} C^{-1} and of 7.5.10^{-5} µmol.mol^{-1}.hPa^{-1}. It has been checked that the PAS does not deviate significantly if the temperature varies from 23°C to 47°C. The deviation is lower than the resolution. Concerning the influence of the pressure, it has been checked in the range of 101 to 103 kPa. The deviation is also lower than the resolution.

Spectrometer stability

According to the manufacturer, the zero drift is estimated to 0.0050 µmol.mol^{-1} per month, while the sensitivity drift[9] is estimated to 0.83% per month. Considering that the manufacturer has adjusted the spectrometer in order to obtain the fitting $C_s = 1 \times C_{read}$ before delivering the apparatus, the first calibration of the spectrometer gives a first estimation of the apparatus stability:

- The range drift is about 0.3% per months, and
- The zero drift is about 0.024 µmol.mol^{-1} per month.

Thus the zero drift seems to be higher than expected. However, as the spectrometer aims at measuring a variation of concentration, the zero drift has not to be taken into account in the calculation of the uncertainty on the variation of the concentration. On the contrary, the sensitivity drift is a component of the uncertainty on the measurement of the variation of the concentration: it seems that this component was overestimated by the manufacturer.

In fact the analyzer was calibrated twice. Therefore, a first estimation of the stability of the concentration measurements can be done: the range drift is less than 0.72% in two months, which means a drift of 0.36% per month. It seems that the spectrometer stability value is lower than the manufacturer estimation. As the analyzer was calibrated only twice, the value of the manufacturer will be taken into account.

Uncertainty budget of the concentration measurement

The following budget of uncertainty (see Table 3.2) is a summary of the identified uncertainty components for the concentration measurements: only the components that impact the variation value of the concentration with time are taken into account. The repeatability is not considered yet: this component will be estimated by repeating the leak flow rate measurement. The combined uncertainty is expressed from the combined standard uncertainties calculated for the lower limit of the range and the upper limit of the range: U = (0.076 + 0.011 x C) µmol.mol^{-1}.

Table 3.2. Uncertainty budget related to the measurement of the concentration.

Components of uncertainty	**Unit**	**Standard uncertainty** */ unit*	**Sensitivity coefficient** */ µmol.mol^{-1}.unit^{-1}*	**Standard uncertainty**
Calibration	x C	2.6 x 10^{-4}	1	2.6 x 10^{-3} x ***C***
Temperature	°C	5.8 x 10^{-1}	1.5 x 10^{-3}	8.7 x 10^{-4} *µmol.mol^{-1}*
Pressure	hPa	5.8	7.5 x 10^{-5}	4.3 x 10^{-4} *µmol.mol^{-1}*
Stability (1 month)	x C	4.8 x 10^{-3}	1	4.8 x 10^{-3} *µmol.mol^{-1}*
Non applied correction				
Deviation of the model	0.074 *µmol.mol^{-1}*			

[9] Called the « range drift » by the manufacturer.

3.4 Measurement of the pressure

The pressure gauges used in this test bench have been calibrated in order to qualify the pressure measurement. Therefore, components of the uncertainty have been identified:

- components due to the characteristics of instruments: 2 digital barometers,
- component due to the correction that will be made on the indications of the pressure gauges (uncertainty due to the fitting),
- component due to the homogeneity of the pressure inside the test bench, and
- component due to the pressure variations due to the suction of the spectrometer micro-fan.

3.4.1 Calibration of the pressure gauges

Every 6 months, the calibration of the pressure gauge is performed by a direct comparison with a piston gauge of the LNE at the temperature of (20 ± 1)°C. The comparison is made from 100 hPa to 1300 hPa and from 1300 hPa to 100 hPa (see Figure 3.8). The uncertainty of the standard is (0.30 Pa + 3.0 x 10^{-5} x P). Then, the hysteresis, the stability, the resolution, and the correction to be made on the pressure indications of the pressure gauges can be established. The influence of the temperature on the pressure measurement can be established via the manufacturer information.

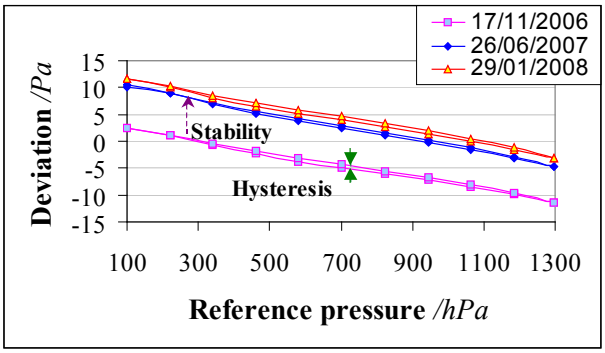

Figure 3.8. Deviation of the indication of the pressure gauge from the reference pressure as a function of the latter pressure.

The hysteresis is then verified. The hysteresis for a reference value is defined as the difference between the two measurements made for the same reference value: one made during the measurement from 100 hPa to 1300 hPa and one made during the measurement from 1300 hPa to 100 hPa. The hysteresis value of the instrument is quantified as the maximum value, considering every reference pressure.
The pressure gauges are calibrated every 12 months to check their stability. The stability for a reference pressure value is defined as the difference of the current deviation of the indication provided by the pressure gauge measuring the reference value and the former one. The instrument stability is quantified as the maximum value considering every reference value, as the shift is more or less a zero drift.

Some characteristics of the pressure gauge are also considered. The resolution of the apparatus is 0.1 Pa. According to the manufacturer, the pressure gauge is influenced by the temperature. In a room controlled at (20 ± 1)°C, the pressure uncertainty component due to the influence of the temperature is (1.2 x 10^{-5} x P).

Finally, based on measurements made during the calibration, the indications of the pressure gauge can be corrected. A relationship [3.13] between the reference pressure values and the related indications of the pressure gauge is determined thanks to the least squares method:

$P_{corr} = coeff1_P \times P_{read} + coeff0_P$, where [3.13]

$$coeff1_P = \frac{\sum_i\left(\frac{1}{u_2(P_{si})}\right)\cdot\sum_i\left(\frac{1}{u_2(P_{si})}\cdot P_{si}\cdot P_{readi}\right)-\sum_i\left(\frac{1}{u_2(P_{si})}\cdot P_{si}\right)\cdot\sum_i\left(\frac{1}{u_2(P_{si})}\cdot P_{readi}\right)}{\sum_i\left(\frac{1}{u_2(P_{si})}\right)\cdot\sum_i\left(\frac{1}{u_2(P_{si})}\cdot P_{readi}^2\right)-\left[\sum_i\left(\frac{1}{u_2(P_{si})}\cdot P_{readi}\right)\right]^2}, \text{ and} \quad [3.14]$$

$$coeff0_P = \frac{\sum_i\left(\frac{1}{u_2(P_{si})}\cdot P_{si}\right)\cdot\sum_i\left(\frac{1}{u_2(P_{si})}\cdot P_{readi}^2\right)-\sum_i\left(\frac{1}{u_2(P_{si})}\cdot P_{si}\cdot P_{readi}\right)\cdot\sum_i\left(\frac{1}{u_2(P_{si})}\cdot P_{readi}\right)}{\sum_i\left(\frac{1}{u_2(P_{si})}\right)\cdot\sum_i\left(\frac{1}{u_2(P_{si})}\cdot P_{readi}^2\right)-\left[\sum_i\left(\frac{1}{u_2(P_{si})}\cdot P_{readi}\right)\right]^2}. \quad [3.15]$$

The uncertainty due to the fitting is defined as the maximum absolute value of the residuals. This value is about 0.65 Pa.

Thus, the components of the pressure uncertainty due to the characteristics of the pressure digital pressure gauge and due to the correction applied to the measurement (linear fitting) has been identified and quantified. The following paragraphs discuss the homogeneity of the static pressure according to the altitude and the possible variations of the pressure during the calibration (due to the suction of the spectrometer micro-fan).

3.4.2 Homogeneity of the static pressure inside the accumulation volume

The static pressure in the installation is not homogenized. It depends on the altitude. Therefore, a correction must be made according to the local pressure. Figure 3.9 represents a diagram with the main components of the bench and the notation and definition of their related altitudes. The altitudes were measured with a ruler whose resolution is 1 mm (see Table 3.3). The reference altitude was taken at the manometer basement.

Considering the dependence between the pressure and altitudes, the indications of the pressure must be corrected. The correction of the pressure is expressed by Equation [3.16]:

$$Corr_P(z) = \rho_{gas} \cdot g \cdot (z - z_{mano}) . \quad [3.16]$$

The accumulation volume is composed of the accumulation cell, the PAS, the accumulation pressure gauge, and the fittings. Its height is estimated to (466.5 ± 4.3) mm. It means that the pressure inside the accumulation volume varies of about 5.5 Pa.

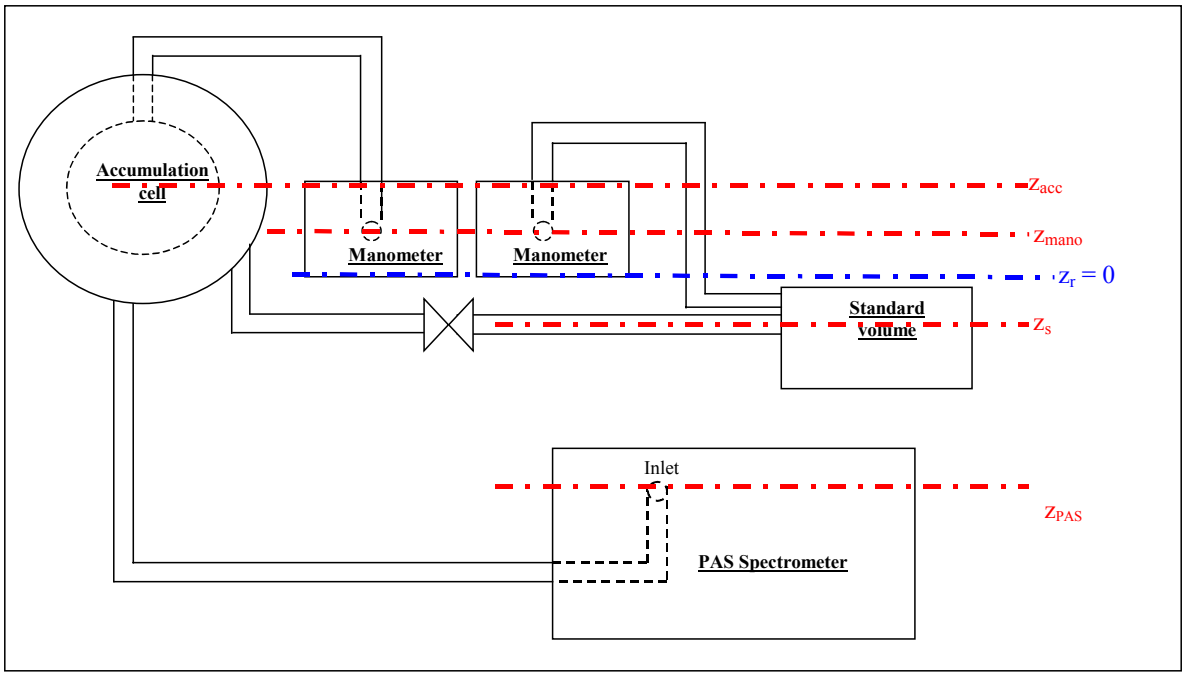

Figure 3.9. Diagram of the altitude of main components of the test bench.

Table 3.3. Summary of the different altitudes where to consider the pressure.

Altitude	Value of the altitude [mm]	Uncertainty of the altitude (k=2) [mm]	Description
z_{mano}	51.5	3.0	Altitude of the pressure gauges from a reference z_r.
z_{Acc}	149.0	3.0	Altitude of the center of the accumulation volume from a reference z_r.
z_s	67.5	3.0	Altitude of the center of the fittings connecting the volumes from a reference z_r.
z_{PAS}	-151.0	3.0	Altitude of the inlet of the PAS from a reference z_r.

3.4.3 Analysis of the influence of the PAS micro-fan suction on the pressure

As the PAS alternates a dynamic and a static mode (see Section 2.5.1), the influence of the suction of the spectrometer micro-fan on the pressure inside the accumulation volume must be studied. Therefore, variations along the time of the pressure inside the accumulation volume and of the differential pressure are studied in parallel during the calibration of a 7 g/yr^{-1} leak flow rate (see Figure 3.10).

The differential pressure gauge is stable when the PAS is measuring the tracer gas sample. Then, it indicates (0.8 ± 0.1) hPa. In parallel, the accumulation pressure rises with an amplitude of about 20 Pa, while the PAS is sucking. The phenomenon might be due to the installation of connections on the accumulation volume: the connection between the manometer and the accumulation volume is near the connection between the PAS outlet and the accumulation volume. Therefore, when there is an air circulation due to the suction of the PAS micro-fan, the pressure near the PAS outlet tends to increase. On the contrary, when the PAS is measuring, the pressure inside the accumulation volume decreases to finally stabilize at a minimum value. It can be noticed that, during the calibration, this minimum

pressure value tends to rise with the time – about 3 Pa.min^{-1}. It is due to the presence of the refrigerant leak. It implies an increase of the gas quantity inside the accumulation volume.

Considering these observations, the correction of the concentration with the pressure must be done carefully. The pressure must be the pressure at the accurate moment when the PAS takes the tracer gas sample which will be closed in the PAC. However, as the PAS is sucking, the pressure is not stabilized at this moment. It is then assumed that the pressure at the end of the previous measurement interval is similar to the pressure of the sample gas at the moment of its enclosure inside the PAC.

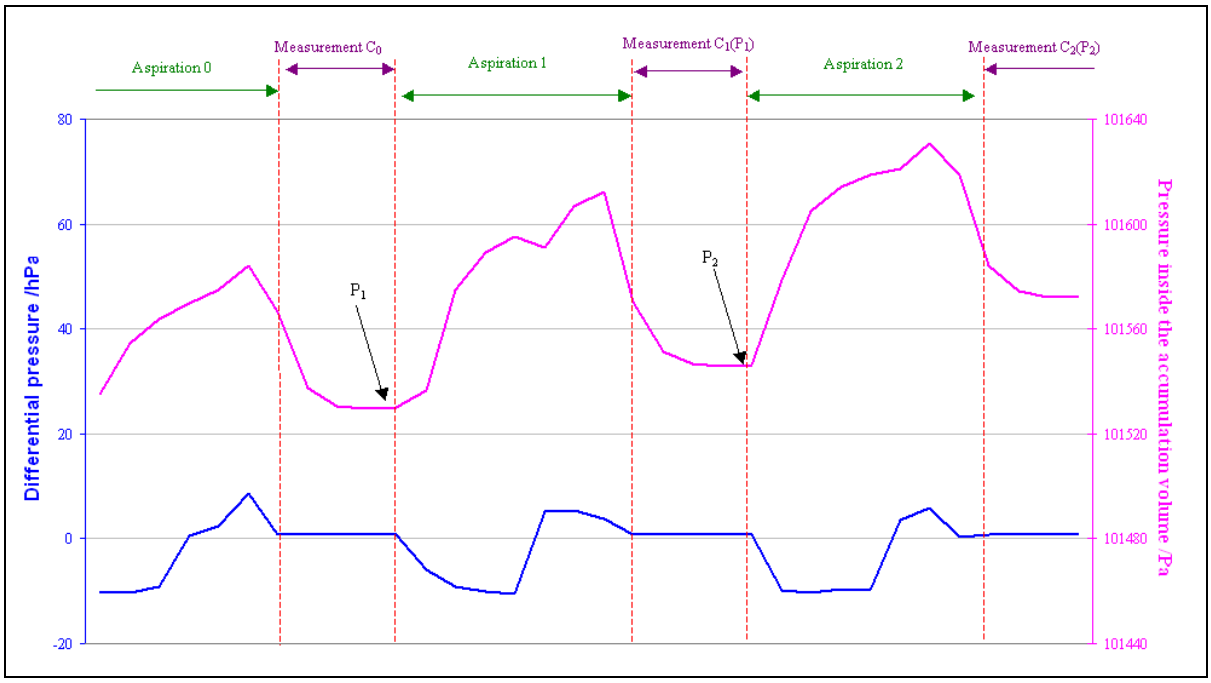

Figure 3.10. Sample of measurements of the differential pressure and the pressure inside the accumulation volume: calibration of a leak flow rate whose nominal value is 7 g/yr.

3.4.4 Expression of the pressure uncertainty

To conclude, the combined uncertainty of the pressure gauge connected to the accumulation volume is then $U = (5 + 2.1 \times 10^{-5} \times P)$ Pa (see Table 3.4). The uncertainty is lower than 8.0 Pa in the range of 10 kPa to 130 kPa. The combined uncertainty of the pressure gauge connected to the standard volume is then $U = (1.4 + 3.4 \times 10^{-5} \times P)$ Pa (see Table 3.5). The uncertainty is lower than 6.0 Pa in the range of 10 kPa to 130 kPa.

However, in the case of a leak flow rate calibration, only a difference of pressure is considered. The calibration is fixed at a pressure near the atmospheric pressure. Therefore, some components of uncertainty do not have to be considered:

- The stability of the apparatus is not considered as the calibration is done in less than one day
- The hysteresis is negligible
- The deviation from the model is less than 0.10 Pa for a pressure around 101 kPa.

For the calibration of a leak flow rate, the expanded uncertainty of the pressure in the accumulation volume is: $U = (0.43 + 3.8 \times 10^{-5} \times P)$ Pa (see Table 3.6). The uncertainty is lower than 5.0 Pa in the range of 100 kPa to 105 kPa.

Table 3.4. Uncertainty budget of the pressure measurement inside the accumulation volume: volume calibration.

Source of the uncertainty	Uncertainty	Standard uncertainty	Expression of the sensitivity coefficient	Standard uncertainty	Standard uncertainty
Calibration	0.36 Pa 3.0×10^{-5} x P	0.18 Pa 1.5×10^{-5} x P	1	0.18 Pa	1.5×10^{-5} x P
Resolution	0.10 Pa	0.06 Pa	1	0.058 Pa	
Hysteresis	4.0 Pa	2.31 Pa	1	2.3 Pa	
Deviation of the model (CNA)	0.63 Pa				
Stability (12 month)	4.0 Pa	2.00 Pa	1	2.0 Pa	
Temperature	1.0 °C	0.6 °C	2.0×10^{-05} Pa/°C		1.2×10^{-5} x P
Fluid column	3.0 mm	1.0 mm	1.1×10^{-07} Pa/mm		1.1×10^{-7} x P
Combined expanded uncertainty of the pressure measurement in the range from 10 kPa to 130 kPa (k = 2) $(6.6 + 1.6 \times 10^{-5} \times P)$ Pa					

Table 3.5. Uncertainty budget of the pressure measurement inside the accumulation volume: calibration of a refrigerant leak flow rate.

Source of the uncertainty	Uncertainty	Standard uncertainty	Expression of the sensitivity coefficient	Standard uncertainty	Standard uncertainty
Calibration	0.36 Pa 3.0×10^{-5} x P	0.18 Pa 1.5×10^{-5} x P	1	0.18 Pa	1.5×10^{-5} x P
Resolution	0.10 Pa	0.058 Pa	1	0.058 Pa	
Deviation of the model (CNA)	0.10 Pa				
Temperature	1.0 °C	0.58 °C	2.0×10^{-05} Pa/°C		1.2×10^{-5} x P
Fluid column	3.0 mm	1.0 mm	1.1×10^{-07} Pa/mm		1.1×10^{-7} x P
Combined expanded uncertainty of the pressure measurement in the range from 100 kPa to 105 kPa (k = 2) $(0.43 + 3.8 \times 10^{-5} \times P)$ Pa					

Table 3.6. Uncertainty budget of the pressure measurement inside the standard volume: volume calibration.

Source of the uncertainty	Uncertainty	Standard uncertainty	Expression of the sensitivity coefficient	Standard uncertainty	Standard uncertainty
Calibration	0.33 Pa 3.0×10^{-5} x P	0.18 Pa 1.5×10^{-5} x P	1	0.18 Pa	1.5×10^{-5} x P
Resolution	0.10 Pa	0.06 Pa	1	0.058 Pa	
Hysteresis	0.25 Pa	2.31 Pa	1	2.3 Pa	
Deviation of the model (CNA)	0.54 Pa				
Stability (12 month)	0.76 Pa	2.00 Pa	1	2.0 Pa	
Temperature	1.0 °C	0.6 °C	2.0×10^{-05} Pa/°C		1.2×10^{-5} x P
Fluid column	3.0 mm	1.0 mm	1.1×10^{-07} Pa/mm		1.1×10^{-7} x P
Combined expanded uncertainty of the pressure measurement in the range from 10 kPa to 130 kPa (k = 2) $(1.3 + 3.5 \times 10^{-5} \times P)$ Pa					

3.5 Measurement of the temperature

3.5.1 Description of the measurement chain of the temperature

Measurand

The temperature is measured by platinum resistance thermometers. There are 5 Pt100 probes in the test bench. Considering the platinum resistance thermometers whose sensors are placed inside the accumulation volume, the measurand is defined as the temperature of the gas inside the accumulation volume. Considering the platinum resistance thermometers whose sensors are placed in contact of the lateral wall of the accumulation volume, the measurand is defined as the temperature of the accumulation volume walls. Considering the platinum resistance thermometer whose sensor is placed inside the lateral wall of the standard volume, the measurand is defined as the temperature inside the walls of the standard volume.

Indication of the Pt100

Resistance thermometers, also called resistance temperature detectors (RTDs), are temperature sensors that exploit the predictable change of the electrical resistance of some materials while changing the temperature. The resistance thermometers are gained with stainless steel. Therefore, in the case of the Pt100 placed inside the accumulation volume for instance, the temperature of the platinum is neither the temperature of the air inside the accumulation volume nor the temperature of the air in contact with the stainless steel. The indication given by a Pt100 is a resistance value. They are four-wire ones, in order to compensate the addition of the resistances of wires.

Indication of the digital multimeter

A 6.5 digits multimeter is connected to the Pt100 and allows reading the resistance indications of the thermometers. Therefore, considering one Pt100, its measurand is the indication given by this Pt100. The digital multimeter gives an indication of the read resistance or an indication of the temperature, by using the standard relationship between the resistance and the temperature.

Summary

Figure 3.11 aims at summarizing the measurement chain of the temperature, considering all the cases.

3.5.2 Calibration of the digital multimeter

The calibration of the digital multimeter is performed by a direct comparison with the standard resistances RES110 and RES100 whose nominal values are respectively 110 Ω and 100 Ω. These resistances are calibrated at the temperature of (20 ± 1)°C, by the electrical metrology division of the LNE. The digital multimeter is configured to measure resistances of Pt100 with 4 wires and to indicate a resistance value.

Then, the indication given by the multimeter can be corrected: a linear relationship [3.17] between the indication and the standard values can be given:

$$RES_{corr} = SENS_{mult} \cdot (RES_{read} - RES100_{read}) + RES100 \text{ , where:} \quad [3.17]$$

$$SENS_{mult} = \frac{RES110 - RES100}{RES110_{read} - RES100_{read}} . \quad [3.18]$$

The combined uncertainty of a resistance measurement of the digital multimeter is composed of:

- the calibration of the standard resistances,
- the stability of the standard resistances,
- the resolution of the multimeter indication, and
- the accuracy of the indication of the multimeter.

The uncertainty budget is given in Table 3.7.

Table 3.7. Uncertainty budget of the indication of the multimeter, which measures the resistance indicated by a Pt100.

Source of the uncertainty	Uncertainty [Ω]	Distribution law	Standard uncertainty [Ω]	Expression of the sensitivity coefficient	Sensitivity coefficient value	Standard uncertainty of the indication of the multimeter [Ω]
Resolution	0.0001	√12	0.000029	1	1	0.000029
Calibration of the resistance RES_{100}	0.0001	2	0.000050	$1+(R-RES_{100}^{read}) \times (RES_{110}^{read}-RES_{100}^{read})/(RES_{110}-RES_{100})^2$	1	0.000054
Calibration of the resistance RES_{110}	0.00055	2	0.00028	$-(R-RES_{100}^{read}) \times (RES_{110}^{read}-RES_{100}^{read})/(RES_{110}-RES_{100})^2$	-0.078	0.000021
Stability of the resistance RES_{100}	0.0004	√12	0.00012	$1+(R-RES_{100}^{read}) \times (RES_{110}^{read}-RES_{100}^{read})/(RES_{110}-RES_{100})^2$	1.078	0.00012
Stability of the resistance RES_{110}	0.0001	√12	0.000029	$-(R-RES_{100}^{read}) \times (RES_{110}^{read}-RES_{100}^{read})/(RES_{110}-RES_{100})^2$	-0.078	0.0000023
Accuracy	0.0016	√12	0.00046	1	1	0.00046
Combined standard uncertainty of the resistance measurement [Ω] 0.00048						

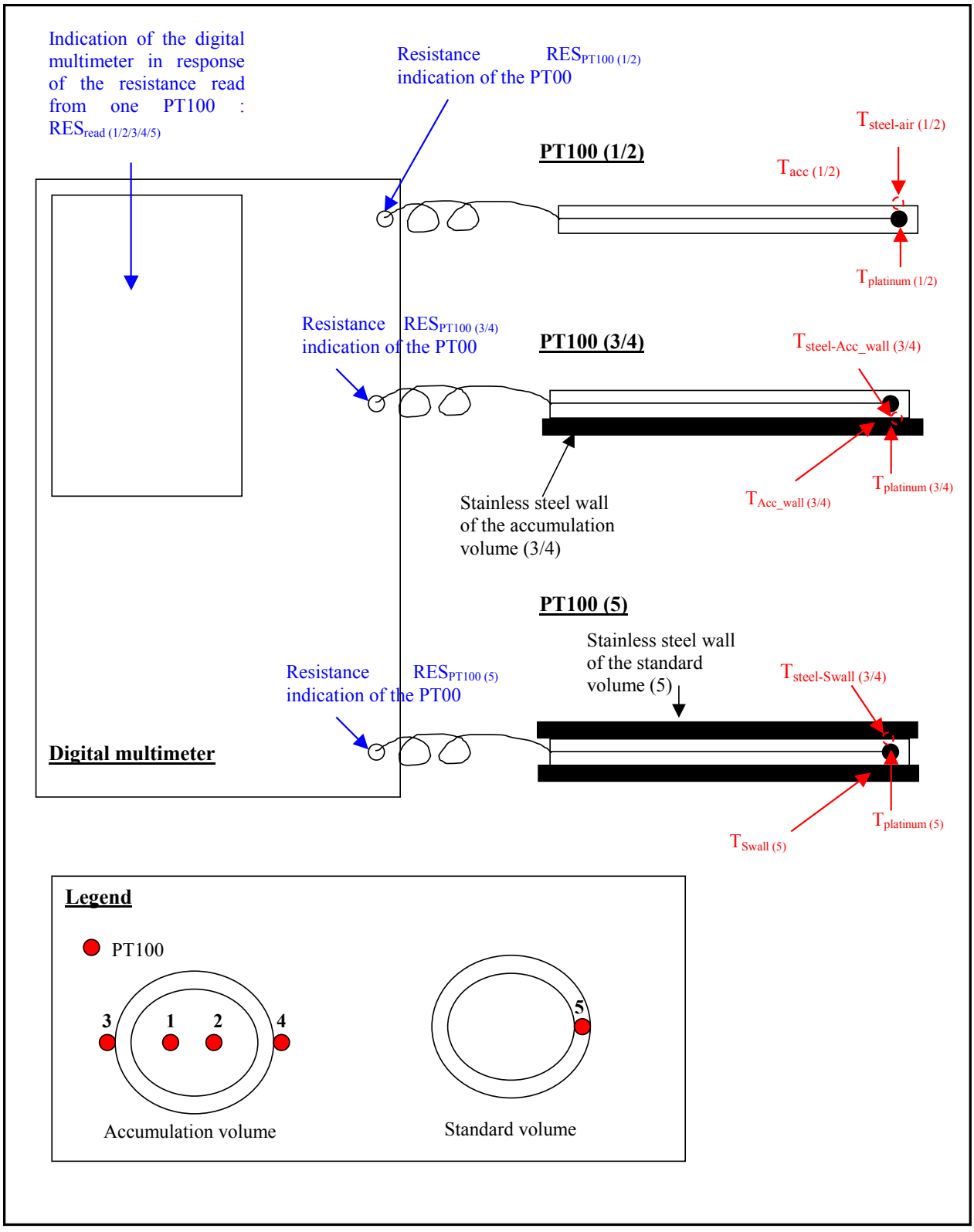

Figure 3.11. Diagram of the temperature measurement chain in the bench to calibrate refrigerant leaks.

3.5.3 Calibration of the Pt100

The calibration of the Pt100 is carried out by comparison with a standard Pt100 in a constant-temperature bath at 0°C and at 20°C. The uncertainty due to the calibration is U = 0.030 °C. This uncertainty was calculated considering the standards, the calibration means, the environment, the contribution of the calibrated instrument, the repeatability etc.

According to the standard NF EN 60751, a relationship between the temperature and the corresponding resistance is standardized. Equation [3.19] is available for the range from 0 °C to 850 °C:

$RES_{Pt100} = 100 . (1 + coeff1_{Pt100} . T + coeff2_{Pt100} . T^2)$, with [3.19]

$Coeff1_{Pt100} = 3.90802 \times 10^{-3}\ °C^{-1}$, and

$Coeff0_{Pt100} = -5.802 \times 10^{-7}\ °C^{-1}$.

However, in this case, the relationship [3.20] between the temperature and the corresponding resistance is considered as a linear relationship:

$RES_{Pt100} = SENS_{Pt100} . (T-T_{20°C}) + RES_{20°C}$, where [3.20]

$$SENS_{Pt100} = \frac{RES_{20°C} - RES_{0°C}}{T_{20°C} - T_{0°C}} . \quad [3.21]$$

The temperature room in the laboratory is about (20 ± 1) °C. In this range, the relationship can be considered as linear: there is however a deviation due to the fitting. The deviation generated by a linear fitting is determined as 0.010 °C for a temperature varying in the range (20 ± 1) °C. This correction is not applied on the measurement results.

Besides, as the platinum resistance thermometers are calibrated every 4 years, it is necessary to determine an uncertainty component due to the stability of the thermometers. As these thermometers are recent ones, the uncertainty component due to the stability cannot be calculated via measurements yet. According to the data base of the LNE, the stability of similar Pt100 is less or equal to U = 0.030 °C.

The combined uncertainty of the measurement by a Pt100 is then composed of:

- The calibration of the Pt100, and
- The stability of the Pt100 for 4 years.

Besides, as the resistance is fitted with the temperature linearly, an additional uncertainty component NAC is considered. Thus, the uncertainty budget can be established (see Table 3.8). The combined uncertainty is expressed by Equation [3.22]:

$$u_{Pt100} = \sqrt{u^2_{calibration} + u^2_{stability}} + NAC_{fitting} . \quad [3.22]$$

Table 3.8. Uncertainty budget of the measurement of the temperature of the gas near the sensor by the Pt100

Source of the uncertainty	Uncertainty *(°C)*	Distribution law coefficient	Standard uncertainty *(°C)*	Sensitivity coefficient	Standard uncertainty *(°C)*
Calibration	0.030	2	0.015	1	0.015
Stability (4 years)	0.030	2	0.015	1	0.015
Fitting	0.010				

3.5.4 Expression of the temperature uncertainty

The corrected value of the temperature is then expressed by Equation [3.23]:

$$T = \frac{\left(SENS_{mult} \cdot \left(RES_{read} - RES100_{read} \right) + RES100 \right) - RES_{20°C}}{SENS_{Pt100}} + T_{20°C} . \qquad [3.23]$$

The combined uncertainty of the temperature measurement is due to:

- the multimeter calibration,
- the Pt100 calibration, and
- the homogeneity in the system.

Typically, the deviation between the corrected measurement of the temperature by the 2 Pt100 in contact with the walls of the accumulation volume are inferior or equal to 0.20 K. The homogeneity of the temperature inside the accumulation volume is inferior to 0.20 K. It will be assumed that the homogeneity of the temperature inside the accumulation volume takes also the value of 20 °C following a rectangular law with a range of (20 ± 0.20)°C. The deviation of the corrected measurement between the Pt100 in contact with the walls of the accumulation volume and the Pt100 inside the lateral wall of the standard volume is inferior or equal to 1.0°C.

This significant deviation is due to the fact that the standard volume is located near the spectrometer and the pressure gauges on the contrary near the accumulation volume. Therefore there is a small gradient of temperature between both volumes. A system to isolate the volumes from the instrument is going to be build in order to improve the homogeneity of the temperature of the test bench. A difference exists between the measured quantities. The Pt100s related to the accumulation volume are only in contact with the lateral wall, while the Pt100 related to the standard volume is placed in the middle of the lateral wall of the standard.

Thus, Table 3.9 presents the uncertainty budget of the measurement of the temperature related to one of the volume. The expanded combined uncertainty of the temperature related to one volume is: U_T (1 volume) = 0.14°C. As the homogeneity of the temperature of both volumes is inferior or equal to 1.0°C, the expanded combined uncertainty of the temperature related to both volumes is U_T (Both volumes) = 0.59°C.

With an isolation of both volumes from the instruments, an improvement of the uncertainty of the temperature measurement is expected. It will be due to an improvement of the homogeneity of the temperature of both volumes.

Table 3.9. Uncertainty budget of the measurement of the gas temperature inside the accumulation volume or of the lateral wall of the accumulation volume.

Source of the uncertainty	Uncertainty	Distribution law coefficient	Standard uncertainty	Sensitivity coefficient	Standard uncertainty (°C)
Calibration of the multimeter	0.0020 Ω	2	0.0010 Ω	$1/SENS_{Pt100}$ °C/Ω	0.0031
Calibration of the Pt100	0.070°C	2	0.035°C	1	0.035
Homogeneity of the temperature inside one volume	0.20°C	√12	0.058°C	1	0.058

3.6 Measurement of the volume

3.6.1 Description of the standard volume

The accumulation volume value can be deduced from the value of the standard volume and from Equation [2.23]. The design of the standard volume aims at making a volume with simple shapes in order to calibrate it dimensionally [REDG99] with a relative uncertainty of 0.1% or better. Therefore, the volume is a cylinder made of stainless steel 316L - the "main cylinder" - sealed with O-rings and mainly composed of an opened cylinder and two lids manufactured by the LNE. The combined uncertainty of the standard volume will be mainly due to the tolerances related to the dimensions, the roughness of the interior walls, and the parallelism of the opposite interior walls. These parameters were controlled in the manufacturing process.

The standard volume is also composed of:

- the fittings between the accumulation volume and the standard volume, including the dead volume of the valve VVE0,
- the fittings between the main cylinder and the pressure gauge, and
- the dead volume of the pressure gauge.

Considering the system {Accumulation volume + Standard volume} as leak free, a simulation of the uncertainty of the size of the accumulation volume has been performed taking into account the thermal phenomena involved by the gas expansion. This simulation aimed at determining the optimal size of the standard volume compared to the nominal value of the accumulation volume size (see Chapter 2). The optimal nominal value of the standard volume was estimated to 0.5 dm^3.

3.6.2 Calibration of the standard volume

The main cylinder is calibrated by a tri-dimensional standard machine. It estimates:

- the mean value of the cylinder diameter,
- the deviation from the mean value of the diameter at different heights,
- the cylinder length,
- the flatness of both lids, and
- the parallelism of the opposite interior walls.

Considering those parameters, the main cylinder and its expanded uncertainty (k = 2) were calculated:

V_{cyl} = (0.50818 ± 0.00035) dm^3 (see Table 3.10).

The additional volumes, as the volume of the fittings, the dead volumes of the valve VVE0, and pressure gauge, are calculated based on the suppliers' scaling drawings and information. Consequently, the standard volume and its expanded uncertainty (k = 2) were calculated:

V_s = 0.51279 ± 0.00056 dm^3, which represents a relative expanded uncertainty of 0.11%.

Table 3.10. Uncertainty budget related to the calibration of the standard volume.

Main cylinder						
Components	**Unit**	**Uncertainty**	**Distribution law coefficient**	**Standard uncertainty**	**Sensitivity coefficients**	**Standard uncertainty [mm^3]**
Uncertainty of the diameter	*mm*	0.0034	2	0.0017	12320 mm²	21
Deviation of the diameter from the mean value	*mm*	0.011	3	0.0037	12320 mm²	45
Uncertainty of the measurement of the length of the cylinder	*mm*	0.010	2	0.0050	5346 mm²	27
Uncertainty in the determination of the flatness of the flanges	*mm*	0.0015	2	0.0008	5346 mm²	4
Flatness of the upper flange	*mm*	0.0070	√3	0.0040	5346 mm²	22
Flatness of the lower flange	*mm*	0.047	√3	0.027	5346 mm²	150
Deviation in the definition of the reference plane	*mm*	0.024	√3	0.013	5346 mm²	74
Thermal expansion	*K*	1 K	√3	0.58 K	24.4 mm^3.K^{-1}	14

3.6.3 Description of the instrumentation

In order to measure directly the accumulation volume, a pneumatic circuit "the standard volume circuit" was added in comparison to the previous test benches developed by the CEP: it is mainly composed of the standard volume and series of valves (see Figure 2.12 in Chapter 2). A pressure gauge measures the pressure inside the standard volume with an uncertainty of U = 8 Pa. A platinum resistance thermometer measures the temperature of the walls of the standard volume. Therefore the temperature of the gas inside the volume is not directly measured. The temperature of walls is not significantly influenced by the quick variation of temperature inside the volume: according to the initial conditions, the total mass of air inside both volumes is around 2.8 g, while the mass of the stainless steel standard volume is around 12 000 g, and the mass of the stainless steel accumulation cell is around 4 000 g. Thus, a variation of air temperature inside both volumes hardly initiates a variation of the temperature of walls. For instance, an air variation of 1 K implies a variation of about 0.002 K of the temperature of the accumulation-volume walls and a variation about 0.0005 K of the temperature of the standard-volume walls, which is less than the sensitivity of the thermometer [HOL65].

A similar pressure gauge measures the pressure inside the accumulation cell with an uncertainty of 15 Pa. A couple of platinum resistance thermometers measures the temperature inside the accumulation cell and another couple measures the wall temperature of the accumulation cell. The thermometer diameters are around 3 mm. Even if the temperature inside the accumulation cell is measured, the response time of the thermometer is too long. Therefore, in case of a quick temperature variation, the amplitude of changes cannot be correctly detected. In order to ensure that the system has reached the equilibrium, a minimum stabilization time must be estimated. Consequently the thermal phenomena were studied, as described below.

3.6.4 Determination of the stabilization time of the thermal phenomena

The influence of the volumes ratio is defined for a system at the equilibrium state [HOL69], [JIT90]. During the transient regime, gas compression in a volume implies gas heating, while an expansion implies gas cooling in the range of the studied pressure and temperature [PICK48]. However, the changes of temperature during transient regime cannot be measured with the formerly described apparatus as the changes are too fast. Therefore, the parameters must be considered at the equilibrium state and the needed time δ for equilibrating the system must be determined [HOL65].

3.6.4.1 1D thermal modeling

In order to estimate δ, a thermal modeling study of 1D was carried out using the Thermette software developed by the CEP. This modeling allows calculating the temperature spatial fields in dynamic mode as a function of thermo-physical properties and solicitations. However, in order to integrate the equations of the model, the knowledge of the flow rate and the convection coefficients are necessary.

Fitting of the expanded flow rate

To fit the expanded flow rate, the regular and singular losses between volumes were established according to the theory ([IDEL69], [BOU90], and [CARL72]), the design and the fittings of the test bench. The studied system is only composed of tubes, fittings, and valves connecting the accumulation volume to the standard volume. The following assumptions are considered:

- the expanded gas inside both volumes during the calibration of the accumulation volume is clean air, considered as a perfect gas,
- the expansion in the studied system is isenthalpic.

By considering the perfect gas law, the equation of continuity - the Bernoulli equation - the expanded flow rate was modeled by iteration. The flow rate is fitted as a function of the pressure difference between both volumes and of the gas density inside the accumulation volume: $Q = f(\Delta P, \rho)$.

First, as density depends on the pressure, the system will be divided in several parts where the density is considered as constant (see Figure 3.12). The gas is perfect. Therefore, the density is known by the perfect gas law [3.24]:

$$\rho = \frac{P.M}{R_g.T} \qquad [3.24]$$

where

M	Molar Mass
P	Pressure
R_g	Perfect gas constant
T	Temperature
ρ	Density

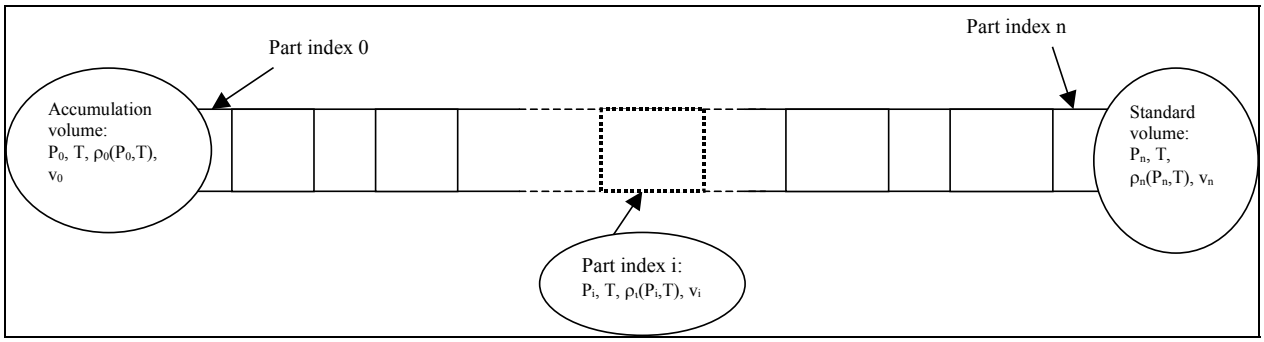

Figure 3.12. Modeling the expanded flow rate: representation of the studied system divided in n parts.

Considering one part of the system, the gas is incompressible and the flow regime is permanent. Therefore, the difference between the upstream and the downstream pressures of the part (index i) can be calculated from the Bernoulli Equation [3.24] knowing the average gas speed, the average density, and the singular and the regular pressure losses inside the concerned part of the system:

$$\Delta\Pi_{i+1\to i}=\Delta P_{i\to i+1}+\rho_i\cdot g\cdot\Delta z_{i\to i+1}+\rho_i\cdot\frac{\Delta v^2_{i\to i+1}}{2}, \qquad [3.24]$$

where

g	Acceleration of gravity
T	Temperature
$\Delta P_{i\to i+1}$	Variation of the pressure between the part (index i) and the part (index i +1)
$\Delta v_{i\to i+1}$	Variation of the speed between the part (index i) and the part (index i +1)
$\Delta z_{i\to i+1}$	Variation of the altitude between the part (index i) and the part (index i +1)
$\Delta\Pi_{i+1\to i}$	Pressure loss between the part (index i) and the part (index i +1)
ρ_i	Mean density in the part (index i)

and

$$\Delta\Pi_{i+1\to i}=\frac{\psi_i^{\,regular}\cdot\rho_i\cdot v_i^2\cdot l}{2\cdot D_i}+\frac{1}{2}\cdot\sum_j\cdot\psi_j^{\,singular}\cdot\rho_i\cdot v_i^2 \qquad [3.25]$$

where

D_i	Characteristic diameter of the part (index i)
l	Length
$\psi_i^{regular}$	Regular pressure loss coefficient
$\psi_i^{singular}$	Singular pressure loss coefficient

The regular and all the singular losses (index j) in each part were calculated using the architecture of the system and literature sources ([IDEL69], [BOU90], [CARL72]).

Finally, the law of mass conservation for a permanent flow allowed establishing a relation between the average speed and the average density of a part i of the system. Indeed the flow rate of the expanded gas $Q_m=\rho.v.S$ inside the system is constant for fixed values of pressure inside both volumes.

Therefore by iteration on the average speed in the part 0 of the system, the mass flow rate can be calculated as a function [3.26] of the difference of the pressures respectively in the accumulation volume (P_0) and the standard volume (P_n), and of the density $\rho_0(T)$ (see Figure 3.13):

$$Q_m=(A_6\cdot\rho+B_6)\Delta P^6+(A_5\cdot\rho+B_5)\Delta P^5+(A_4\cdot\rho+B_4)\Delta P^4+(A_3\cdot\rho+B_3)\Delta P^3+(A_2\cdot\rho+B_2)\Delta P^2+(A_1\cdot\rho+B_1)\Delta P \qquad [3.26]$$

with A_6=-5.782 x 10^{-32} $m^3.s^{-1}.Pa^{-6}$; A_5=1.573 x 10^{-26} $m^3.s^{-1}.Pa^{-5}$; A_4=-1.662 x 10^{-21} $m^3.s^{-1}.Pa^{-4}$;
A_3=8.616 x 10^{-17} $m^3.s^{-1}.Pa^{-3}$; A_2=-2.316 x 10^{-12} $m^3.s^{-1}.Pa^{-2}$; A_1=3.988 x 10^{-8} $m^3.s^{-1}.Pa^{-1}$;
B_6=-1.391 x 10^{-31} $kg.s^{-1}.Pa^{-6}$; B_5=5.366 x 10^{-28} $kg.s^{-1}.Pa^{-5}$; B_4=5.675 x 10-23 $kg.s^{-1}.Pa^{-4}$;
B_3= 2.950 x 10^{-18} $kg.s^{-1}.Pa^{-3}$; B_2= 7.985 x 10^{-14} $kg.s^{-1}.Pa^{-2}$; B_1=1.366 x 10^{-9} $kg.s^{-1}.Pa^{-1}$.

The relative deviation between the modeled mass flow rate and the one calculated by iteration reaches a maximum of 8.5%.

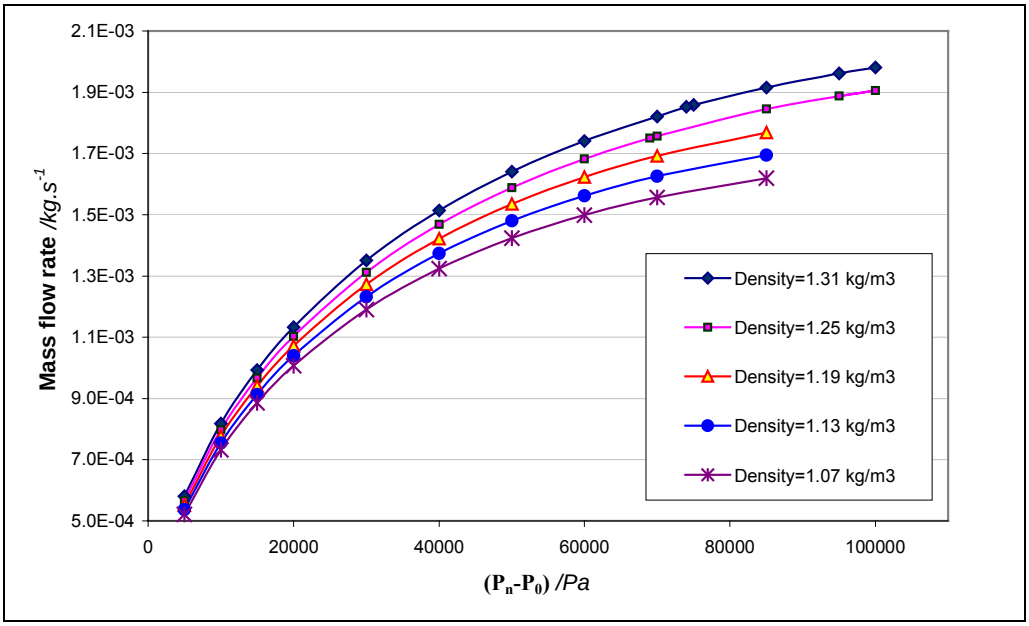

Figure 3.13. Calculated mass flow rate versus the pressure difference between the accumulation and the standard volumes and the density in the accumulation volume.

Model of the thermal transfers

Once the expression of the mass flow rate is established, the accumulation and the standard volumes are studied as two independent entities. Only the mass transfer from the accumulation volume to the standard volume is considered. A platinum resistance thermometer is also simulated inside the accumulation volume.

Each volume and the platinum resistance thermometer are considered separately during the transient regime. Considering that the walls are rigid, an explicit integration of the temperature can be deduced from the first law of the thermodynamics:

$$\frac{dE_{int}^{*}}{dt} = \sum_{e-s} Q_m \cdot h^{*} + \dot{E}_{heat}$$

$$\Rightarrow T_{gas}(t+\Delta t) = \frac{\Delta t}{m(t)\cdot C_V}\cdot\left[h_{gas}\cdot S_{Wall}\cdot\left(T_{Wall}-T_{gas}(t)\right)-Q_m\cdot\left(\frac{R_g}{M}\cdot\left(T_{gas}(t)-T_0\right)+h_0-e_{int0}\right)\right]+T_{gas}(t) \qquad [3.27]$$

where:

C_v	Heat capacity at constant volume
D	Diameter
E_{int}	Internal energy
e_{int0}	Internal energy of 1 kg of gas at T_0
E_{heat}	Heat energy
h*	Enthalpy of 1 kg of gas
h_0	Reference enthalpy of 1 kg of gas at T_0
h_{gas}	Convection coefficient of the gas
M	Molar Mass
m(t)	Mass at the instant t
Q_m	Mass flow rate
S_{wall}	Wall surfaces
T_0	Reference temperature (= 293.15 K)
$T_{gas}(t)$	Gas temperature at the instant t
T_{wall}	Wall temperature
t	Time

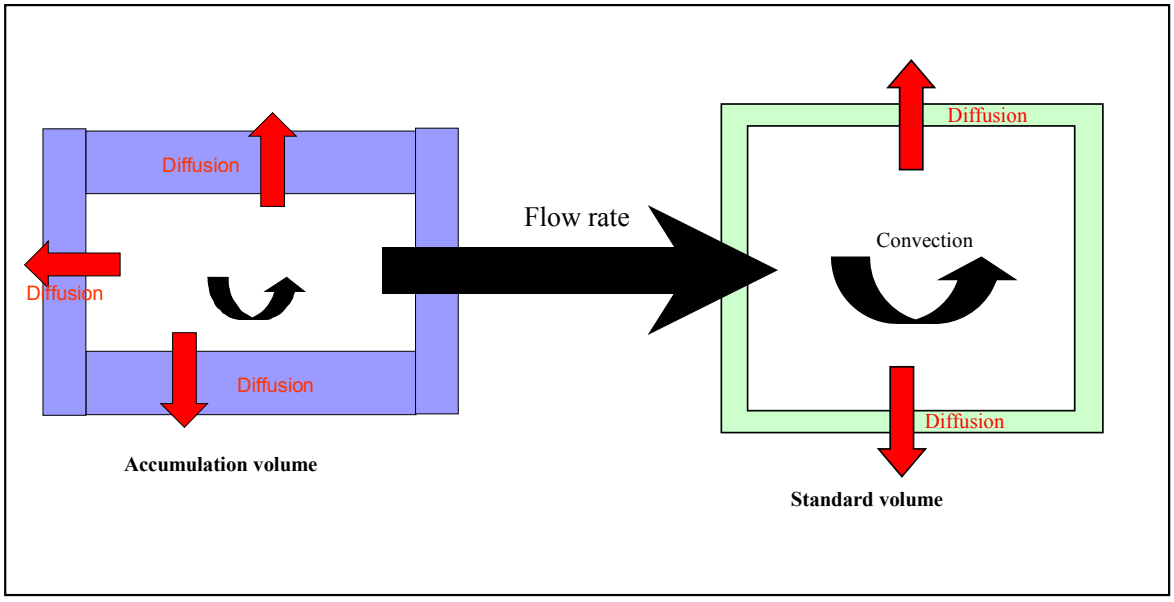

Figure 3.14. Modeling of thermal and mass transfers of two distinct systems: the accumulation and the standard volume.

Therefore it was necessary to determine the convection coefficient h_{gas}. The standard volume and the accumulation volume, as well as the platinum resistance thermometer, were assumed horizontal and isothermal cylinders. The external convection coefficient for each volume or thermometer can be

deduced from the expression of the Nusselt Number $\mathrm{Nu_D} = \frac{h_{gas} \cdot D}{K}$.

The Nusselt number is fitted by the Morgan equation: $\mathrm{Nu_D} = \mathrm{A} \cdot \mathrm{Ra_D^n}$. Values of the real numbers in the couple *(A,n)* depend on the value of Ra_D. Ra_D the Rayleigh number defined by:

$$\mathrm{Ra_D} = \frac{\mathrm{g} \cdot \beta_\mathrm{V} \cdot \rho^2 \cdot \mathrm{C_p} \cdot \left|\mathrm{T_{wall}} - \mathrm{T_{gaz}}\right| \cdot \mathrm{D}^3}{\mathrm{K} \cdot \mu} \quad . \qquad [3.28]$$

The couples (A,n) are evaluated in Table 3.11 according to the literature [PAD05] and [PET_ECP].

Table 3.11. Values of the parameters A and n as a function of the Ra_D value [PAD05].

A	**n**	**Ra_D**
0.675	0.058	10^{-10} à 10^{-2}
1.020	0.148	10^{-2} à 10^{2}
0.850	0.188	10^{2} à 10^{4}
0.480	0.250	10^{4} à 10^{7}
0.125	0.333	10^{7} à 10^{12}

However, a model of the internal convection coefficient is available for vertical cylinders only: the Elenbaas' model (see [PAD05] and [PET_ECP]). It will be used to estimate the internal convection coefficient relative to each volume as there is no model for horizontal cylinders:

$$\overline{\mathrm{Nu}} = \frac{\mathrm{Ra}^*}{16}\left[1 - \exp\left(-16 \cdot \left(\frac{1}{2 \cdot \mathrm{Ra}^*}\right)^{3/4}\right)\right], \qquad [3.29]$$

with the modified Rayleigh number Ra^* is defined by: $\mathrm{Ra_D^*} = \mathrm{Ra_D} \cdot \mathrm{D} \cdot \mathrm{L}^{-1}$.

Once the flow rate and the convection coefficients are fitted, the pressure and the temperature of each volume and the temperature measured by the platinum resistance thermometer can be simulated (see Figure 3.15).

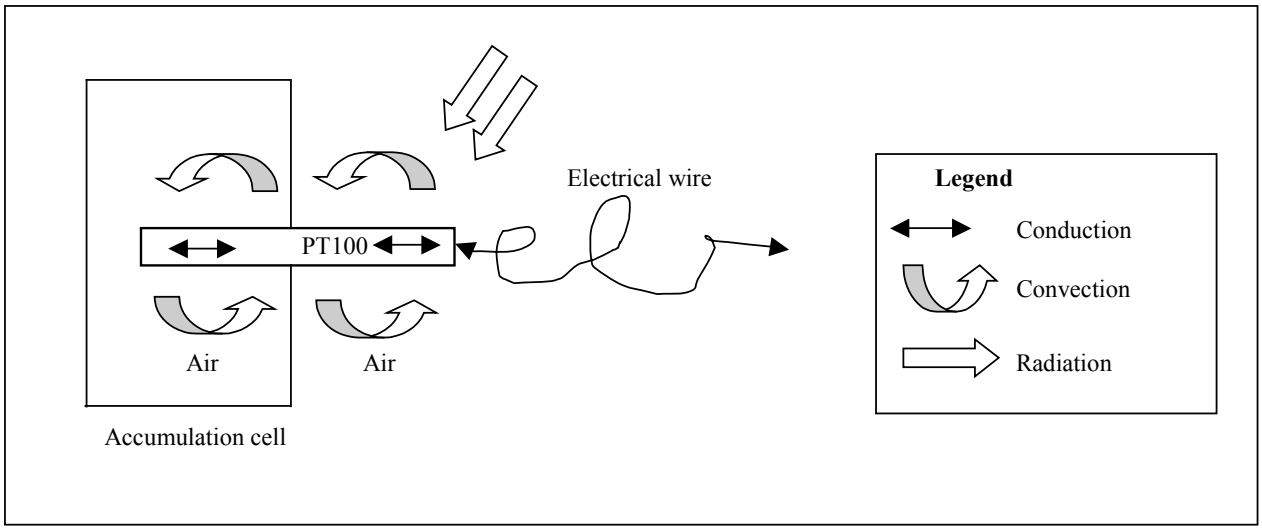

Figure 3.15. Modeling of heat transfer relative to the platinum resistance thermometer.

The temperature is estimated thanks to the first law of thermodynamics and the pressure is estimated via the perfect gases' law. By integrating these equations in the software Thermette, the changes in temperatures and pressures as a function of time when the valve is opened are simulated.

Results of the simulation

The pressures calculated by the model reach the equilibrium after a short period of time, typically after 150 s (see Figure 3.16). Changes of temperature in the standard volume, initially at 20 kPa, and in the accumulation volume, initially at 117 kPa, increased by more than 20 K and decreased by about 5 K respectively. They stabilize at a temperature around the wall temperature from the beginning of the expansion after 150 s (see Figure 3.17). The wall temperature is hardly influenced by these changes, which is in agreement with the theory. The simulated platinum resistance thermometer Pt100 with a diameter of 3 mm (see Figure 3.18) underlines the fact the changes of temperature are highly attenuated: according to the simulation results, a variation of less than 0.5 K in 25 s is measured by the Pt100 while there is in reality a change of 5 K inside the volume in less than 10 s. The measurements of the Pt100 are not stabilized 400 s after the beginning of the expansion, while the temperature of the gas in the model is in reality stabilized around 150 s after that beginning.

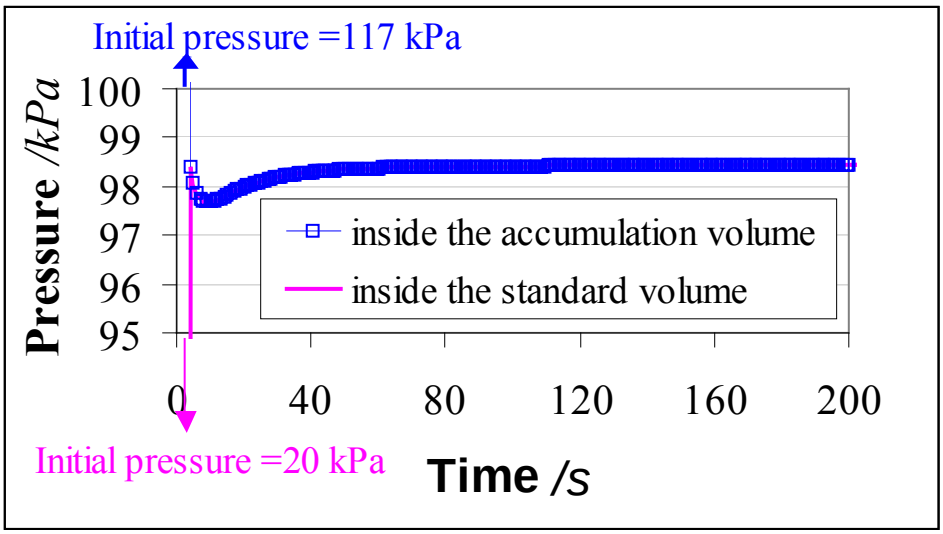

Figure 3.16. Simulation of an expansion from the accumulation volume to the standard volume: variation of pressures.

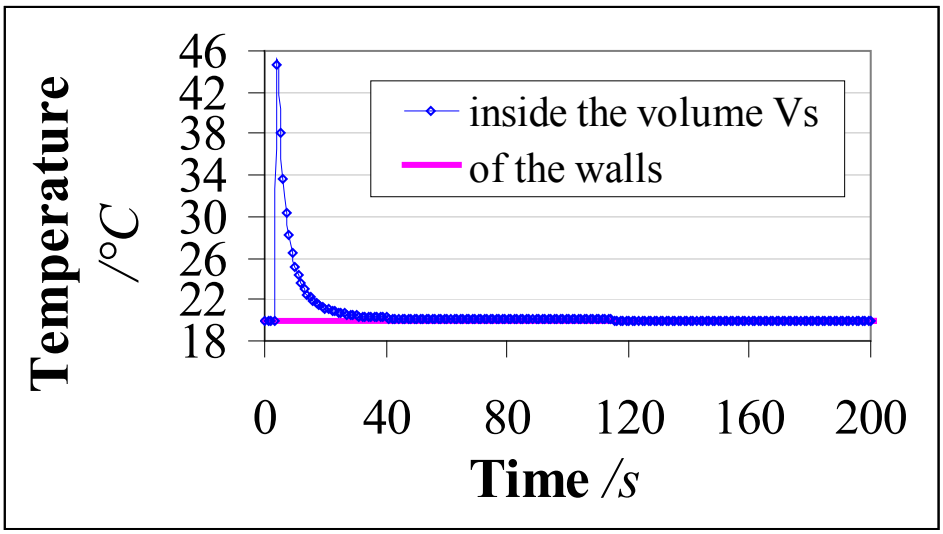

Figure 3.17. Simulation of an expansion from the accumulation volume to the standard volume: variation of the standard volume wall temperature and gas temperature.

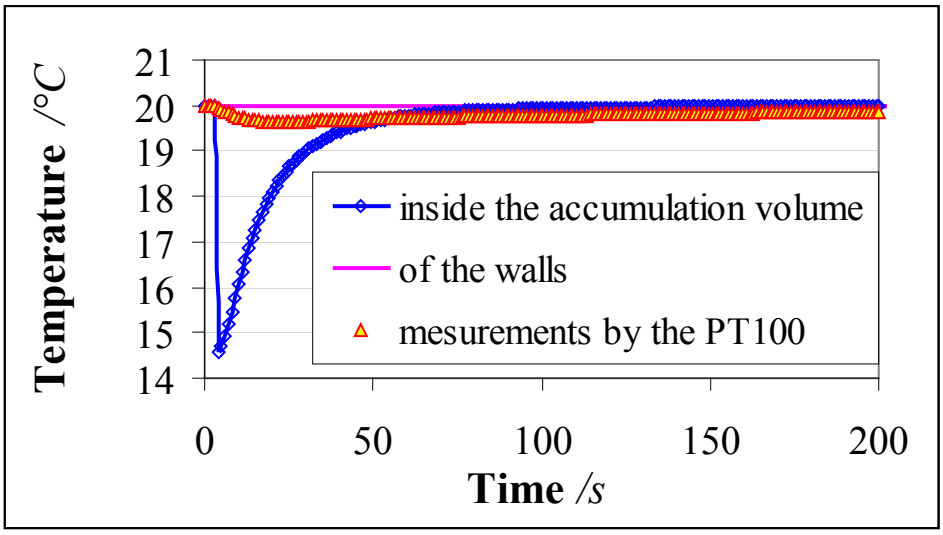

Figure 3.18. Simulation of an expansion from the accumulation volume to the standard volume: variation of the accumulation volume wall temperature, of the gas temperature and its measurement by a Pt100.

The convection coefficient is low and has no significant impact on the stabilization time. However, the simulated expansion flow rate may have a huge impact on the changes of temperature and on the stabilization time. It is difficult to estimate the reliability of the simulated value of those parameters. Therefore the main issue is to evaluate the influence of the expansion flow rate. Experimentations must then complete the analyses. As the temperatures are not measured with a sufficiently small response time, the discussion will mainly concern the pressure measurements.

3.6.4.2 Experimentation: expansion between two volumes

Due to the gas monitor, the pressure in the accumulation volume cannot exceed 110 kPa. The initial pressure is then around 108 kPa in this experiment. The initial pressure inside the standard volume is fixed around 20 kPa. The pressure inside both volumes, the temperature inside the accumulation volume, the temperature of the walls of each volume are measured every second. The results are presented in Figure 3.19 and Figure 3.20.

As predicted by the theory, the temperature of the walls is hardly affected by any change of the temperature of the gas inside the accumulation volume. The Pt100 inside the volume only measures a change of the temperature around 4 or 5 K and stabilized 400 s after the beginning of the expansion (see Figure 3.19), which is consistent with the simulation. As already discussed, the pressure measurements are the most reliable. The uncertainty of the stabilization time is mainly due to the expansion flow rate model and cannot be easily estimated. The pressure inside both volumes (see Figure 3.20) is however in agreement with the model: the stabilization time of pressures is also around 150 s.

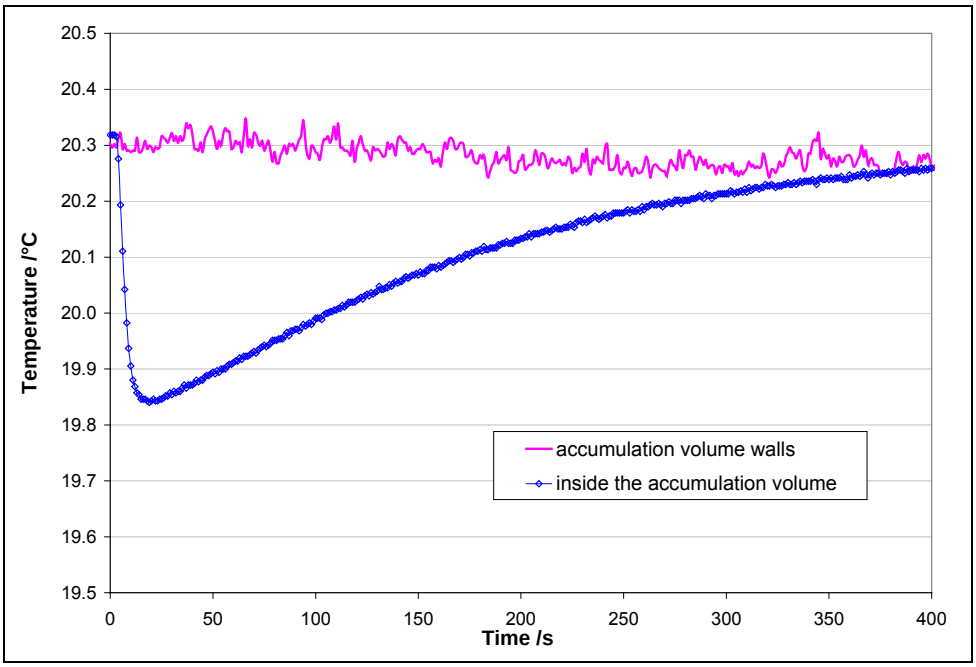

Figure 3.19. Expansion from the accumulation volume to the standard volume: measurement of the temperature inside the accumulation volume and of the temperature wall.

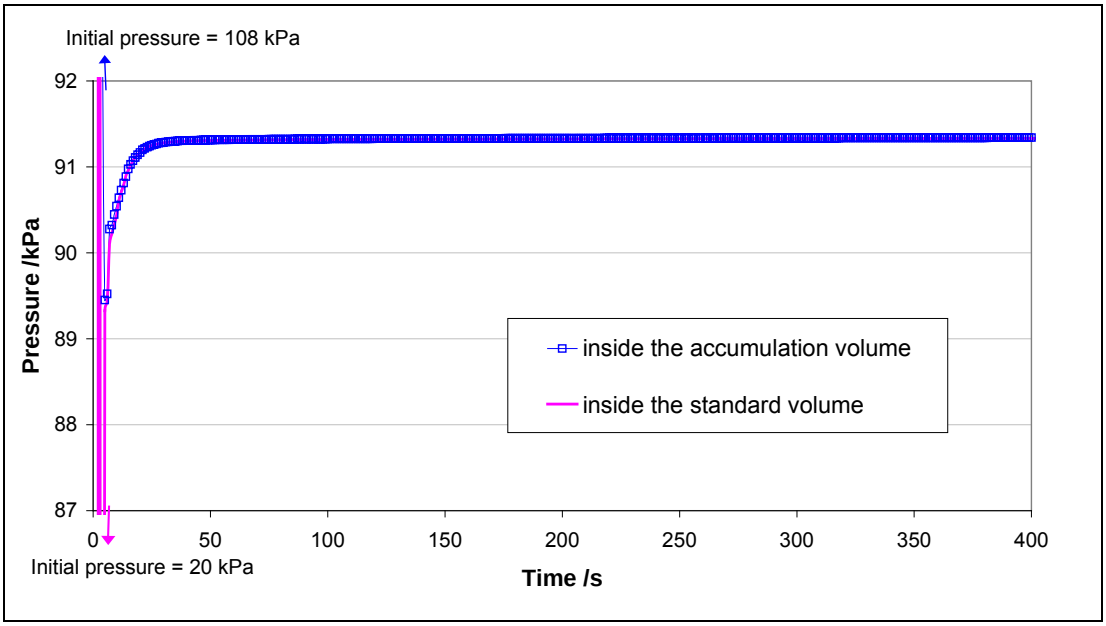

Figure 3.20. Expansion from the accumulation volume to the standard volume: measurement of the pressures inside both volumes.

In order to confirm this result, similar experiments with a type K thermocouple (response time checked around 1 s) were carried out. The measured changes of temperature are more significant and the stabilization time is shorter, around 150 s.

From these results, a minimum stabilization time of 150 s of the system {accumulation volume + standard} has been considered as necessary.

3.6.5 Operating principle

At the beginning, clean air is swept across the system composed by the two volumes. The pressure in the accumulation volume is fixed at 108-110 kPa to preserve the gas monitor. The pressure inside the standard volume is fixed between 15 and 35 kPa. After the expansion beginning, the system is allowed stabilizing during a minimum of 150 s before recording the measurements of pressure and temperature. As an example, Figure 3.21 presents a diagram of the variations of the ratio P/T that can be measured during a calibration.

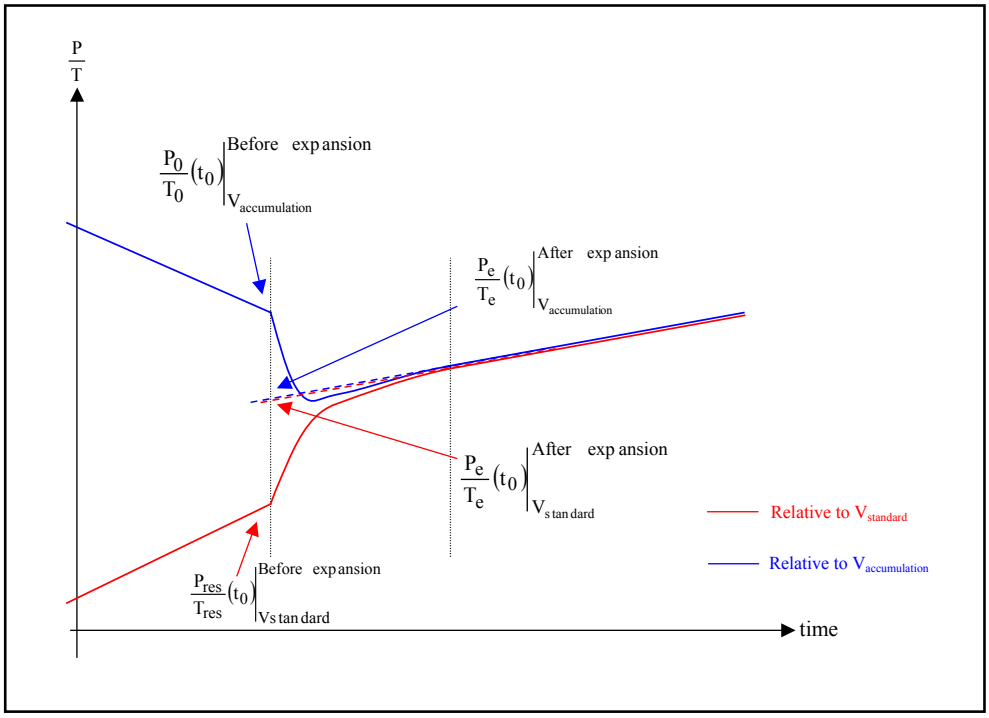

Figure 3.21. Variations of the P/T as a function of time for both volumes during a calibration.

The accumulation volume is expressed by Equation [3.30]:

$$V = V_s \cdot \frac{\left.\frac{P_e}{T_e}(t_0)\right|_{\{\text{Standard volume} + \text{Accumulation volume}\}}^{\text{After expansion}} - \left.\frac{P_{res}}{T_{res}}(t_0)\right|_{\text{Standard volume}}^{\text{Before expansion}}}{\left.\frac{P_0}{T_0}(t_0)\right|_{\text{Accumulation volume}}^{\text{Before expansion}} - \left.\frac{P_e}{T_e}(t_0)\right|_{\{\text{Standard volume} + \text{Accumulation volume}\}}^{\text{After expansion}}} - V_{fittings} \quad [3.30],$$

where $V_{fittings}$ represents the added volumes of the fittings between the standard volume and the accumulation volume. It is defined by valves 1, 2, and 3 (see Figure 3.22). The expansion is generated by opening valve 2.

The ratios *P/T* are extrapolated at the time of the valve opening in order to take into account an eventual residual leakage and adsorption of the walls during the calibration [HOL69], [HOL65], and [BER04].

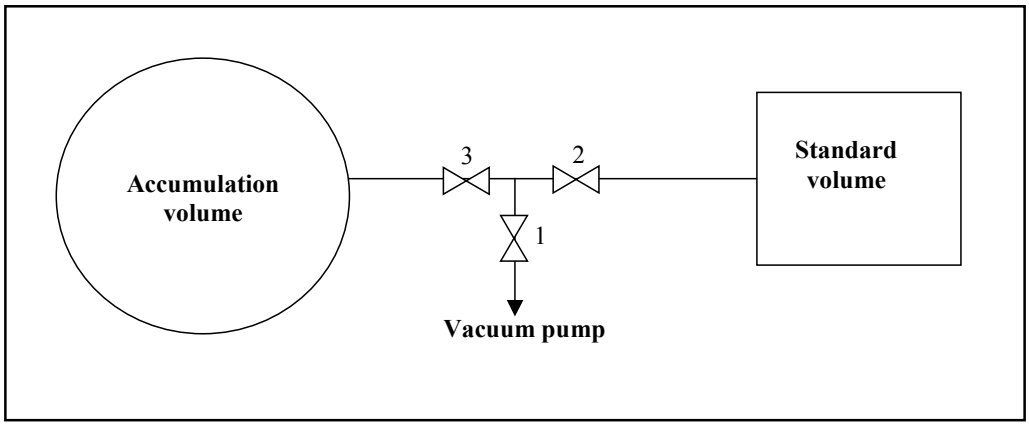

Figure 3.22. Diagram of the connections between the accumulation volume, the standard volume, and the vacuum pump.

3.6.6 Expression of the volume uncertainty

The standard uncertainties have been calculated from the contribution of uncertainties originating :

- from the pressure measurement,
- from the temperature measurement,
- from the homogeneity of the temperature inside both volumes,
- from the calibration of the standard volume,
- from the value of the ratios P/T extrapolated at the time of the valve opening.

The size of the accumulation volume is calculated as: V = (2.161 ± 0.029) dm^3. The uncertainty budget is presented in Table 3.12.

3.6.7 Comparison with the results of the LNE volume metrology unit

A 1-dm^3 volume is used as a transfer standard for a comparison of the static expansion method to the conventional gravimetric method. Its shape is cylindrical and simpler than the accumulation volume. The transfer standard was connected to the primary leak standard. The volume size was calibrated using the static expansion system. The volume size of the transfer standard was estimated to be: $V_{Pressure}$ = (0.9936 ± 0.0093) dm^3. Using the gravimetric method, the mass laboratory of the LNE has also done a calibration of the volume size of the transfer standard. The method consists in first evacuating the standard. After weighing it, the transfer standard is filled with water. The volume size at 20°C is calculated using the density of the water. The result is: V_{Volume} = (0.99630 ± 0.00030) dm^3.

The standard error $EN = \left(V_{Volume} - V_{\mathrm{Pr}essure}\right) \cdot \left(U^2_{Volume} + U^2_{\mathrm{Pr}essure}\right)^{-1/2}$ is then calculated. Its value is + 0.29. Therefore both results are consistent. However, the uncertainty of the static expansion system is significantly higher than the uncertainty of the other method: it is mainly due to the homogeneity of the temperature of the transfer standard and the standard volume of the primary leak standard (Figure 3.23). A thermal insulation of the volumes from the environment has then to be integrated in order to reduce significantly the uncertainty.

Table 3.12. Example of an uncertainty budget of the calibration of the accumulation volume.

Description	Unit	Uncertainty	Distribution law coefficient	Standard uncertainty	Sensibility coefficient	Standard uncertainty of V_{acc}
		[unit]		*[unit]*	*dm^3/[unit]*	*dm^3*
Repeatability	*dm3*			0.0022	5.2×10^{-1}	1.2×10^{-3}
P0/T0 : modeling	*Pa/K*			0.0010	-4.3×10^{-2}	4.4×10^{-5}
P0/T0 : resolution of time	*Pa/K*			0.000051	-4.3×10^{-2}	2.2×10^{-6}
P0: calibration of the pressure gauge	*Pa*	15	2	7.5	-1.5×10^{-4}	1.1×10^{-3}
T0 : calibration of the thermometers	*K*	0.060	2	0.030	5.4×10^{-2}	1.6×10^{-3}
T0 : calibration of the multimeter	*K*	0.00080	2	0.00040	5.4×10^{-2}	2.2×10^{-5}
T0: homogeneity	*K*	0.14	√12	0.040	5.4×10^{-2}	2.2×10^{-3}
Pres/Tres : Modelisation	*Pa/K*	0.010	1	0.010	-1.0×10^{-2}	1.0×10^{-4}
Pres/Tres : Resolution of time	*Pa/K*	0.0001	1	0.0001	-1.0×10^{-2}	1.5×10^{-6}
Pres: calibration of the pressure gauge	*Pa*	15	2	7.5	-3.5×10^{-5}	2.7×10^{-4}
Tres : calibration of the thermometers	*K*	0.060	2	0.030	4.2×10^{-3}	1.3×10^{-4}
Tres : calibration of the multimeter	*K*	0.00080	2	0.00040	4.2×10^{-3}	1.7×10^{-6}
Tres: homogeneity	*K*	0.14	√12	0.040	4.2×10^{-3}	1.7×10^{-4}
Pe/Te : modeling	*Pa/K*	0.0010	1	0.0010	5.3×10^{-2}	5.4×10^{-5}
Pe/Te : resolution of time	*Pa/K*	0.000069	1	0.000069	5.3×10^{-2}	3.7×10^{-6}
Pe: calibration of the pressure gauge	*Pa*	15	2	7.5	1.8×10^{-4}	1.4×10^{-3}
Te : calibration of the thermometers	*K*	0.060	2	0.030	-5.8×10^{-2}	1.7×10^{-3}
Te : calibration of the multimeter	*K*	0.00080	2	0.00040	-5.8×10^{-2}	2.3×10^{-5}
Te : homogeneity	*K*	1.00	√12	0.29	-5.8×10^{-2}	1.7×10^{-2}
Standard volume	*dm^3*	0.00057	2	0.00029	4.126	1.2×10^{-3}
Correction $V_{fittings}$	*dm^3*	0.00021	2	0.00010	-1	1.0×10^{-4}

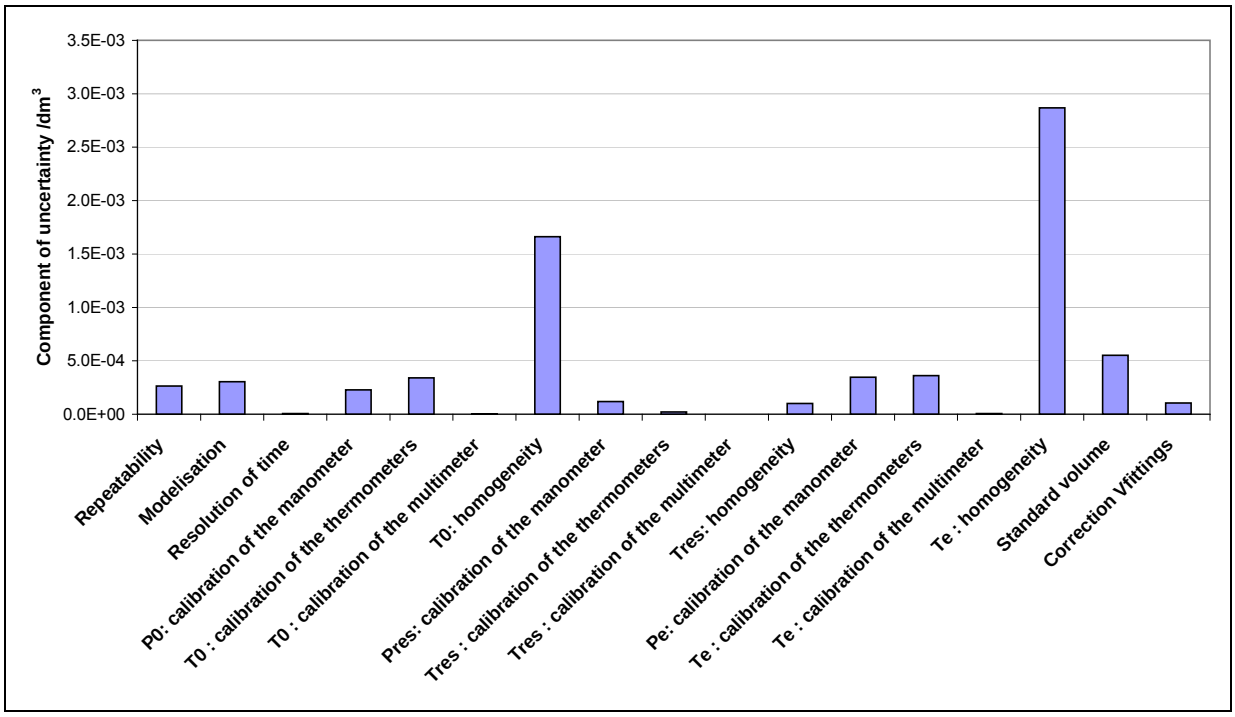

Figure 3.23. Components of the uncertainty of the size of the 1 dm^3-volume using the static expansion system: example of one measurement.

3.7 Expanded uncertainty of refrigerant leak flow rate measurement by the primary standard

Once the PAS and the accumulation volume are calibrated, the uncertainty due to the primary standard can be estimated.

3.7.1 Expression of the leak flow rate

A low concentration of gas C_{gas} is generally expressed in µmol/mol, which means there is n_{gas} moles of the gas in one billion of moles of the mixture:

$$C_{gas} = \frac{n_{gas}}{10^6 \cdot n_{mixture}} \qquad [3.31].$$

Considering the perfect gas law, Expression [3.31] becomes:

$$n_{gas} = C_{gas} \cdot n_{mixture} = C_{gas} \cdot \frac{P \cdot V}{R \cdot T} \qquad [3.32].$$

In this case, as the volume is a constant one (the accumulation volume), the expression of the leak flow rate can be expressed by Equation [3.33]:

$$Q_m = \frac{M_{gas} \cdot V_{Acc}}{R_g} \cdot \frac{\partial\left(\frac{P_{Acc}}{T_{Acc}} \cdot C_{gas}\right)}{\partial t} \qquad [3.33].$$

As the gas tends to be absorbed by the walls or captured in the dead volumes, a strict rinsing must be done before measurement. Despite the rinsing, R-134a rises inside the accumulation volume, even if there is no calibrated leak connected to the primary standard. The residual leak flow rate must then be checked every month (the frequency will be adjusted with better acknowledgement).

3.7.2 Modeling of the variation of the corrected concentration as a function of time

As the gas analyzer measures a sample of gas from the accumulation volume every minute, Equation [3.33] must be discretized.

The first way to discretize the equation is to consider the variation of the product PC/T as a function of the corresponding time variation:

$$Q_m = \frac{M_{gas} \cdot V_{Acc}}{R_g} \cdot \frac{\partial\left(\frac{P_{Acc}}{T_{Acc}} \cdot C_{gas}\right)}{\partial t} \Rightarrow Q_m = \frac{M_{gas} \cdot V_{Acc}}{R_g} \cdot \frac{\Delta\left(\frac{P_{Acc}}{T_{Acc}} \cdot C_{gas}\right)}{\Delta t} \qquad [3.34]$$

In order to minimize the uncertainty, the interval of time must be long enough. Thus if n measurements are done, the leak flow rate will be expressed from the variation of the concentration from the beginning to the end of the calibration:

$$Q_m = \frac{M_{gas} \cdot V_{Acc}}{R_g} \cdot \frac{\left[\frac{P_{Acc}}{T_{Acc}} \cdot C_{gas}(n \cdot \Delta t) - \frac{P_{Acc}}{T_{Acc}} \cdot C_{gas}(0)\right]}{n \cdot \Delta t}$$

[3.35].

However, this method:

- gives too much weight to the first measurement, which has the highest uncertainty, on the result
- does not consider the intermediate measurements, which could give a more reliable result and a statistical indication of the deviation of the result.

The second way to discretize the equation is to use the least mean squares method. The method of least squares, also known as regression analysis, is used to model numerical data obtained from observations by adjusting the parameters of a model so as to obtain an optimal fit of the data. The best fit is characterized by the sum of squared residuals at its least value. A residual is defined as the difference between an observed value and the value given by the model. This is called the Gauss criterion (Carl Friedrich Gauss around 1794). This method will be used to estimate the variation of the corrected concentration along time.

The following assumptions have been considered:

- As the leak flow rate is assumed to be constant, it is assumed that PC/T can be linearly fitted: $P \cdot C \cdot T^{-1} = a \times t + b$, with ***a***[10] and ***b*** constant.
- The time value is not biased.
- The measurements of the quantities P, C, and T have respective variances: $U^2(P) = 64\ Pa^2$; $U^2(C) = (0.035 + 0.011 \times C)^2\ \mu mol^2.mol^{-1}$ and $U^2(T) = 0.14\ K$.
- The measurements of the quantities P, C, and T are not correlated.

As the variances of the observations of C along time are not equal, the method used was precisely the weighted least squares method [TOM92]. The calculation of $(PC/T)_i$ is performed using the observations. Then a weighted coefficient for each observation (index *i*) is defined as:

$$g_i = \left[U\left(P \cdot C \cdot T^{-1}\right)_i \right]^{-2}.$$

The criterion of Gauss implies that the quantity Resi(***a***,***b***) is minimal:

$$\mathrm{Resi}(a,b) = \sum_i g_i \cdot \left[\left(P \cdot C \cdot T^{-1}\right)_i - a \cdot t_i - b \right].$$

The estimation of ***a***, $\hat{a}$, and its variance are then expressed by Equations [3.30] and [3.31]:

$$\hat{a} = \left[\sum_i g_i \cdot \sum_i \left(g_i \cdot t_i \cdot P_i \cdot C_i \cdot T_i^{-1}\right) - \sum_i \left(g_i \cdot t_i\right) \cdot \sum_i \left(g_i \cdot P_i \cdot C_i \cdot T_i^{-1}\right)\right] \cdot \left[\sum_i g_i \cdot \sum_i \left(g_i \cdot t_i^2\right) - \left(\sum_i \left(g_i \cdot t_i\right)\right)^2\right]^{-1}, \quad [3.30]$$

$$U^2\left(\hat{a}\right) = \sum_i g_i \cdot \left[\sum_i g_i \cdot \sum_i \left(g_i \cdot t_i^2\right) - \left(\sum_i \left(g_i \cdot t_i\right)\right)^2\right]^{-1}. \quad [3.31]$$

3.7.3 Uncertainty budget of leak flow rate

To estimate ***a*** and the uncertainty related to the fitting, the uncertainty related to the quantity *PC/T* must be calculated. The combined uncertainty related to *PC/T* can be estimated according to the combined uncertainties of the measurement of temperature, pressure, and concentration. An uncertainty budget (see Table 3.13) can be established. The calibration is done until the concentration reaches the linear limit of the PAS 150 µmol.mol^{-1}. Therefore, the combined uncertainty is determined for (PC/T) in the range of 0 Pa.K^{-1} to 0.052 Pa.K^{-1}:

$$U_{PC/T} = \left(0.020 \times PC/T + 2.6 \times 10^{-5}\right)\ Pa.K^{-1}.$$

[10] The quantity ***a*** is then defined as ($a = \partial\left(P \cdot C \cdot T^{-1}\right)/\partial t$) and expressed in Pa.K^{-1}.s^{-1}.

Table 3.13. Uncertainty budget of the quantity PC/T.

Description of the quantity	Standard uncertainty of the quantity	Standard uncertainty of PC/T
Pressure	4.0	3.9×10^{-5} x [PC/T]
Temperature	0.070	2.4×10^{-4} x [PC/T]
Concentration	$(9.7 \times 10^{-4} + 5.5 \times 10^{-3}$ x C) *µmol.mol^{-1}*	(0.33 + 5.5×10^{-3} x [PC/T]) *Pa.µmol.mol^{-1}.K^{-1}*
Non applied correction		
	Value	
Concentration fitting	25 *Pa.µmol.mol^{-1}.K^{-1}*	

The uncertainty of ***a*** is an uncertainty calculated by the type A-method. It mainly depends on the observations. A permeation leak whose nominal value is 20 g.yr^{-1} has been calibrated as an example. Results are presented in Table 3.14. The uncertainty budget has been established (see Table 3.15). The leak flow rate is estimated to: (17.01 ± 0.24) g.yr^{-1}. It means a relative uncertainty of U = 1.5%.

Table 3.14. Calibration of a permeation leak whose nominal value is 20 g.yr^{-1}, with the standard uncertainty of the quantity ***a'***[11].

Cycle	Leak flow rate	u(*a'*)
	g.yr^{-1}	g.yr^{-1}
1	17.006	0.051
2	17.042	0.051
3	16.996	0.051

Table 3.15. Example of an uncertainty budget of the calibration of the 20 g.yr^{-1}-permeation leak.

Description	Unit	Standard uncertainty *[Unit]*	Sensibility coefficient *g.yr^{-1}.[Unit]$^{-1}$*	Standard uncertainty of Qm *g.yr^{-1}*
Repeatability	*g.yr^{-1}*	2.4×10^{-2}	1	2.4×10^{-2}
Measure of the concentration variation	*Pa/K*	6.6×10^{-8}	7.74×10^{5}	5.1×10^{-2}
Volume	*m3*	1.5×10^{-5}	8334	1.2×10^{-1}
Residual leak flow rate	*g.yr^{-1}*	7.0×10^{-4}	1	7.0×10^{-4}

[11] The quantity ***a'*** is defined as : ($a' = Cst \cdot M \cdot R_g^{-1} \cdot V \cdot a$). *Cst* is a constant in order to express ***a'*** in g.yr^{-1}.

The main component of the uncertainty is due to the calibration of the accumulation volume. As previously mentioned, this component can be minimized by thermal insulation of the accumulation and the standard volumes during the calibration.

3.8 Conclusions

As the test bench was designed, realized, and qualified, the LNE can now provide calibration of R-134a leaks, in their operating conditions with a relative **expanded uncertainty** around **1-2%**. The objective was to provide a bench to measure R-134a leak flow rate with an uncertainty of 1%. The objective is then almost achieved.

This new method has required to adapt the static expansion method in order to calibrate a complex volume. Therefore, the LNE can calibrate complex volumes with a relative expanded uncertainty of about 1-2%. It corresponds to the main uncertainty of the MFR measurement. However, the static expansion method can be optimized by thermal insulation of {the accumulation volume and the standard volume} system. Consequently, it will improve the leak flow rate measurement.

The other main uncertainty component of the MFR measurement is due to the concentration measurement. It has required the manufacturing of R-134a mixtures in order to calibrate the PAS. The uncertainty on the concentration is then about 1-2% on the concentration value. However, as the calculation needs a variation of concentration and not the value of the absolute concentration, some systematic errors are compensated. The uncertainty due to the concentration variation measurement is then about 1% of the MFR value. A study of the residuals shows that the fitting could be improved for concentrations lower than 20 $\mu mol.mol^{-1}$. The uncertainty may be done by a study at lower concentrations: a comparison between the PAS concentration indication with the theoretical ones due to previously calibrated refrigerant leaks may be carried out.

Thus, as the refrigerant leaks can now be traceable to the SI units, the European standard EN 14624, the ASHRAE standard that is currently in production, and the SAE standard can be applied to qualify the refrigerant detectors with R-134a leaks. The primary leak standard is a good support to ensure the traceability of the qualification of refrigerant detectors. However, like the primary standard, the standard to qualify refrigerant detectors is a tool for industrials in order to control the leak tightness of their refrigerating equipment. It is however necessary to understand the relevance of the tests, the parameters that are qualified in order to take the needed precautions during the test: it is the goal of Chapter 4.

Chapter 4 - Analysis of the qualification tests of refrigerant leak detectors according to existing standards

4.1 Objective

According to the European regulations, the leak tightness of equipment containing refrigerant must be controlled by refrigerant leak detectors and room controllers, whose respective sensitivities are lower than 5 $g.yr^{-1}$ and 10 $\mu mol.mol^{-1}$. The sensitivity of these devices has to be confirmed by qualification tests defined in EN 14624 [AFN05] or in the future ASHRAE standard. The performances of room controllers are tested by using standard concentrations, which are easily traceable. The performances of hand leak detectors are tested by comparing the calibrated leak MFR and the indication of the detectors. As the refrigerant calibrated leaks can be traceable to SI units thanks to the new primary standard (see Chapters 2 and 3), the standard EN 14624 or other standards to qualify the refrigerant hand leak detectors can now be applied.

However, in order to qualify the leak detectors in the best conditions, complementary technical requirements are necessary once the calibrated leaks have been standardized. It is necessary to identify the precautions that must be taken during the performance tests. Besides, the operators that use these devices must be aware of the differences between laboratory conditions and in the field conditions, and their influences on the results. This chapter aims at defining what is the real measurand of a hand leak detector and what are the parameters tested by the standard. Even in a laboratory, the operating conditions are not perfect. It is then necessary to identify the influence parameters and to control them carefully. As the hand leak detector is used in an industrial environment, it is also necessary to underlines the differences between the conditions obtained during the performance tests and the real operating conditions. The precautions to take during the qualification tests and during a field detection must then be clearly identified in order to improve the quality of the controls.

To summarize, the objectives of this chapter are the following ones:

- To identify the measured quantity by a refrigerant detector
- To analyze the objectives of the existing standards to qualify refrigerant detectors
- To study the mass transfers during a leak detection, in order to define the precautions to take during the tests defined in the standards
- To define the precautions to take during the leak detection in real conditions

4.2 Description of the three main methods of refrigerant leak detection

4.2.1 Example of an infrared detector

4.2.1.1 Operating principle

Infrared light is directed through a cell. If there is a refrigerant gas through the cell, it absorbs the infrared light energy according to the Beer's law. The amplitude drop is then detected by a sensor. The sensor relies on the operating principle that infrared light heats the sensor via an absorption coating. By this change in temperature, electrical charges are released in certain materials like $LiTaO_3$ (Lithium Tantalate). If the light is modulated, this heating will generate an electric AC signal (see Figure 4.1).

Unlike the infrared photo-acoustic spectrometer, it is not the light that is modulated. In fact, a three-way valve changes the gas entering the cell several times per second between ambient air ("reference gas") and the gas escaping from a leak – the test gas. Therefore, it is the composition of the gas that is modulated and generates an alternative signal, which is related to the gas concentration [MAL95], [CLO98-7].

4.2.1.2 Advantages and disadvantages of a reference gas

The gas admission ports at the tip of the probe are designed in a way that the opening for the reference gas is located as close as possible to the test gas inlet. Indeed the concentrations of interfering gases are not constant, but have gradients even over short distances. It is a real advantage to compare the sample at the measuring line to the sample at the reference line, because it takes into account the ambience changes. Therefore, the detector is less dependent from the changes in environment than other technologies.

Nonetheless, the two openings must not be so close to each other because gas from the leak will enter through the reference gas inlet to the sensor, and may distort the results.

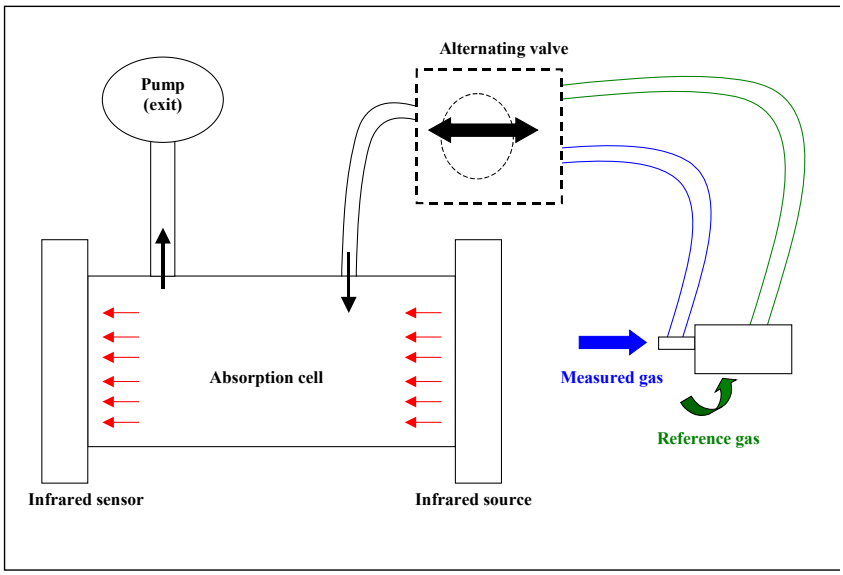

Figure 4.1. Diagram of the operating principle of an infrared refrigerant detector

4.2.1.3 Calibration of the refrigerant detector

As the measurand is a concentration, the manufacturer calibrates the detector in order to obtain a relation between the measured concentration and the leak flow rate. The refrigerant detector is then directed to a refrigerant leak whose flow rate is directly compared to the electrical signal. However, the way to identify the influence parameters and to take them into account is not explained by the manufacturer.

4.2.2 Detector with a heated sensor

4.2.2.1 Operating principle

This method is based on the high electro-negativity of the halogens. Therefore, detectors that use this kind of detection are composed with two elements: an emitter and a collector. The emitter is a platinum cylinder, inside which a ceramic is inserted. The collector is a platinum coil located around the emitter.

When the detector is switched on, the elements are heated at more than 500°C. The alkaline atoms are migrating at the surface of the emitter and the halogens atoms capture the electrons and ionize. Therefore a current due to the ionization of the alkaline atoms - proportional to the concentration of the halogen gas - is generated from the emitter to the collector [MAL95], [CLO98-7].

4.2.2.2 Interest of the method

This method can be used for the detection of HFC gases. The halogen electrical configuration of the layer of the valence at the fundamental state is $ns^2\ np^5$, which corresponds to 3 pairs of electrons and one single electron. Their electro-negativities are very high, which means that they easily capture an electron in order to reach the electronical configuration of rare gases (8 pairs of electrons). They are then easily ionized. In particular, fluorine is the element whose electro-negativity is the highest of the Mendeleïev table.

However, according to the literature ([CLO98-7], [MAL95]), this method is more adequate for CFCs than for HFCs. In order to improve the sensitivity of the detection of HFCs, the emitter temperature is settled at a very high temperature, which weakened the sensor. This kind of detectors is easily saturated due to the ionization of all the alkaline atoms.

4.2.3 Catharometer

4.2.3.1 Operating principle

A catharometric cell, also called a thermal capacity cell, consists of two heated filaments of a metal with high coefficient of resistance, e.g. platinum. They form two arms of a Wheatstone bridge circuit.

The two filaments are situated in separate channels in a heated metal block. Similarly to the infrared detector, the gas is drawn into one of the channels (called the measure circuit) while the ambient air - the reference gas - is drawn into the other channel (called the compensation circuit). The rate of heat loss from each filament determines its temperature and therefore its resistance: $R=R_0(1+\alpha.T)$, where α is the temperature coefficient of resistance for the conductor material.

A change in thermal conductivity of the gas flow in the sample channel arising from elusion of a sample component alters the temperature and hence the resistance of the filament in that channel. This produces an out-of-balance signal in the bridge circuit [ACCOR94], [SEE05], [CLO98-7], [FIF95].

4.2.3.2 Interest of the method

The thermal conductivity detector is robust and reliable. However it has only moderate overall sensitivity that varies from compound to compound.

The sensitivity depends on the difference between the thermal capacities. For instance, the thermal conductivity of the air is about 26.2 $mW.m^{-1}.K^{-1}$, while the thermal conductivity of R-134a is about 13 $mW.m^{-1}.K^{-1}$. It can be noticed that this method is best suited for CFC gases. For instance the thermal conductivity of R-12 is only about 9.46 $mW.m^{-1}.K^{-1}$. Hence, the difference between the conductivities of air and R-12 is larger than between the conductivities of air and R-134a.

Response has a limited linear range and is sensitive to changes in temperature gradient of the environment. The suction speed of the detector has to be stable in order to give a reliable measurement. Therefore this method of detection is not particularly suitable for quantitative work. Also this detector is not selective. The presence of other gases than R-134a or air will unbalance the Wheatstone bridge, as their conductivities are different from the air thermal conductivity.

4.3 Theoretical relation between the measurand and the nature of the measured quantity

Whatever detection method is considered, a detector measures a concentration and not directly a leak flow rate. The relation between concentration and leak flow rate must be studied.

4.3.1 Theory of accumulation

In this session, the analysis is based on Annex B from the European standard EN 14624 [AFN05]. Annex B is based on the second tests to qualify a hand leak detector: it is the test to measure the sensitivity threshold when the detector is moving. The leak detector is installed on a mobile platform, moving from left to right and vice-versa in front of an adjustable leak orifice – adjusted for some discrete values between 1 $g.yr^{-1}$ to 50 $g.yr^{-1}$. The lowest flow rate that the detector can detect when it is in front of the leak orifice is considered as the sensitivity threshold when the detector is moving at 2 $mm.s^{-1}$.

Contrary to the accumulation method, there is no enclosed volume on which the leak is connected: the gas from the leak diffuses in the room. In order to express a relation between the concentration and the MFR, it is considered that the gas from the leak is mainly accumulated in a control volume near the leak outlet. The second test of the standard showed that the detector nose must be at 2 mm from the orifice of the leak, when their axes are superimposed. The control volume is then defined as a sphere whose diameter is 2 mm (see Figure 4.2). The volume size is 4.2 mm^3. During the test, the detector translates at both sides of the leak at a 2 $mm.s^{-1}$ speed. Consequently, the detector crosses the control volume in 1 s.

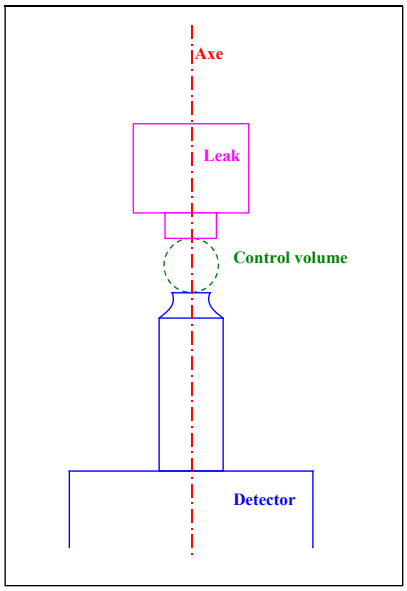

Figure 4.2. Control volume of a portable leak detector [AFN05]

As a control volume is defined, the relation between the MFR and the concentration can be expressed by Equation [4.1]:

$$Q_m = M_{R-134a} \cdot \frac{V_{Control}}{V_{mol}} \cdot \frac{\partial C}{\partial t} . \qquad [4.1]$$

with V_{mol}= 24 $m^3.kmol^{-1}$.

In a thermo-controlled room at (20.0 ± 1.0) °C at a pressure (101.3 ± 2,0) kPa, the presence of a standard leak of 5 $g.yr^{-1}$ (U = 15%[12]) generates a concentration change of (35100 ± 5000) µmol.mol^{-1} per second in the control volume. This calculation has been done for several MFRs and control volume sizes (see Figure 4.3). This simulation underlines the correlation between the leak flow rate and the gas accumulation in the control volume. It indicates that the distance between the leak and the detector nose influences this correlation.

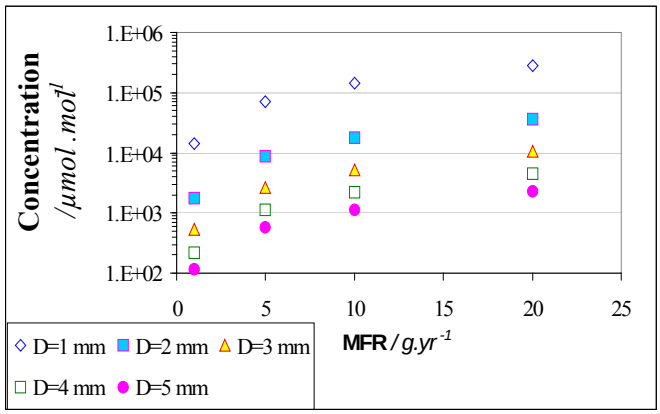

Figure 4.3. Variation of the concentration every second in the control volume (logarithmic scale) as a function of the MFR and of the distance between the leak and the detector nose.

This study aims at calculating the average accumulation of gas in the control volume. However, this study considers the control volume as an enclosed volume. It does not take into account the air movement due to the suction of the R-134a/air mixture by the detector. Therefore a theoretical study introducing a suction rate of the detector has been carried out.

[12] This relative uncertainty is the maximum uncertainty tolerated by the standard [AFN05].

4.3.2 Mass balance

Considering a domain defined by a refrigerant detector nose installed in front of a refrigerant calibrated leak (see Figure 4.4), the mass balance of R-134a is expressed by Equation [4.2].

$$Q_m^{Leak} = C_{R-134a} \cdot \rho_{R-134a} \cdot Q_v^{detector} \quad [4.2]$$

This equation is based on the following assumptions:

- The suction rate of the detector is higher than air flows due to air turbulence, there is no effect of gravity and of temperature gradient in the room. Therefore, it is considered that there is only air in the lateral zone of the control volume ("Zone of air only").
- There is no accumulation of gas, because the volumetric flow rate (VFR) of the detector is significant.
- The calibrated leak is filled with pure R-134a ("Zone with R-134a only").

Thus, the concentration seen by the detector is expressed by Equation [4.3]:

$$C_{R-134a} = \frac{Q_m^{Leak}}{\rho_{R-134a} \cdot Q_V^{Detector}} \quad [4.3]$$

A graph has been established using Expression [4.3]: the concentration seen at the inlet of the detector nose is represented as a function of the detector VFR (see Figure 4.5) and as a function of the R-134a leak flow rate. This graph underlines the influence of the detector VFR on the concentration seen by the detector. The lower the VFR, the higher the concentration seen by the detector. It seems that the concentration is lower than 100 $\mu mol.mol^{-1}$ for MFR between 1 and 50 $g.yr^{-1}$, even if the accumulated concentration in the control volume is huge (see Section 4.3.1).

Thus the theory shows that the concentration seen by the detector depends on the VFR of the detector. However, assumptions have been made to simplify the equations: the air speed and the gravity are for instance considered as negligible. Yet, because of the gravity, the R-134a tends to fall as it is heavier than air and the openings of the room tests can influence the detection of the leak detector. The distance between the detector nose and the outlet of the leak are not considered. The gas in the control volume is not homogeneous: the concentration calculated by this method is an average. The concentration gradient in the control volume is not established by this method. Consequently, a phenomenological study must be carried out in order to identify the main influence parameters.

A phenomenological study with the CFD software FLUENT has been carried out in steady state. These simulations aim at considering the dispersion and the dilution phenomena. The objective is to establish the concentration gradient of R-134a in the control volume in order to identify some parameters that can relevantly influence this relation.

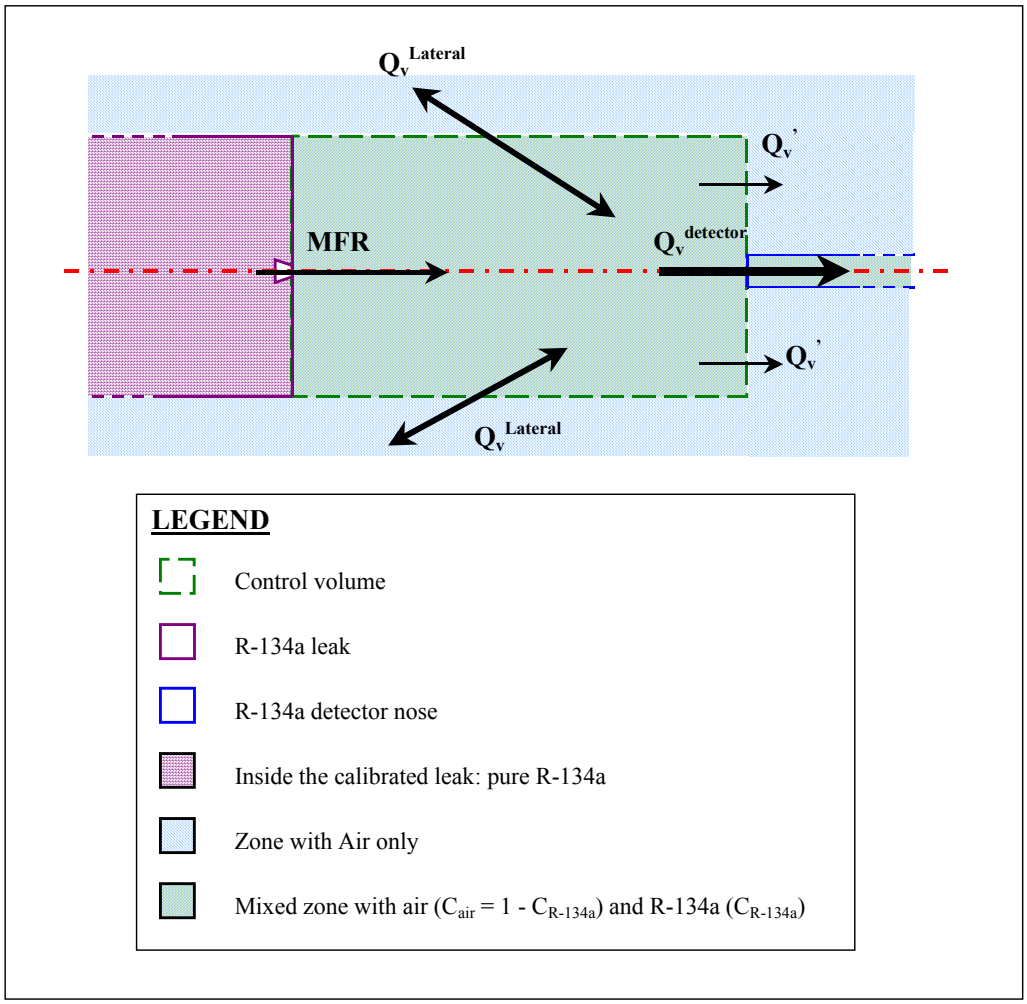

Figure 4.4. Studied domain to express the mass balance during the detection of a leak by a refrigerant detector.

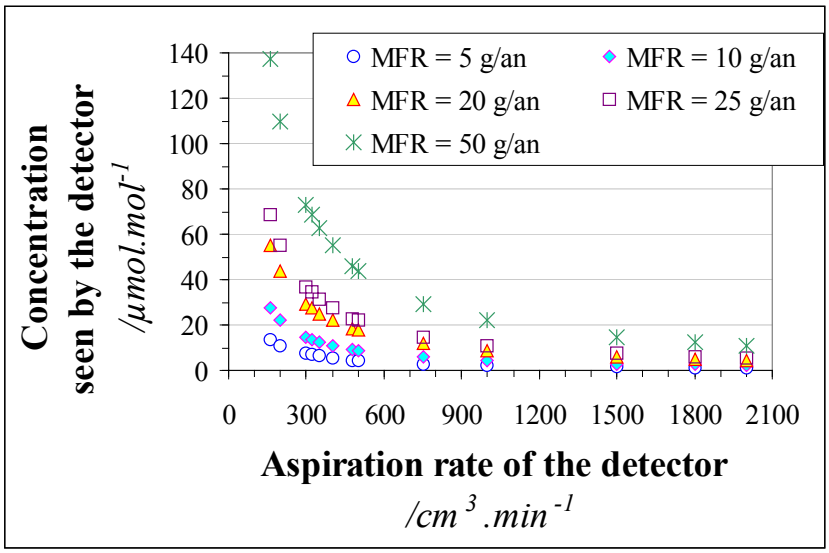

Figure 4.5. Concentration seen by the detector as a function of the R-134a leak flow rate and of the VFR leak detector, using the expression [4.3].

4.4 Concentration gradient near a calibrated leak

The accumulation theory (see Section 4.3) has established that the larger the control volume, the lower the average variation of concentration. Using FLUENT software, the concentration in the control volume - defined Figure 4.6 - has been established for a 50 $g.yr^{-1}$ leak.

4.4.1 Influence of the distance from the leak

4.4.1.1 Phenomenological study

Description of the studied system

The studied control volume is a cylinder. Its length is defined as the distance between the leak and the detector nose. Because some supplied capillary leaks have a tube (diameter about 1 cm) at the end where it leaks, the diameter of the control volume is set equal to 10 mm. The study is reduced to this control volume in order to have a highly refined grid mesh. At one end of the volume, a refrigerant leak flows at a constant rate (limit condition called in FLUENT "Mass flow inlet" from the leak). This end is composed by a 2 mm-diameter circle as it is in the calibrated leak. At the second one, a hand leak detector draws up at a constant rate (limit condition called "Mass flow inlet" of the detector). The control volume is represented in Figure 4.6.

Setting of the simulation by FLUENT

- Once the control volume is drawn and meshed, the calculation by FLUENT needs to enter some parameters relative to the properties of the existing fluids and materials, to the flow regime, to the boundary conditions and to the initial conditions. The system is studied when the flow circulation is in steady state.
- The viscous regime is considered following the laminar model. For a characteristic diameter of 1 cm and a volume flow rate of 320 $cm^3.min^{-1}$, the Reynolds number is low (<100).
- The boundary conditions are described in Figure 4.6.
- R-134a is defined at 20°C and at atmospheric pressure as the temperature and the pressure are constant. The value of each physical parameter of the gas is calculated via the software developed by NIST, REFPROP 7.
- The diffusion of R-134a and air is described by the kinetic theory.

The kinetic theory defines the diffusion coefficient of R-134a in air using the Chapman-Ensog theory [CUS84]. The accuracy of Equation [4.4] is announced equal to 8%.

$$D_{R-134a/air} = \frac{1{,}86 \cdot 10^{-3} \cdot T^{2/3} \cdot \left(1/M_{air} + 1/M_{R-134a} \right)^{1/2}}{P \cdot \Phi^2_{R-134a/air} \cdot \Omega} \qquad [4.4]$$

with P the pressure expressed in atm., T the temperature in K, M_{air} and $M_{R\text{-}134a}$ the respective molar mass of the air and R-134a. $\Phi_{R134a/air}$ is the collision diameter expressed in Angströms between R-134a and air. This diameter is defined by Equation [4.5]. Ω is the collision integral defined thanks to standard tables and to the knowledge of the quantity $k_BT/\varepsilon_{R134a/air}$. $\varepsilon_{R134a/air}$ is the interaction energy between R-134a and air: it is defined by Equation [4.6]:

$$\Phi_{R134a/air} = 0{,}5.(\Phi_{R134a} + \Phi_{air}) \qquad [4.5]$$

$$\varepsilon_{R-134a/air} = \sqrt{\varepsilon_{R-134a} \cdot \varepsilon_{air}} \qquad [4.6]$$

Parameters σ and ε are Lennard-Jones parameters, whose values for the air were extracted from the literature [CUS84]. Values of the Lennard-Jones parameters of R-134a were estimated by NIST [HUB03]. Considering the uncertainty of the formula, the pressure, the temperature (20 ± 1)°C and the uncertainty of the values of the Lennard-Jones parameters, the diffusion coefficient is ($9.0 \times 10^{-8} \pm 2.2 \times 10^{-8}$) m²/s, which means an uncertainty of U = 24%.

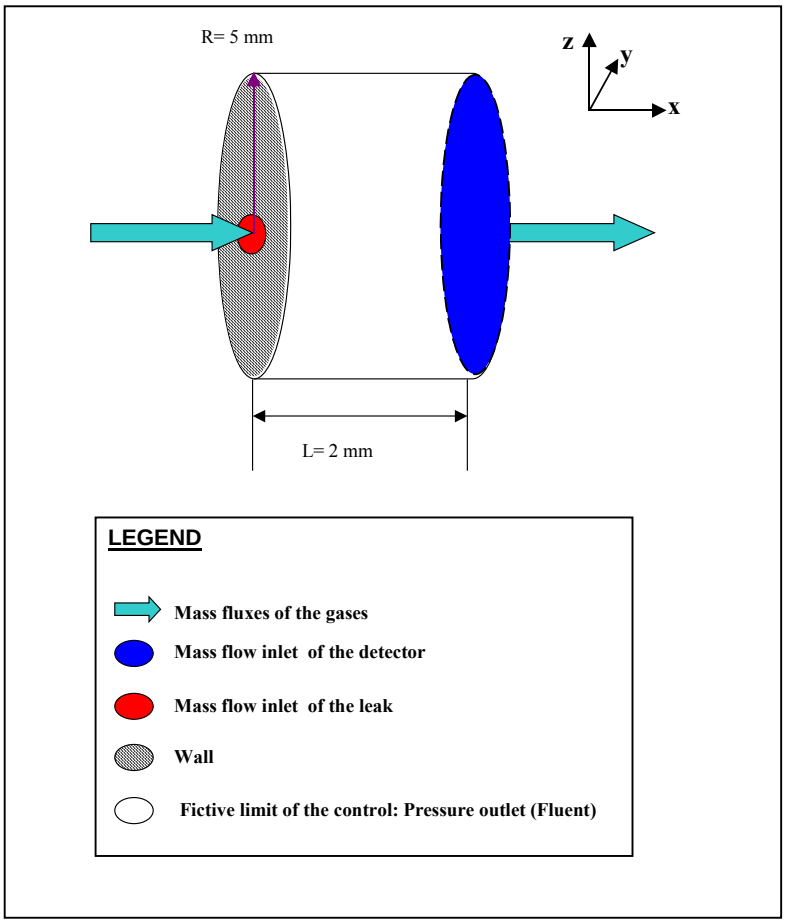

Figure 4.6. Description of the control volume and the boundary conditions used for FLUENT simulations.

Convergence criterion

The convergence is checked thanks to the mass balance. In steady state regime, there is no accumulation of gas. Therefore, the solution is assumed to be converged when the accumulation of gas is about $10^{-3} \times Q_m$, where Q_m is the value of the MFR set at the limit condition "mass leak flow rate" and when the average concentration of R-134a at the inlet of the detector (see Figure 4.7) is stabilized at (value ± 0.2) µmol.mol^{-1}.

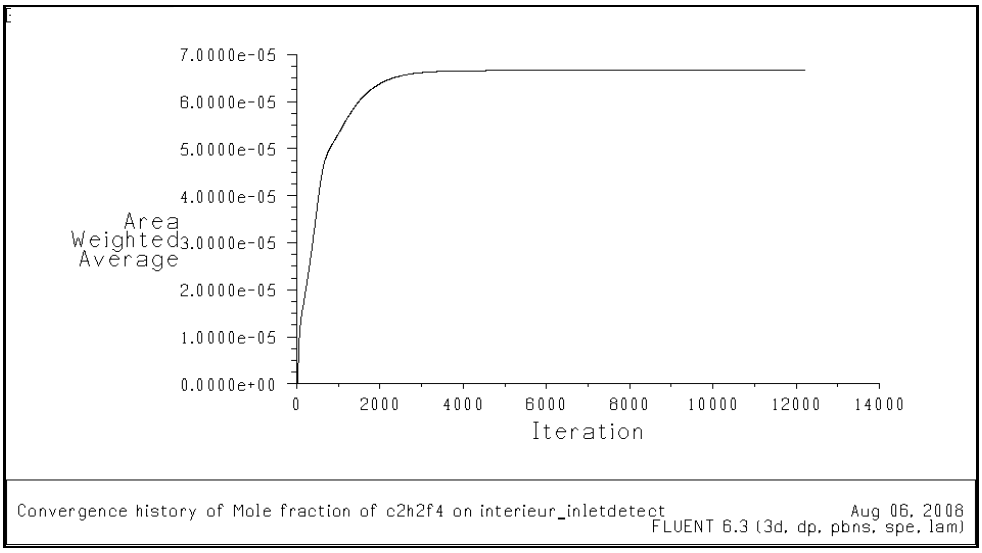

Figure 4.7. Graph of the convergence history of R-134a concentration in µmol.mol^{-1}.

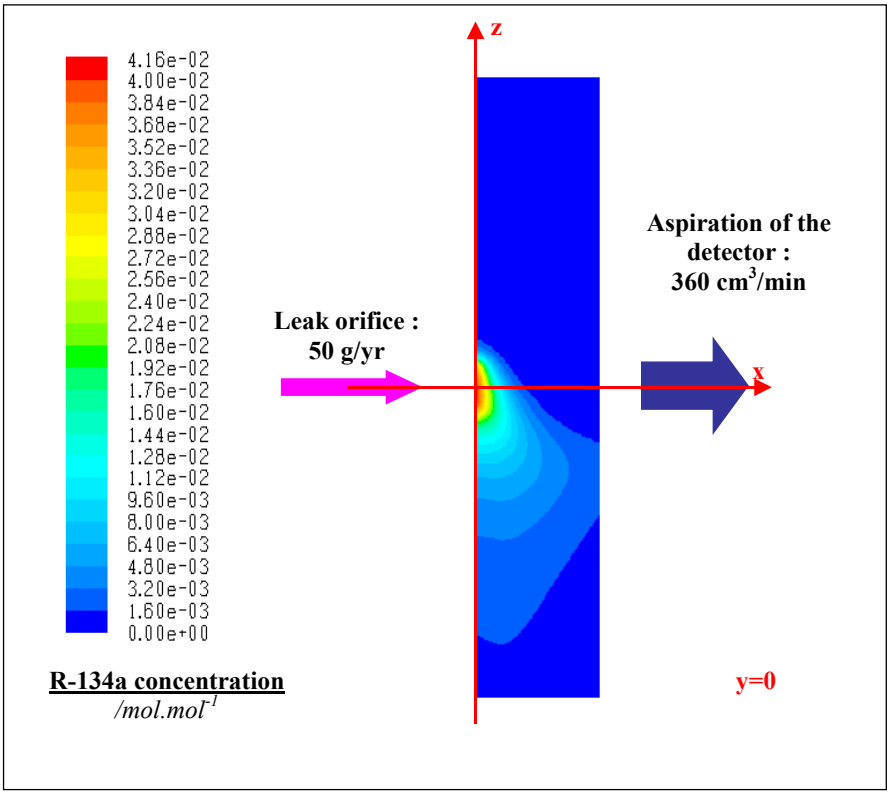

Figure 4.8. Molar fraction of R-134a (mol.mol^{-1}) in the cylindrical control volume, in the plane y =0.

Results

The concentration of R-134a expressed in mol.mol^{-1} can be calculated by FLUENT in the control volume. The simulation can represent the gradient of concentration in the whole control volume. The example of 50 g.yr^{-1}-MFR and 360 cm^3.min^{-1}-suction rate detector is considered. Figure 4.8 presents the concentration of R-134a in µmol.mol^{-1} in the plane y = 0 mm. The graph in Figure 4.9 presents the concentration as a function of the distance from the leak (coordinate: x) on the line defined by the coordinates (x, z = 0 mm, y = 0 mm).

In Figure 4.8, it can be noticed a dissymmetry of the repartition of R-134a concentration with altitude. Indeed, R-134a is heavier than air and tends to "fall". However, this matter will be discussed later in § 4.4.2. As expected, the concentration of R-134a seen by the detector due to a leak value around 50 g.yr^{-1} tends to significantly decrease (along an exponential to be characterized) as a function ofthe distance from the leak (the coordinate x). The distance from the leak is a relevant influence parameter. Therefore, refrigerant detectors are efficient only close to the leak source. Thus, to control a potential leak source, the operator must move the detector around the potential leak source and close to the potential source (less than the distance checked in the standard, i.e. 2 mm). If it is not the case, the operator must be aware that the sensitivity threshold of the moving detector is worse than the one measured according to the standard [AFN05]. It may be relevant to check the sensitivity threshold of a detector at different distances. In order to complete and to validate this study, an experimental study has been carried out.

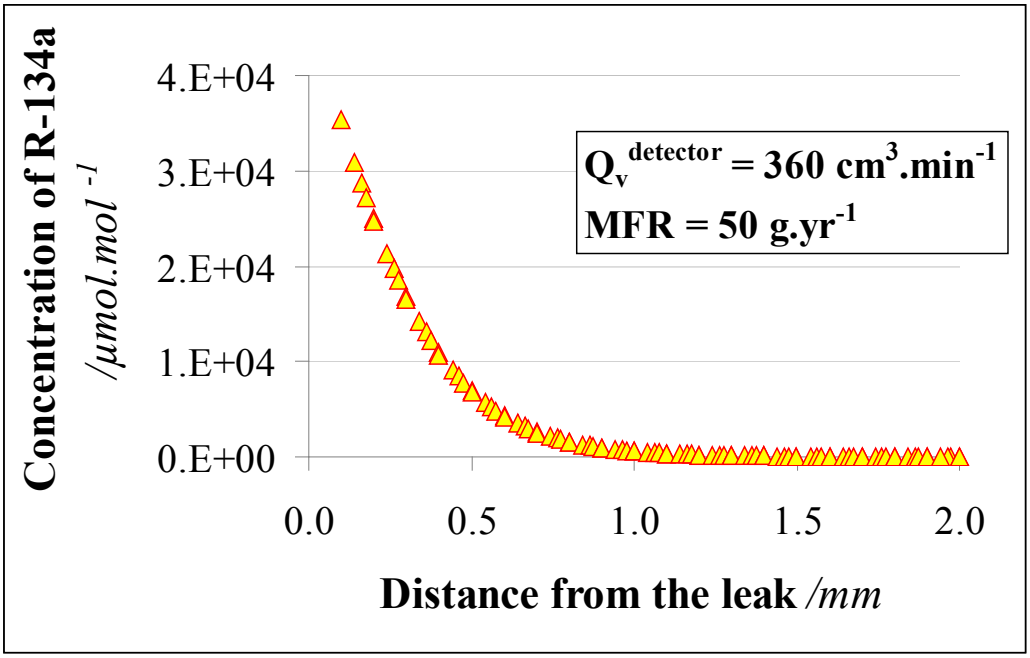

Figure 4.9. Changes of R-134a molar fraction in the cylindrical control volume as a function of coordinate x in the line (x; z = 0; y = 0), due to a 50 g.yr-1 leak and to a 360 cm3.min-1 suction of the detector installed at 2 mm from the leak.

4.4.1.2 Experimental study

This study aims at drawing a cartography of the concentration near a R-134a calibrated leak in order to validate the tendency shown on the phenomenological CFD study. Therefore, the PAS nose is placed at different positions near a calibrated leak and the concentration is measured. Several measurements (minimum 3 measurements) are done in order to check the repeatability.

The concentrations are checked at different distances from the leak and different altitudes.

Description of the experimental stand

The test bench is composed of (see Figure 4.10):

- a mobile platform to which the leak detector is attached,
- a support for positioning the calibrated leak standard,
- a fixed stage to maintain the detector nose,
- a mobile stage for height adjustments of the detector nose,
- a mobile stage to adjust the distance of the detector nose from the leak.

The study is done for 2 leaks whose nominal values are 20 $g.yr^{-1}$ and 50 $g.yr^{-1}$.

This test bench is designed to allow the adjustments of the position of the nose according to the position of the leak. Therefore the position of the detector nose can be controlled and maintained thanks to micrometer adjustment screws (resolution of 0.1 mm). However, the combined uncertainty of the parameter is U = 1 mm: it is mainly due to the parallelism of the detector nose.

The detector is a PAS. The PAS suction rate is not constant: during 20 s, it is about 1800 $cm^3.min^{-1}$ and then it is about 300 $cm^3.min^{-1}$ during 10 s before the analysis of the gas sample.

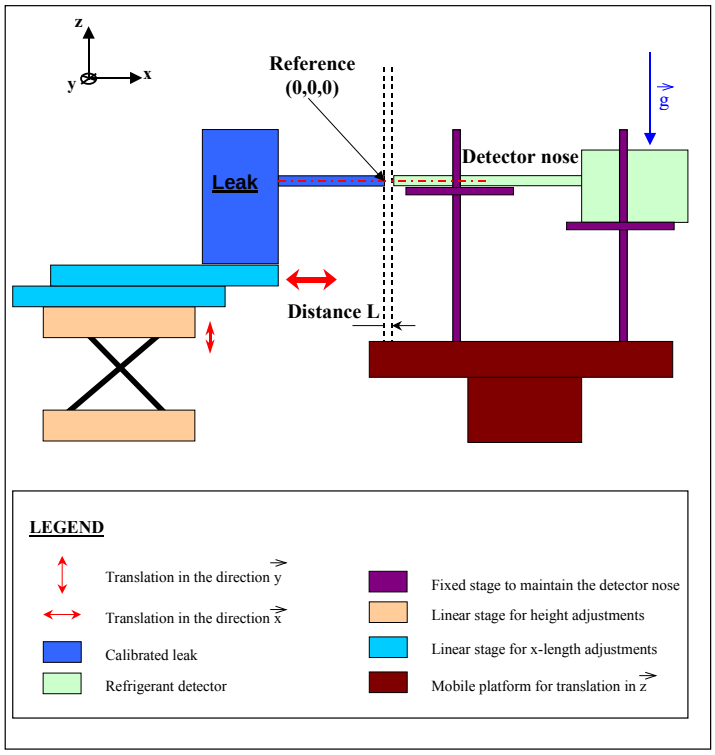

Figure 4.10. Description of the experiment: test bench designed according to the standard E 35422.

Results

Results are reported in Figure 4.11. As expected, the concentration decreases significantly with the distance of the detector probe from the leak. However, if the detector probe is directed as the axis of the leak, it is constant about 54-56 $\mu mol.mol^{-1}$ until it reaches a distance of 5 mm from the leak. The concentration is still detected at a distance of 15 mm, even if it is attenuated.

In this case, the measured concentration is the concentration seen at a certain distance x, when the detector probe is placed at coordinate x, which corresponds to the distance from the leak. However, in the simulation by Fluent, the detector nose does not move. As the main cause of the concentration of R-134a at 2 mm in the simulation is due to the detector VFR, it may explain why in the simulation this phenomenon does not appear. With no detector VFR, only the diffusion of R-134a in the air and the

convection of the air will be considered: the gravity will have a higher influence and R-134a will tend to “fall” instead of moving and reach a distance of 2 mm.

However, the concentration does not remain constant after a distance of 5 mm or when the axis of the detector is not the same as the one of the leak: it decreases and the standard deviation increases with this distance (see Figure 4.11). The tendency shown in the simulation is then verified.

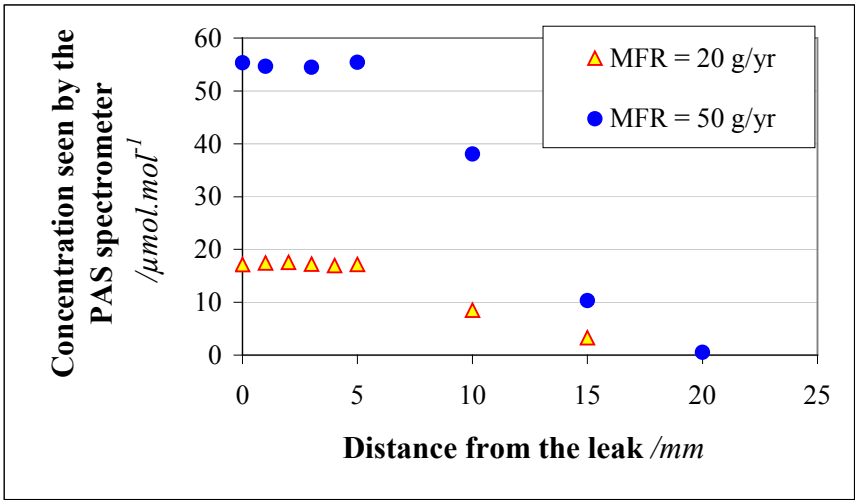

Figure 4.11. Indicated concentration of R-134a as a function of the distance from the calibrated leak to the PAS nose: the nose is centered to the leak orifice (altitude z = 0 corresponds to the center of the leak orifice).

4.4.2 Influence of altitude and gravity

R-134a is heavier than air: its density at 101 kPa and at 20 °C is 4.36 kg/m^3. In theory, R-134a tends to « fall » due to the gravity. The simulation by FLUENT underlines this phenomenon (see Figure 4.12).

The concentration of R-134a decreases when the altitude increases, which means that coordinate z increases. In the simulation, the acceleration due to gravity is defined parallel to the line (0 mm; z ;0 mm). Figure 4.12 presents the graph of the R-134a concentration in the line (x = 2 mm; z; y = 0 mm): the studied surface corresponds to the detector inlet. As expected, the concentration of R-134a follows a dissymmetric repartition because of the gravity.

Results of the phenomenological study show a high influence of the gravity for a detector VFR of 360 cm^3.min^{-1} (see Figure 4.12). As the resolution of FLUENT is not good enough to have accurate results, the study only gives the tendency of the concentration gradient as a function of the altitude: the altitude is given as a function of the R-134a concentration in the line (x = 2 mm; z; y = 0). It also shows that the influence of gravity decreases when the detector suction rate increases (see Figure 4.13). The detector VFR tends to compensate the gas movement due to gravity; this tendency was expected.

According to the simulation, a leak can be better detected if the detector nose is directed to the leakage direction. Besides, the repartition of the concentration is denser at the bottom of the leak than above the leak. An experiment has been carried out: a refrigerant detector whose sensitivity threshold is about 7 g.yr^{-1} is used to detect a mass leak flow rate from a MAC system fitting and confirms the tendency shown by the CFD study (see Section 4.6.3).

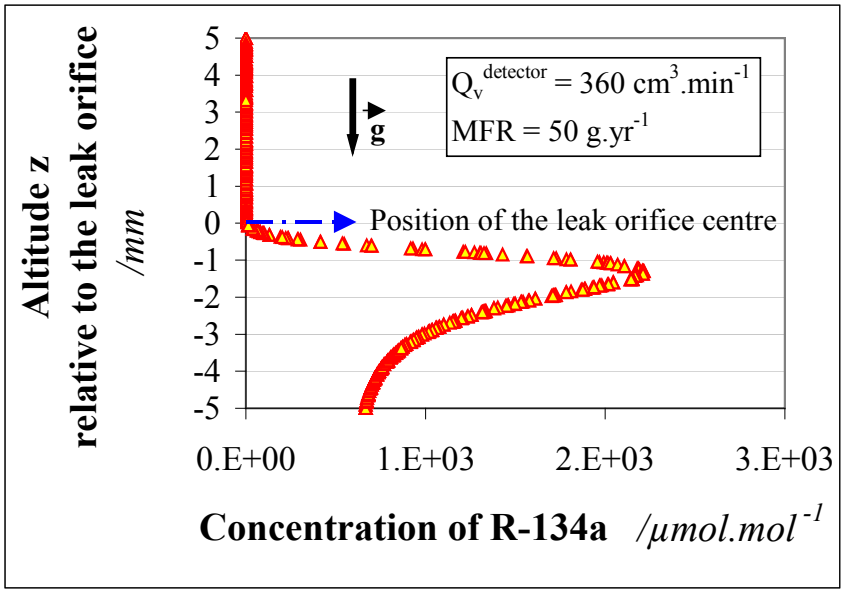

Figure 4.12. Changes of the R-134a concentration in the cylindrical control volume as a function of altitude, in the line (x = 2 mm; z; y = 0), due to 50 g.yr^{-1} leak and to 360 cm3.min^{-1} VFR of the detector installed at 2 mm from the leak.

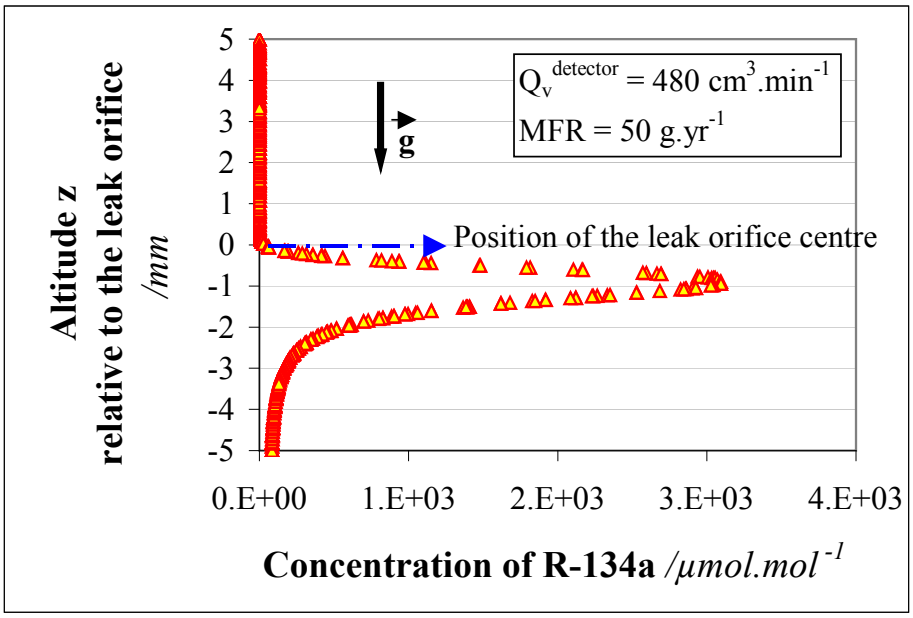

Figure 4.13. Changes of the R-134a concentration in the cylindrical control volume as a function of altitude, in the line (x = 2 mm; z; y = 0), due to 50 g.yr^{-1} leak and to 360 cm3.min^{-1} VFR of the detector installed at 2 mm from the leak.

4.4.3 Conclusions

The concentration seen by the detector probe - which is placed in front of a calibrated leak - is significantly lower than the values calculated by the theory of accumulation in the control volume. The average concentration seen at the inlet of the detector – placed in front of a 50 g.yr^{-1} leak - is about 69 µmol.mol^{-1} according to the phenomenological study and about 55 µmol.mol^{-1} according to the experiment. Consequently, the accumulation method seems to be the best method to detect a refrigerant gas leakage. The wrapping detection method is then more efficient than a classical

detection: if the leakage localization is wrapped – for instance in a vinyl sheet – the concentration seen by the detector will be more significant than if the detector nose is just face to the non-wrapped leakage localization.

Another significant result is the constancy of the concentration seen by the detector when its nose is centered to the leak and at a distance lower than 5 mm. It underlines the fact that in laboratory conditions, the measurement of a refrigerant detector can be repeatable in these conditions. Consequently, during the qualification of a refrigerant detector, it is necessary to impose a distance of the detector nose during the test lower than 5 mm. The standard imposes 2 mm.

The concentration near the calibrated leak also changes with the altitude. The CFD study and the experimental study (see Section 4.4.2) have shown that because of the gravity effect, R-134a tends to "fall": the concentration below the leak is higher than the concentration above the leak. However, according to the experimental measurement of concentration close to a calibrated leak, the difference is not significant when there is no obstacle below the leak. The studies has indeed shown that the maximum concentration detected is when the detector nose is placed in the same direction as the flow direction: the detector VFR tends to compensate the gravity effect.

As the standards to qualify refrigerant detector aim at qualifying the sensitivity threshold of refrigerant detectors in order to control accurately the refrigerant leak detectors and room controllers, this accumulation effect must be avoided. Therefore, during the tests, there must be no obstacles below the calibrated leak. Performances of the detector should be qualified or quantified by considering the detector nose in front of the leak orifice, although the European standard does not require to control the direction of the probe[13]. It must be clear to the user that the qualified sensitivity threshold is relevant only when the detector nose is placed in front of the leak and at the same direction: the direction must then be specified in the result report transmitted to the operator.

4.5 Test bench to qualify the refrigerant leak detector according to the existing standards

Considering the influence parameters identified in the previous sections, a test bench was designed and realized in order to qualify the refrigerant leak detectors according to the standard EN 14624. In reality, other standards are in project – the ASHRAE standard [ASH08] or recently published [SAE06]. A presentation of those three standards (purpose and description of the tests) is done in Sections 4.5.1 and 4.5.2

4.5.1 Objectives of the standards

In order to design the test bench, the objectives of the standards must be clearly defined.

4.5.1.1 European standard and ASHRAE standard

The main objective of those standards is to measure the sensitivity threshold of a locating refrigerant leak detector. The first performance of a leak detector is its minimum sensitivity threshold, which has to be measured by the standard test.

However, the way to use the detector may influence its sensitivity threshold. For instance, a detector that does a zeroing regularly can detect a 5 $g.yr^{-1}$-leak when it is moving, but it might not detect the

[13] In the SAE standard J1627, the direction of the detector is clearly expressed.

leak flow rate when it is stationary. The detector may be saturated when it is placed in a polluted ambiance or when the detector was previously placed in front of a high leak flow rate: its detection performances can be deteriorated. Consequently the standard describes four tests in order to measure:

1. the sensitivity threshold when the detector is stationary,
2. the sensitivity threshold when it is moving in a low R-134a concentration room,
3. the sensitivity threshold when it is moving in a polluted ambiance, and
4. the recovery time of the detector that was previously saturated.

These parameters define the performances of the detector and give information relative to the conditions of use of the locating detector:

- Is this detector conform to the regulation[14] when stationary?
- Is this detector conform to the regulation when moving?
- Is this detector conform to the regulation when in a polluted ambience?
- If the detector is saturated, how much time does the detector need to recover its sensitivity threshold?

4.5.1.2 SAE standard

The purpose of this standard [SAE06] is different from the European standard and the ASHRAE standard. It does not intend to measure the sensitivity threshold of a refrigerant leak detector used to control any refrigerating equipment. It aims at establishing minimum performance criteria for electronic probe-type leak detector for use in automotive air conditioning systems operating with R-134a.

4.5.2 Description of the tests to qualify hand detectors defined in the standards

4.5.2.1 European standard EN 14624

The 4 tests of the standard to qualify the performances of a locating refrigerant leak detector are described here below.

E-1. The detector probe is placed "in contact with"[15] the orifice of several calibrated leaks: 1 $g.yr^{-1}$, 5 $g.yr^{-1}$, 10 $g.yr^{-1}$, 20 $g.yr^{-1}$, and 50 $g.yr^{-1}$. The lowest flow rate that the detector can detect is considered as the sensitivity threshold when the detector is stationary.

E-2. It has to be reminded that the leak detector is placed on a mobile platform (see Figure 4.14), moving from left to right and vice-versa in front of an adjustable leak orifice – adjusted from 1 $g.yr^{-1}$ to 50 $g.yr^{-1}$ at a speed of 2 $mm.s^{-1}$. When the detector is in front of the leak, the distance between the center of the leak and the inlet of the detector is 2 mm. The lowest flow rate that the detector can detect when it is in front of the leak orifice is considered as the sensitivity threshold when the detector is moving at 2 $mm.s^{-1}$.

[14] Its sensitivity threshold must be lower than 5$g.yr^{-1}$ [ARRETE07].

[15] Quotation from the standard [AFN05].

E-3. The second test is repeated in a polluted ambiance. The test bench is installed in a sub-volume where the concentration is twice lower than the practical limit fixed by the manufacturer.

E-4. The leak detector is installed first in contact with a calibrated leak whose flow rate is about the detector maximum threshold (defined by the manufacturer). Just after, the calibrated leak is switched with one whose flow rate is equal to the detector minimum sensitivity threshold. The time needed for the detector to recover its minimal sensitivity threshold is recorded: it is the recovery time.

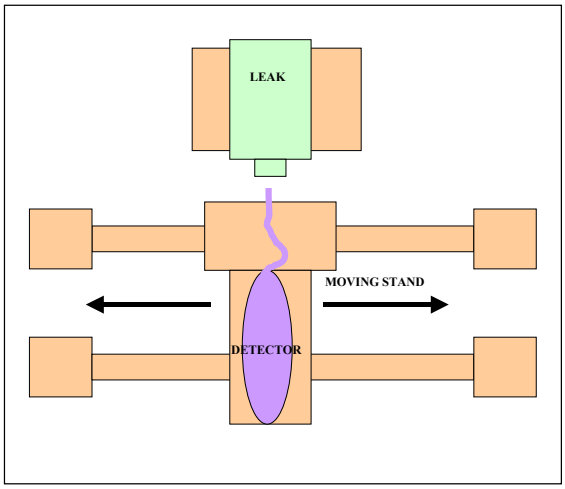

Figure 4.14. Diagram of the testing stand [CLO02].

4.5.2.2 ASHRAE standard

In North America, the ASHRAE is currently developing a new standard dealing with the method to qualify refrigerant leak detectors. The standard is not published yet and may still be slightly modified. Therefore, the description of the standard deals with the draft version [ASH08]. This standard is highly inspired from the European standard EN 14624.

A-1. The detector probe is placed at the testing stand. Periodically, the detector is moved in front of the center of the leak during 5 s: it is placed not "in contact with"[16] but at 1 mm from the orifice of several calibrated leaks between 1 $g.yr^{-1}$ and 50 $g.yr^{-1}$. The lowest flow rate that the detector can detect is considered as the sensitivity threshold when the detector is stationary.

A-2. Test A-2 is similar to Test E-2 the European standard. However, the test is performed for two detector translation speeds (3 $mm.s^{-1}$ and 50 $mm.s^{-1}$) and two distances (3 mm and 5 mm).

A-3. Test A-3 is an additional test: it consists in performing Test E-1 in order to measure the time needed by the detector to stop giving a measurement when it goes away from the leak.

A-4. Test A-4 is similar to Test E-3 in the European standard, but the concentration is fixed to 500 µmol.mol-1.

A-5. Test A-5 is similar to test E-4.

[16] Quotation from the standard [AFN05].

4.5.2.3 SAE standard J1624

According to the standard, the detector shall have three scales that can be manually selected: 4 $g.yr^{-1}$, 7 $g.yr^{-1}$ and 14 $g.yr^{-1}$, and the detector shall detect the selected leak flow rate and higher leaks. But it shall not detect leak flow rate lower than the selected value. Some tests are described in the standard to check this criteria. Only two tests are required:

Test S-1 is similar to Test E-2 of the European standard. However, the distance between the leak center and the detector inlet is about 9.5 mm and the average translation speed is about 75 $mm.s^{-1}$. When the detector reaches an extremity of the test bench, the detector is stopped during (9 ± 1) seconds. The distance from the leak orifice must be horizontal or up to 45° downward offset. Three calibrated leaks (4 $g.yr^{-1}$, 7 $g.yr^{-1}$, and 14 $g.yr^{-1}$) are checked for each scales. The test is performed in a chamber filled with clean air.

Test S-2 is similar to Test S-1. However, R-134a has been injected in the chamber in order to get a contaminated atmosphere (500 µmol.mol-1 at least).

The following paragraphs will specially deal with the European standard [AFN05] and the ASHRAE draft standard [ASH08]. However, since tests are similar, some results can be applied to the SAE standard [SAE06] as well.

4.5.3 Description of the testing stand and precautions

As seen previously, several parameters can influence the expression of the conversion of the concentration to a leak flow rate, particularly from a certain distance (for instance 5 mm as demonstrated for a 50 $g.yr^{-1}$-leak):

- The distance from the leak,
- The direction of the detector nose relatively to the leak axis,
- The gravity.

Therefore, some precautions must be taken into account during the qualification tests described in the standard. These parameters must be controlled in order to ensure the repeatability of the sensitivity threshold measurements.

4.5.3.1 Needed adjustments of the detector position relatively to the calibrated leak

Distance from the leak

In Section 4.4, it was shown that the detector nose must be at a distance lower than 5 mm and ideally lower than 2 mm. In order to confirm those values, a measuring detector has been purchased by the LNE. It is an infrared detector – HLD5000 – that measures with a resolution of 0.1 $g.yr^{-1}$. This detector can detect an 1 $g.yr^{-1}$ leak. Using this apparatus, an analysis of the distance influence in the detector performances is then possible.

Test 1 –described in the European and ASHRAE standards – has been carried out for several distances from the leak. Distances were measured with a micrometer adjustment screw (resolution of 100 µm): see Table 4.1. The detector capability to detect a 1 $g.yr^{-1}$ leak decreases with the distance. It still detects at a distance of 2 mm. However, the signal response is lower than the signal of the detector when it is placed at 1 mm from the leak. At 3 mm, the detector does not always detect: the deviation of the signal is about 100% of the signal. In order to obtain a reasonable repeatability of the results, the distance must be defined lower than 2 mm when stationary.

Table 4.1. Measurements of a calibrated leak (1 g/yr) by a stationary measuring detector (stationary time of 10 s) at several distances from the leak (1 mm; 2 mm; 3 mm).

Distance = 1 mm		Distance = 2 mm		Distance = 3 mm	
Leak Flow rate *g/yr*	**Deviation** *g/yr*	**Leak Flow rate** *g/yr*	**Deviation** *g/yr*	**Leak Flow rate** *g/yr*	**Deviation** *g/yr*
1.0	0.1	0.4	0.2	0.2	0.2
0.7	0.1	0.6	0.2	0.2	0.2
1.3	0.1	0.5	0.1	0.1	0.1
1.0	0.5	0.4	0.1	0.2	0.1
1.3	0.3	0.6	0.2	No detection	0.2
1.2	0.2	0.5	0.1	0.2	0.1
1.0	0.4	0.5	0.1	0.2	0.1
1.4	0.1	0.3	0.2	0.2	0.2
1.2	0.1	0.5	0.2	No detection	0.2
1.2	0.2	0.6	0.1	No detection	0.1
Average value *g/yr*	**Maximum deviation** *g/yr*	**Average value** *g/yr*	**Maximum deviation** *g/yr*	**Average value** *g/yr*	**Maximum deviation** *g/yr*
1.1	**0.5**	**0.5**	**0.2**	**0.2**	**0.2**

Test 2 - described in the European and ASHRAE standards – has been carried out for several distances. For a distance above 1 mm, the signal is significantly attenuated (see Table 4.2). The defined distance between the detector and the calibrated leak must then be lower than 3 mm. For instance, the European standard imposes (2.0 ± 0.1) mm. The test bench must include a micrometer adjustment screw to control the distance between the detector probe and the leak orifice.

Table 4.2. MFR maximum value indicated by the moving measuring detector in response to the presence of a calibrated leak whose value is (1.33 ± 0.053) $g.yr^{-1}$.

	Detector average translation speed	
	2 $mm.s^{-1}$	50 $mm.s^{-1}$
Distance between the detector and the leak: D	**Maximum mass flow rate indicated by the detector**	
mm	$g.yr^{-1}$	
1	2.3	0.6
2	0.7	0.2
3	0.4	0.3
5	0.2	No detection

Direction of the detector nose

In Section 4.4, it was also shown that the detector nose must be centered to the leak. But in the European standard, there is no reference to the direction of the nose, which is also important to ensure the repeatability of the tests[17]. Consequently, a system of linear stages for height and length adjustments is included in the test bench in order to place the detector probe in front of the leak orifice. Fixed stages are designed to ensure that the detector probe direction is fixed during the movement. However, the operator must be aware that the measured threshold corresponds to the sensitivity of the detector when it is detecting a leak whose direction is the same as the nose of the detector: it means that if he does not direct the detector probe towards the leak direction, the real sensitivity threshold of the detector will be different.

[17] In the SAE standard J1627, the direction of the detector is clearly expressed.

Gravity influence

In Section 4.4.2, it was shown that the influence of gravity may not be significant. But, if there is an obstacle below the leak, there will be accumulation of refrigerant. In this case, the sensitivity threshold will be overestimated. Therefore, the test bench was designed in order not generating any accumulation: the calibrated leak is 200 mm above any obstacle.

This precaution is specified in the ASHRAE standard, but not in the European standard. The SAE standard realizes the tests in an enclosed cell. Although it allows maintaining a still environment, there is a risk of accumulation, especially for the tests needing a long time.

4.5.3.2 Influence of the leak detector translation speed: test of the European and ASHRAE standards

Regarding the theory of accumulation presented in Section 4.3.1, the control volume is defined by the distance D between the detector and the calibrated leak when their axis are superimposed and by the detector translation speed v_X. If the distance traveled in one second by the detector is equal to D, the control volume is assimilated to a sphere whose diameter is D (see Annex B in the European standard EN 14624 [AFN05]). However, if the distance traveled in one second by the detector is different from the value D, the control volume shape is more a cylinder than a sphere: the diameter will be equal to (v_X.dt) with (dt = 1 s) and the length will be (l = D). Consequently, the control volume is rising with the detector translation speed. The concentration accumulated in one second in the control volume rises then (see Section 4.3.1). The example of the calculation for a 5 g.yr^{-1} leak is illustrated in Figure 4.15.

Thus, if the detector movement speed is too high, the detector performances are lower than expected and measured according to the European standard EN 14624 [AFN05]. The detector sensitivity threshold is measured when its translation speed is about 2 mm.s^{-1}. The influence of the parameter is not checked in this standard.

However, it is checked in the ASHRAE standard. As previously mentioned, the main difference between the European standard and the ASHRAE standard concerns the test when the sensibility threshold of the detector is measured when moving – called "***test n°2"***. While in the European standard, the distance D between the detector and leak is fixed at 2 mm and the detector translation speed is fixed at 2 mm.s^{-1}, two distances D are tested (3 mm and 5 mm) and two average translation speeds are tested (3 mm.s^{-1} and 50 mm.s^{-1}).

In order to underline the relevance of checking two values, Test n°2 was performed on a measuring infrared refrigerant detector[18], for different distances D and different speeds v_x. The measurements are reported in Table 4.2. The leak measured by the detector decreases when both distance D and detector translation speed increase. Although the apparatus detects a 1 g.yr^{-1} calibrated leak at a distance lower than 3 mm whatever its translation speed, the sensitivity is lower as the MFR value indicated by the detector is lower. At a distance of 5 mm, the detector hardly manages to measure a 1 g.yr^{-1} leak when it moves at 2 mm.s^{-1}, but it does not succeed to detect the leak at 50 mm.s^{-1}. For a distance of 5 mm and a speed of 50 mm.s^{-1}, the sensitivity threshold is between 1 g.yr^{-1} and 3 g.yr^{-1}. Finally, the response time of the detector is also underlined by this test. At the average speed of 50 mm.s^{-1}, the maximum value is indicated by the detector with a delay (~ 1 s - ~2 s).

[18] The resolution of the detector is 0.1 g.yr^{-1}.

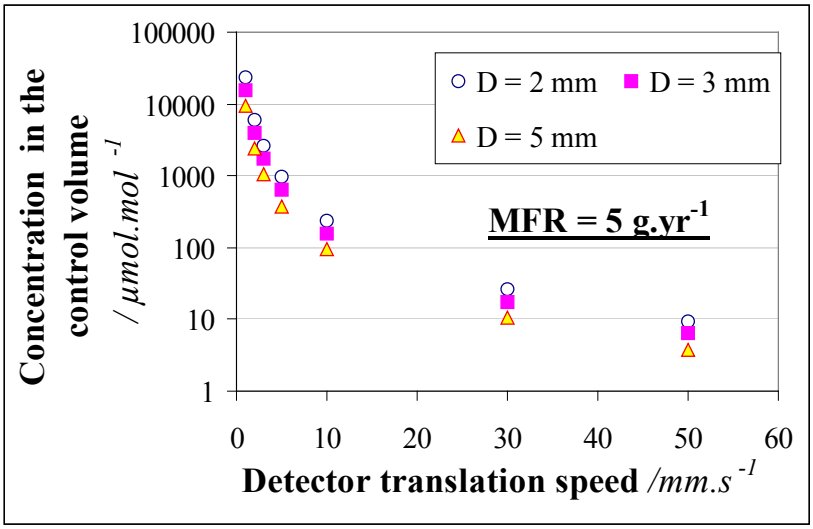

Figure 4.15. Variation of the concentration every second in the control volume (logarithmic scale) as a function the detector translation speed and the distance between the detector and the calibrated leak when their axis are superimposed.

To conclude, when an operator uses a qualified detector to control refrigerating equipment, he must know the distance D_{used} and the translation speed $(v_x)_{used}$ used to measure its sensitivity threshold and take the necessary precautions, i.e.:

- The detector must be moved at a speed lower than vx,
- The potential leak sources must be checked by the detector at a distance lower than D.

It is thus relevant to check the performances of a refrigerant detector at different distances D and speeds v_x.

4.5.3.3 Test bench to qualify refrigerant detectors

The test bench was designed and realized. A description of the testing stand is presented in Figure 4.10 and its photo in Figure 4.16.

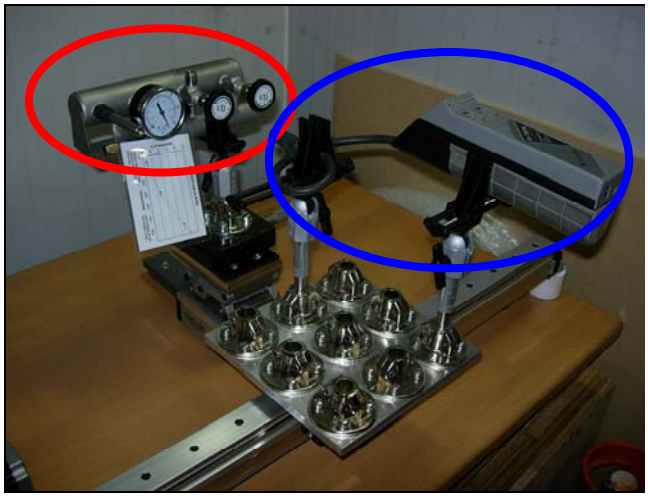

Figure 4.16. Photo of the moving stand installed at the LNE according to the standard EN 14624.
(Blue circle: example of a leak detector in the moving stand ; red circle : example of a calibrated leak)

4.5.4 Precautions in the operating conditions

The gradient of the concentration near a calibrated leak was studied in order to show that the distance, the direction, and the gravity have an impact on the result quality of the tests done according to the standards. However, they are not the only influence parameters: the operating conditions - like the air speeds in the room, the detector VFR and the room temperature – may influence the results and the repeatability of the tests. The testing stand is installed in a room with temperature and air speed controls. Air movements must be avoided (see Section 4.4.1.2). Room doors must not be opened during tests and operators must limit their movements.

4.5.4.1 Influence of the air convection in the room

It seems that the smaller the distance between the detector nose and the leak orifice, the lower the influence of other parameters (the air speed in a room, gravity and so on). When the detector nose is at a distance of 10 mm from the leak, the opening of the room door influences the results. Two openings of a door have been done during the measurement at 10 mm from the leak:

- The first one has made the concentration decrease from 43.7 µmol.mol^{-1} to 0.53 µmol.mol^{-1}.
- The second one has made the concentration increase from 43.6 µmol.mol^{-1} to 51.8 µmol.mol^{-1}.

It has caused a standard deviation of 43% (see Table 4.3). Therefore, the air speed induced from the opening of the door highly influences the detection performances of a detector whose sensitivity is about 0.015 µmol.mol^{-1}. Influenced by this factor and several other non-identified factors, the concentration randomly changes: it is not predictable. Thus, this highly sensitive detector seems to be not capable to always detect a high leak if it is at a distance longer than 5 mm.

Table 4.3. Measurements of the concentration by the PAS as a function of the distance of its nose from the 50 g.yr^{-1}-leak, at the altitude z = 0 mm, which corresponds to the center of the leak orifice.

Distance of the detector nose from the 50 g.yr^{-1}-leak */mm*	**Average concentration** */µmol.mol^{-1}*	**Standard deviation** */µmol.mol^{-1}*	**Relative standard deviation**
0	55.33	0.12	0.21%
1	54.67	0.29	0.53%
3	54.48	0.90	1.7%
5	55.44	0.42	0.75%
10	38	16	43%
15	10.3	7.6	74%
20	0.51	0.30	59%

4.5.4.2 Influence of the leak detector VFR

As the air speed in the room has an influence on the results, the detector VFR should have an influence parameter too. The influence is shown by Equation [4.3]. It means that the repeatability of results will also depend on the tested apparatus itself. The simulation of the R-134a concentration in the control volume has been also carried out for several VFRs. The example of a 50 g.yr^{-1}-leak is presented in this session. Figure 4.17 represents the average concentration of R-134a seen by the detector at its inlet. The simulation has been done for several VFRs of the refrigerant detector: 160 cm^3/min, 320 cm^3/min and 480 cm^3/min.

The theory is set thanks to strong hypothesis. The resolution of the FLUENT software is not good enough to have accurate results. As the leak flow rate is very low, the mesh must be very refined, which is not possible because of a lack of computer memory. The leak orifice is defined as the orifice seen by the operator, but the permeation element is not at the reachable leak orifice. There is then already a larger dilution source of R-134a. The current calculations by Fluent need to have a concentrated leak from an orifice. This value has been adjusted according to the experimental results for a detector VFR of 320 $cm^3.min^{-1}$. Thus the deviation of the theory and the simulation can reach about 50% of the value, when the VFR is different from 320 $cm^3.min^{-1}$.

Results are thus not accurate, but they show the tendency, which is the objective of the current study. According to the theory, the R-134a concentration decreases when the detector VFR rises. This tendency shown by the theory is confirmed by the simulation: the higher the detector VFR, the more significant the dilution.

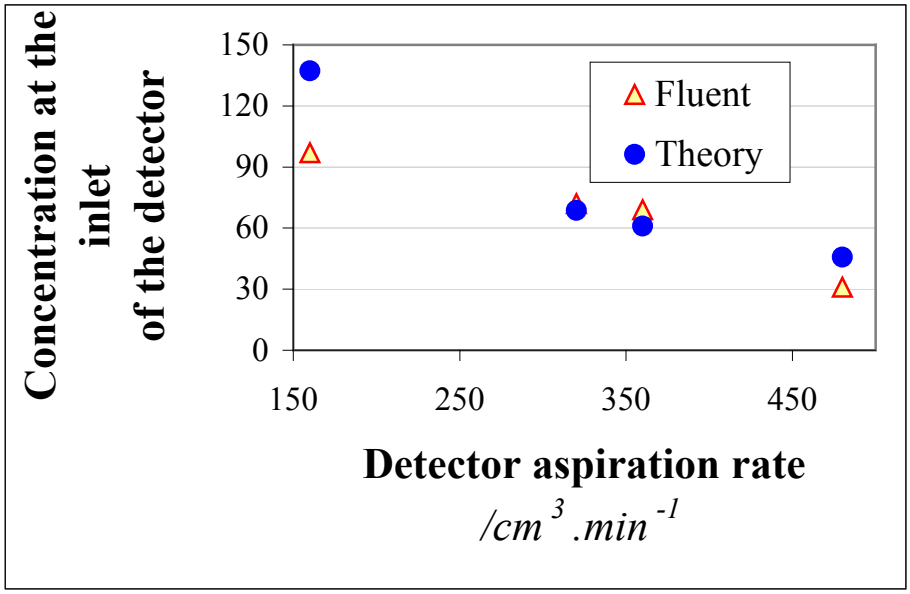

Figure 4.17. R-134a average concentration seen at the inlet of the detector due to a 50 $g.yr^{-1}$ leak as a function of the detector VFR installed at 2 mm from the leak, according to the theory and the simulation by FLUENT.

4.5.4.3 Room temperature

As it was shown in Chapter 1 (Section 1.3.4), leak MFR depends on the temperature, especially permeable leak. The measurement of the leak MFR must be carried out at a constant temperature and the leak MFR value must be the value measured at the same temperature.

The test bench to qualify leak flow rate has the been installed in the same room as the primary standard. The room is temperature-controlled: (20 ± 0.2)°C.

4.5.5 Example of an empirical fitting $Q_m = f(C)$ using the first test of the standard

The PAS probe is placed at 1 mm from the orifice of several refrigerant leak orifices whose nominal values are: 1 $g.yr^{-1}$, 3 $g.yr^{-1}$, 7 $g.yr^{-1}$, 17 $g.yr^{-1}$ and 50 $g.yr^{-1}$. Contrary to any locating refrigerant leak detector, the indicated measurement is a concentration. Its expanded uncertainty is about U = 1.3%.

The calibrated leaks were previously calibrated using the primary standard. Their expanded uncertainties are about U = 2%. The test is done in a temperature controlled room: (20 ± 0.2) °C.

Values are reported in Table 4.4 and the graph CcorrPAS = f(MFR) is presented in Figure 4.18. However, the graph is related to the PAS and its characteristics (the VFR, the performance of the apparatus etc.). It is also related to the conditions of the experiment: air speed in the room, temperature, pressure, gravity and so on. Other influence parameters may not have been identified. There is no guarantee that this conversion of the concentration to a leak flow rate is reproducible: it cannot be reliably predictable as it depends on too many factors.

The only cases to convert concentration into flow rate seems to be when the detection is done at a low distance from the leak and in the direction of the leak flow or when the detection is done in a enclosed volume.

Table 4.4. PAS corrected measurements of the concentration at 1 mm in front of several leaks calibrated by the primary standard.

Calibrated leak MFR $g.yr^{-1}$	**Corrected concentration** C_{corr}^{PAS} $\mu mol.mol^{-1}$
(1.326 ± 0.053)	(1.49 ± 0.045)
(3.808 ± 0.015)	(4.34 ± 0.091)
(6.77 ± 0.27)	(6.77 ± 0.13)
(16.92 ± 0.34)	(17.92 ± 0.31)
(52.50 ± 0.92)	(56.99 ± 0.94)

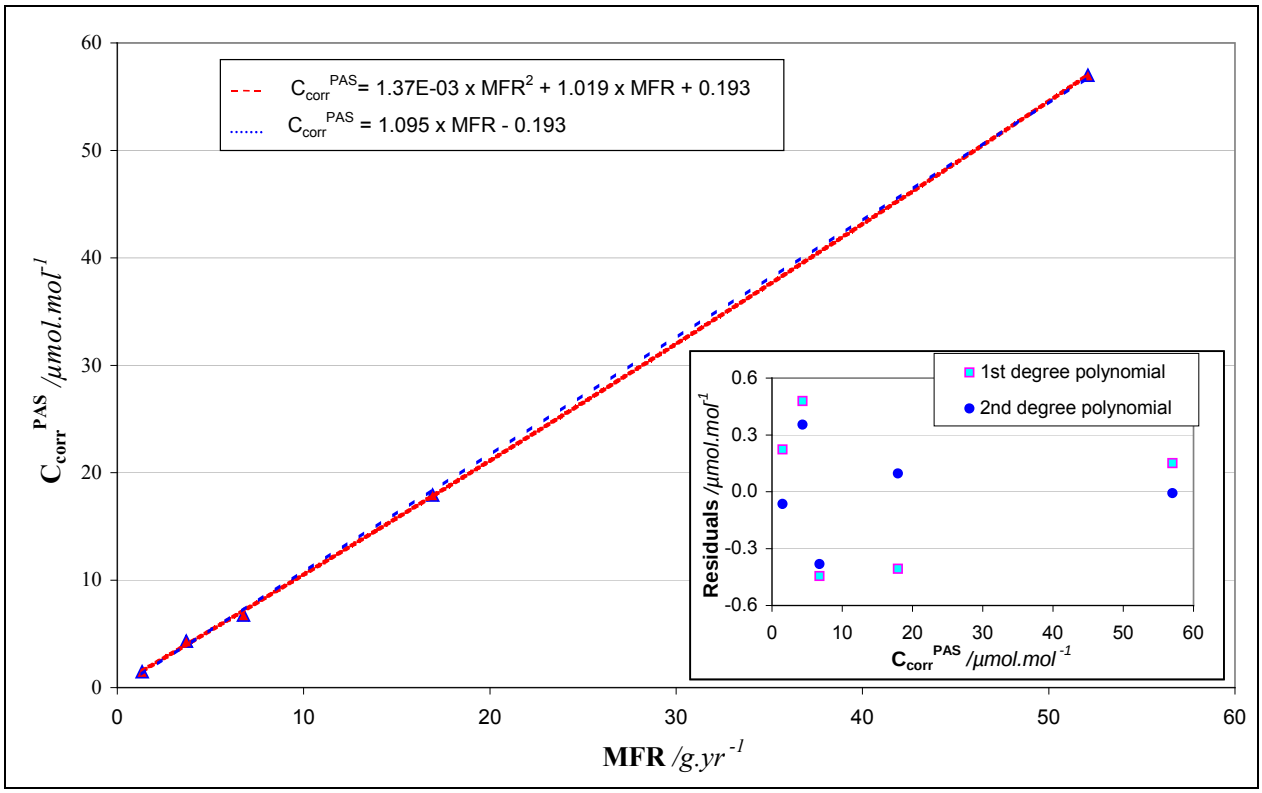

Figure 4.18. Example of a polynomial graph CcorrPAS = f(MFR), established according to Test 1 of the standard EN14624, and its associated residuals.

4.6 Leak detection in real conditions

According to the previous paragraph, the detection of a leak flow rate by a locating detector depends on several parameters, as a refrigerant locating detector measures in reality a concentration. Even if the detection is done in a laboratory with calibrated leaks, the measurements are not always repeatable. It seems that all the parameters are not identified and not well-controlled.

In real conditions, these parameters are even less controlled. For instance, the air speed (temperature gradient in the room, opening of doors, forced ventilation and so on) and the R-134a concentration in the ambient are generally higher. The measurement of the leak detector can then be disturbed. Also, if the temperature room is not controlled, it can influence the leak flow rate.

Finally, the leak is not a calibrated leak but a real leak:

- it is not always unidirectional,
- it is not always a stable value and so on.

Indeed, in some cases, a leak about 10-20 g/yr is not detected by a refrigerant detector whose sensibility was measured about 5 g/yr according to the standard EN 14624. This paragraph aims at explaining these cases.

4.6.1 Leak sources

A leak is a small passage or permeable element through which leakage may occur under the action of pressure or concentration difference across the passage or elements [EHR92].

Calibrated leaks

A calibrated leak has a known, measured leakage rate for a specific gas under specific conditions. Permeation and capillary leaks are the most widespread calibrated leaks [EHR92]:

- The leak element in a permeation leak is made from a material which allows diffusion of one or more species of gas through it. This kind of leak is temperature dependent.
- A capillary leak is a physical leak in which the leak element – a capillary tube or drawn capillaries or crimped metal capillary tube element – provides a physically restricted flow path between the reservoir and the process connection.

In both cases, the calibrated leaks are designed in order that the gas flows through an orifice or a small diffusive surface. Moreover it is located and well-determined for the user. Therefore, the user knows how the detector nose must be directed to detect the leak. The calibration of the leak by the national reference (see Chapters 2 and 3) consists in calibrating the leak flow rate from this orifice only.

Real leaks

Contrary to a calibrated leak, a real leak is not always localized and it can be the combination of several passages or/and several permeable elements. There are many leak causes. The leak can be due to [CAZ08]:

- A structure default of the materials, of the fabrication or else,
- A bad choice or a default of the materials that ensure the leak tightness of the component (VCR fittings, O'rings …),
- An inadequate surface conditions,
- Inadequate dimensions or tolerances of the components,
- Incompatibility between the materials or the fluids and materials….

Therefore, there is not just one point of control in a real leak, there are several.

4.6.2 Real leaks: several control points

Where there is a connection between two fittings or where there is a permeable element, there can be a leakage (see Figure 4.19). For instance, a MAC system – mobile air-conditioning system – is composed of many components (see Figure 4.20):

1. the compressor with its fittings,
2. the discharged line without fittings,
3. the condenser with its fittings,
4. the liquid line without fittings,
5. the TXV (thermal expansion valve),
6. the evaporator with its fittings,
7. the suction line.

A study related to the MAC systems was carried out by the CEP [YU06].

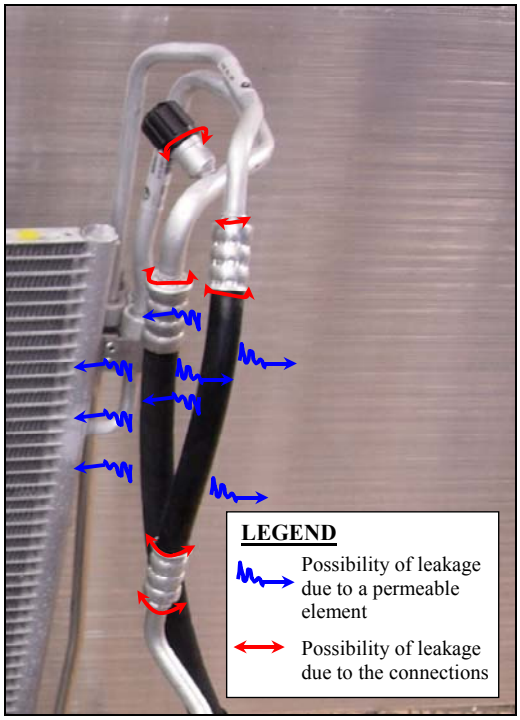

Figure 4.19. Example of possible localizations of leakage in a component of a part of a MAC system.

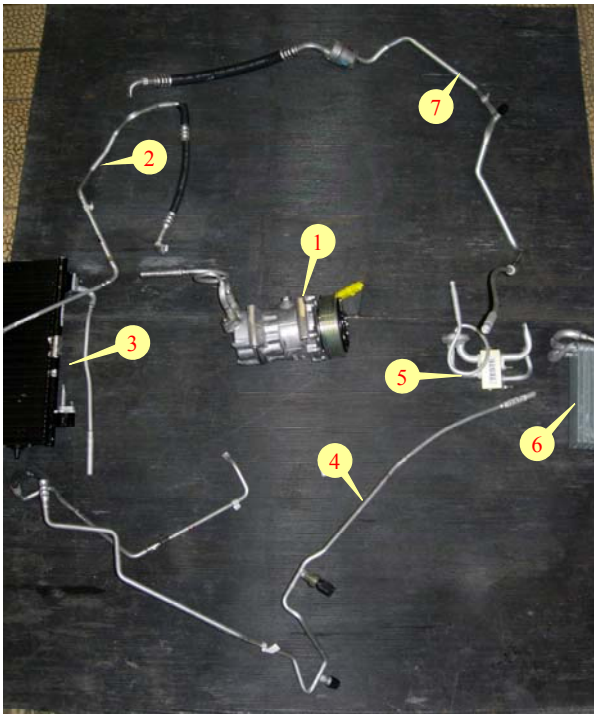

Figure 4.20. Example of a MAC system cut into parts [YU06].

In this study, the leakage of the components with their fittings was measured considering the whole MAC system and then considering the components one by one. 0 presents the results obtained for one MAC system at 40 °C. The leakage from the compressor and the suction line are above 5 g.yr^{-1}, but the other components leak at a rate lower than the maximum tolerated value fixed by the regulations [ARRETE07] 5 g.yr^{-1}. However, the whole system leaks about 30-40 g.yr^{-1}, which is significantly higher than 5 g.yr^{-1}. The total contribution of these components is measured equal to 6.3 g.yr^{-1}. It is not significantly higher than 5 g.yr^{-1}. Nonetheless, a detector whose sensitivity threshold is exactly 5 g.yr^{-1} – for instance - must detect this leak even if the uncertainty of the MFR measurement is about 15%. The leakage sources are from several localizations where it leaks lower than 5 g.yr^{-1}. Therefore, a detector whose sensibility threshold is exactly 5 g.yr^{-1} will not detect those leaks.

Table 4.5. Summary table of the MFR measurement of the components of a MAC system and of the whole MAC system.

Reference	Description	MFR */g.yr^{-1}*
1	Compressor with its fittings	16.5
2	Discharged line without fittings	0.9
3	Condenser with its fittings	2.6
4	Liquid line without fittings	1.7
5	TXV (thermal expansion valve)	1.0
6	Evaporator with its fittings	< 0.1
7	Suction line	5.5
1+2+3+4+5+6+7	**Sum of all MFR**	**28.3**
	Whole system	**37**

4.6.3 Gas escape from a real leak: direction and heterogeneity

Even if there is just one control point, a real leak is not necessarily unidirectional, contrary to a calibrated leak. For instance, a leak can be caused by the default of a O-ring: the leak can be localized in a region of the O-ring or can be from the whole O-ring. Therefore if the total leak from the fitting with this O-ring is higher than 5 $g.yr^{-1}$, it is not certain that a hand leak refrigerant detector, which sucks in one direction only, will detect the leak even if its sensitivity threshold is qualified between 1 and 5 $g.yr^{-1}$.

To illustrate this case, a leak was created in order to have a non-unidirectional leak. The upstream of a micro-valve is connected to a boiler. This boiler is set up at 590 kPa. Downstream of the valve are connected some fittings. A cap is installed at the end of it, in order to make the leak spreading all around (see Figure 4.21).

Direction of the leak

A refrigerant detector whose sensitivity threshold is about 7 $g.yr^{-1}$ is used to detect a leak mass flow rate around the cap. The detector detects at first when it is directed from the top to the bottom (see Figure 4.22.a) and next from the bottom to the top (see Figure 4.22.b). In this case, the leak is directed to the bottom (see Figure 4.21): if the detector probe is directed from the bottom, then its direction is the same as the leak flow direction. The leak direction is defined in Figure 4.21.

According to the CFD study (see Section 4.4.2), a leak can be detected more efficiently if the detector nose is directed to the leakage direction. The repartition of the concentration is denser at the bottom of the leak than above the leak. Therefore, the detector must detect better in the second case. The gravity makes the detection easier as the leakage is in the same direction.

Results confirm the expectations: while the detector does not detect the leak when the nose is directed to the leak from the top, it detects from the bottom. It shows that the detection is more efficient if the nose is placed in the same direction as the diffusion of the leak. On the contrary, if the nose is not placed in the same direction, the VFR of the detector increases the dilution of R-134a in the air[19]: it implies that the VFR has an influence on the detection of the leak.

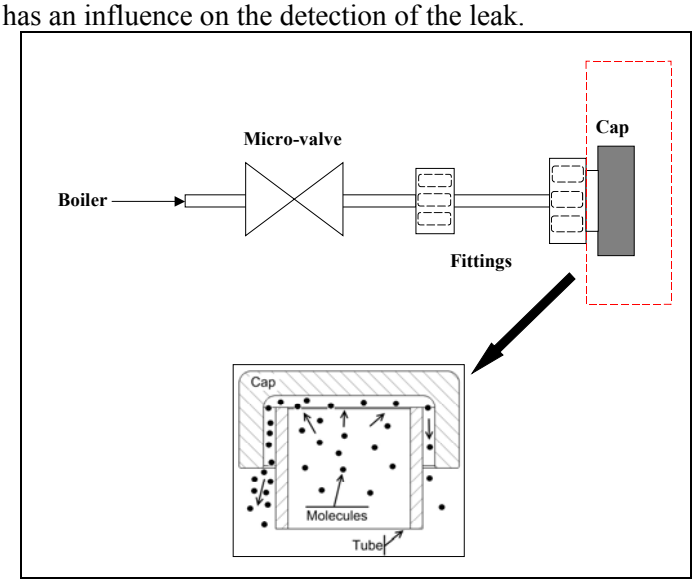

[19] It also implies that the VFR has an influence on the detection of the leak.

Figure 4.21. Diagram of a leak made in order to be non-unidirectional

Figure 4.22.a. Detection from the top of a R-134a leak from a MAC system fitting, using a 7 g.yr-1 sensitivity threshold – detector.

Figure 4.22.b. Detection from the bottom of a R-134a leak from a MAC system fitting, using a 7 g.yr-1 sensitivity threshold – detector.

In order to confirm these results, the experiment described in Section 4.4.1.2 has been done for several altitudes. The concentration seen by the PAS was reported as a function of 3 altitudes (see Figure 4.23):

- z = 0 mm: the leak axis and the detector axis are similar,
- z = -5 mm: the detector axis is 5 mm below the leak axis,
- z = 5 mm: the detector axis is 5 mm above the leak axis.

As expected, the concentration is lower above the leak orifice than below the leak orifice. However, the maximum concentration is seen when the detector nose is placed at an altitude between the leak orifice altitude and the relative altitude -5 mm. It is certainly due to the fact that a calibrated leak is unidirectional contrary to a real leak and that the detector VFR is significant. Contrary to the cap leakage case, these results confirm the phenomenological study results.

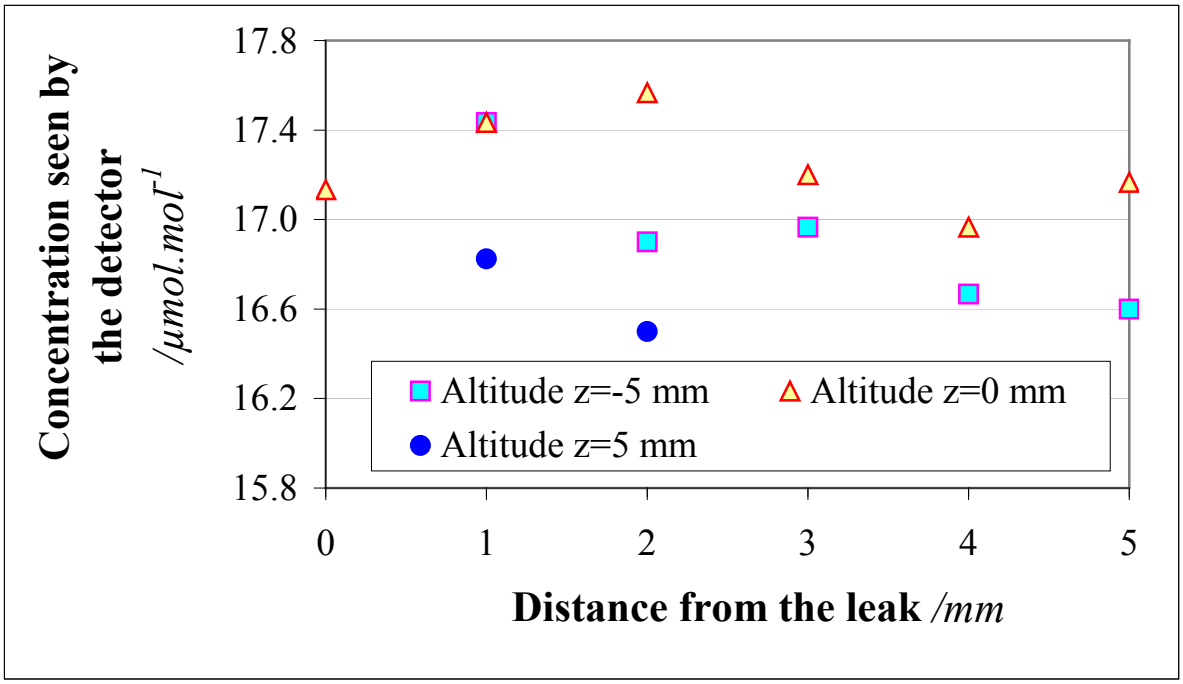

Figure 4.23. Concentration of R-134a seen by the PAS during the detection of 20 g.yr^{-1}-leak, according to the distance from the leak and to the altitude of the detector nose relative to the leak axis (z = 0 mm).

Heterogeneity of a leak

It was just shown that the detection of a leak is easier if the detector is placed in the direction of the flow. However, a leak is not always unidirectional. The leak can flow in several directions in an heterogeneous way. In order to illustrate that, the nose of a measuring leak detector[20] is moved around the outlet of the cap. The detector has shown a response time of 5 s and its accuracy is about 0.5 g.yr^{-1}, when it measures a calibrated leak whose flow rates is between 1 g.yr^{-1} and 50 g.yr^{-1}.

Results – the average value and the standard deviation of N measurements - are reported in Figure 4.24. They show that the escape appears all around the cap and that the leak flow rate is not homogeneous. Indications of the refrigerant detector is not always above 5 g.yr^{-1}.

[20] HLD5000 manufactured by INFICON.

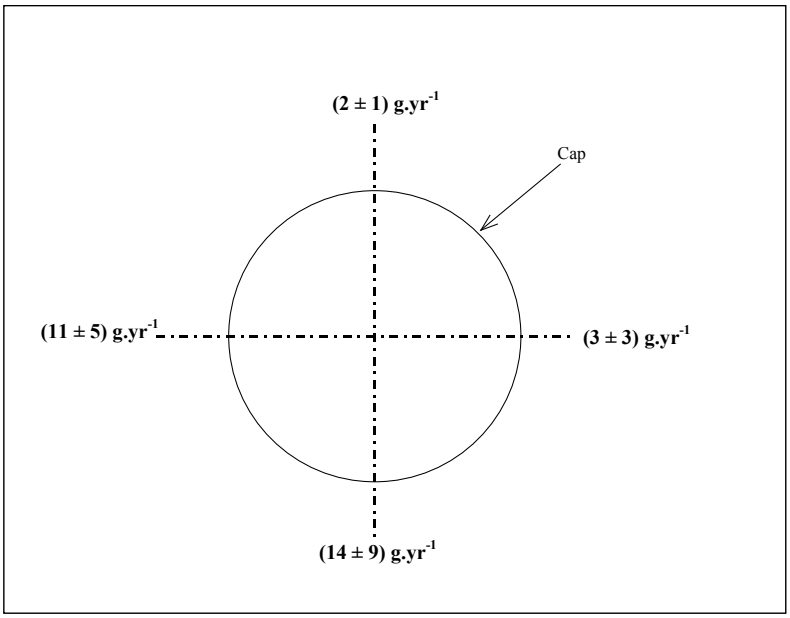

Figure 4.24. Measurements at 4 control points around the cap by an infrared measuring refrigerant detector.

However, as shown in Figure 4.24, the standard deviation of the measurements of the detector are significant. The leak is not stable, which is confirmed by the PAS. The PAS was used to check if this instability was due to the detector or to the leak. The concentration indicated by the PAS also varies with a relevant standard deviation. It shows that a real leak is not always stable. It can significantly vary, which does not allow the detector to stabilize. It shows that the leak detection by the sniffing method[21] is not easy and that if the detector detects some leak briefly, it can be an error or it can be an unstable leak. As the leak was unstable, the experiment could not be repeated. It cannot be confirmed if the total leak is near the sum of the leaks of the four control points or not. Finally, it shows that a real leak, even above 10 g/yr, can be detected or not, even with high sensitivity leak detector.

The total leak measured by the envelopment method is an average leak flow rate of this instable leak. The envelopment method [CLO00] consists in enveloping the control point in a vinyl sheet closed by adhesive tape or in an closed cell (see Figure 4.25). The total leak was estimated: (19.8 ± 3.5) $g.yr^{-1}$. The relative uncertainty is U = 18% and includes the uncertainty components due to:

- pressure,
- temperature,
- air tightness of the cell (checked by measuring the CO_2 variations),
- volume of the cell,
- model deviation of dC/dt.

The leak flow rate is lower than the sum of the average leak flow rate at the four point controls, but it is higher than the leak flow rate seen by the detector punctually in one point control.

This heterogeneity may explain why a highly sensitive detector (sensitivity about 1 $g.yr^{-1}$) does not always detect a leak whose flow rate is higher than 10 $g.yr^{-1}$. But if the leak source is enveloped in a vinyl sheet or in an enclosed cell, the apparatus will detect the leak. In order to illustrate that, the cap was adjusted to make a leak that is not detected by a 7 $g.yr^{-1}$ sensitivity threshold detector. After

[21] The sniffing method consists on directing the detector sniffer in front of the leak and see the response of the detector.

checking that the detector does not detect the leak, the cap is enveloped by a transparent small cell. The PAS is connected to the cell. The concentration inside the cell is analyzed as a function of time. The leak rate is then calculated (see the accumulation method used for the primary standard): it is about (20 ± 2) $g.yr^{-1}$. After the measurement, the detector nose is introduced into the cell: the leak is detected.

To conclude, in some cases, even if the detector is conform to the regulation (sensitivity lower than 5 $g.yr^{-1}$), it may not detect a huge leak (about 10 - 20 $g.yr^{-1}$). Consequently, component wrap in of the component prior to perform leak search ensure the leak localization.

Figure 4.25. Photo of the envelopment of the cap by a closed cell.

4.6.4 Conclusion

The sniffing method depends on too many influence parameters. It is more difficult to control it in the field than in a laboratory. The operators must then be aware that the sensitivity threshold - according to the standard EN 14624 - is measured in a temperature-controlled room using a well-defined calibrated leak (the flow rate and the leakage axis are known). The distance of the detector nose to the leak is 2 mm; the detector speed is 2 mm/s for the sensitivity threshold relative to the movement of the detector. The laboratory method allows the comparison under controlled conditions of the detection performances of the different leak detectors proposed on the market. The correct method of detection in the field depends on the real life conditions and must be analyzed on a case-by-case approach.
Therefore, in the field, operators must:

- Control many directions near a possible leak source,
- The detector speed must be low, about 2 mm/s. If the sensitivity threshold of the detector is checked at a higher speed, the speed can be increased.
- The recovery time of a detector after the detection of a high leak flow rate - measured according to the standard - must be respected.
- The air speed of the ambient should be relatively low.

However, as all the influence parameters may not be defined, as it is not easy to take those precautions, it may not be enough to ensure the quality of a leakage control. The most reliable way to convert concentration in leak flow rate is to enclose the leak. It is clearly verified in the case of a real leak: as the leak is not always localized and stable, the best way to detect a leak is to wrap the leak into

a vinyl sheet and put the detector nose inside the envelopment after a certain time. If there is a leak, the concentration will quickly reach the concentration sensitivity threshold of the detector.

4.7 Conclusions

Hand leak detector sensors are based on several principles; three of them have been presented in this chapter. This literature study underlines the fact that whatever detection method is considered, a hand leak detector measures a concentration and not directly a leak flow rate. As the standard aims at qualifying the MFR sensitivity of the detector in $g.yr^{-1}$ when it does not move, when it moves, and when it is placed in a polluted ambiance, the relationship between concentration and leak flow rate must be known. It has then be studied in this chapter thanks to theory, experiments and simulations using Fluent.

The relationship between the two quantities is not well-defined for the detection conditions. It depends on several parameters; some of them have been identified in the chapter:

- The distance from the leak,
- The gravity: its influence decreases when the detector VFR increases,
- The direction of the detector nose relatively to the leak axis,
- The detector VFR, and
- The ambient air speed.

Those parameters have to be controlled for ensuring the repeatability of the tests. Only the detector VFR depends on the manufacturer and cannot be stabilized if not. A test bench to qualify the detector according to the standards has been designed and realized in order to control the other influence parameters. The test bench is installed in a controlled-temperature room - temperature of $(20 \pm 0.2)°C$ - with low air movements.

As the refrigerant detectors aim at controlling leak tightness of refrigerating and air-conditioning systems, the differences between the operating conditions in a laboratory and in an industrial environment have been analyzed according to the identified influence parameters. The influence parameters cannot be easily controlled during leak detection in real conditions. The operators must be aware of the differences. They must know the results of the qualification in order to understand how to use the detectors. A number of precautions must be taken, and not all are easy to fulfill.

The best way to ensure a well-defined relationship between concentration and MFR remains the relationship used for the primary standard: it means that the wrapping detection method is the most efficient method to localize leaks. If the leakage localization is wrapped – for instance in a vinyl sheet – the concentration seen by the detector will be more significant and repeatable than if the detector nose is just face to the non-wrapped leakage localization. However, as the volume is not well-known, once the leak is localized, the qualified detector can measure the leak MFR.

General conclusion

Nowadays, leak detection is widely used in various fields such as the automotive and the refrigeration industries. The leak tightness of installations charged with refrigerants must be controlled periodically by refrigerant gas detectors, qualified by refrigerant leaks. The implementation of regulation on leak-tightness inspections requires then to implement a complete measurement chain from a primary standard to measure calibrated leak flow rate to the qualification of the performances of refrigerant leak detectors.

At the present time, national laboratories of metrology can calibrate standard leaks of helium using especially vacuum techniques. Based on literature research, some techniques have been explained in this dissertation. The main information is that, in evacuated systems, leak flows are characterized by molecular or transient regime. However, since refrigerant leaks at atmospheric pressure and higher, its flow is characterized by a viscous regime. The transient regime model is not sufficiently accurate yet for the required uncertainties of the calibrate leak flow rate by the regulations. Based on this observation, a new method developed by the CEP is presented in the dissertation. This method is the **infrared method** based on accumulation: it consists in measuring the gas accumulation due to the refrigerant leak inside a closed volume at atmospheric pressure. Based on the observations relative to the previous techniques, **the interests of this method** has been presented:

- **the calibration is done at atmospheric pressure**, which respects the working flow regime of the leaks. It uses R-134a as the tracer gas: at atmospheric pressure this gas is an **excellent gas tracer**
- the infrared detection is **selective**
- by using the infrared detection method, the **accumulation** principle can be used. Therefore, the longer the calibration, the lower the uncertainty.

The primary standard has then been designed according to this technique. The design is based on the experience of the CEP. However, some metrological improvements had to be done, especially concerning the measurements of the concentration and of the accumulation volume. The dissertation has then demonstrated that the **photo-acoustic spectrometer** was metrologically a better choice than the spectrophotometer to measure the concentration in the accumulation volume. The argumentation is based on theoretical and experimental comparisons.

Literature review has allowed listing and analyzing the main techniques to measure a volume: the dimensional method, the gravimetric method, and the static expansion system. An analysis of the accumulation volume characteristics and the establishment of the uncertainty budget relative to the techniques has been carried out in order to established the most appropriate one. The accumulation volume was then defined too complex and could not be easily measured via a dimensional method. The theoretical and minimal uncertainty relative to the gravimetric method already reaches the relative value of 2.1%. It implies a value of 2.1% of the minimal relative uncertainty of the MFR. Using this method, it is not possible to realize a primary standard to measure refrigerant leak MFR with an uncertainty of 1%. Therefore, a static volume expansion method has been defined and analyzed. It is a vacuum technique used to measure pressure knowing two volumes. In this case, a volume is measured knowing the pressures and one of the two volumes. The theoretical and minimal uncertainty relative to this method reaches the value of 0.35%. **The static expansion method** has then been selected.

Based on those results, the primary standard has been designed with some improvements. The main one is the design and the realization of a standard volume to measure the accumulation volume. This volume has been designed to be calibrated by the dimensional method. Therefore, the volume is a

cylinder whose dimensions are controlled with restrictive tolerances. The uncertainty of the standard volume is about **0.1%**. Some improvements – such as the integration of a differential pressure gauge to control the measurement cycle of the spectrometer - has been done thanks to the spectrometer comparison study: the operating principle of the spectrometer is indeed better acknowledged. The test bench has then been realized considering those improvements.

Like the design phase, concentration and volume measurements are the key points of the qualification. The pressure and the temperature are not the main elements of the uncertainty as it is possible to measure the quantities with reasonable uncertainties. One of the main uncertainty component of the MFR measurement has then been identified as the concentration measurement. An analysis of the measurement chain and the potential causes of uncertainties has shown that there are many elements of the spectrometer that must be checked. To simplify the calibration procedure of the photo-acoustic spectrometer, the dissertation has then presented the spectrometer as a box where the concentration gas sample enters and makes the spectrometer give a concentration indication. The comparison of the measurand and the spectrometer indication has then required the manufacturing of R-134a mixtures. The uncertainty of the concentration is about **1%** on the concentration value. However, as the calculation of the leak MFR needs a variation of concentration and not the value of the absolute concentration, some systematic errors are compensated.

The second main uncertainty components of the MFR measurement is the accumulation volume measurement. Thanks to theory, a thermal phenomenological study and experimental results, the LNE can calibrate complex volumes with a relative expanded uncertainty of about **1-2**% using the static expansion method. The studies have established that the uncertainty is mainly due to the temperature homogeneity in the volume.

As the test bench was designed, realized, and qualified, the LNE can now provide calibration of R-134a leaks, in their operating conditions with a relative **expanded uncertainty** around **1-2%**. The objective was to provide a bench to measure R-134a leaks flow rate with an uncertainty of 1%. The objective is then almost achieved. Some improvements can be done. Concerning the spectrometer calibration, a better calibration of the spectrometer can be done by increasing the number of gas standard mixtures and by developing a new fitting method to correct the measurement based for instance on the generalized least squares method. A new concept of photo-acoustic spectrometer can be also developed based on the results of this dissertation: the issue will be to improve the measurement chain based on the analysis of the uncertainty causes. The accumulation volume measurement can also be improved by thermally insulating the system {the accumulation volume and the standard volume}. Finally, the primary standard can now measure R-134a leak flow rate. An extension to other gases can be studied.

The primary leak standard is a good support to ensure the traceability of the calibrated leaks needed to qualify the refrigerant detectors. However, a literature review of some detector operating principles underlines the fact that whatever detection method is considered, a hand leak detector measures a concentration and not directly a leak flow rate. Then, the relationship between the calibrated leak flow rate and the indication of the detector depends on many influence parameters that are not always easily controlled. Analyzing the goals of the standards to qualify detectors, it is clear that this relationship must be repeatable. The main influence parameters have then been identified in this work thanks to theory, experiments and simulations using Fluent. Some precautions have been defined according to the identified influence parameters.

As the refrigerant detectors aim at controlling leak tightness of refrigerating and air-conditioning systems, a study of the differences between the operating conditions in a laboratory and in an industrial environment has then been initiated. Some detection experiments on real leaks have been carried out and presented in the work. They establish that real leaks are not always **unidirectional, stable, and homogeneous.** All the experiments were not repeatable. The best way to ensure a well-defined relationship between concentration and MFR remains the relationship used for the primary standard: it means that the wrapping detection method is the most efficient method to localize leaks. If

the leakage localization is wrapped – for instance in a vinyl sheet – the concentration seen by the detector will be more significant and repeatable than if the detector nose is just face to the non-wrapped leakage localization. However, as the volume is not well-known, once the leak is localized, the qualified detector is necessary to measure the leak MFR. As it is presented in this work, the knowledge of the leak direction improves the detection results. It shows that the knowledge of the leak behavior will allow improving leak detection in industrial sites. To go further, it is then required to study real leak flow behavior by studying the different causes of leaks, the stress in the structure, the permeation mass transfers thanks to theory and CFD software in order to improve the knowledge of the leak flow and to characterized better the measurement of a real leak with a hand refrigerant detector.

Bibliography

Chapter 1

[AFN02] *Essais non destructifs — Contrôle d'étanchéité, Guide pour la sélection des instruments utilisés pour le mesurage des fuites gazeuses*, AFNOR, Norme française NF EN 13625, mars 2002.

[AFN05] *Performances des détecteurs de fuite mobiles et des contrôleurs d'ambiance de fluides frigorigènes halogénés (Performance of portable halogenated refrigerant leak detectors and room controllers)*, AFNOR, European standard, NF EN 14624, July 2005.

[ARRETE00] Arrêté du 12 janvier 2000 relatif au contrôle d'étanchéité des éléments assurent le confinement des fluides frigorigènes utilisés dans les équipements frigorifiques et climatiques.

[ARRETE07] Arrêté du 7 mai 2007 relatif au contrôle d'étanchéité des éléments assurant le confinement des fluides frigorigènes utilisés dans les équipements frigorifiques et climatiques.

[BER06] M. Bergoglio, G. Brondino, A. Calcatelli, G. Raiteri, G. Rumiano, *Mathematical model applied to the experimental calibration results of a capillary standard leak,* Flow Measurement and Instrumentation 17 (2006) 129–138.

[BLA91] B. Blanc, R.P. Henry, and J. Leclerc, *Guide de l'étanchéité* (Guidebook of Leak Tightness), Paris, Société Française du Vide, 1991.

[BOI06] F. BOINEAU, J.C. LEGRAS, P. OTAL *Calibration of helium leaks: reference method and dissemination. Range from* 4.10^{-14} *mole.s*$^{-1}$ (10^{-10} *Pa.m*^{3}*.s*$^{-1}$) *to* 4.10^{-6} *mole.s*$^{-1}$ (10^{-2} *Pa.m*^{3}*.s*$^{-1}$), Salamanca, 2006, 26-28 juin, Spain, WS 18.

[CLO98-1] Denis Clodic*, Zero Leaks,* ch.1, ASHRAE 1998.

[CLO98-6] Denis Clodic*, Zero Leaks,* ch.6, ASHRAE 1998.

[CLO98-8] Denis Clodic*, Zero Leaks,* ch.8, ASHRAE 1998.

[CLO00] D. Clodic, *Measurement and Control of Refrigerant Leaks*, dans AICARR Conference, 2000.

[CLO02] D. Clodic, N. Torbey, F. Fayolle, *Qualification des détecteurs de fuite - Etalonnage des fuites calibrées*, Colloque Effet de Serre III. Paris, 26 septembre 2002.

[CUL87] K.E. Mc Culloh, C.R. Tilford, C.D. Ehrlich, F.G. Long, *Low-range flowmeters for use with vacuum and leak standards,* National bureau of Standards, J. Vac. Scl. Technol. A5 (3), May/Jun 1987.

[DECRET98] Vu le décret n° 92-1271 du 7 décembre 1992 relatif à certains fluides frigorigènes utilise dans les équipements frigorifiques et climatiques, modifié par le décret n° 98-560 du 30 juin 1998

[DECRET07] Décret no 2007-737 du 7 mai 2007 relatif à certains fluides frigorigènes utilisés dans les équipements frigorifiques et climatiques.

[DELA61] J. Delafosse et G. Mongodin*, Les calculs de la technique du vide*, Société Française des Ingénieurs et Techniciens du vide, 1961 (p.34).

[EHR90] C.D. Ehrlich, S.A. Tison, H.Y. Hsiao and D.B. Ward, *A study of the linearity of transfer leaks and a helium leak detector*, Journal of Vacuum Technology A 8 (6), Nov/Dec 1990.

[EHR92] C.D. Ehrlich, J.A. Basford, *Recommended practices for the calibration and use of leaks*, Journal of Vacuum Technology A vol.10 n°1, Jan/Feb, 1992.

[EHR96] C.D. Ehrlich, *A note on flow rate and leak rate units,* Journal of Vacuum Technology A, vol. 4, n°5, Sept/Oct 1996.

[HYL96] R.W. Hyland, C.D. Ehrlich and C.R. Tilford, *Transfer leak studies and comparisons of primary leak standards at the National Bureau of Standards and Sandia National Laboratories*, Journal of Vacuum Technology, vol.4, n°3, pps. 334-337, May/Jun 1996.

[IVE82] M.V. Iverson and J.L. Hartley, *Methods for calibration of standard leaks*, Journal of Vacuum Technology, vol. 20, n°4, April 1982.

[JOU02] K. Jousten, H. Menzer, R. Niepraschk, *A new fully automated gas flowmeter at the PTB for flow rates between 10^{-13} mol/s and 10^{-6} mol/s*, Metrologia, 2002, 39, pp. 519-529.

[LEG97] J.C. Legras, J. LE Guinio, "L'étalonnage des fuites de référence au BNM/LNE", dans le 8ème Congrès International de Métrologie, 1997.

[NIST92] Charles D. Ehrlich, Stuart A. Tison*, NIST Leak Calibration Service*, NIST Special Publication 250-38, 1992.

[REGLEM06] Règlement (CE) n°842/2006 du parlement européen et du conseil du 17 mai 2006 relatif à certains gaz à effet de serre fluorés.

[TIS93] S.A. Tison, *Experimental data and theoretical modeling of gas flows through metal capillary leaks*, Vacuum, vol.44, n°11, n°12, 1993, p. 1171-1175.

[TOR02] N. Torbey, D. Clodic, *Méthode d'étalonnage sur un étalon primaire des fuites calibrées permettant la vérification des performances des détecteurs de fuites des fluides frigorigènes*, étude réalisée pour l'ADEME (01 74 084/11243), décembre 2002

Chapter 2

[AFN75] *Spectromètre de masse, Détecteurs de fuites, Etalonnage,* AFNOR, French standard, NF X 10530, November 1975.

[AND93] Frédéric André, *Spectroscopie photo-acoustique*, Techniques de l'Ingénieur, Traité Mesures et Contrôles, April 1993.

[B&K90-1] J. Christensen, *The Brüel & Kjaer Photo-acoustic Transducer system and its Physical Properties, Danemark: The Brüel & Kjaer Technical Review*, 1990, n°1.

[B&K90-2] J. Christensen, *The Brüel & Kjaer Photo-acoustic Transducer system and its Physical Properties, Danemark: The Brüel & Kjaer Technical Review*, 1990, n°2, pp. 4-19.

[CLO00] D. Clodic, *Measurement and Control of Refrigerant Leaks*, dans AICARR Conference, 2000.

[CLO02] D. Clodic, N. Torbey, F. Fayolle, *Qualification des détecteurs de fuite – Etalonnage des fuites calibrées* , in Colloque à effet de Serre III, 2002.

[HAR00] F.J.M. Harren, G. Cotti, J. Oomens and S. L. Hekkert, *Photoacoustic Spectroscopy in Trace Gas Monitoring, Encyclopedia of Analytical Chemistry*, Wiley, Chichester (2000), p. 2203.

[ISO06] *Préparation des mélanges de gaz pour étalonnage : méthode gravimétrique*, AFNOR, French standard, NF EN ISO 6142, December 2006.

[MOR07] I. Morgado, J.C. Legras, D. Clodic, *Etalon primaire pour les débits de fuites frigorigènes*, Actes de conférences au Congrès de métrologie, 2007, Lille, France.

[ROS80] Rosencwaig, *Photo-acoustics and photo-acoustic spectroscopy,* John Wiley and Sons, 1980.

[SHAF99] S. Schäfer, A. Miklós, P. Hess, *Photo-acoustic Spectroscopy, Theory*, Encyclopedia of Spectroscopy & Spectrometry, Lindon J, Tranter G, Holmes J, Eds, 1999, pp. 1815-1822.

[TOR02] N. Torbey, D. Clodic, *Méthode d'étalonnage sur un étalon primaire des fuites calibrées permettant la vérification des performances des détecteurs de fuites des fluides frigorigènes*, étude réalisée pour l'ADEME (01 74 084/11243), décembre 2002.

[URAS] *Photomètre – Principe de base,* ABB, presentation, Automation Products GmbH Training Analytical.

[VECHT06] M. Vecht, J. Rosendhal*, A photo-acoustic approach to measure refrigerant leaks rate,* VDA Alternative refrigerant winter meeting, 2006.

[VIM94] *Vocabulaire international des termes fondamentaux et généraux de métrologie*, AFNOR, French standard, NF X 07-001, December 1994.

[VOLT00] A. Del Volta, *Mise au point de la Méthode d'Etalonnage par Volumes d'Expansion*, Rapport interne, Laboratoire National de Métrologie et d'Essais, 2000.

[WRI03] J.D. Wright, A.N. Johnson, M.R. Moldover, *Design and Uncertainty Analysis for a PVTt Gas Flow Standard,* Journal of Research of the National Institute of Standards and Technology, vol. 108, n°1, Jan/Feb 2003, 21-47.

Chapter 3

[ALLAN87] D. W. Allan, *Should the Classical Variance be used as a basic measure in standards metrology ?,* Instruments and Measurement, vol. IM-36, n°2, June 1987.

[AND93] Frédéric André, *Spectroscopie photo-acoustique*, Techniques de l'Ingénieur, Traité Mesures et Contrôles.

[B&K90-1] J. Christensen, *The Brüel & Kjaer Photo-acoustic Transducer system and its Physical Properties, Danemark: The Brüel & Kjaer Technical Review*, 1990, n°1.

[B&K90-2] J. Christensen, *The Brüel & Kjaer Photo-acoustic Transducer system and its Physical Properties, Danemark: The Brüel & Kjaer Technical Review*, 1990, n°2, pp. 4-19.

[BER04] M Bergoglio and A Calcatelli, *Uncertainty evaluation of the IMGC-CNR static expansion system*, Metrologia, Vol. 41, pp 278-284, June 2004.

[BONN83] J. Bonnin, *Écoulement des fluides dans les tuyauteries*, Techniques de l'Ingénieur, A738, May 1983.

[BOU90] A. Boussicaud, *Calcul des pertes de charge*, Editions Parisiennes, 1990.

[CARL72] M. Carlier, *Hydraulique générale et appliquée*, Collection du Centre de Recherches et d'Essais de Chatou, Eyrolles, 1972.

[GREEN06] J.C. Greenwood, *Simulation of the operation and characteristics of static expansion pressure standards*, Vacuum, 2006.

[GUM99] *Guide pour l'expression de l'incertitude de mesure,* AFNOR, French standard, NF ENV 13005, August 1999.

[HAR00] F.J.M. Harren, G. Cotti, J. Oomens and S. L. Hekkert, *Photoacoustic Spectroscopy in Trace Gas Monitoring, Encyclopedia of Analytical Chemistry*, Wiley, Chichester (2000), p. 2203.

[HOL69] R. Hollanda, *Evaluation of a volume-ratio system for vacuum gage calibration from 10^{-8} to 10 torr*, NASA TN D-5406, 1969.

[HOL65] R. Hollanda, *Evaluation of a volume-ratio system for vacuum gage calibration from 10^{-6} to 10^{-3} torr*, NASA TN D-3100, 1965.

[IDEL69] I.E. Idel'cik, *Mémento des pertes de charge*, Eyrolles, 1969.

[JIT90] W. Jitschin, J.K. Migwit, G. Grosse, *Gauge calibration in the high and medium vacuum range by a series expansion standard*, Vacuum, Vol. 41, pp 1799-1801, 1990.

[MIK01] A. Miklos, P. Hess, and Z. Bozoki, *Application of acoustic resonators in photoacoustic trace gas analysis and metrology*, Review of Scientific Instruments, vol. 72, n°4, April 2001, 1937-1955.

[MOR07] I. Morgado, J.C. Legras, D. Clodic, *Etalon primaire pour les débits de fuites frigorigènes*, Actes de conférences au Congrès de métrologie, 2007, Lille, France.

[PAD05] J. PADET, *Convection thermique et massique, Nombre de Nusselt, Partie 1*, Techniques de l'Ingénieur, BE 8 206, October 2005.

[PET_ECP] J.P. Petit, *Convection naturelle*, cours ECP.

[PICK48] G.L. Pickard, F.E. Simon, *A Quantitative Study of the Expansion Method for Liquefying Helium,* Proc. Phys. Soc., Vo.l 60, Part 50, n°341, 1 May 1948.

[REDG99] F.J. Redgrave, A.B. Forbes, P.M. Harris, *A discussion of methods for the estimation of volumetric ratios determined by multiple expansions*, Vacuum, Vol. 53, pp 159-162, 1999.

[ROS80] Rosencwaig, *Photo-acoustics and photo-acoustic spectroscopy,* John Wiley and Sons, 1980.

[TASK05] D.G. Tasker, J.H. Goforth, H. Oona, P.A. Rigg, D. Dennis-Koller, J. King, D. Torres, D. Herrera, F. Sena, F. Abeyta, L. Tabaka, *Results from isentropic compression experiments (ICE),* American Physical Society, 14th APS Topical Conference on Shock Compression of Condensed Matter, July 31-August 5, 2005.

[TOM92] R. Tomassone, S. Audrain, E. Lesquoy-de Turckheim and C. Millier, *La régression : nouveau regards sur une ancienne méthode statistique*, Masson, 1992, 46-47.

[TOR02] N. Torbey, D. Clodic, *Méthode d'étalonnage sur un étalon primaire des fuites calibrées permettant la vérification des performances des détecteurs de fuites des fluides frigorigènes*, étude réalisée pour l'ADEME (01 74 084/11243), décembre 2002.

[VECHT06] M. Vecht, J. Rosendhal*, A photo-acoustic approach to measure refrigerant leaks rate,* VDA Alternative refrigerant winter meeting, 2006.

[VIM94] *Vocabulaire international des termes fondamentaux et généraux de métrologie*, AFNOR, French standard, NF X 07-001, December 1994.

[VOLT00] A.Del Volta, *Mise au point de la Méthode d'Etalonnage par Volumes d'Expansion*, Rapport interne, Laboratoire National de Métrologie et d'Essais, 2000.

[WRI03] J.D. Wright, A.N. Johnson, M.R. Moldover, *Design and Uncertainty Analysis for a PVTt Gas Flow Standard,* Journal of Research of the National Institute of Standards and Technology, vol. 108, n°1, Jan/Feb 2003, 21-47.

[WUTH06] C. Wüthrich, M. Coulibaly, *Determination of volume ratios by gas depletion through multiple expansions*, Vacuum 81, pp. 453-458, 2006.

[ZEN90] V. Zeninari, V.A. Kapitanov, D. Courtois, Y.N. Ponomarev, *Design and characteristics of a differential Helmholtz resonant photoacoustic cell for infrared gas detection,* Infrared Physics & technology, vol. 40, Issue 1, 1999, 1-23.

Chapter 4

[ACCOR94] A. Accorsi, *Explosimètres. Détecteurs de gaz*, Techniques de l'Ingénieur, R 2 380, January 1994.

[AFN05] Performances des détecteurs de fuite mobiles et des contrôleurs d'ambiance de fluides frigorigènes halogénés (Performance of portable halogenated refrigerant leak detectors and room controllers), AFNOR, European standard, NF EN 14624, July 2005.

[ARRETE07] Arrêté du 7 mai 2007 relatif au contrôle d'étanchéité des éléments assurant le confinement des fluides frigorigènes utilisés dans les équipements frigorifiques et climatiques.

[ASH08] Method of Test to Determine the Performance of Halocarbon Refrigerant Leak Detectors, ASHRAE standard draft, January 2008.

[BER06] M. Bergoglio, G. Brondino, A. Calcatelli, G. Raiteri, G. Rumiano, *Mathematical model applied to the experimental calibration results of a capillary standard leak*, Flow Measurement and Instrumentation 17 (2006) 129–138.

[CAZ08] X. Cazauran, *Guide de bonnes pratiques pour la détection des fuites de fluides frigorigènes*, CETIM, n°2F30, 2008.

[CLO98-7] D. Clodic, *Zero Leaks*, ch. 7, pps. 105-112, ASHRAE 1998.

[CLO99] D. Clodic, *Qualification des performances des contrôleurs d'ambiance et des détecteurs de fuites de fluides frigorigènes HFC*, (Characterization of performances of HFC refrigerant leak detectors and room controllers), Journée Française du Froid, Interclima – Interconfort. November 9, 1999.

[CLO00] D. Clodic, *Measurement and control of refrigerant leaks*, Evoluzione tecnologica et impiantistica nella refrigerazione commerciale, AICARR Conference, Verone, 14 April 2000

[CLO02] D. Clodic, N. Torbey, F. Fayolle, *Qualification des détecteurs de fuite - Etalonnage des fuites calibrées*, Colloque Effet de Serre III. Paris, 26 septembre 2002.

[DECRET07] Décret no 2007-737 du 7 mai 2007 relatif à certains fluides frigorigènes utilisés dans les équipements frigorifiques et climatiques.

[EHR90] C.D. Ehrlich, S.A. Tison, H.Y. Hsiao and D.B. Ward, *A study of the linearity of transfer leaks and a helium leak detector*, Journal of Vacuum Technology A 8 (6), Nov/Dec 1990.

[EHR92] C.D. Ehrlich, J.A. Basford, *Recommended practices for the calibration and use of leaks*, Journal of Vacuum Technology A vol.10 n°1, Jan/Feb, 1992.

[FIF95] F.W. Fifield, D. Kealey, *Principles and Practice of Analytical Chemistry*, Blackie Academic & Professional, 4th Edition, 1995, ch. 4, pp. 97.

[HUB03] M.L. Huber, A. Laesecke, R.A. Perkins, Model for the viscosity and thermal conductivity of refrigerants, including a new correlation for the viscosity of R134a, Ind. Eng. Chem. Res., 2003, Vol. 42, pp.3163-3178.

[LOY02] D. Clodic, J.C. Loyer, *Analyse des performances de 3 contrôleurs d'ambiance selon la norme E35-422*, MAD L'Outil Froid, Septembre 2002.

[MAD00] D. Clodic, *Mesure des performances de détecteurs manuels de HFC selon la norme E 35422*, MAD L'Outil Froid, mai 2000, n° 21. pp 78-81.

[MAL95] A. Malek, *Detecteurs de fuites: Principe et offre commerciale, Revue Générale du Froid*, 33-41, June 1995.

[SAE06] Minimum performance criteria for electronic refrigerant R-134a leak detector, SAE, standard J1627, 2006.

[SEE05] B. Seemann, *Détection de fuite*, Techniques de l'Ingénieur, R 2 055, March 2005.

[TOR02] N. Torbey, D. Clodic, *Méthode d'étalonnage sur un étalon primaire des fuites calibrées permettant la vérification des performances des détecteurs de fuites des fluides frigorigènes*, étude réalisée pour l'ADEME (01 74 084/11243), décembre 2002

[YU06] Y. Yu, D. Clodic, *Research study on the definition of the implementation of a method of measurement of annual leak flow rates (LFRs) of MAC systems*, ACEA, 2006.

RESUME EN FRANCAIS

Introduction générale

La détection des fuites est une activité de plus en plus réglementée, notamment dans l'industrie automobile et dans la réfrigération. Les équipements contenant des fluides frigorigènes doivent être régulièrement contrôlés en étanchéité avec des détecteurs qualifiés via des fuites frigorigènes calibrées. La thèse vise à mettre en place une chaîne complète d'étalonnage pour la mesure des débits de fuites frigorigènes afin rendre ces contrôles traçables. Elle est composée de quatre chapitres. Les trois premiers chapitres concernent l'étalon primaire pour la mesure des débits de fuites calibrées (en R-134a). Le dernier concerne la méthode de qualification des détecteurs et vise à définir les précautions à prendre lors d'une détection.

Le chapitre 1 décrit les enjeux et la nécessité de mettre en place une nouvelle chaîne d'étalonnage spécifique aux débits de fuites frigorigènes. Un inventaire et une analyse des méthodes existantes – essentiellement des méthodes adaptées aux fuites hélium et des techniques du vide – sont effectués afin de mettre en évidence la nécessité de développer une nouvelle chaîne de mesure spécifique aux fuites calibrées de frigorigènes. De cette analyse, les avantages de la méthode infrarouge développée par le Centre d'Energétique et des Procédés (CEP) seront déduits : elle sera utilisée comme principe de mesure des débits de fuite frigorigène.

Le chapitre 2 présente les différentes étapes de la conception de l'étalon primaire utilisant la méthode infrarouge. Des bancs de mesure ont déjà été conçus par le CEP. La conception du banc se base sur cette expérience tout en améliorant et en optimisant les performances métrologiques du banc. Les points clés identifiés sont : la mesure de la concentration et la mesure du volume d'accumulation. L'étude de conception cherche donc en particulier à présenter les techniques de mesures disponibles. En outre, les performances de ces techniques sont analysées afin d'identifier les plus adaptés à l'objectif : mesurer un débit de fuite avec une incertitude de l'ordre de 1%.

Une fois l'étalon primaire réalisé suivant les spécifications établies dans le chapitre 2, la mesure du débit de fuite peut être qualifiée. Le chapitre 3 présente la procédure d'étalonnage des différents éléments de mesure (instruments, méthodes etc.) des grandeurs nécessaires au calcul du débit de fuite, à savoir la concentration, la pression, la température et le volume d'accumulation. Les causes d'incertitudes des mesures associées aux différentes grandeurs sont en outre analysées et quantifiées. Le budget d'incertitude de mesure du débit de fuite pourra alors être établi.

Une fois qualifié, le banc peut étalonner les fuites calibrées avec une incertitude de l'ordre de 1 %. Ces fuites n'ont d'intérêt que pour qualifier les détecteurs de fuites suivant les normes existantes, en particulier la norme européenne EN 14624. Il est donc intéressant de s'assurer de la traçabilité et de la répétabilité de ces tests en assurant le suivi de ces fuites, mais aussi en identifiant les précautions à prendre lors de ces tests. Le chapitre 4 cherche à définir les précautions à prendre grâce à des études théoriques, phénoménologiques et expérimentales permettant de définir les différents paramètres susceptibles d'influer sur la qualification des performances des détecteurs. Face aux résultats obtenus, une discussion sur les précautions à prendre lors d'une détection en situation réelle sera effectuée.

Chapitre 1 Etat de l'art des méthodes existantes pour la mesure de débit de fuite

1.1 Contexte

Au titre de la décision 2002/358/CE du conseil du 25 avril 2002 relative à l'approbation, au nom de la Communauté européenne, du protocole de Kyoto, la communauté et ses états membres sont tenus de réduire de 8% au cours de la période 2008-2012 leurs émissions de gaz à effet de serre, notamment une grande partie des gaz fluorés tels que le R-134a. Le règlement européen n°842/2006 ayant pour objectif la réduction des gaz à effet de serre vise à une politique de contrôle de l'étanchéité des équipements contenant plus de 3 kg de fluide, la fréquence du contrôle variant en fonction de la charge de fluide. En France, l'arrêté du 7 mai 2007 spécifie la méthode de contrôle d'étanchéité des équipements frigorifiques et climatiques : les contrôles doivent être effectués par un détecteur de fuite manuel avec une sensibilité de 5 g/an ou un contrôleur d'ambiance avec une sensibilité de 10 µmol/mol. Ces sensibilités doivent être mesurées suivant la norme EN 14624. Cette norme préconise l'utilisation de fuites calibrées de fluide frigorigène - R-134a - dont le débit varie de 1 à 50 g/an. Il est indispensable de disposer de fuites étalons permettant de vérifier les mesures effectuées.

1.2 Objectifs

Les objectifs de ce premier chapitre sont les suivants :

- Analyser la pertinence de l'utilisation des méthodes de mesure des débits de fuite déjà existantes, pour mesurer des débits de fuites frigorigènes.
- Présenter la méthode utilisée pour mesurer un débit de fuite frigorigène.
- En déduire l'intérêt de cette méthode.

1.3 Méthodes d'étalonnage de débit de fuite existantes

Bien que la réglementation exige l'utilisation de fuites calibrées de R-134a pour qualifier des détecteurs de fuites, il n'existait jusqu'à présent aucune installation pour mesurer le débit de ces fuites. Toutefois, une chaîne de mesure des débits de fuites hélium est largement mise en place. Par exemple, un étalon primaire est disponible au National Institute of Standards and Technology (NIST) aux USA [NIST92] et est basé sur la comparaison entre le débit issu d'un débitmètre et le débit de la fuite. De même, un étalon primaire basé sur une autre méthode a été développé au Laboratoire National de Métrologie et d'Essais (LNE), en France [LEG97], [BOI06]. Ces étalons mesurent des débits de fuite hélium de 10^{-6} mol/s à 10^{-12} mol/s, ce qui correspond à des débits massiques d'hélium entre (1.3×10^{-4}) g.an^{-1} et (1.3×10^{2}) g.an^{-1}.

1.3.1 Etalon primaire du NIST pour la mesure des débits de fuite hélium

1.3.1.1 Principe de mesure

L'étalon primaire du NIST vise à étalonner des fuites calibrées de gaz hélium [NIST92], [EHR90] de débits estimés entre 10^{-6} mol.s^{-1} and 10^{-12} mol.s^{-1}, ce qui correspond à un débit massique d'hélium entre (1.26×10^{-4}) g.an^{-1} and 126 g.an^{-1} et à un débit de R-134a entre

(3.22×10^{-4}) g.an^{-1} and (3.22×10^{3}) g.an^{-1} [EHR96] . Il est composé de deux éléments principaux (cf. Figure 1.1):

- un système mis sous vide composé d'une chambre supérieure et d'une chambre inférieure,
- d'un débitmètre à pression constante.

Le principe repose sur deux techniques de mesure : la technique d'écoulement par la chambre supérieure et la technique de mesure par division de flux.

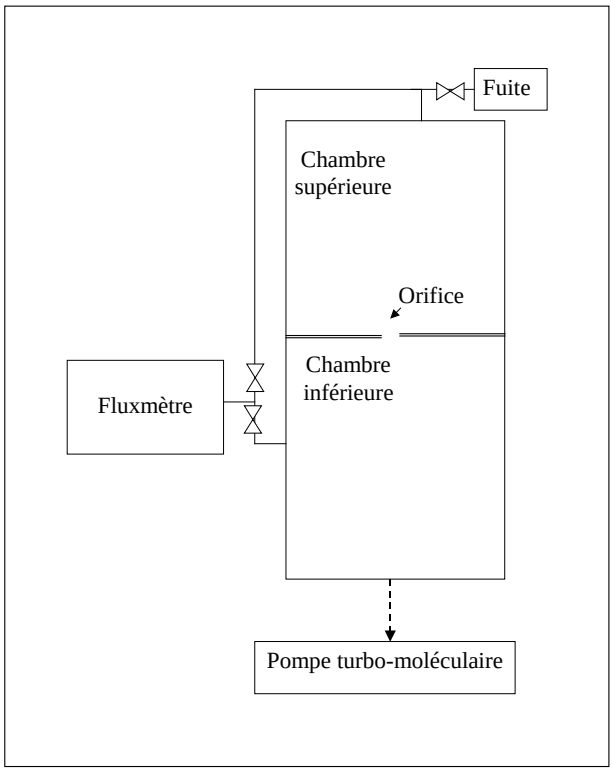

Figure 1.1 Schéma de l'étalon primaire au NIST [NIST92]

Technique d'écoulement par la chambre supérieure

Le capteur différentiel de micro pression permet de mesurer l'écart de pression entre les deux chambres (supérieure et inférieure), l'orifice intermédiaire générant un écart de pression mesurable. En faisant circuler alternativement :

- le débit de fuite en provenance de la fuite à étalonner (1ère mesure),
- celui en provenance du débitmètre (2ème mesure),

il est possible de régler le débit provenant du débitmètre tel qu'il génère le même écart de pression différentielle entre les 2 chambres que celui mesuré pour la fuite étalon. Le débit de la fuite hélium à étalonner peut alors être calculé à partir de la mesure du débit issu du débitmètre.

Le débitmètre (cf. Figure 1.2) est composé d'un volume de référence, d'un volume variable, de deux pistons, d'un système de régulation du déplacement du piston et d'instruments de mesure de la pression. La génération d'un débit de gaz issu du débitmètre entraîne une baisse de la pression dans le volume variable, comparé au volume de référence. Le déplacement des pistons (cf. Figure 1.3) permet alors de faire varier le volume de telle sorte que la pression dans le volume variable reste constante.

Cette technique mesure des débits entre 10^{-6} mol.s^{-1} and 10^{-12} mol/s. Toutefois, les débits de l'ordre de 10^{-12} mol/s sont mesurés avec une incertitude autour de 12%. Afin d'améliorer cette incertitude, une technique par division de flux a été développée par le NIST.

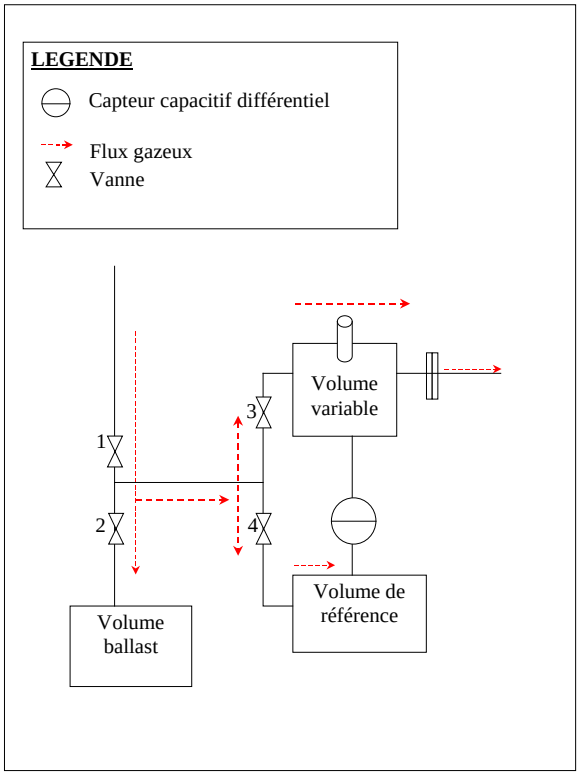

Figure 1.2 Réglage du débitmètre

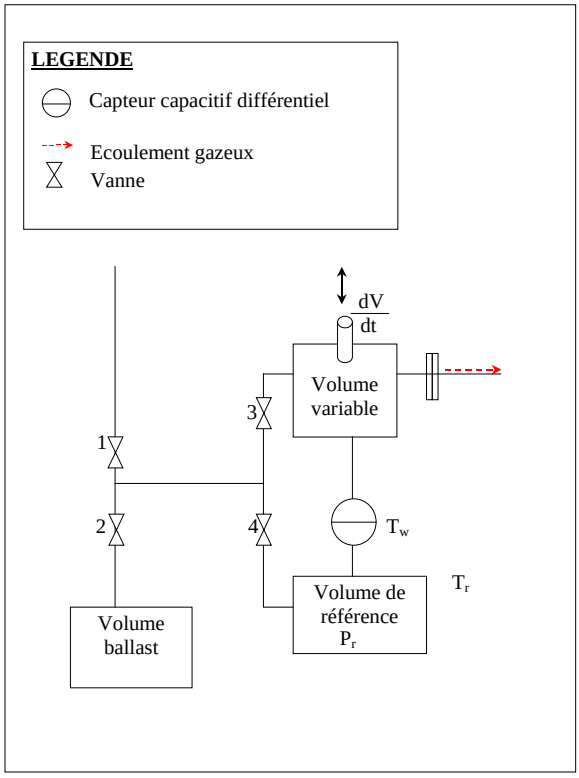

Figure 1.3 Mesure du débit de fuite généré par le débitmètre

Technique de mesure par division de flux

L'objectif de cette technique est d'étendre le domaine de mesure à 10^{-12} mol/s avec une incertitude inférieure à 10%. Le principe de la technique repose sur l'observation suivante : en régime moléculaire, à conductance de l'orifice constante et à pompage constant, le rapport entre le débit entrant dans la chambre supérieure tel que la pression soit P_u et le débit entrant dans la chambre inférieure tel que la pression dans la chambre supérieure soit aussi égale à P_u est constant. Il est noté $R_{u/L}$.

Ce rapport peut donc être déterminé pour des débits supérieurs afin de minimiser l'incertitude. Le débitmètre débite tout d'abord dans la chambre supérieure et la pression P_u est mesurée. Une fois le débit généré par le débitmètre mesuré, il débite ensuite dans la chambre inférieure de telle sorte que la pression soit voisine de P_u. A nouveau le débit généré est mesuré. Le ratio $R_{u/L}$ peut alors être déduit. Une fois ce rapport connu, le débit provenant de la fuite connectée à la chambre supérieure (pression P_u) peut se déduire de ce rapport et du débit du débitmètre entrant dans la chambre inférieure de telle sorte que la pression dans la chambre supérieure soit égale à P_u .

1.3.1.2 Budget d'incertitude

Les composantes d'incertitudes définies par le NIST sont principalement dues à:

- La mesure du débit généré par le débitmètre et détaillée dans l'article [CUL87],
- La mesure de la pression dans la chambre supérieure,
- La mesure de la température dans la chambre,
- La mesure de la vitesse de pompage,
- La mesure de la conductance,
- La mesure du ratio $R_{u/L}$ dans le cas de la technique par division de flux.

Toutefois, le calcul du débit de fuite est basé sur une théorie valable uniquement en régime moléculaire. Une autre méthode basée sur une théorie plus facilement transposable à un régime visqueux a donc été analysée et est présentée dans le paragraphe §1.3.2.

1.3.2 Méthode par variation de pression et/ou de volume

La loi des gaz parfait permet d'établir à température constante une relation entre le débit exprimé en $Pa.m^3.s^{-1}$, la variation de la pression et la variation de volume (cf. équation [1.1]).

$$PV = nRT \rightarrow \frac{dQ}{dt} = R_g T \frac{dn}{dt} = P\frac{dV}{dt} + V\frac{dP}{dt} \qquad [1.1].$$

Trois possibilités se présentent alors:

- seul le volume varie,
- seule la pression varie, ou
- la pression et le volume varient.

Ces possibilités sont décrites dans la littérature: [IVE82], [HYL96], [LEG97], [BOI06].

Ainsi le NIST mesure une variation de volume pour estimer le débit généré par le débitmètre de son étalon primaire (cf. §1.3.1). L'étalon primaire développé au LNE repose sur la variation de pression à température et volume constants [LEG97], [BOI06]. Tandis que la fuite débit dans un volume étalon mis sous vide, un capteur capacitif mesure la variation de pression dans le temps. Le débit peut alors être calculé à partir de cette mesure, de la mesure du volume étalon, de la mesure des volumes morts dus aux connections et au capteur capacitif et de la mesure du débit résiduel (augmentation de pression en l'absence de débit de fuite).

Cette méthode permet de mesurer des débits de fuite entre (2×10^{-7}) $Pa.m^3.s^{-1}$ (ou 8×10^{-11} $mol.s^{-1}$) et (1×10^{-1}) $Pa.m^3.s^{-1}$ (ou (5×10^{-5}) $mol.s^{-1}$), dans des systèmes sous vide, quel que soit le gaz considéré [EHR96]. L'incertitude associée à cette méthode est de l'ordre de 2% pour des débits autour de (1×10^{-1}) $Pa.m^3.s^{-1}$ et peut atteindre 8% pour des débits de l'ordre de (2×10^{-7}) $Pa.m^3.s^{-1}$.

1.3.3 Adaptabilité des méthodes à la mesure des débits de fuite frigorigène aux conditions opératoires

Les deux méthodes présentées – celle utilisée au NIST et celle utilisée au LNE – indiquent que des débits de fuite en hélium – débitant sous vide – peuvent être mesurés avec une incertitude entre 1,3% et 2,7% pour des débits variant entre 10^{-6} et 10^{-10} mol/s. Or les fuites

frigorigènes utilisées ont des débits entre 1 et 50 g/an, ce qui correspond à des débits entre (3.1×10^{-10}) mol/s et (1.6×10^{-8}) mol/s. Ces méthodes pourraient donc les mesurer sous vide.

Néanmoins, les fuites frigorigènes sont utilisées à pression atmosphérique. Leur écoulement est donc caractériser par un régime visqueux et non moléculaire. L'étalon du NIST n'est pas facilement adaptable à la pression atmosphérique car la théorie n'est valable qu'en régime moléculaire. Il semble plus aisé d'adapter la méthode par variation de pression à un système à la pression atmosphérique.

1.3.3.1 Influence de la température

La variation de pression dans un système mis sous vide est beaucoup moins influencé par les fluctuations de température que celle dans un système mis à la pression atmosphérique. Ainsi une variation de température de 1 K peut entraîner une variation de 0,07 Pa lorsque le système est à 20 Pa et une variation de 350 Pa lorsque le système est à la pression atmosphérique.

Ce paramètre est très difficile à contrôler et oblige à augmenter le temps d'étalonnage afin de permettre une variation de pression suffisamment importante pour être détectable. Ceci tend à augmenter les paramètres non maîtrisés tels que la stabilité de la fuite, la stabilité de la température et la stabilité du débit résiduel durant ce laps de temps par exemple.

Il semble alors plus aisé d'établir une méthode de conversion d'une mesure du débit de fuite d'un gaz A -tel que l'hélium - en un débit de cette même fuite débitant un autre gaz B tel qu'un gaz frigorigène.

1.3.3.2 Conversion d'un débit mesuré en régime moléculaire ou intermédiaire à un régime visqueux

Une étude Euromet (n°911) a été initiée par le LNE et l'Istituto Nazionale di Ricerca Metrologica (INRIM) afin de mettre en place cette méthode de conversion dans le cas de fuites capillaires. En effet, si les modèles moléculaires et visqueux peuvent être modélisés, les différents modèles développés pour le régime intermédiaire sont peu probants (cf. [BLA91], [DELA61], [TIS93], [BER06], [NIST92]).

Pour l'instant, des mesures ont été faites sur une fuite capillaire pincée par la méthode de variation de pression avec un système mis sous vide puis à pression atmosphérique. L'INRIM a effectué des mesures à l'aide d'un débitmètre sur la même fuite pour le gaz hélium. Les résultats comparés ne sont pour l'instant pas concluants. La modélisation suivant la littérature entraîne des écarts supérieurs à 10%.

Enfin, si le nombre de Knudsen permet de définir le régime d'écoulement d'une fuite capillaire, il est plus difficile de déterminer le diamètre de référence nécessaire au calcul du nombre dimensionnel pour une fuite capillaire pincée.

1.3.4 Méthode par pesée

Face à ce défaut de traçabilité des débits de fuites frigorigènes, certains industriels étalonnent leurs fuites par une méthode de pesée : il s'agit de mesurer la variation de masse dans le temps. Les fuites étant très faibles, l'étalonnage dure plusieurs mois. Or la fuite n'est pas obligatoirement stable. Notamment, les fluctuations de température et de pression sont

susceptibles de faire varier le débit. Cette méthode ne permet donc de mesurer qu'un débit moyen. Une estimation grossière de l'incertitude permet d'établir qu'elle atteint au minimum 26% du débit. Pour rappel, la qualification des détecteurs nécessite des fuites dont le débit est connu avec une incertitude inférieure à 15%.

1.4 Méthode par spectrométrie infrarouge spécifique aux fuites frigorigènes

Face à une réglementation de plus en plus stricte, le Centre Energétique et Procédés de l'Ecole des Mines de Paris, a développé une méthode propre aux fluides frigorigènes.

1.4.1 Principe de mesure

La méthode repose sur la capacité d'un spectromètre infrarouge à détecter les gaz frigorigènes. Elle consiste à mesurer la variation dans le temps de la concentration de gaz émis par la fuite à étalonner dans un volume d'accumulation fermé. Le volume est à une pression voisine de la pression atmosphérique et à une température voisine de 20 °C.

Chaque minute, la mesure de concentration effectuée par le spectromètre est acquise. La valeur de concentration obtenue est ensuite corrigée par des mesures simultanées de température et de pression. La variation dans le temps de la concentration du gaz étudié dans le volume fermé est établie par la méthode des moindres carrés. Une bonne connaissance du volume d'accumulation permet alors de calculer le débit massique suivant l'équation [1.2]

$$Qm = \frac{M}{R_g}.V.\frac{\partial\left(\frac{P.C}{\mathrm{T}}\right)}{\partial t} \qquad [1.2]$$

1.4.2 Avantages de la méthode

La méthode présente plusieurs avantages :

- Les mesures sont effectuées dans les conditions opératoires de la fuite,
- La méthode procède par accumulation.

Les mesures de débit à pression atmosphérique évitent d'introduire des modèles de conversion d'un régime moléculaire/intermédiaire à un régime visqueux contrairement aux précédentes méthodes. Entre outre, cela permet d'utiliser le gaz lui-même comme gaz traceur. En effet, en régime visqueux, plus la viscosité d'un gaz est faible, plus la conductance est élevée. Par conséquent, le R-134a dont la viscosité est 30% plus faible que l'hélium est un excellent gaz traceur à pression atmosphérique.

Enfin, la spectrométrie infrarouge permet de procéder par accumulation. Or plus le temps s'écoule, plus la concentration dans le volume fermé est élevée. Il suffit alors d'augmenter le temps d'étalonnage pour augmenter la sensibilité de la méthode. Des débits aussi faibles que 1 g/an peuvent alors être mesurés.

1.5 Conclusion

Les textes réglementaires [ARRETE00], [DECRET98], [DECRET07], [REGLEM06] obligent aujourd'hui à mesurer le seuil de sensibilité des détecteurs de fuite frigorigène. Ce dernier doit être inférieur à 5 g/an. Cette mesure est effectuée en accord avec la norme européenne EN 14624 qui préconise l'utilisation de fuites calibrées en R-134a dont le débit doit être raccordé au système d'unité SI.

Actuellement, il existe une chaîne de mesure pour les débits de fuite hélium, mais les mesures sont principalement effectuées sous vide. Ces méthodes sont difficilement transposables à des systèmes en pression atmosphérique. Une étude Euromet entre le LNE et l'INRIM pour établir une méthode de conversion des flux mesurés dans des systèmes sous vide – c'est à dire en régime moléculaire ou intermédiaire – à des flux débités en pression atmosphérique a été initiée, mais ne laisse pas envisager des mesures avec des incertitudes inférieures à 10%. Ces incertitudes seraient donc trop élevées pour des étalons de transfert vers l'industrie.

Afin de répondre à la réglementation, le CEP a développé une méthode basée sur la spectrométrie infrarouge. Elle permet de mesurer les débits de fuites frigorigènes en utilisant le fluide lui-même comme gaz traceur, dans les conditions d'utilisation de la fuite. Afin de permettre la mise en place d'une chaîne d'étalonnage de ces fuites calibrées, le LNE et le CEP ont développé dans le cadre d'un financement de l'ADEME une référence nationale à partir de cette méthode de mesure.

Chapitre 2 Conception du banc d'étalonnage des débits de fuites frigorigènes

2.1 Objectifs

La méthode infrarouge développée pour mesurer le débit de fuite d'une fuite frigorigène – présentée au chapitre 2 – implique que le débit est calculé à partir de la variation de concentration du gaz traceur, de la pression, de la température dans le volume d'accumulation et de la capacité du volume d'accumulation. La pression et la température étant facilement mesurées, les points clés de la conception consistent à sélectionner le meilleur spectromètre infrarouge pour mesurer la variation de concentration de R-134a et de CO_2 et à déterminer la meilleure méthode de mesure de la capacité du volume d'accumulation. Peu de spectromètres infrarouges mesurant de faibles concentrations de R-134a (~ 1 µmol.mol^{-1}) sont disponibles sur le marché. Deux appareils définis sur des techniques différentes sont utilisés au CEP : le spectrophotomètre photo-acoustique et le spectrophotomètre. En ce qui concerne la détermination du volume d'accumulation, trois méthodes principales sont présentées et comparées, afin de déterminer la plus adéquate.

Ce chapitre présente les étapes de la conception de l'étalon primaire pour la mesure de débits de fuites frigorigènes avec une incertitude d'environ 1%. Les objectifs de ce chapitre sont les suivants :

- Evaluer et comparer les performances des deux spectromètres infrarouges détectant les concentrations de R-134a et de CO_2, afin de choisir l'analyseur le plus adéquat.
- Etudier les méthodes d'étalonnage de volume afin de choisir la plus adaptée aux contraintes du banc.
- Définir la capacité optimale des volumes composant le banc.
- Définir l'architecture du banc.

2.2 Choix de la technique de détection infrarouge

2.2.1 Principes de mesure

Il existe actuellement deux spectromètres infrarouges permettant de mesurer des concentrations de R-134a. Les deux techniques se basent sur le phénomène suivant :
Lorsqu'une molécule absorbe l'énergie lumineuse, son amplitude de vibration augmente. Les chocs entre molécules sont donc plus nombreux et la vitesse des molécules augmente. La température, directement liée à la vitesse, augmente également. Par conséquent, si le gaz considéré est confiné dans un volume, la pression augmente aussi. Par le biais de la pression, la concentration peut être connue.

Dans le cas du spectromètre photo-acoustique, et pour effectuer une mesure, un échantillon du mélange gazeux est introduit dans un petit compartiment fermé hermétiquement, la cellule photo-acoustique. Il est alors irradié par de la lumière pulsée à travers les parois de ce compartiment. Lorsque la lumière est absorbée par l'échantillon gazeux, par effet photo-acoustique, l'ambiance va se chauffer et se dilater, entraînant une augmentation de pression. La lumière irradiée étant transmise sous forme de pulsations, la chaleur est également émise sous forme de pulsations. C'est l'effet photo-acoustique : c'est une pression acoustique qui est

mesurée. La concentration de l'échantillon de gaz prélevée peut être directement déduite de cette mesure. En théorie, la relation est quasi-linéaire et peut donc s'écrire simplement:

$$C_{PAS}=Z_{PAS}.p_{PAS}\ , \qquad [2.1]$$

où C_{PAS} est la concentration du gaz à mesurer, p_{PAS} est la pression acoustique mesurée par un microphone et Z_{PAS} un coefficient dépendant de la fréquence du hacheur, de la fréquence d'absorption etc.

Dans le cas du spectrophotomètre, la lumière n'est pas pulsée : c'est une élévation de pression qui est mesurée en permanence. Cette élévation de pression permet de mesurer l'intensité lumineuse entrant dans le photomètre. En effet, l'intensité en sortie de la cuve où circule le gaz à mesurer (cuve de mesure) est détectée par un photomètre. Ce dernier est composé de deux cavités fermées : une empli d'un gaz absorbant, l'autre emplie d'un gaz neutre. Dans la cavité emplie du gaz absorbant, la pression augmente donc. De la mesure de cette élévation, l'intensité entrante dans le photomètre peut être déduite. Si l'intensité sortante de la cuve de mesure est mesurée alternativement avec l'intensité sortante d'une cuve de référence où l'intensité n'a pas été absorbée (cuve emplie d'un gaz neutre), alors la concentration peut être mesurée par la loi de Beer-Lambert. La méthode est donc moins directe que dans le cas de la spectrométrie photo-acoustique. La relation peut s'écrire de manière simplifiée par l'équation [2.2].

$$C=\frac{1}{Z_I}\left[1-\frac{\Delta P^{1}_{Spectrophotomètre}}{\Delta P^{0}_{Spectrophotomètre}}\right] \qquad [2.2]$$

où C est la concentration, $DP^{1}_{spectrophotomètre}$ l'élévation de pression mesurée lorsque la source à traverser la cuve de mesure, $DP^{0}_{spectrophotomètre}$ l'élévation de pression mesurée lorsque la source à traverser la cuve de référence et Z_I est un coefficient dépendant principalement des caractéristiques des cuves, de la source infrarouge, du photomètre et des propriétés du gaz à mesurer et du gaz absorbant dans le photomètre.

2.2.2 Comparaison des méthodes

Afin de déterminer l'impact de la méthode de mesure sur le résultat, les valeurs de l'incertitude sur la mesure de la pression acoustique et de la différence de pression ne sont pas considérées dans cette analyse : par hypothèse, ces incertitudes sont considérées comme égales, soit :

$$\sigma_{PAS} = \sigma^{0}_{Spectrophotomètre} = \sigma^{1}_{Spectrophotomètre} = \sigma\ .$$

L'incertitude relative au spectromètre photo-acoustique u_{CPAS} et l'incertitude liée au spectrophotomètre $u_{CSpectrophotomètre}$ s'expriment donc après calculs par les équations [2.3] et [2.4]

$$u_{C_{PAS}} = Z_{PAS}.\sigma \qquad [2.3]$$

$$u_{C\,Spectrophotometer} = \sqrt{\frac{1}{\Delta P^{0}_{Spectrophotometer}{}^{2}} + \frac{1}{\Delta P^{l}_{Spectrophotometer}{}^{2}}} \cdot \left| \frac{\Delta P^{l}_{Spectrophotometer}}{Z_I . \Delta P^{0}_{Spectrophotometer}} \right| \sigma \qquad [2.4]$$

Puisque les concentrations étudiées sont très faibles (de l'ordre du µmol.mol^{-1}), il peut être considéré que $\left| \frac{\Delta P^{l}_{Spectrophotomètre}}{\Delta P^{0}_{Spectrophotomètre}} \right| \approx 1$, d'où :

$$\frac{u_{C_{Spectrophotomètre}}}{u_{C_{PAS}}} \approx \sqrt{2} \frac{1}{Z_I . Z_{PAS}} . \frac{1}{\Delta P_{Spectrophotomètre}} \qquad [2.5]$$

Après calculs, dans le cas du R-134a, le rapport est estimé à environ 50. Or les fabricants annoncent un seuil de détection de 0,015 µmol/mol pour le spectromètre photo-acoustique et de 0,5 µmol/mol pour le spectrophotomètre, soit un rapport d'environ 34.

2.2.3 Comparaison expérimentale des spectromètres

En premier lieu, il est nécessaire de déterminer quel mesurande doit être considéré et quels paramètres de performances doivent être comparés.

2.2.3.1 Mode opératoire

Les deux analyseurs de gaz mesurent des concentrations. Pour analyser et comparer leurs performances, il est pertinent de définir un mesurande de même nature. Aussi le mesurande doit-il être la concentration du gaz étudié.

Dans notre expérimentation, le mesurande est défini comme la concentration de R-134a maintenue dans le banc de mesure à une température donnée. Une concentration étalon est donc injectée dans le banc à chaque essai et maintenue. Etant donné les faibles débits envisagés, les concentrations que le banc doit mesurer à un instant donné sont faibles. Il a été décidé de faire la comparaison des deux analyseurs au voisinage de leur seuil de détection. Les concentrations étalons sont donc de l'ordre de 10 nmol.mol^{-1} à 2 000 nmol.mol^{-1} pour le R-134a. L'étalonnage consiste à comparer la valeur de la concentration étalon injectée dans le banc avec la concentration mesurée par chacun des instruments.

L'enceinte d'accumulation est reliée aux deux spectromètres à comparer mis en parallèle. En outre, un mélangeur, composé de deux contrôleurs de débits appropriés, est ajouté au montage. Le mélangeur permet de maintenir en amont du banc une concentration connue du gaz étudié en le diluant dans de l'air reconstitué.

Afin de créer des mélanges aussi faibles, les concentrations étalons sont obtenues par dilution d'un mélange mère de R-134a/Air reconstitué avec un mélange uniquement constitué d'air reconstitué. Les « concentrations mères » ont été créées à partir de la méthode gravimétrique [ISO06]. Les valeurs des mélanges $C_{mélange}$ sont respectivement (42,4 ± 0,1) µmol.mol^{-1} et (100,0 ± 0,1) µmol.mol^{-1}. L'incertitude élargie sur les mélanges obtenus est estimée à 2,7 %.

Pour une concentration étalon donnée, plusieurs mesures sont effectuées. Afin de vérifier le comportement des spectromètres en fonction de la température du gaz, la température dans le banc a été régulée dans une fourchette de 23 à 47 °C.

2.2.3.2 Critères de performances

Classiquement, un spectromètre ou spectrophotomètre est évalué à partir des paramètres tels que la fidélité, la justesse, la linéarité, la stabilité etc. [VIM94], [AFN75]. Toutefois, un analyseur mesure une concentration. Or la grandeur recherchée dans notre cas est un débit de fuite à température et pression données. De ce fait, tous les paramètres classiquement utilisés pour évaluer les performances de ce type d'instrument ne sont pas pertinents. En effet, pour calculer un débit, il est nécessaire de pouvoir mesurer une variation de concentration et non une concentration absolue. De ce fait, les paramètres tels que la fidélité, la linéarité et la stabilité de la sensibilité de l'analyseur sont les plus importants. A court terme, la stabilité ne peut être estimée. La comparaison se fera donc sur la fidélité et la linéarité des appareils.

2.2.3.3 Résultats obtenus

Les résultats montrent que la répétabilité des analyseurs associée à 25 mesures est inférieure à la résolution respective de chaque analyseur annoncée par le fabricant, à savoir 15 nmol/mol pour le spectromètre photo-acoustique et 500 nmol.mol^{-1} pour le spectrophotomètre. De même, les résultats montrent que l'écart de linéarité du spectromètre photo-acoustique et l'écart de linéarité du spectrophotomètre sont respectivement de 0,011 % et de 0,6 % de l'étendue de mesure de 0 à 150 µmol/mol, domaine de fonctionnement qui nous intéresse pour l'étalonnage des fuites. Ces écarts de linéarité sont inférieurs ou équivalents à la résolution des analyseurs. La résolution de l'analyseur photo-acoustique à faible concentration est telle que des changements de concentration très faibles – entre 0 et 1,3 µmol/mol – sont parfaitement décelables (cf. Figure 2.1).

Optimiser la qualité des mesures des débits de fuites et le temps de mesure revient à choisir le spectromètre ayant la meilleure sensibilité, et le signal de sortie le plus linéaire. Bien que les résultats affichés ne donnent que des résultats sur une gamme restreinte, à savoir 0 à 1,3 µmol/mol, ces résultats permettent tout de même d'établir que la détection infrarouge photo-acoustique est la plus adaptée à la méthode de mesure des débits de fuites frigorigènes. Un point supplémentaire à 40 µmol/mol a permis de conforter cette décision.

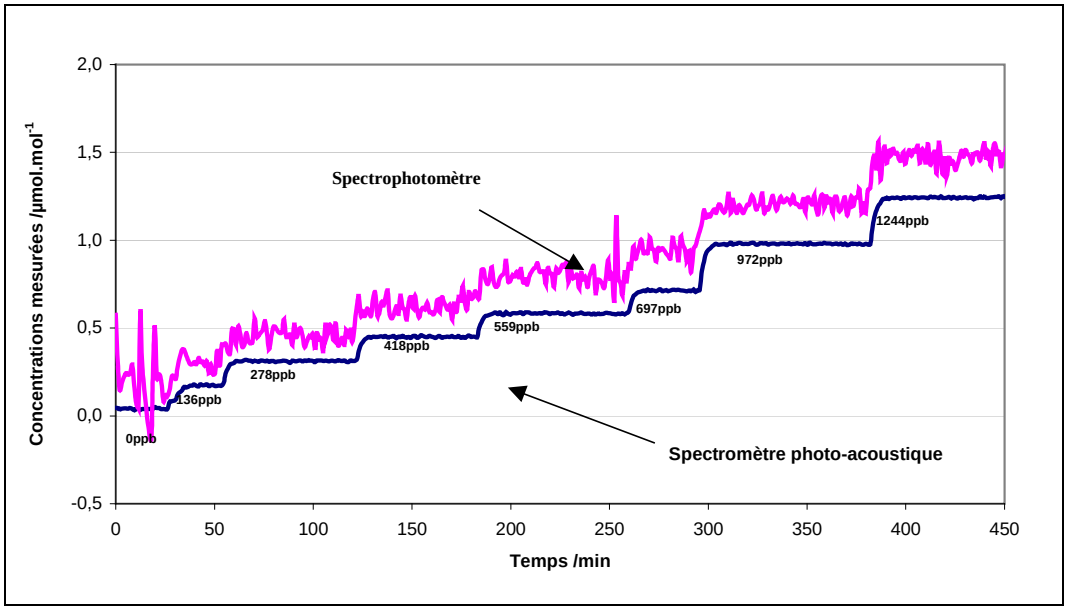

Figure 2.1. Mesures par le spectromètre photo-acoustique et par le spectrophotomètre d'un échantillon de 0 à 1,30 µmol.mol^{-1} de R-134a – *1 ppb = 0,001 µmol.mol^{-1}*

2.3 Choix de la méthode d'étalonnage du volume d'accumulation

Trois méthodes sont principalement utilisées pour étalonner un volume :

- La méthode dimensionnelle,
- La méthode gravimétrique,
- La méthode par les volumes d'expansion.

Elles ont été analysées afin de déterminer laquelle était la plus appropriée afin d'obtenir une incertitude relative significativement inférieure à 1%.

La méthode dimensionnelle consiste à étalonner les différentes dimensions du volume (cylindricités, diamètres, longueurs, rugosité, parallélisme etc.) et de calculer le volume à partir de ces mesures. Le volume d'accumulation est trop complexe pour permettre d'utiliser une telle méthode.

La méthode gravimétrique consiste à injecter une certaine masse d'un gaz tel que l'argon dans le volume d'accumulation mis initialement sous vide et de mesure la variation de masse volumique dans le volume. Comme le spectromètre infrarouge ne peut être soumis à une pression en dessous de 90 kPa, une première mesure doit s'effectuer en isolant le spectromètre. Une deuxième mesure doit ensuite être faite avec le spectromètre. Une simulation des mesures du volume (spectromètre isolé) indique que l'incertitude est d'environ 2,1 %. Bien que cette incertitude théorique ne prenne pas en compte toutes les sources d'incertitude, elle est déjà trop élevée pour permettre la mesure d'un débit de fuite à 1 %.

La méthode par les volumes d'expansion consiste à effectuer une détente adiabatique de gaz entre un volume mis en surpression et un volume mis en dépression, initialement isolés par une vanne. Il possible dans ce cas de mettre le volume d'accumulation en légère surpression pour que la pression reste dans les limites tolérées par le spectromètre. Une estimation grossière des incertitudes permet d'établir que l'incertitude peut être inférieure à 1 % suivant les capacités du volume d'accumulation et du volume étalon.

2.4 Optimisation de la capacité des volumes

2.4.1 Optimisation de la capacité du volume d'accumulation

Puisque la méthode utilisée pour mesurer les débits de fuites frigorigènes est basée sur l'accumulation du gaz traceur, la taille du volume d'accumulation a un impact sur la durée de l'étalonnage. L'étalonnage ne doit pas durer trop longtemps afin de limiter les composantes d'incertitude liée à l'environnement. Le volume doit donc être le plus petit possible. En effet, plus le volume est petit, plus la concentration du gaz traceur augmente rapidement dans le volume. Toutefois l'étalonnage doit être suffisamment long afin d'avoir suffisamment de points pour exploiter les données acquises. En outre, plus le volume d'accumulation est petit, plus l'incertitude sur la détermination de sa valeur risque d'être importante. Le choix de la taille du volume d'accumulation doit donc être un compromis devant ces contraintes.

Il peut être établi que la taille du volume d'accumulation ne peut dépasser 1 ou 2 dm^3, afin de ne pas excéder un temps d'étalonnage de 1 heure. En effet, un volume plus important entraînerait des temps d'étalonnage trop long pour atteindre une incertitude de l'ordre de 1 % [TOR02], [MOR07]. Toutefois, la mesure d'un débit de fuite de 50 g/an implique une forte variation de la concentration dans le temps. Des essais effectués montrent que 10 mesures de

concentration sont suffisantes pour mesurer un débit de l'ordre de 50 g/an. Afin d'éviter la saturation des circuits du spectromètre, l'échelle de mesure prise en compte est de 0,015 µmol/mol à 150 µmol/mol. Un volume de 1 dm^3 serait donc trop petit pour effectuer l'étalonnage d'une fuite de 50 g/an. Pour conclure, un volume d'accumulation de 2 dm^3 semble le plus adéquat.

2.4.2 Optimisation de la taille du volume étalon

Le volume étalon a été conçu dans l'optique de mesurer le volume d'accumulation par la méthode des volumes d'expansion. Il doit être le plus simple possible afin d'être étalonné à partir de mesures dimensionnelles. Le volume étalon est composé d'un volume cylindrique principal, d'une vanne isolant le volume étalon du volume d'accumulation, des raccords entre le volume principal et la vanne, des raccords entre le volume principal et le manomètre. Seuls les volumes intérieurs sont à déterminer.

Comme l'analyseur de gaz est compris dans le volume d'accumulation, la pression dans le volume d'accumulation doit obligatoirement être comprise dans la gamme acceptable par l'instrument de sorte qu'il ne soit pas détérioré: entre 90 kPa et 110 kPa. Ainsi, en fixant les pressions initiale et finale dans le volume d'accumulation, une estimation des composantes d'incertitudes dues à la mesure des pressions, à la mesure des températures et à la connaissance de la taille du volume étalon en fonction du rapport des deux volumes peut être effectuée. Il s'agit d'une première estimation qui peut être sous-évaluée. Néanmoins, il ne s'agit pas de qualifier la méthode pour l'instant mais de déterminer la taille optimale du volume étalon.

L'incertitude est établie en considérant que :

- la température suit une loi rectangulaire d'incertitude (20 ± 0,10) °C,
- la pression suit une loi normale d'incertitude U = 15 Pa, et
- le volume étalon est réalisé de telle sorte que son volume puisse être connu avec une incertitude relative de U = 0,10 %.

En conclusion, le rapport optimal théorique des deux volumes $\frac{V_{Acc}}{V_E}$ est environ de 4 pour une pression initiale entre 10 à 35 kPa dans le volume étalon et entre 105-110 kPa dans le volume d'accumulation. L'incertitude relative estimée sur le volume d'accumulation est de 0,35 %.

2.5 Conception du banc de l'étalon primaire

Une fois le spectromètre et la méthode d'étalonnage du volume choisis, l'architecture de l'étalon primaire peut être établie. Le calcul du débit d'une fuite de frigorigène nécessite la mesure du volume d'accumulation, de la concentration accumulée, de la pression et de la température dans le volume d'accumulation. Le banc doit par conséquent pouvoir:

- Mesurer la concentration et la pression/température associées dans le volume d'accumulation,
- Mesurer le volume d'accumulation
- Rincer le volume d'accumulation et le volume étalon afin de s'assurer qu'il n'y a pas de pollution dans les volumes (notamment pollution en CO_2 et en vapeur d'eau).

- Se mettre sous une pression voisine de la pression atmosphérique.

Afin de pouvoir assurer toutes ces fonctions, l'architecture du banc est décomposée en plusieurs circuits (cf. Figure 2.2).

Circuit de mesure

Le circuit de mesure représente tous les éléments de mesure du banc reliés à l'enceinte de mesure, en particulier le circuit lié au spectromètre photo-acoustique et isolé de l'enceinte de mesure par deux vannes. Ce circuit représente le volume d'accumulation.

Circuit d'alimentation en air reconstitué

Le circuit d'alimentation en air reconstitué est isolé de l'enceinte par une vanne. Ce circuit a pour premier rôle d'assurer la mise sous pression des circuits fluidiques à une pression voisine de la pression atmosphérique, tout en assurant une ambiance non polluée composée essentiellement d'air reconstitué.

Circuit de mise sous vide

Le circuit de mise sous vide du volume d'accumulation (ou de l'enceinte de mesure uniquement) et/ou du volume étalon comprend une pompe à vide sèche et est délimité par une vanne qui isole la pompe à vide du volume étalon et de l'enceinte de mesure.

Ce circuit a un double objectif :
- mettre en dépression le volume étalon lors de l'étalonnage du volume d'accumulation par la méthode des volumes d'expansion,
- évacuer les impuretés des circuits pneumatiques de la référence.

Circuit d'étalonnage du volume d'accumulation : « circuit volume étalon »

Le circuit d'étalonnage du volume d'accumulation permet l'étalonnage du volume d'accumulation par la méthode des volumes d'expansion. Il relie le volume au volume étalon, isolés l'un de l'autre par un jeu de vannes.

Le volume principal est un volume cylindrique de valeur nominale 0,5 dm^3 créé exclusivement à cet effet. Comme il doit être relié au volume d'accumulation et au manomètre, des volumes additionnels (tubes, raccords et volumes intérieurs de la vanne et du manomètre) doivent être pris en compte. Toutefois, ces pièces étant des pièces standards, les seules tolérances pouvant être exigées lors de la fabrication du volume sont les tolérances sur les dimensions du cylindre, sans considérer les pièces additionnelles. Ce cylindre sera nommé « cylindre principal ». Il est décomposé en trois pièces :
- Un cylindre creux ouvert aux extrémités,
- Deux couvercles fermant le cylindre aux extrémités : l'étanchéité est assurée par des joints toriques.

Il a été exigé que le cylindre principal ait les caractéristiques suivantes:
- Le diamètre interne du cylindre est fixé à (82,50 ± 0,02) mm à n'importe quelle hauteur du cylindre,
- La longueur interne du cylindre (de la surface interne d'un couvercle à celle du second couvercle) est fixée à (95,05 ± 0,03) mm,
- La tolérance sur la rugosité des parois internes est de (± 0,01) mm,

- La tolérance sur le parallélisme entre les surfaces internes des couvercles est de ± 0,01 mm.

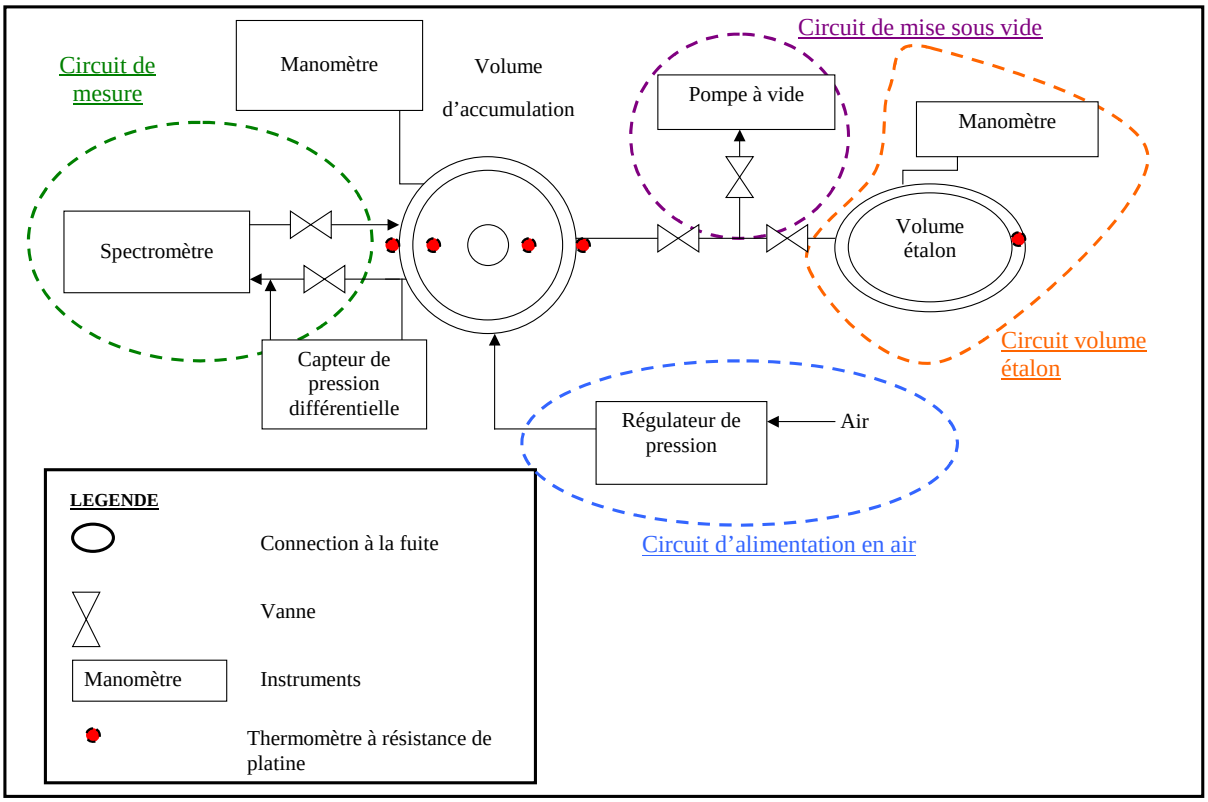

Figure 2.2. Architecture du banc de mesure des débits de fuites frigorigènes

2.6 Conclusion : réalisation du banc

En se basant sur les spécifications décrites dans ce chapitre, l'étalon primaire a été réalisé. Une fois que ce banc sera qualifié (cf. Chapitre 3), il permettra d'étalonner des fuites calibrées qui seront utilisées pour qualifier les détecteurs de fluides frigorigènes suivant les normes prévues à cet effet.

Chapitre 3 Qualification de l'étalon primaire

3.1 Objectifs

Il a été établi dans le chapitre 1 que la réalisation de l'étalon primaire nécessitait une phase de conception et une phase de qualification. En effet, un étalon est un « système de mesure destiné à définir, réaliser, conserver ou reproduire une unité ou une ou plusieurs valeurs d´une grandeur pour servir de référence ». Dans ce cas, la quantité à définir est un débit de fuite et son unité le $g.an^{-1}$. Un étalon primaire est un étalon particulier: il est « désigné ou largement reconnu comme présentant les plus hautes qualités métrologiques et dont la valeur est établie sans se référer à d´autres étalons de la même grandeur » [VIM94].

La conception du banc visait à améliorer les bancs précédemment construits au CEP afin d'optimiser l'incertitude de la mesure. Il reste encore à qualifier la chaîne de mesure permettant d'obtenir un débit de fuite en fonction de quantités d'une autre nature, c'est à dire à partir de la pression, de la température, du volume et de la concentration. La qualification de l'étalon primaire consiste à identifier et quantifier les sources d'incertitudes sur la mesure finale du débit de fuite.

Les objectifs de ce chapitre sont les suivants :

- Résumer les bases générales pour l'expression de l'incertitude de mesure.
- Enumérer et quantifier les différentes sources d'erreurs dans la mesure du débit de fuite.
- Etablir le budget d'incertitudes pour la mesure du débit d'une fuite frigorigène d'une valeur nominale comprise entre 1 et 50 g/an.

Après avoir rappelé les bases générales pour l'expression de l'incertitude de mesure en se basant sur les documents [VIM94] et [GUM99], le chapitre reprend les différentes quantités qui permettent le calcul du débit de fuite : la concentration, la pression, la température et le volume.

3.2 Mesure de la concentration

La mesure du débit de fuite repose principalement sur la capacité du spectromètre photo-acoustique à mesurer la concentration accumulée dans le volume. Il est donc nécessaire d'étalonner l'instrument. Si les principales causes d'incertitude sur la mesure du spectromètre peuvent être identifiées, il est plus simple d'étalonner l'appareil par comparaison avec des concentrations étalons.

3.2.1 Méthode d'étalonnage

Dans un premier temps, la méthode par dilution a été envisagée : il s'agit de réaliser des concentrations étalons en maîtrisant le rapport de dilution entre un mélange en air reconstitué et un mélange en R-134a/air reconstitué qui sera appelé mélange mère. Deux inconvénients sont apparus dans l'utilisation de cette méthode.

Le premier concerne un défaut lors du mélange : les essais ont mis en évidence un défaut d'homogénéisation du mélange lorsque le débit d'air est trop faible. Des concentrations étalons ont été créées par dilution à partir du mélange-mère de 1 023,5 µmol.mol^{-1} de telle sorte que leur valeur soit proche. Les rapports de débit sont volontairement distincts. L'indication de l'analyseur diffère suivant le rapport de débit considéré. La répétabilité de l'analyseur étant meilleure que sa résolution de 0,015 µmol.mol^{-1}, ces écarts sont significatifs.

Le second inconvénient concerne le niveau d'incertitude sur les concentrations diluées. En effet, comme il a été présenté au chapitre 2, l'incertitude relative sur la concentration étalon diluée est de U = 2,7 %, ce qui ne permettra pas d'obtenir une incertitude de l'ordre de 1% sur le débit de fuite.

Afin d'améliorer l'incertitude sur les concentrations étalons, il a donc été décidé de comparer directement les indications lues du spectromètre avec des mélanges mères R-134a-air reconstitué. Trois mélanges ont été créés à cet effet: (10,660 ± 0,055) µmol.mol^{-1} ; (77,83 ± 0,14) µmol.mol^{-1} ; (148,42 ± 0,30) µmol.mol^{-1}. En outre, un point en absence de R-134a peut être effectué en balayant le volume avec de l'air reconstitué.

3.2.2 Estimation de l'incertitude

Hystérésis

L'écart entre la concentration lue lors de la phase de montée en concentration et la concentration étalon, et l'écart équivalent en phase descendante de concentration, différent d'une valeur supérieure à la répétabilité pour une concentration de l'ordre de 80 µmol.mol^{-1}. Ce phénomène d'« hystérésis » n'est cependant pas à prendre en compte, puisque la mesure du débit d'une fuite induit la mesure d'une concentration en phase de montée en concentration.

Résolution

L'appareil dispose d'une résolution limitée à 3 chiffres. Toutefois, cette résolution influe directement sur l'incertitude de la modélisation et est donc considérée comme prise en compte au niveau de la modélisation.

Modélisation

La modélisation se fait donc sur les mesures effectuées en phase montante. Une modélisation linéaire entraîne alors un écart au modèle (résidu maximal) de 0,58 µmol.mol^{-1}. Une modélisation polynomiale de second degré entraîne alors un écart au modèle (résidu maximal) de 0,033 µmol.mol^{-1}.

Environnement

Selon le fabricant, le spectromètre est influencé par la température et la pression. Il varierait de 0,0015 µmol.mol^{-1}.°C^{-1} et de 7,5.10^{-5} µmol.mol^{-1}.hPa^{-1}. Il a été vérifié expérimentalement que l'influence de la température est inférieure à la résolution de l'appareil (tests de 23 °C à 47 °C). L'influence de la pression n'a pu être vérifiée que sur une faible variation de 101 kPa à 103 kPa et est inférieure à la résolution de l'appareil.

Stabilité du spectromètre

En un mois, la dérive de zéro annoncée est de 0,0050 µmol.mol^{-1} tandis que la dérive de sensibilité de l'appareil est de 0,83 %. En considérant que le constructeur a étalonné l'appareil

et l'a calibré pour obtenir une relation $C_E = 1 \times C_{lue}$ avant livraison, la sensibilité de l'appareil semble avoir dérivé d'environ 6 % en 19 mois et le zéro de - 0,46 µmol.mol^{-1}. La dérive de la sensibilité de l'appareil – de l'ordre de 0,3 %/mois - semble donc inférieure à ce qu'annonce le constructeur.

Dans un premier temps, la sensibilité de l'instrument sera vérifiée en deux points tous les mois, et une incertitude type de 0,3 % sera prise en compte. La valeur du constructeur sera donc conservée. Par contre, le zéro semble avoir dérivé de manière plus significative qu'annoncé. Toutefois, l'objectif est de mesurer une variation de concentration et non une concentration absolue. Ce paramètre n'entre donc pas en compte dans le budget d'incertitude.

Budget d'incertitude

Le budget d'incertitude peut donc être établi (cf. Tableau 3.1). L'incertitude élargie composée est alors calculée et estimée à : U = (0,076 + 0.011 x C) µmol.mol^{-1}.

Tableau 3.1. Budget d'incertitude du spectromètre photo-acoustique

Composantes d'incertitude	**Unité**	**Incertitude-type** */ unité*	**Coefficient de sensibilité** */µmol.mol^{-1}.unité$^{-1}$*	**Incertitude-type**
Etalonnage	x C	2.6×10^{-4}	1	$2.6 \times 10^{-3} \times \boldsymbol{C}$
Température	°C	5.8×10^{-1}	1.5×10^{-3}	8.7×10^{-4} *µmol.mol^{-1}*
Pression	hPa	5.8	7.5×10^{-5}	4.3×10^{-4} *µmol.mol^{-1}*
Stabilité (1 mois)	x C	4.8×10^{-3}	1	4.8×10^{-3} *µmol.mol^{-1}*
Correction non appliquée				
Ecart au modèle	0.074 *µmol.mol^{-1}*			

3.3 Mesure de la pression

Tous les 6 mois, les baromètres sont étalonnés par comparaison directe avec un étalon de pression du LNE. L'étalonnage est effectué dans un laboratoire climatisé à (20 ± 1) °C. L'incertitude de l'étalon est de (0,30 Pa + 3,0.10^{-5} x P). La comparaison est effectuée de 100 hPa à 1 300 hPa puis de 1 300 hPa à 100 hPa.

L'incertitude composée pour le baromètre connecté au volume d'accumulation est $U = (5 + 2{,}1 \times 10^{-5} \times P)$ Pa. Cette incertitude est inférieure à 8.0 Pa sur une échelle de mesure de 10 kPa à 130 kPa. Elle est surévaluée puisque l'appareil mesure à une pression voisine de la pression atmosphérique. L'incertitude composée pour le baromètre connecté au volume étalon est de $U = (1.4 + 3.4 \times 10^{-5} \times P)$ Pa. Cette incertitude est inférieure à 6,0 Pa pour la mesure d'une pression entre 10 kPa et 130 kPa.

3.4 Mesure de la température

L'incertitude de la mesure de la température est due :

- A l'étalonnage du multimètre numérique de résolution 6,5 digits.
- A l'étalonnage des sondes Pt100,
- A la définition du mesurande-mesuré analysé dans ce paragraphe,
- A l'homogénéité de la température.

L'incertitude composée associée est alors de : U = 0,14 K. En considérant la mesure de la température dans un système composé des deux volumes, l'incertitude composée est supérieure, puisque l'écart d'homogénéité entre les températures est supérieur : U = 0,59 K. Une enceinte d'isolation thermique va être intégrée au banc afin d'améliorer cette composante d'incertitude.

3.5 Mesure du volume d'accumulation

3.5.1 Description du volume étalon

le volume total est décomposé en plusieurs éléments:

- le cylindre principal en inox 316L,
- le volume de la connexion entre le volume étalon et un manomètre,
- le volume ajouté de la connexion entre le volume étalon et le volume à mesurer.

3.5.2 Etalonnage du volume étalon

L'étalonnage du cylindre principal a consisté à déterminer les dimensions nécessaires au calcul du volume cylindrique par la relation simple : $V=\pi.R^2.H$, à savoir le rayon R et la hauteur H, et d'estimer les composantes d'incertitudes associées à ces grandeurs, notamment les incertitudes associées à l'étalon, à la planéité et à la cylindricité. Il a été réalisé dans une salle climatisée à (20 ± 0,5) °C à l'aide d'une machine de mesure tridimensionnelle raccordée aux étalons nationaux. La valeur du cylindre principal est donc estimée à:

V_{cyl} = (0,50818 **±** 0,00035) dm^3.

Les capacités des tubes, raccords et vannes permettant de raccorder le volume étalon au volume d'accumulation et ceux permettant de raccorder le volume étalon au manomètre, ainsi que le volume interne du manomètre, ont été évalués par l'intermédiaire des schémas techniques fournis par les fournisseurs. En cas de volume interne complexe, le volume a été déterminé par le biais du logiciel AUTOCAD. Le volume étalon est estimé à V_E = (0,51861 **±** 0,00056) dm^3.

3.5.3 Description de l'instrumentation

Lors d'une détente, des phénomènes thermiques ont lieu. Dans le volume initialement en surpression, la température a tendance à baisser de manière significative. Dans le volume initialement en dépression, la température augmente au même titre que la pression [PICK48]. Ainsi ce déséquilibre des températures doit être pris en compte dans la mesure du volume. Par

conséquent des sondes de température PT100 ont été mises en place pour mesurer la température dans les deux volumes. Par souci de précision de la valeur du volume étalon, la sonde de température associée à ce volume n'a pas été placée à l'intérieur du volume.

Si une détente est effectuée entre le volume d'accumulation mis en surpression et le volume étalon mis en dépression, il peut être observé que seules les sondes de température à l'intérieur du volume d'accumulation détectent un refroidissement. Une étude énergétique peut confirmer ce phénomène. A l'équilibre, ces sondes tendent vers la température des sondes de parois. Il est donc nécessaire de connaître le temps de stabilisation nécessaire au système pour pouvoir considérer que la mesure de la sonde de paroi du volume étalon correspond à la mesure du gaz à l'intérieur du volume. Il a été établi par des études phénoménologique et expérimentale que ce temps peut être estimé à 150 s.

Le volume d'accumulation se déduit de l'expression [3.1] :

$$V = V_s \cdot R - V_{fittings} = V_s \cdot \frac{\left.\frac{P_e}{T_e}(t_0)\right|_{Average}^{After\ expansion} - \left.\frac{P_{res}}{T_{res}}(t_0)\right|_{S}^{Before\ expansion}}{\left.\frac{P_0}{T_0}(t_0)\right|_{Acc}^{Before\ expansion} - \left.\frac{P_e}{T_e}(t_0)\right|_{Average}^{After\ expansion}} - V_{fittings} \quad [3.1]$$

où $V_{fittings}$ représente le volume additionnel dus aux connections entre le volume étalon et le volume d'accumulation.

L'extrapolation des rapports P/T est effectuée de sorte que les phénomènes thermiques, l'étanchéité imparfaite du système et les phénomènes d'adsorption des parois soient pris en compte et corrigés dans le résultat [HOL69], [HOL65].

Les composantes d'incertitudes sont définies comme dues à :

- L'incertitude sur les extrapolations des rapports P/T,
- L'incertitude due à la mesure du temps (résolution de 1 s),
- L'incertitude sur la mesure de pression,
- L'incertitude sur l'étalonnage des sondes Pt100,
- L'incertitude sur l'étalonnage du multimètre numérique,
- L'incertitude sur l'homogénéité de la température T_0 associée au volume d'accumulation établie à partir de la mesure de l'écart des indications entre les deux sondes installées en opposition, au contact de la paroi latérale du volume d'accumulation,
- L'incertitude sur l'homogénéité de la température initiale associée au volume étalon T_{res} estimée égale à l'incertitude sur l'homogénéité de T_0,
- L'incertitude sur l'homogénéité de la température à l'équilibre dans le système { Volume d'accumulation + Volume étalon + tubes de connexions et vannes} établie comme l'écart des indications entre la moyenne des mesures effectuées par les sondes associées au volume d'accumulation et la mesure effectuée par la sonde placée dans la paroi du volume étalon,
- L'incertitude sur le volume étalon, et
- L'incertitude sur le volume additionnel dû à la présence de tubes et vannes connectant les deux volumes.

Des essais permettent de mesurer le volume d'accumulation avec une incertitude élargie de l'ordre de 1 %. L'utilisation d'un volume plus simple comme étalon de transfert a permis une comparaison avec un autre laboratoire. Les résultats sont concluants : l'écart normalisé est de +0,29.

3.6 Mesure du débit de fuite

Le débit de fuite se calcule à partir des mesures de pression, température, concentration acquises chaque minute et de la mesure du volume d'accumulation suivant l'expression [1.2]. L'incertitude sur la mesure du débit dépend donc en partie de l'incertitude composée du produit PC/T. Après étude, cette incertitude est estimée à

$$U_{PC/T} = \left(0.020 \times PC/T + 2.6 \times 10^{-5}\right) \text{ Pa.K}^{-1} .$$

L'incertitude dépend donc de la valeur de PC/T.

Afin de modéliser la variation du produit PC/T dans le temps, une modélisation de PC/T(t) par la méthode des moindres carrés pondérés est utilisée. L'incertitude sur la variation de PC/T au cours du temps est déduite par cette méthode et prise en compte dans le budget d'incertitude. L'incertitude dépend du débit de fuite et du temps d'étalonnage. Un exemple de mesure d'une fuite de 20 g/an a donc été présenté (cf. Tableau 3.2). Après étalonnage, sa valeur est estimée à : (17,01 ± 0,24) $g.an^{-1}$, soit une incertitude élargie de 1,5 %.

Tableau 3.2. Exemple de budget d'incertitude après étalonnage d'une fuite de valeur nominale 20 g/an

Description	**Unité**	**Incertitude-type** *[Unité]*	**Coefficient de sensibilité** $g.an^{-1}.[Unité]^{-1}$	**Incertitude-type sur Qm** $g.an^{-1}$
Répétabilité	$g.an^{-1}$	$2,4 \times 10^{-2}$	1	$2,4 \times 10^{-2}$
Mesure de la variation de PC/T(t)	*Pa/K*	$6,6 \times 10^{-8}$	$7,74 \times 10^{5}$	$5,1 \times 10^{-2}$
Volume	*m3*	$1,5 \times 10^{-5}$	8334	$1,2 \times 10^{-1}$
Débit de fuite résiduel	$g.an^{-1}$	$7,0 \times 10^{-4}$	1	$7,0 \times 10^{-4}$

3.7 Conclusions

L'étalon primaire permet de mesurer des débits de fuite avec une incertitude de 1 à 2 % suivant la valeur de la fuite et le temps d'étalonnage. Toutefois, certaines améliorations peuvent être faites sur :

- l'étalonnage du volume d'accumulation : l'incertitude est principalement due à l'homogénéité de la température. L'intégration d'un caisson d'isolation permettrait de réduire cette incertitude.
- L'étalonnage du spectromètre : l'étalonnage du spectromètre ne se fait qu'à l'aide de trois mélanges, ce qui est faible pour établir une modélisation de second degré. En outre, une analyse des résidus de PC/T(t) tous cycles confondus permet de mettre en

évidence un défaut de modélisation pour des concentrations inférieures à 20 µmol/mol. Plus de mélanges vont donc être fabriqués.

- La modélisation des moindres carrés pondérés se base sur le fait que les mesures ne sont pas corrélées, ce qui n'est pas forcément vérifié. La méthode des moindres carrés généralisés sera donc développée afin de mieux déterminer le débit de fuite.

Les fuites frigorigènes calibrées peuvent donc aujourd'hui être étalonnées : les normes visant à qualifier les détecteurs frigorigènes peuvent donc être mises en œuvre. Les essais peuvent être tracés. Toutefois, afin d'assurer au mieux la traçabilité des essais, les précautions à prendre lors des essais doivent aussi être identifiés (cf. chapitre 4).

Chapitre 4 Analyse des tests de qualification des performances des détecteurs de fuites mobiles suivant les normes existantes

4.1 Objectifs

Afin de définir les précautions à prendre, il est nécessaire d'analyser le fonctionnement de ces détecteurs et d'établir ce qui est à mesurer et ce qui est mesuré. De la même manière, les normes seront présentées, ainsi que leurs objectifs.

A partir de ces informations, l'analyse des paramètres pouvant influencer les résultats de la qualification pourra être effectuée. Des études théoriques, expérimentales et phénoménologiques ont donc été menées.

Enfin, les détecteurs sont qualifiés dans le but de répondre à une réglementation de plus en plus stricte en matière de contrôle des équipements frigorifiques. Il est donc intéressant de discuter la pertinence des résultats obtenus lors des essais en laboratoire et les précautions à prendre pour une utilisation de ces détecteurs en milieu industriel devant des fuites réelles.

Les objectifs de ce chapitre sont donc les suivants :

- Identifier la quantité mesurée par un détecteur frigorigène.
- Analyser les objectifs de la norme EN 14624
- Etudier les mécanismes de dilution lors des essais de détection afin de définir les précautions à prendre lors de la réalisation des tests décrits dans la norme EN 14624.
- Définir les précautions à prendre lors de la détection d'une fuite dans des conditions réelles.

4.2 Présentation de 3 techniques de détection

Une étude sur le fonctionnement de 3 types de détecteurs a été menée. Les principes de fonctionnement d'un détecteur infrarouge, d'un détecteur à diode chauffée et d'un catharomètre ont été tour à tour analysés. Cette étude a permis de mettre en évidence l'écart entre la grandeur recherchée et la mesure effectuée par le détecteur. En effet, un détecteur mesure une concentration et non un débit de fuite.

Bien que les détecteurs soient utilisés pour la détection de débits de fuite de gaz frigorigènes, il s'avère qu'ils ne mesurent pas un débit, mais une concentration. Selon les constructeurs, la conversion d'une concentration à un débit est effectuée par comparaison directe du signal indiqué par le détecteur et des débits de fuites étalons. Toutefois, les paramètres pouvant influencer la relation entre le débit indiqué et le mesurande doivent être clairement identifiés et analysés afin de déterminer les précautions à prendre lors de ces étalonnages ou bien lors des tests de qualification des performances des détecteurs. Il est donc intéressant de mettre en évidence la relation entre le débit et la concentration.

4.3 Relation entre le débit et la concentration

La relation entre le débit et la concentration est évidente dans un volume fermé. Elle reprend la relation utilisée pour le calcul du débit de fuite à partir de la mesure de la variation de concentration. Le volume de contrôle est défini arbitrairement comme une sphère de diamètre égal à la distance entre la fuite et le détecteur, soit 2 mm dans le cas décrit par la norme européenne, la variation de concentration est alors très élevée.

Toutefois, lors de la détection d'une fuite, le volume est en général ouvert. La théorie est alors complexe. La concentration dans le volume de contrôle n'est pas homogène. En outre, si la concentration issue d'une fuite calibrée est intégralement aspirée par le détecteur dans l'instant, une relation entre la concentration perçue par le détecteur et la vitesse d'aspiration du détecteur peut être mise en évidence. Il apparaît donc que la relation entre le débit de la fuite et la concentration perçue par le détecteur dépend de la distance entre la fuite et le nez du détecteur et de la vitesse d'aspiration du détecteur.

Cette simplification de la théorie ne rend pas compte de la répartition non uniforme du R-134a dans le volume de contrôle. De ce fait, une étude phénoménologique a été menée, utilisant l'outil CFD Fluent. Elle considère un volume de contrôle cylindrique décrit en Figure 4.1. Cette étude a permis de confirmer l'hétérogénéité de la concentration dans le volume de contrôle, l'influence du débit d'aspiration du détecteur et l'influence de la gravité : le R-134a a tendance à s'accumuler vers le bas de la fuite. En outre, de cette étude, il a été établi que la concentration dépend aussi de la direction de la fuite. Ainsi si le détecteur est positionné dans la même direction que l'écoulement de la fuite, il détectera la fuite plus aisément.

Ces résultats ont été en outre confirmés par l'expérimentation. Afin de déterminer la concentration autour d'une fuite, le tube d'aspiration du spectromètre photo-acoustique est placé en différents points de l'espace par rapport à la fuite. Il en ressort que:

- la mesure de concentration est stable et répétable lorsque le tube d'aspiration est à moins de 5 mm de l'orifice de la fuite et à 0 mm d'altitude,
- la mesure n'est plus répétable au-delà d'une distance de 5 mm.

Il semble donc que dans la direction de la fuite, la mesure de concentration vue par le détecteur de fuite est relativement constante jusqu'à une distance de 5 mm. Si le tube d'aspiration n'est pas tout à fait centré sur la fuite, la mesure est légèrement inférieure mais relativement constante jusqu'à une distance de 2 mm. A partir de cette distance, la concentration diminue avec la distance et semble être influencée par différents paramètres. Par exemple, l'ouverture de la porte du laboratoire peut engendrer un mouvement d'air tel que les mesures peuvent varier jusqu'à 100 % de la valeur voire plus, si le tube d'aspiration est à plus de 5 mm de distance. Cette variation est totalement aléatoire et ne peut donc être corrigée. Le mouvement d'air doit donc être limité lors des essais de qualification. Cette étude indique que le détecteur n'est vraiment performant que jusqu'à une distance de 2 mm, voire 5 mm si le nez du détecteur est centré sur la fuite.

Ainsi, la relation entre le débit de la fuite et la concentration vue par un détecteur est influencée par différents paramètres tels que la distance du renifleur à la fuite, la direction du renifleur par rapport à la fuite, le débit d'aspiration du détecteur, la gravité, les mouvements de l'air ambiant etc.

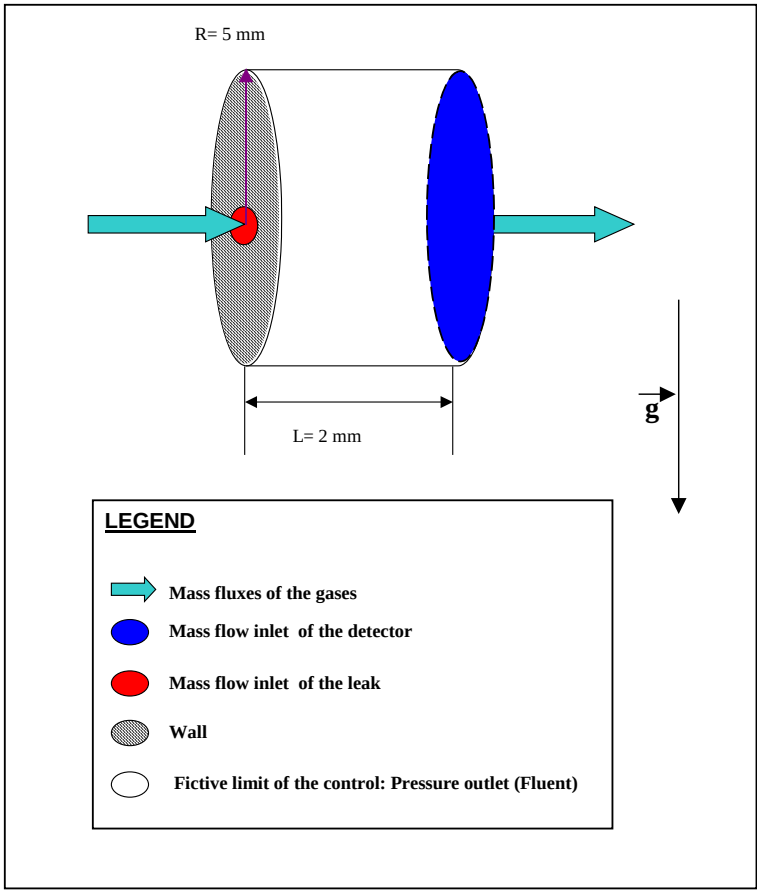

Figure 4.1. Volume de contrôle considéré pour l'étude phénoménologique

4.4 Banc de qualification des détecteurs

Le banc de qualification des détecteurs a été conçu et réalisé afin de répondre à la réglementation qui spécifie que les contrôles d'étanchéité des équipements frigorifiques doivent être effectués avec des détecteurs de fuites frigorigènes. Or les principaux critères de qualification de ces détecteurs sont:

- la sélectivité, c'est-à-dire la capacité à détecter un type de gaz ou une famille de gaz,
- l'échelle de mesure ou la possibilité de disposer de plusieurs échelles de mesures
- la répétabilité de l'indication de la mesure,
- le temps nécessaire pour la détection,
- l'intervalle de temps nécessaire pour réaliser une nouvelle détection après en avoir effectué une préalablement,
- la capacité à détecter lorsque la tête de détection est en mouvement,
- la capacité à détecter en position fixe,
- la capacité à détecter en ambiance polluée.

Deux normes visant à caractériser ces éléments ont été rédigées : la norme européenne EN 14624 et la norme SAE J1627. Une norme ASHRAE est en cours de rédaction : elle s'inspire de la norme européenne. Par l'arrêté du 7 mai 2007, il est obligatoire de qualifier les détecteurs suivant la norme européenne EN 14624. Cette norme a en effet pour objectif de définir les performances des détecteurs de fuite, alors que la norme SAE a pour objectif de définir les critères de performances minimales nécessaires à un détecteur de fuite. Dans les

deux normes, des tests sont explicités pour déterminer les performances des détecteurs. En ce qui concerne la qualification des détecteurs manuels, la norme européenne décrit 4 tests :

- Le premier test – le « test fixe » - vise à mesurer le seuil de sensibilité d'un détecteur de fuite manuel lorsque ce dernier est mis à l'arrêt.
- Le second test – le « test mobile » - mesure le seuil de sensibilité lorsque le détecteur est en mouvement : il est mis en mouvement aller-retour devant une fuite calibrée.
- Le troisième test – le « test en ambiance polluée » - vise à mesurer le seuil de sensibilité du détecteur en ambiance polluée.
- Enfin le dernier test – le « test de récupération » - vise à mesurer le temps de récupération du détecteur après avoir été soumis à un débit élevé, afin de l'amener à saturation.

La norme SAE prévoit un détecteur possédant trois échelles de mesure à sélectionner manuellement : 4 g/an, 7 g/an et 14 g/an. Ces échelles de mesure sont vérifiées par deux tests reprenant le test mobile et le test en ambiance polluée.

La norme ASHRAE prévoit de reprendre les tests de la norme européenne mais en les réitérant à plusieurs distances entre le nez du détecteur et l'orifice de la fuite et à plusieurs vitesse de translation du détecteur durant le test mobile.

Il a été vu précédemment que la détection d'une fuite est fortement influencée par divers facteurs comme la distance à la fuite, la direction de l'écoulement de la fuite, la vitesse de l'air ambiant etc. Lors des essais de qualification, ces paramètres doivent donc être maîtrisés au mieux. Face à ce constat, le banc de qualification a été conçu et installé au LNE en prenant quelques précautions :

- le banc a été installé dans un laboratoire où les mouvements d'air sont faibles (inférieur à 0,2 m/s).
- les essais sont effectués portes fermées.
- la fuite est installée sur un support de telle manière que l'orifice est à un minimum de 20 cm au-dessus de la table de travail, afin d'éviter toute accumulation.
- des vis micrométriques permettent d'établir avec une résolution de 10 µm la position du renifleur et de le centrer par rapport à la fuite.
- des pinces ont été installées afin de stabiliser le détecteur lors du mouvement de va-et-vient.
- un dispositif de mesure permettant de contrôler la concentration de R-134a dans l'enceinte polluée.

4.5 Détection en situation réelle

Lors des contrôles sur site, les paramètres d'influence définis précédemment ne peuvent être maîtrisés aussi bien qu'en laboratoire. Les mouvements d'air ambiant sont généralement supérieurs à 0,2 m/s. Une fuite n'est pas forcément unidirectionnelle, stable - fluctuations de température, de pression etc. - et n'est pas obligatoirement localisée en un point de contrôle. Ainsi, bien que le détecteur utilisé par l'opérateur soit performant, il n'est pas aisé de localiser une fuite :

- il faut réduire au maximum les mouvements d'air.
- le déplacement du détecteur sur les points de contrôles doit être très lent : vitesse de l'ordre de 2 $mm.s^{-1}$ pour que le seuil de détection du détecteur soit le plus proche possible de la valeur mesurée en utilisant la norme européenne ou la norme ASHRAE.
- le détecteur doit être positionné le plus près possible du point de contrôle.

- peu de gaz réfrigérant doit être présent dans la zone de contrôle.
- le nez du détecteur doit être déplacé dans tous les sens afin de rechercher la direction d'une éventuelle fuite et de détecter au mieux.

En outre, comme une fuite réelle n'est pas obligatoirement stable et unidirectionnelle, tout signal – même bref – du détecteur doit être considéré comme susceptible d'être potentiellement généré par une fuite. La mise en place d'une procédure d'utilisation du détecteur incluant les précautions à prendre devient néanmoins plus aisée puisque la traçabilité de l'étalonnage des détecteurs est aujourd'hui assurée. Il est donc important que l'industriel sache ce qui est testé et dans quelles conditions. Le LNE peut en outre adapter les conditions des tests de qualification selon la demande : faire varier la distance du détecteur par rapport à la fuite, la vitesse de translation du détecteur etc.

Toutefois, ces paramètres d'influence peuvent être négligés dans le cas d'un volume fermé : la relation entre la concentration et le débit de fuite est alors définie par l'équation [1.2]. Comme cela a été vu, la concentration accumulée atteint très vite des valeurs élevées dans le cas d'une fuite de l'ordre de plus de 5 g/an, en comparaison avec la valeur réellement vue par un détecteur dans un volume de contrôle ouvert. Aussi l'enveloppement reste-t-il la méthode la plus adaptée et la plus aisée pour localiser une fuite : il suffit d'envelopper les points de contrôle avec des feuilles de vinyle et d'y insérer le renifleur au bout d'un certain temps. Toutefois, en raison de la difficulté à mesurer ce volume d'accumulation, la détection d'une fuite sans enveloppement par un détecteur qualifié reste le moyen le plus simple pour mesurer la fuite, une fois celle-ci localisée.

Conclusion générale

La détection des fuites est une activité de plus en plus réglementée, notamment dans l'industrie automobile et dans la réfrigération. Les équipements contenant des fluides frigorigènes doivent être régulièrement contrôlés en étanchéité avec des détecteurs qualifiés via des fuites frigorigènes qui doivent être traçables. Il est donc indispensable de disposer de fuites étalons permettant de vérifier la mesure effectuée par les différents dispositifs et équipements.

Les laboratoires nationaux de métrologie sont capables d'étalonner des débits de fuites hélium. Pour cela, ils utilisent en particulier des techniques du vide. En se basant sur la littérature, certaines techniques ont été présentées dans ce rapport. Il ressort que ces techniques caractérisent des écoulements moléculaires ou intermédiaires. Or les fuites frigorigènes débitent à pression atmosphérique : leur écoulement est donc caractérisé par un régime visqueux. Comme les modélisations de la conductance dans le cas d'un régime intermédiaire ne sont pas suffisamment exactes pour les besoins en terme d'incertitudes, une nouvelle méthode a été développée par le CEP et est présentée dans le rapport de thèse. En considérant les observations faites sur les techniques du vide ou autre, les avantages de la méthode sont présentés :

- L'étalonnage est effectué à pression atmosphérique, ce qui respecte les conditions d'utilisation des fuites frigorigènes. En outre, le R-134a est un excellent traceur dans le cas d'un régime visqueux et peut donc être utilisé comme tel.
- La détection infrarouge est sélective.
- Le recours à la détection infrarouge permet d'utiliser une méthode par accumulation. Ainsi, plus l'étalonnage dure, plus la concentration à mesurer est importante et plus l'incertitude est faible.

Un étalon primaire basé sur cette méthode a donc été conçu à partir de l'expérience du CEP. Les étapes clés de la conception visent à améliorer la chaîne de mesure du débit, en particulier à établir la méthode de mesure de la variation de concentration et du volume d'accumulation. L'étude présente donc les raisons pour lequel un spectromètre photo-acoustique disponible sur le marché a été choisi, plutôt qu'un spectrophotomètre (également disponible sur le marché). Le choix est basé sur des études comparatives théorique et expérimentale. En outre, une étude bibliographique a permis d'énumérer et d'analyser les techniques principales pour la mesure des volumes : les méthodes dimensionnelle, gravimétrique et la méthode des volumes d'expansion. Une analyse des caractéristiques du volume d'accumulation a permis d'établir que le volume était trop complexe pour qu'une méthode d'étalonnage dimensionnel soit possible. Une première estimation théorique de l'incertitude sur les volumes en fonction de la méthode utilisée a aussi été effectuée afin de déterminer laquelle parmi la méthode gravimétrique et la méthode des volumes d'expansion était la plus adaptée à l'objectif : mesurer un débit de fuite avec une incertitude de l'ordre de 1 %. Avec une incertitude estimée de 2,1 %, la méthode gravimétrique n'est pas retenue. La méthode des volumes d'expansion a, elle, été retenue : incertitude estimée inférieure à 0,35 %.

A partir de ces études, l'étalon primaire a été conçu avec quelques améliorations par rapport aux bancs précédemment développés au CEP. La principale amélioration concerne l'intégration d'un volume étalon conçu de telle sorte qu'il puisse être étalonné dimensionnellement avec une incertitude de l'ordre de 0,1%. En outre, l'étude comparative des spectromètres a permis d'améliorer la connaissance du cycle de mesure du spectromètre

photo-acoustique pour une meilleure gestion de la correction des concentrations en pression et température. A partir des spécifications décrites, l'étalon primaire a pu être réalisé.

Comme lors de la phase de conception, la qualification du banc a porté sur le processus de mesure de la concentration et du volume. En effet, si les méthodes d'étalonnage des instruments de pression et de température sont bien établies, les méthodes d'étalonnage du spectromètre et du volume d'accumulation ont dû être mises au point. La chaîne de mesure du spectromètre photo-acoustique a été analysée : les sources d'incertitudes ont été identifiées. Afin de simplifier la procédure d'étalonnage, le spectromètre a finalement été considéré comme une boîte noire mesurant une concentration et indiquant une concentration. Par conséquent, l'étalonnage s'effectue par comparaison entre l'indication du spectromètre et la valeur de mélanges étalons de R-134a/Air reconstitué fabriqués à cet effet. L'incertitude obtenue est de l'ordre de 1 %. De même la méthode d'étalonnage du volume d'accumulation a été mise au point en se basant sur des études théoriques, phénoménologiques et expérimentales, afin notamment de déterminer le temps de stabilisation du système, d'optimiser la mesure de la température et la mesure du volume étalon. L'incertitude obtenue élargie est de l'ordre de 1 à 2 %. Elle est principalement due à l'homogénéité de la température dans le système.

Aujourd'hui, le LNE est donc en mesure d'étalonner des débits de fuites frigorigènes avec une incertitude composée élargie de l'ordre de 1 à 2 %. L'incertitude obtenue est donc proche de l'objectif (1 %). Des améliorations peuvent cependant être réalisées. En ce qui concerne l'étalonnage du spectromètre, le nombre de mélanges de gaz peut être augmenté afin d'améliorer la modélisation du comportement du spectromètre. En outre, la méthode généralisée des moindres carrés peut être développée afin de prendre mieux en compte la corrélation entre les mesures. L'étalonnage du volume d'accumulation peut aussi être amélioré en intégrant un caisson isolant thermiquement le système {volume d'accumulation et volume étalon}. Enfin, la possibilité d'une extension de la méthode de mesure à d'autres gaz ou mélanges de gaz peut être étudiée.

L'étalon primaire est un bon outil pour assurer la traçabilité des fuites calibrées nécessaire à la qualification des détecteurs de frigorigènes suivant les normes existantes. Cependant, une étude bibliographique sur trois techniques de détection a mis en évidence le fait qu'un détecteur mesure une concentration et non un débit. Or la relation concentration-débit est susceptible d'être influencés par plusieurs paramètres. Des études théoriques, phénoménologiques à partir de l'outil CFD Fluent et des études expérimentales ont permis d'établir que cette relation dépendait notamment de la distance du détecteur à la fuite, de la vitesse d'aspiration de la fuite, de la vitesse de translation de la fuite, de la gravité, de la direction du détecteur par rapport à la fuite, de la vitesse de l'air ambiant etc. Certaines précautions à prendre ont donc été identifiées et prises en compte lors de la conception du banc de qualification des détecteurs de fuites frigorigènes décrits dans les normes existantes. Ces études ont été étendues à l'utilisation des détecteurs en situation réelle. Après avoir mis en évidence qu'une fuite réelle n'est pas forcément unidirectionnelle, stable et homogène comme une fuite calibrée, des précautions supplémentaires ont été identifiées et appuyées par des essais. La méthode par accumulation semble donc le meilleur moyen de s'affranchir des paramètres d'influence et d'établir une relation répétable entre la concentration et le débit. Pour cela, la méthode par enveloppement semble la plus indiquée. Elle ne permet que la localisation globale d'une fuite. Néanmoins, une fois cette fuite identifiée, il sera plus simple de la localiser pour la traiter.